Silesian University of Technology

Faculty of Energy
and Environmental Engineering

Institute of Thermal Technology

Clausthal University of Technology

Faculty of Energy
and Management

Institute of Energy Process Engineering
and Fuel Technology

Ph.D. thesis

Ecological evaluation
of the pulverized coal combustion
in HTAC technology

Natalia SCHAFFEL-MANCINI

This thesis was realized in the frame of the agreement between
Silesian University of Technology and Clausthal University of Technology
for Ph.D. projects

Gliwice - Clausthal-Zellerfeld 2009

Politechnika Śląska
w Gliwicach
Wydział Inżynierii Środowiska
i Energetyki
Instytut Techniki Cieplnej

Uniwersytet Techniczny
w Clausthal
Wydział Energii
i Nauk Ekonomicznych
Instytut Energetycznej Inżynierii Procesowej
i Technologii Paliw

Praca doktorska

Ocena ekologiczna
procesu spalania pyłu węglowego
w technologii HTAC

Natalia SCHAFFEL-MANCINI

*Praca doktorska powstała w ramach umowy o podwójnym doktoracie zawartej pomiędzy
Politechniką Śląską w Gliwicach i Uniwersytetem Technicznym w Clausthal*

Gliwice - Clausthal-Zellerfeld 2009

Schlesische Technische Universität
in Gliwice

Fakultät für Energie
und Umwelttechnik

Institut für Hochtemperaturtechnik

Technische Universität
Clausthal

Fakultät für Energie-
und Wirtschaftswissenschaften

Institut für Energieverfahrenstechnik
und Brennstofftechnik

Dissertation

Ökologische Bewertung
der HTAC-Kohlestaubverbrennungsmethode

Natalia SCHAFFEL-MANCINI

Diese Dissertation wurde im Rahmen der Doppelpromotionsvereinbarung zwischen der Schlesischen Technischen Universität und der Technischen Universität Clausthal ausgefertigt

Gliwice - Clausthal-Zellerfeld 2009

Author:

Mgr inż. **Natalia Schaffel-Mancini**

Silesian University of Technology

Faculty of Energy

and Environmental Engineering

Institute of Thermal Technology

ul. Konarskiego 22

PL-44 100 Gliwice, Poland

e-mail: `natalia.schaffel@polsl.pl`

Dipl.-Ing. **Natalia Schaffel-Mancini**

Clausthal University of Technology

Faculty of Energy

and Management

Institute of Energy Process Engineering

and Fuel Technology

Agricolastr. 4

D-38 678 Clausthal-Zellerfeld, Germany

e-mail: `natalia.schaffel@ievb.tu-clausthal.de`

Supervisors:

Prof. dr hab. inż. **Andrzej Szlęk**

Silesian University of Technology

Faculty of Energy

and Environmental Engineering

Institute of Thermal Technology

ul. Konarskiego 22

PL-44 100 Gliwice, Poland

e-mail: `andrzej.szlek@polsl.pl`

Prof. Dr.-Ing. **Roman Weber**

Clausthal University of Technology

Faculty of Energy

and Management

Institute of Energy Process Engineering

and Fuel Technology

Agricolastr. 4

D-38 678 Clausthal-Zellerfeld, Germany

e-mail: `roman.weber@ievb.tu-clausthal.de`

Reviewers:

Prof. dr hab. inż. **Marek Pronobis**

Silesian University of Technology

Faculty of Energy

and Environmental Engineering

Institute of Power Engineering

and Turbomachinery

ul. Konarskiego 20

PL-44 100 Gliwice, Poland

e-mail: `marek.pronobis@polsl.pl`

D. Sc. (Tech.), Professor **Antti Oksanen**

Tampere University of Technology

Faculty of Science

and Environmental Engineering

Department of Energy

and Process Engineering

PO Box 589

FIN-33 101 Tampere, Finland

e-mail: `antti.oksanen@tut.fi`

Contents

List of Tables

List of Figures

Abstract

High Temperature Air Combustion (HTAC), named also FLameless OXidation-FLOX or MILD (Moderate and Intensive Low-oxygen Dilution) combustion (often written simple as mild combustion), is probably the most important achievement of the combustion technology in recent years. In HTAC technology chemical reactions take place in almost entire volume of the combustion chamber. Consequently, very uniform both temperature and species concentrations fields are characteristics of this technology. Moreover, the technology features very low NO_x and CO emissions, and high and uniform heat fluxes. So far, HTAC technology was implemented mainly in industrial furnaces fired either with gaseous fuels or light oils. In most of industrial applications, the technology is combined with heat recovery systems and such a combination typically results in substantial fuel savings.

In this work, firstly, the mathematical models describing coal combustion in HTAC technology have been validated against the data generated during an IFRF experiment called HTAC 99. The CFD-based simulations have been performed using FLUENT code. Prior to performing the numerical simulations of HTAC 99 trials, substantial efforts have been allocated to an accurate modeling of combustion of Guasare coal which was used in the IFRF experiments. Subsequently performed numerical simulations of the HTAC 99 experiments have demonstrated that the FLUENT code predicts both the in-furnace measured data and the furnace exit parameters with good accuracy. Such a validated model has then been used in the boiler design studies.

In the second part of the work, applications of HTAC technology to power station boilers fired with pulverized coal have been numerically investigated. Several boiler configurations have been analyzed with the respect to the following key points: existence of an intensive in-furnace recirculation, uniformity of both the temperature and chemical species fields, and of heat fluxes. Special considerations have been given to emissions of NO_x, CO and unburned hydrocarbons. Calculations of the steam cycle have been coupled with the combustion chamber simulations.

The most important advantages of the pulverized coal fired boiler operating under HTAC conditions are as following. Firstly, heat fluxes emitted during combustion process are high and uniform which results in the high firing density and consequently the small size of the boiler. Secondly, low NO_x emissions in comparison with the standard PC burners. Then, used burners have a very simple construction: without air staging, flame stabilizer or swirl which are commonly used in the commercial pulverized coal burners.

Overall, the present study confirmed that HTAC technology could be a practicable, efficient and clean technology for pulverized coal fired boilers.

Streszczenie

Technologia HTAC (High Temperature Air Combustion), znana także pod nazwą FLameless OXidation- FLOX lub MILD (Moderate and Intensive Low-oxygen Dilution) combustion, jest prawdopodobnie najważniejszym odkryciem w dziedzinie spalania w przeciągu ostatnich lat. W technologii HTAC reakcje chemiczne zachodzą w całej objętości komory spalania, czego efektem są równomierne pola temperatury i koncentracji związków chemicznych. Ponadto technologia HTAC cechuje się niskimi emisjami substancji szkodliwych (szczególnie NO_x i CO) oraz wysokimi i wyrównanymi strumieniami ciepła. Jak dotąd, technologia HTAC została zastosowana głównie w piecach przemysłowych opalanych paliwami gazowymi lub lekkim olejem. W większości zastosowań przemysłowych technologia ta jest zintegrowana z systemami odzysku ciepła ze spalin, co pozwala na znaczne zmniejszenie zużycia paliwa.

W pierwszej części pracy sprawdzono poprawność modelu matematycznego opisującego proces spalania pyłu węglowego w technologii HTAC. Weryfikacji modelu dokonano w oparciu o pomiary przeprowadzone w instytucie badawczym IFRF, podczas eksperymentu zwanego HTAC 99. Symulacje, oparte o numeryczną mechanikę płynów, wykonano używając oprogramowania FLUENT. W rezultacie uzyskano dobrą zgodność pomiędzy wynikami pomiarów i obliczeń numerycznych. Opracowany model matematyczny spalania pyłu węglowego w technologii HTAC został zastosowany w procesie projektowania kotła pracującego w tej technologii.

W drugiej części pracy, zbadano możliwość zastosowania technologii HTAC w kotłach energetycznych opalanych pyłem węglowym. Konfigurację badanego kotła analizowano ze względu na trzy kluczowe kwestie: intensywne recyrkulacje wewnątrz komory spalania, wyrównane pola temperatury i koncentracji reagentów oraz równomierne strumienie ciepła. Szczególną uwagę poświęcono zagadnieniom związanym z ochroną środowiska: emisji tlenków azotu, tlenku węgla oraz niewypalonych części stałych. Przetestowano także działanie kotła HTAC przy wybranych parametrach eksploatacyjnych oraz we współpracy z układem parowym.

Najważniejszą zaletą zastosowania technologii HTAC w kotłach energetycznych są wyrównane i wysokie wartości strumieni ciepła, a tym samym duża gęstość energii w komorze kotła. Skutkuje to mniejszymi rozmiarami komory spalania takiego kotła. Kolejną zaletą jest niska emisja substancji szkodliwych, głównie tlenków azotu, w porównaniu ze standardowymi palnikami pyłowymi. Dodatkowo, zastosowane palniki mają niezwykle prostą konstrukcję: bez stopniowania powietrza, stabilizacji płomienia czy zawirowania, które są powszechnie stosowane w palnikach pyłowych.

Przedstawiona praca doktorska potwierdziła, że zastosowanie technologii HTAC w kotłach energetycznych może być praktyczną, wysokoefektywną i czystą metodą spalania pyłu węglowego w celu produkcji energii elektrycznej.

Kurzfassung

Die FLammenlose OXidation (FLOX), im englischen Sprachraum entweder als High Temperature Air Combustion (HTAC) oder als MILD (Moderate and Intensive Low-oxygen Dilution) Combustion bekannt, gehört zu den wichtigsten Forschungsgebieten der Verbrennungstechnik in jüngerer Zeit. Die HTAC-Technologie zeichnet sich dadurch aus, dass die chemischen Reaktionen nahezu im gesamten Volumen des Verbrennungsraumes stattfinden. Dies geht sowohl mit einer sehr gleichmäßigen Temperaturverteilung als auch einer gleichmäßigen Verteilung der chemischen Komponenten einher. Neben sehr niedrigen NO_x- wie auch CO-Emissionen ermöglicht die Anwendung dieser Technologie hohe und gleichmäßige Wärmestromdichten. Bis heute hat die HTAC-Technologie hauptsächlich Anwendung in Industrieöfen gefunden, die mit gasförmigen Brennstoffen oder leichtem Heizöl befeuert werden. Zusätzlich wird bei den meisten industriellen Anwendungen die Restwärme aus dem Prozess zurückgewonnen, was insgesamt zu beträchtlichen Brennstoffeinsparungen führt.

Im Rahmen dieser Arbeit wird zuerst das mathematische Modell, das die Verbrennung von Kohle unter HTAC-Bedingungen beschreibt, mit Hilfe von Messergebnissen validiert, die aus einem IFRF-Experiment stammen, das als HTAC-99 bekannt ist. Besonderes Augenmerk wurde auf die Modellierung des Verbrennungsverhaltens von Guasare-Kohle gelegt, da diese auch in den HTAC-99 Experimenten verwendet wurde. Dabei wurden alle verbrennungs- und strömungstechnischen Untersuchungen mit der CFD-Software FLUENT durchgeführt. Anschließend durchgeführte numerische Simulationen der HTAC-99 Experimente zeigen, dass die Ergebnisse der Modellrechnungen sowohl mit den im Verbrennungsraum gemessenen Daten wie auch mit den im Abgas gemessenen Daten mit guter Näherung übereinstimmen. In den folgenden Untersuchungen zur Kesselauslegung wurde solch ein validiertes Modell verwendet.

Im zweiten Teil werden die Anwendungsmöglichkeiten der HTAC-Technologie in kohlestaubbefeuerten Kraftwerkskesseln numerisch untersucht. Verschiedene Kesselkonfigurationen wurden bezüglich folgender Schlüsselfragen untersucht: Existenz einer intensiven internen Rezirkulation; gleichmäßige Temperaturverteilung; gleichmäßige Verteilung der chemischen Komponenten sowie gleichförmige Wärmestromdichten. Dabei wurden die Emissionen an NO_x, CO sowie unverbrannter Kohlenwasserstoffe einer besonderen Betrachtung unterzogen. Zudem wurde die Berechnung des Dampfkreislaufes mit den Simulationen der Verbrennungsvorgänge im Kraftwerkskessel gekoppelt.

Zusammenfassend folgen die wichtigsten Vorteile der mit Staubkohle befeuerten Kessel, die mit HTAC Technologie funktionieren. Da wären zuerst die hohen und gleichmäßigen Wärmeströme, die während des Verbrennungsprozesses abgestrahlt werden, welche ein Resultat der hohen Befeuerungsdichte und der konsequent kleinen Bauart des Kessels sind. Als nächstes seien die, im Vergleich zu Standard-PC-Brenner, geringen NO_x-Emissionen genannt. Desweiteren sind die Brenner simpel aufgebaut: ohne Luft Stufung, Flammenstabilisator oder Drall Erzeuge, was üblicherweise in kommerziellen Staubkohlebrennern verwendet wird.

Insgesamt ergeben die Rechnungen, dass die HTAC-Technologie eine machbare, effiziente und saubere Technologie für Staubkohle befeuerte Kessel ist.

Acknowledgments

Writing this thesis has been fascinating and extremely rewarding. I would like to take the opportunity to express my sincere appreciation to everyone that has contributed to the final result in many different ways:

I wish to thank my supervisors Professor **Andrzej Szlęk** and Professor **Roman Weber** for their constant availability, attention, time and insightful guidance. Their advice was invaluable for the progress and completion of this thesis. One simply could not wish for better or friendlier supervisors!

In particular, I wish to thank **Marco Mancini** for everlasting assistance in my life. He supports all my undertakes and gives me the extra strength, motivation and love necessary to get things done. He has always inspired me to learn, both as a researcher and as a person. He is my mentor, my husband and my best friend. I am truly fortunate to have been able to enjoy and benefit from such a relationship with him. His belief and generosity are most profoundly acknowledged here with love and respect.

I would also like to thank my **colleagues at ITC** (Institute of Thermal Technology) and **at IEVB** (Institute of Energy Process Engineering and Fuel Technology). Thank you for a great time! Special thanks is given to **Sebastian Werle** for helping me with the polish bureaucracy while I stay in Germany, **Piotr Plis** for the support with the organization of my Ph.D. study in Poland, **Marc Muster** for the advice in German translations and **Jadwiga Wróbel** for companionship not only during the coffee breaks. I thank also all my **friends** for their companionship all the time.

Finally, I thank my **family** for their love, security, understanding and unswerving belief in me. I am truly and deeply indebted to you!

I also must acknowledge my gratitude to **God** for the many opportunities. He has given me the gifts that made those opportunities fruitful.

Introduction

Combustion technology provides more than 90% of our worldwide energy demand [1]. Severe environmental requirements and international agreements on reduction of pollutants emissions (CO_2, CO, NO_x, soot, particles etc.) raise a continuous demand for improved combustion technologies.

Coal is an abundant fuel resource in many of the developing regions and forecasts show that it is likely to remain a dominant fuel for electricity generation in many countries for years to come [2]. Coal-fired power plants currently generate approximately 40% of the world electricity. Since coal dominates the energy supply in the developing countries and still is an important fuel in the industrialized nations it will continue to play an important role in worldwide power generation [3]. Thus the development of advanced coal combustion technologies of a higher performance efficiency and lower pollutants emissions is a major goal of combustion researchers.

The global demand for electricity is projected to grow at an annual rate of 2.5% [3]. In order for coal to continue to be a dominant fuel in power generation there are some important challenges that must be addressed, and they are predominantly environmental. The development of advanced coal fired power plants of higher performance efficiency and lower pollutants emissions is a major goal of combustion researchers. To realize this goal of environmentally friendly coal utilization new concepts are needed while the existing combustion routes and processes have to be continuously improved.

Application of HTAC technology to boilers fired with pulverized coal could be one of the future coal combustion technologies for the clean power generation. Technical and ecological aspects of such applications are analyzed and discussed in this thesis.

Motivation

The ultimate goal of current combustion research in power generation sector is to improve the fuel conversion efficiency and to minimize pollutants emissions. High Temperature Air Combustion provides an opportunity to achieve this goal in certain sectors of energy conversion. In the current situation of growing demand for electricity there is an urgent need for development of advanced coal combustion technologies for power generation. Therefore, it is important to assess whether and how HTAC technology can be implemented in coal fired power station boilers.

Objectives

The main objective of this thesis is to investigate applicability of HTAC technology to power station boilers fired with pulverized coal for environmental friendly electricity production. In order to achieve this main goal, several technical objectives have been formulated.

The first objective is to examine how accurately HTAC combustion of coal can be predicted using numerical modeling methods. To this end several sub-models have been validated against the IFRF measurements. The mathematical model selected in the validation and verification process is then used in all subsequent investigations.

The second objective is to develop a conceptual design of a pulverized coal fired boiler utilizing HTAC technology. This involves determination of the combustion chamber shape, its dimensions, distance between individual burners and positions of the burner block. A successful implementation of HTAC technology requires the following three key points: a strong recirculation of combustion products to fresh reactants, uniform fields of temperature and chemical species inside the boiler, and an intensive radiative heat transfer. These three points are carefully considered while developing of the boiler conceptual design and they are discussed in this work.

The third objective involves examination of the environmental aspects of the HTAC technology implementation. Here one focuses on NO_x, CO and unburned hydrocarbons emissions, as well as on char burnout.

The fourth objective is to examine the boiler operation under different operating conditions like: low air preheat, low jet momentum and low air excess ratio.

The fifth objective is to investigate a whole steam cycle in order to estimate the efficiency of electricity production in such a HTAC boiler.

Chapter 1

Coal in power generation

Solid fuels are an important item in world energy balance. According to all forecasts, this situation will remain unchanged over a foreseeable future [4]. Solid fuels will be of special importance in the regions abundant in coal deposits. One of these regions is the east part of Europe, including Poland, where coal is also the basic fuel in power generation. Coal is also a significant fuel for the West-European countries and the USA since it is an alternative to oil or natural gas which resources are located in politically unstable regions of the world. Therefore, it is important to develop new coal combustion technologies featuring low emissions of harmful substances and a high efficiency.

This Chapter provides a state of the art review of the coal based power generation technologies all over the world. Special attention is given to the role of coal in the power generation of today and tomorrow. In this Chapter the environmental concern of coal combustion and pollutants emissions control policies are also described. Furthermore, forthcoming coal utilization technologies are presented. Finally, current boiler designs are briefly described in order to compare them later with the boiler concept proposed in this thesis.

1.1 Overview of coal utilities

Coal is one of the major energy source for power generation. Coal is by far the largest fossil fuel resource in the world with known reserves of some 1145 billion tons which should suffice for the next 200 years [2]. In contrast, natural gas, its principal fossil fuel competitor for power generation, is a more limited resource. Decreased availability of natural gas is projected to occur in the forthcoming future, thus weakening its ability to compete with coal for power generation in the world. Therefore, coal will remain an indispensable major source of energy for power generation also in the coming decades.

Coal is uniformly dispersed almost all over the world in contrast to oil and gas which are situated only in few regions. Coal-exporting countries can be divided into two classes. To the first group belong the United States, South Africa, Germany, Poland and parts of the former Soviet Union. In these countries coal exports are a relatively small fraction of a substantial domestic market. Other countries mine primarily for export. The leading country in this class is Australia, with Colombia and Venezuela also rapidly increasing coal exports. China is a special case: it is the world's largest producer but almost all of its coal is consumed domestically [1]. Japan is the world's largest coal importer while the fastest import growth is occurring in the rapidly developing Pacific Rim countries, especially Taiwan and South Korea [5]. The European Union (EU) is dependent on import of primary energy and the recent large increase of oil and gas prices shows clearly this dependence. The coal prices remain more stable than gas and oil prices which demonstrates the strategic role of coal in the EU energy mix.

The most important market for coal utilization is electricity generation. Two major market components are: the construction of new generation capacity and the retrofit and rehabilitation of existing plants. The current power station capacity of the EU amounts to 600 GW [1]. At present more than 50% of these installations is more than 25 years old and 30% of which is based on coal. Only 8% of the existing power plants show an efficiency of 40% or higher. Assuming a lifetime of about 40 years, about 50% of presently available capacity will have to be retired by 2030. In order to maintain at least the present supply situation about 300 GW has to be replaced. If the expected increase in electricity demand arises, a total capacity of approximately 500 GW will be needed by that time [1]. The sheer scale of such new plant capacity requirements will have to be met trough the use of range of fuels and as noted above coal will be a part of that energy mix. It is also expected that the gradual succession will be based on the most modern technology with regard to environmental protection and cost effectiveness. Continuous efforts in research and development are therefore necessary in order to achieve these goals [6]. The need for coal fired capacity in China, India, South East Asia, Eastern Europe and the USA is even bigger. So, a competitive, highly-efficient and low-emission coal fired power technology represents an enormous industrial potential, internally in the EU and as an export potential.

Summarizing, coal is a very important fossil fuel and it will play a significant role in the foreseeable future. Therefore, a further development of the present coal technologies and search for new methods are imperative.

1.2 Environmental issues of coal utilization

Environmental concerns will have a major effect on future coal use for power generation in the industrialized countries. Control of SO_2, NO_x, dust, solid wastes, and possibly air toxins, will continue to determine the acceptability of coal based systems, with the states and local environmental requirements posing the most restrictive demands on power plants emissions.

Significant progress has been made over the past decade in the capability of commercial systems to reduce SO_2, NO_x and dust emissions from pulverized coal-fired power plants. The most advanced wet scrubbers reduce SO_2 emissions with the process efficiency of 98%. The most efficient commercial systems are able to remove the particulate emissions up to the 99.9%. Technology for power plant NO_x control has focused on combustion modification methods that currently reduce emissions to about 70-80% control levels. The post-combustion controls achieves up to 90% NO_x reduction levels [7].

Emission limit values for NO_x, SO_x and *dust* (expressed in $\frac{mg}{m_n^3}$, O_2 at 6%) in the case of coal combustion in large combustion plants are controlled by the emissions policies and these limit values for EU [8], Poland [9] and Germany [10] are listed in Tab. 1.1. Furthermore, air toxins are of primary concern to utilities; these are the 10-20 trace substances commonly found in coal, including arsenic, mercury, selenium, nickel, cadmium, and other heavy metals. Regulations of guidelines on emissions of hazardous air pollutants are still in preparation in many countries.

The Kyoto Protocol [11] represents the most important milestone in international climate change mitigation policy and it was the world reaction to the global warming effect. At the same time it has the significant impact on the direction of coal combustion research. The text of this protocol was adopted at the UNFCCC (United Nations Framework Convention on Climate Change) members conference in Kyoto, Japan, on $11th$ December 1997. The Kyoto Protocol came into force on $16th$ February 2005 and required a significant reduction of the greenhouse gasses emission from the participants countries. This provided the driving force for the modernization of the present power plants and investigation of the new low (or zero) CO_2-emissions projects in order to meet the Kyoto agreement. The most cost-effective method of reducing CO_2 emissions from coal based power generation is to improve the systems' overall efficiency. To achieve larger or more rapid reductions in CO_2 emissions new technological options for the removal and storage of CO_2 are needed.

	Thermal input, MW_{th}	Limit values, $\frac{mg}{m_n^3}$
EU		
NO_x	50 to 500	600
	> 500	500
from 1.01.2016		
	50 to 500	600
	> 500	200
SO_2	< 100	2000
	100 to 500	from 2000 to 400*
	> 500	400
dust	< 500	100
	⩾ 500	50
Poland		
NO_x	< 50	400
NO_x	5 to 500	600
	⩾ 500	500
SO_2	< 5	1500
	5 to 50	1500
	50 to 100	1500
	100 to 500	from 1500 to 400*
	> 500	400
dust	< 5	700
	5 to 50	400
	50 to 500	100
	⩾ 500	50
Germany		
NO_x	50 to 100	400
	> 500	200
SO_2	50 to 100	850
	> 100	200
dust		20

Table 1.1: Emission limit values for NO_x, SO_2 and dust in European [8], Polish [9] and German [10] legislation.

(* depended on the thermal input)

Existing technologies for air pollutants control (SO_2, NO_x and particulate) associated with pulverized coal fired power plants are capable of meeting current or forthcoming emission reduction requirements. However, cost reduction is of the primary concern since the cleaning flue gas installations are very expensive. Performance improvements is required especially for NO_x controls. A promising alternative to the commonly used Selective Catalitic Reduction (SCR) de-NO_x methods are low-emission combustion technologies, such as HTAC technology which may eliminate or reduce costly flue gas cleaning installations.

1.3 Coal based technologies for power generation

Global policies which require reduction of CO_2 emission provide a strong driving force for the development of clean and efficiently technologies for power generation, including coal based combustion methods. High natural gas prices could also accelerate the need for such a new capacity. Heightened concerns over global warming could push the drive for high efficiency technology and CO_2 sequestration methods to reduce greenhouse gas emissions. Advanced power systems must not only produce significantly lower emissions than current coal fired plants but also must compete economically with other future options. Higher efficiencies in the new technologies will contribute not only to lower fuel costs but also to improved environmental performance for a given power output. To be competitive overseas, advanced technologies would require the lowest possible capital costs accompanied by the environmental requirements. Summarizing, efficiency, emissions, and costs are the key attributes of advanced coal based technology. The most promising coal technologies for the power generation from thermodynamic, environmental and economic point of view are:

- Pulverized coal (PC) combustion systems

- Fluidized bed combustion (FBC) systems

- Combustion under CO_2/O_2 atmosphere

- Coal gasification (CG) technology

- Integrated Gasification Combined Cycle (IGCC) systems

- Integrated Gasification Fuel Cells (IGFC) systems

These technologies are briefly characterized in Subsections 1.3.1-1.3.6. Magnetohydrodynamics and direct coal-fired heat engines have been omitted since their importance is marginal.

1.3.1 Pulverized coal (PC) combustion systems

Pulverized coal-fired electric power generation involves reducing coal size to a powder and transporting it with combustion air into a boiler, where the fuel is burned. The heat released evaporates water flowing in tubes of boiler walls to form high-pressure, high-temperature steam which is used to drive a turbine connected to an electric generator. The steam is then condensed back to a liquid and returned to the boiler to repeat the cycle (called Rankine cycle, see Section 1.6). A general schematic of a typical PC power plant installation is shown in Fig. 1.1. A wide range of coals from lignites to anthracite are combusted in pulverized coal boilers. Coal cleaning and drying is widely practiced to reduce the coal ash and sulfur content and to raise its heating value due to humidity elimination. Pulverized coal combustion has been practiced for many decades and there is an extensive literature on boiler and system designs [12, 13, 14, 15, 16, 17].
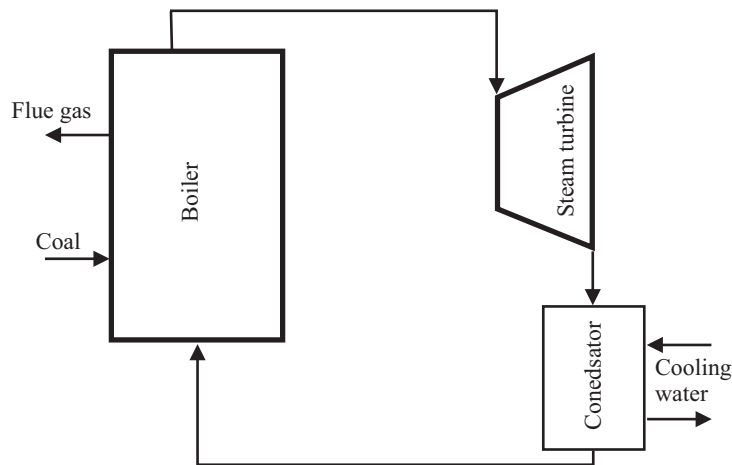
Figure 1.1: General schematic of PC power plant installation

Current boiler designs include usually either low-NO_x combustion technology or advanced flue gas treatment systems (for example, combined SO_2/NO_x removal) or both to achieve cost-effective emissions control. Power generation technology using pulverized coal is commercially mature and it is widely implemented around the world.

1.3.2 Fluidized bed combustion (FBC) systems

Fluidized bed combustion (FBC) technology consists of forming a bed of sand together with finely sized ash, limestone or dolomite (for sulfur oxides removal), and coal particles in a furnace and forcing combustion air up through the mixture, causing it to become suspended or fluidized. The height of bed material suspended above the bottom of the furnace is a function of the velocity of the combustion air entering the bed.

FBC technology can be divided into atmospheric (AFBC) and pressurized (PFBC) application and furthermore, AFBC has two types of practical solutions: bubbling and circulating bed. These two types of fluidized bed are depicted in Fig. 1.2.
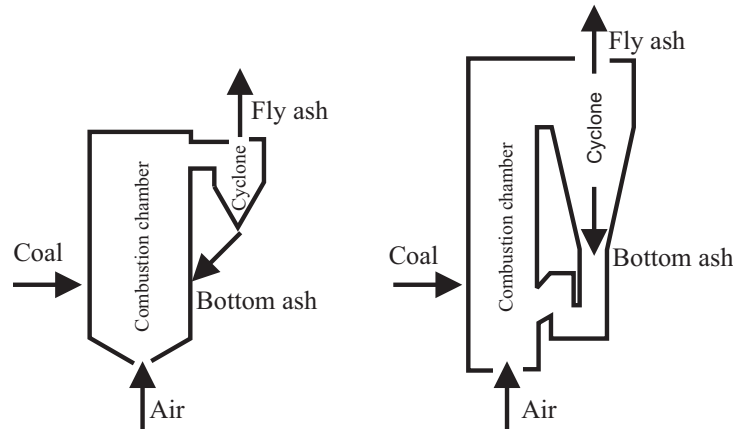
Figure 1.2: Types of fluidized bed arrangement: bubbling bed (left) and circulating bed (right)

AFBC units are operated at near atmospheric pressure in the combustion chamber. The bubbling bed has a fixed height of bed material while in circulating bed, the combustion air enters below the bed at a velocity high enough to carry the bed material out of the top of the chamber, where it is caught in a high temperature cyclone and recycled back into the furnace. This recycling activity improves combustion and reagent utilization. Circulating fluidized bed technology is the most common fluidized combustion design today for coal combustion [18]. In all Atmospheric Fluidized Bed Combustion (AFBC) designs, coal and limestone are continually fed into the furnace and spent bed material is withdrawn at the rate required to maintain the proper amount of bed material for fluidization. The amount of coal fed into the bed is approximately 2-3% of the total weight of the bed material. The fluidization of the bed and the relatively small amount of coal present in the bed at any one time cause good heat transfer throughout the bed material, and the resulting bed temperature is relatively low, about 800-900°C. This low bed temperature together with fluidization process enhance the capture of SO_2 emitted during combustion and retard the formation of NO_x via thermal path. The

features of in-bed capture of SO_2 and relatively low NO_x emissions, plus the fluid bed's capacity to combust the range of different fuels, are the main attractions of FBC as power generation technology. However, under some operating conditions, AFBC units also may produce higher levels of organic compounds, some of which may be potential air toxic. Current studies also indicate that AFBC units emit levels of N_2O (which is classified as a greenhouse gas), higher than other coal combustion systems [19]. AFBC technology has been in commercial use worldwide for well over 50 years. The next generation of FBC technology operates at pressure typically 10-15 times higher than the atmospheric pressure. Operation in this manner allows the pressurized gas stream from a pressurized fluidized bed combustion (PFBC) unit to be cleaned and fed to a gas turbine. The exhaust gas from the turbine is then passed through a heat recovery boiler to produce steam. The steam from the PFBC unit and that from the heat recovery boiler are then fed into a steam turbine. This combined cycle mode of operation significantly increases PFBC system efficiency over the AFBC systems. If the PFBC unit exhaust gas can be cleaned sufficiently without reducing its temperature and as a consequence efficiencies of the order 39-42% [1] can be achieved with PFBC designs, compared wit 34% efficiency of AFBC. To further enhance commercial applications of FBC technologies it is a need to achieve lower capital costs compared with modern pulverized coal (PC) boilers, to improve environmental performance and to increase operating efficiency. Summarizing, reduction of solids in the flue gas, high SO_2 removal efficiencies and low NO_x emissions are the biggest advantages of fluidized bed boilers. Detailed analysis of this technology applications has demonstrated that FBC power plants can be competitive to the PC power plants when FBC power plant is located near to the mine and can utilize low rank coals [20].

1.3.3 Combustion under O_2/CO_2 atmosphere

Combustion under O_2/CO_2 atmosphere is an advanced technology for controlling CO_2 emissions from coal-fired power plants. CO_2 is regarded as the principle component of the greenhouse gases. Therefore, controlling and decreasing CO_2 emissions is an important task for humans. Combustion under O_2/CO_2 atmosphere which replaces combustion under air atmosphere (O_2/N_2) is considered as an advanced technology with a good prospect of eliminating CO_2 emissions from coal-fired power plants. CO_2 concentrations in a flue gas from combustion process using atmospheric air as oxidant are very low and therefore it is difficult to separate CO_2 from such a flue gas. Conversely, it is easier to

---

[1]Throughout this thesis all thermal efficiencies are based on the Low Calorific Value (LCV) of the fuel

separate CO_2 from the flue gas if the CO_2 concentration is high (CO_2 capture). Therefore, the CO_2 concentration in the flue gas should be increased. This can be achieved in combustion under O_2/CO_2 atmosphere. This combustion mode has no formal name and it is often called as: air separate/flue gas recycle technology, oxygen/flue gas recycle combustion or oxyfuel combustion [21, 22]. The IFRF was perhaps the first institution which carried out trials on coal combustion with recirculated flue gas enriched with oxygen [23]. The principle of oxygen/ flue gas recycle combustion technology is shown in Fig. 1.3.
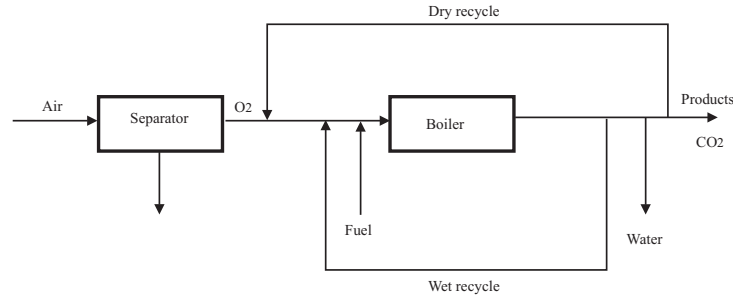
Figure 1.3: Conceptual schematic of the oxygen/flue gas recycle combustion technology

The mixture of O_2 which is separated from air and recycled into flue gas is used as oxidant in this technology. In this method, the concentration of CO_2 can reach above 70% with wet recycle, and up to 90% after dehydrator. Then, the gathering of CO_2 becomes simpler and economical [24, 25]. However, comparing both combustion under O_2/CO_2 and under air atmosphere, the combustion characteristics, particularly the char oxidation of pulverized coal under O_2/CO_2 atmosphere change significantly [23]. In addition, the Selective Catalytic Reduction (SCR) unit and the flue gas desulphurization unit might be omitted in this combustion technique which results in low NO_x emissions and the remaining NO_x and SO_2 present in the flue gas could in principal be left for co-storage with CO_2 or could be separated easily [22]. CO_2 capture reduces the net electricity efficiency by about 10% comparing to the conventional power plants [21].

1.3.4 Coal gasification (CG) technology

Coal gasification is a method of producing a combustible gaseous fuel from almost any type of coal. Conversion of coal to a gaseous fuel in homes and commercial installations has been practiced for over 200 years [26]. The unstable economic and political situation in the petroleum's countries and predictions of impending natural gas shortages resulted in major industry and government programs to develop gasification

systems for production of SNG (synthesis gas, syngas) from coal. The raw gaseous products of coal gasification include hydrogen (H_2), carbon monoxide (CO), carbon dioxide (CO_2), water (H_2O), ammonia (NH_3), hydrogen sulfide (H_2S), nitrogen (N_2), methane (CH_4), and, for the lower temperature processes, higher hydrocarbons and tar. For conversion to clean gas, suitable for combustion in simple equipment or for further processing to other clean fuels or chemicals, the mixture is scrubbed to consist primarily of H_2, CO, CH_4 and N_2.
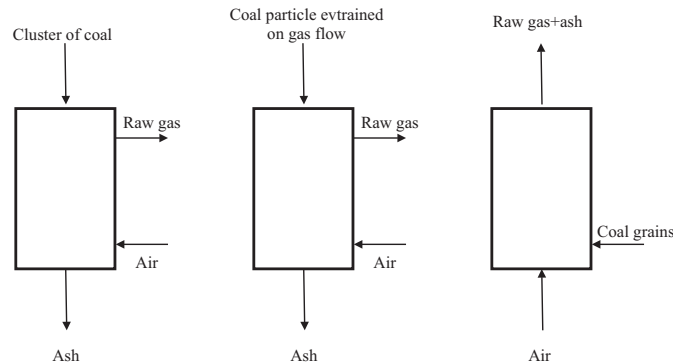
Figure 1.4: General schematic of coal gasifier types: fixed bed (left), entrained flow (center) and fluidized bed (right)

Gasification process can be divided into three major classes: moving fixed bed, entrained flow, and fluidized bed [27]. These three types of the coal gasifier are presented in Fig. 1.4. The fixed-bed and entrained-flow reactors can be designed as countercurrent or cocurrent. In Fig. 1.4 countercurrent type is shown; oxidant is fed from the bottom while coal is supplied from the top. Fluidized bed reactors can be applied with bubbling and with circulating beds. Air or oxygen can be used as an oxidizer. Produced syngas can be cleaned with the so called hot or cold methods. For obtaining a maximum efficiency, the following general guidelines are applicable: a minimum gasification temperature should be used to reduce heat losses and a minimum oxygen consumption to maximize methane production. The use of catalysts to allow lower temperature operations appears attractive to achieve significant improvements in efficiency and to minimize the production of tars. The cost of using catalysts would be a disadvantage. Energy losses in gasification and gas cleanup amount to about 15-20% of the total coal energy input, resulting in a loss of 5-10 percentage points in power generation efficiency. Thus, to improve a gasifier design in order to minimize energy losses is one of the key points of increasing the system efficiency. Development of an efficient gasification technology is thus essential for future high efficiency utilization of coal for both gas turbine (IGCC) and fuel cell (IGFC) systems.

1.3.5 Integrated Gasification Combined-Cycle (IGCC) systems

IGCC electric power systems include components such as advanced coal gasifier, high-temperature gas cleanup system and gas turbine. Schematic diagram of IGCC concept is shown in Fig .1.5.
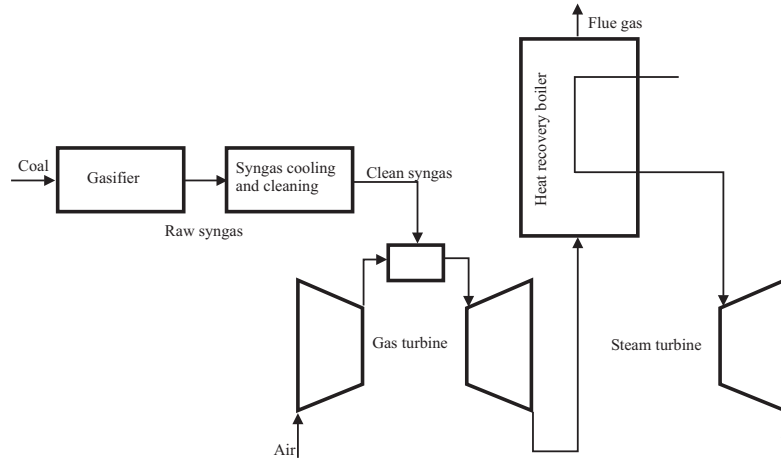
Figure 1.5: General schematic of IGCC concept

An improvement of gasifier design has a key importance for advanced conversion of coal to electricity using IGCC systems. Future advances in gasification based power production are linked to increases in a gas turbine firing temperature, hot gas cleanup of the fuel gas, co-production of both chemicals and electricity and integration of gasification with advanced cycles and fuel cells [28]. The first generation IGCC plants have already demonstrated outstanding operability and environmental performance at commercial scale. These systems can operate at around 45% efficiencies, while efficiencies approaching 60% are foreseen [29]. IGCC offers a coal based power technology with low emissions, the potential for higher thermal efficiency, and the capability for phased construction. However, the key issue for this technology is the high capital cost and its impact on economic competitiveness.

1.3.6 Integrated Gasification Fuel Cells (IGFC) systems

Fuel cells are electrochemical energy conversion devices that convert the chemical energy in a fuel and oxidant directly to electricity without standard combustion. They can be thought of a gas batteries where the electrochemically active materials are gases that can be supplied to the electrodes from outside the battery case. The reaction products are also gases and can be removed similarly. A fuel cell can be discharged continuously

11

to produce electricity as long as the reactants are supplied and the products removed. Environmentally, the electrochemical reactions do not involve direct combustion, so thermal NO_x production is negligible. Reactants are consumed exactly in proportion to the electric energy output, so the efficiency remains high even when the level of power production is reduced. In practice, fuel cell system efficiencies remain limited by energy losses and inefficiencies inherent in most engineered systems. An attractiveness of fuel cell systems is in that both natural gas or coal derived gas are suitable fuels for running a fuel cell system. Fuel cells first came to public attention in the $60s$ because of their importance in the manned space program. Today, commercially available fuel cell systems based on phosphoric acid fuel cell (PAFC) technology are configured for small scale commercial and residential cogeneration applications. These systems use natural gas or other light hydrocarbons as a fuel. They typically yield 36% net electrical efficiency and 70% total efficiency, if thermal energy is used [30]. Fuel cells can readily be integrated also with coal gasifiers and this application is called IGFC. General diagram of this technology is presented in Fig. 1.6.
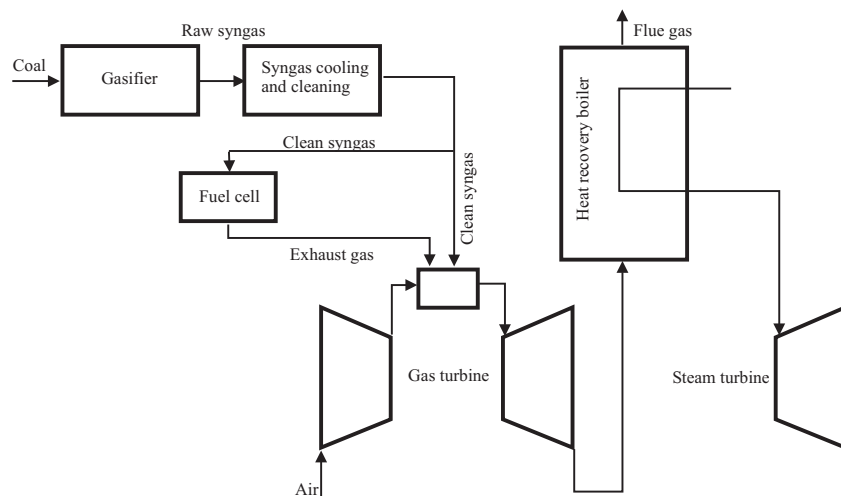
Figure 1.6: General schematic of IGFC concept

IGFC will not materialize for utility scale electricity generation until the fuel cells are fully developed commercially. Furthermore, the capital costs of the fuel cells are extremely high.

1.4 Pulverized coal fired power plants

In PC plants, pulverized coal is combusted with excess air in a boiler to produce high-pressure/high-temperature steam which is expanded in a steam turbine to generate

electricity [7]. The major challenge facing the power generation industry based on pulverized coal combustion over the coming decades will be to increase the efficiencies of the power plants while also meeting more stringent environmental goals. Especially, there is a need to reduce the emissions of NO_x, SO_x and CO_2. At the same time, plant reliability, availability, maintainability and operation costs, as well as the cost of electricity, must not be compromised.

Today the total world installed capacity of coal fired boilers is of the order of 1000 GW and they generate a large majority of the electricity produced from coal which itself is used for 38.7% of total global electricity generation [5]. In the EU old 15 countries at present, the market for new coal fired electricity generation plants is fairly restricted. This is mainly due to a deregulated energy market which provides utilization of natural gas on a large scale. However, the market situation in Europe is expected to change. Likewise, the recent enlargements of the EU with predominantly old installations will offer considerable market opportunities in order that their capacity can approach EU standards. Because several of the new partner states are coal producers, and so operate coal fired power stations, the latest technologies will need to be installed to replace the present low efficiency, environmentally unacceptable, and cost inefficient plants. The installed capacity in the USA is approximately 830 GW, of which 40% is coal fired. In the past Japan was strongly depended on fuel oil (together with hydro, gas and nuclear) for electricity generation. Since the oil crises (1973 and 79), the need for diversification of energy sources was recognized, and has given rise to increase of coal utilization and a fast development of new more efficient technologies. Nowadays, Japan has a total installed capacity for all energy sources of 230 GW with coal accounting for 13% [31]. Finally, the world market, in particular in coal rich regions such as China and India with low efficiency industrial plants, offers large additional opportunities for the modern European technologies. The need for technological advances in these regions is strongly supported by the increasing awareness of environment pollution and the legislative actions for emission control in line with their national policies.

The supply of heat and electricity at competitive cost is a decisive factor for the market penetration of new coal based conversion concepts in a liberalized energy market. For this reason, future efforts must concentrate on reducing investment expenditure and, in particular, operation costs. Modern coal fired power plants can achieve very low levels of pollutants, including particulate and metals emissions. At the same time, there is a need to continue the optimization of emissions control systems in order to minimize any operational and capital cost issues. Furthermore, it can be expected that future legislation for the control of emissions other than carbon dioxide will require

compliance with more stringent limitations than are applied today. Thus, there will be a need for environmentally more efficient and cost competitive techniques for both the fuel conversion process and for flue gas treatment.

From the point of view of steam parameters, pulverized coal fired power plants can be divided into [18]:

- subcritical (under critical point of water [2], usually 19 MPa and 535^oC)

- supercritical (over critical point of water, usually up to 24.1 MPa and 565^oC)

- ultra-supercritical (USC) (over supercritical conditions, usually 30 MPa and 600^oC)

1.4.1 Subcritical installations

Currently, the majority of coal-fired boilers are subcritical. Subcritical plants are well established and relatively easy to control, with overall energy conversion efficiencies in the range of around 30% to 40%. While the efficiencies of older power plants in developing countries like China and India are still around 30%, modern subcritical cycles have attained efficiencies close to 40% [18]. Further improvement in efficiency can be achieved by using supercritical and ultra-supercritical steam conditions. One percent increase in efficiency reduces by two percent specific emissions of CO_2, NO_x, SO_x and particulates [16].

In practice, up to an operating pressure of around 19 MPa in the evaporator part of the boiler, the cycle is subcritical. This means that there is a non-homogeneous mixture of water and steam in the evaporator part of the boiler. In this case mostly a drum-type boiler is used because the steam needs to be separated from water in the drum of the boiler before it is superheated and led into the turbine (for details see Section 1.8).

1.4.2 Supercritical installations

In order to improve coal-fired power plant efficiency leading to a proportional reduction in coal consumption and carbon dioxide emissions, it is widely accepted that the power industry must move from subcritical to supercritical steam cycles. The supercritical design not only improves efficiency by increasing the working fluid pressure but it allows superheating of the steam to higher temperatures which provides significant steam cycle efficiency improvement. Current supercritical coal fired power plants have efficiencies above 45%.

---

[2]The critical point of water is 22.06 MPa and t=375^oC, and above these parameters, there is no distinct water-steam phase transition [32]

The life cycle costs of supercritical coal fired power plants are lower than those of subcritical plants. Current designs of supercritical plants have installation costs that are only 2% higher than those of subcritical plants [13]. Fuel costs are considerably lower due to the increased efficiency and operating costs are at the same level as subcritical plants. The first supercritical power plants had a lot of mechanical and metallurgical problems. Most of these were due to high thermal stresses and fatigue cracking of the heavy section components. Today, the supercritical technology has overcome the earlier problems and offers a more favorable cost of electricity with higher efficiency and lower emissions. Some 400 supercritical coal fired power plants are currently operating around the world [4]. The supercritical technology plays dominant role for the newly built power plants, however the installed technology is dominated by subcritical steam cycles.

1.4.3 Ultra-supercritical installations

As mentioned above, today state of the art in supercritical coal fired power plants permits efficiencies that exceed 45%, depending on cooling conditions. Options to increase the efficiency above 50% in ultra-supercritical power plants rely on elevated steam conditions as well as on improved process and component quality. This increase of efficiency should result in 25% reduction in CO_2 and all other emissions [33]. Steam temperatures in initial USC units was about 600^oC and pressure 24.1 MPa with the goal for future designs being 760^oC and 34.5 MPa or higher [18]. USC steam plants in service or under construction are located in Europe and in Japan. Only 13 units are in operation [31].

1.5 High temperature materials for steam power plants

The fundamental problems in achieving ultra-supercritical conditions lie in the availability of suitable materials for construction. As shown in Fig. 1.7, there is an upper temperature limit of steels, above which much more expensive nickel alloys will be required for high temperature components: boiler membrane wall, superheater and reheater tubes, thick-walled headers and steam turbines. A sustained commitment to materials technology development is needed to produce these advanced alloys and several projects are ongoing all over the world.

In Europe, intense research has been carried out on the development of USC boiler technologies. The major development project, initiated in 1998, is the AD 700 project, which involved the participation of the most important industrial research centers and universities [34]. The goal of the AD 700 project is to demonstrate that it is possible to
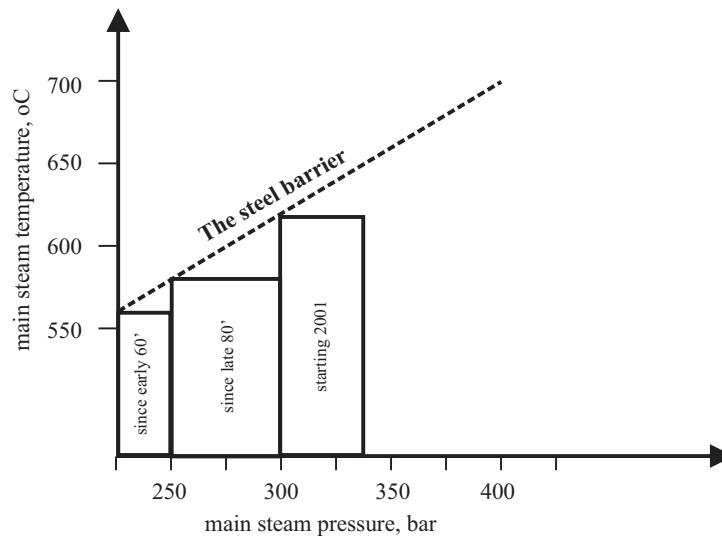
Figure 1.7: Steel barrier in recent years and prediction for future

operate USC steam plants with steam conditions of $700/720^oC$ [3] and 37.5 MPa. Two further major development programs in progress, the Thermie Project of the EC, and the Ultra-Supercritical Materials Consortium in the US by Palkes, aim at steam parameters of 37.5 $MPa/700^oC/720^oC$ and 37.9 $MPa/730^oC/760^oC$, respectively [35].

Currently, advanced steels for boilers operated at pressures up to 30 MPa represent the state of the art [36]. New martensitic high creep strength 9-12%Cr steels allow increased steam parameters in steam headers and steam lines. Similar martensitic steels are used for rotors, casings and valves of advanced steam turbines. Superheater steels must have high corrosion and oxidation resistance. Steam conditions up to 30 $MPa/600^oC/620^oC$ are achieved using steels with 12% chromium content. Up to 31.5 $MPa/620^oC/620^oC$ is achieved using austenite which is a proven but expensive material. Nickel based alloys would permit 35 $MPa/700^oC/720^oC$, yielding efficiencies up to 48%. Steels for furnace panels need to be welded without post weld heat treatment and also for this purpose new ferritic and martensitic steels are available. With the materials development described above it is nowadays possible to construct a USC plant with steam parameters 32.5 $MPa/610^oC/630^oC/630^oC$ and an efficiency approaching 50%. Future developments will address the use of nickel or cobalt based superalloys for boilers, steam lines and turbines. This may lead to efficiencies in the range 52-55% [37].

---

[3]Superheated steam temperature/Reheated steam temperature

1.6 Rankine cycle

Most of the power stations are operated according to the Rankine cycle. The working fluid in this cycle is water/steam and it undergoes various states along the cycle, as shown in Fig. 1.8. The simple Rankine cycle incudes four main processes: heat addition to the system, work done by the system, heat ejected from the system and work done on the system. They will be briefly explained in the following Paragraphs.
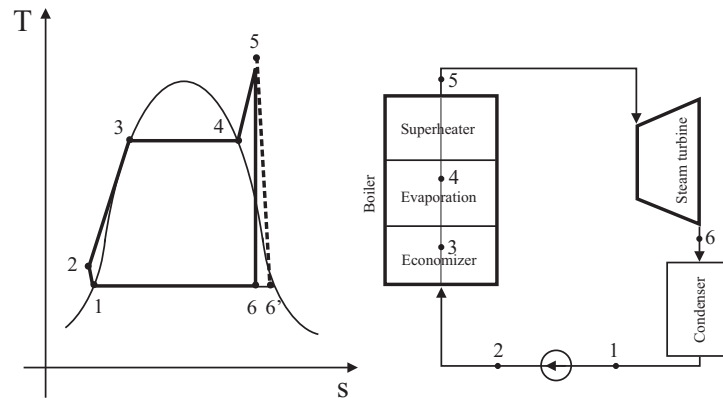
Figure 1.8: T-s diagram of the Rankine cycle (left) and components of the power plant utilizing the Rankine cycle (right)

Heat addition This process occurs in the boiler and can be divided generally into: heat addition to raise the pressurized subcooled water to its saturation temperature corresponding to the boiler pressure (between points 2-3, see Fig. 1.8), latent heat addition to vaporize the saturated water into steam (processes 3-4) and preheat of the steam above the saturation temperature (4-5).

Expansion in the turbine This process occurs in the various stages of the steam turbine and it is driven by the steam jets impinging on the blades mounted on discs. Due to this impingement, the discs rotate and hence the turbine output is transferred to an electric generator to produce electricity. In Fig. 1.8 this process is represented by the line 5-6 for ideal conditions where no friction is encountered. When friction is considered, an increase in the entropy results in a reduced output (5-6').

Heat rejection The heat rejection process returns the exhaust steam from the turbine to the saturated liquid state at low pressure. This process occurs in the condenser (between 6-1) which is a heat exchanger where the cooling water absorbs the heat from the condensing steam.

Pumping water In order to complete the thermodynamic cycle, the water must return to state 2. A pump is needed to raise the water temperature and pressure to state 2. In most practical power stations calculations, pumping work can be disregarded with respect to the turbine output [12].

Rankine cycle efficiency The Rankine cycle efficiency is proportional to the pressure and temperature of heat addition to the cycle, and is inversely proportional to the condenser pressure, and therefore to the temperature of the cooling medium. Based on the nomenclature presented in Fig. 1.8, Rankine cycle thermal efficiency η_R can be described as follows (disregarding pumping work $i_1 = i_2$):

$$\eta_R = \frac{i_5 - i_6}{i_5 - i_1} \tag{1.1}$$

The Rankine cycle presented in Fig. 1.8 and described above is called as simple Rankine cycle. Practically, in industrial steam power stations Rankine cycle is used with reheating and heat regeneration in order to increase its efficiency [32] but these issues are not crucial for this work and therefore they are not discussed here. Reheating and regeneration are also not taken into consideration during the calculations of the steam cycle with the HTAC boiler (see Chapter 10).

1.7 Issues for higher efficiency

The overall efficiency of a pulverized coal power generation cycle is affected by many factors, including the thermodynamic cycle design, steam conditions (temperature and pressure), coal grind, combustion air/fuel ratio, fuel mixing, air leakage into the system, cooling (condenser) water temperature and parasitic energy loads for auxiliary equipment such as grinding mills, pumps, fans, and environmental control systems [12, 17].

The most important factors for improving the pulverized coal fired power plants efficiency are:

- increase of the steam parameters (pressure and temperature)

- increase of the boiler efficiency due to reduction of the physical and chemical losses

and they will be taken into consideration in this work.

1.7.1 Steam pressure

By increasing the final steam conditions above those developed in the condenser, the cycle efficiency is driven higher. The obvious limit is the practical containment of

such high pressures, with regard to both the cost of material and the wall thickness of components. The thickness of pressure vessels is of concern in this part of the boiler which is subjected to the temperature cycles of the ramps, since the resulting stresses must be properly managed. The increased costs due to an increased greater wall thicknesses of the pressure section are largely compensated by the lower costs of the smaller fuel/air/flue-gas path. An increase of the designed steam pressure from 16.5 to 29 MPa increases the net plant efficiency by approximately 2.7% points [18].

1.7.2   Steam temperature

Increasing the steam temperature differential in the power cycle will yield higher efficiency. Current units drive the superheat and reheat temperatures to 620^oC. Metal component strength, stress, and distortion are of concern at elevated temperatures in both the boiler and the steam turbine. The tube metal temperature is higher than that of the steam and concern for accelerated corrosion and oxidation will also influence materials selection. By increasing the steam temperatures from $538/538^oC$ to $593/621^oC$, the net plant efficiency increases by another 2% points [18].

1.7.3   Exit gas temperature

The major physical loss from the boiler is the enthalpy of the exit flue gas. Reduction of the exit gas temperature is typically limited by material selection and concern for dew point and corrosion. Sulfuric acid vapor increases the dew point of the flue gas and hence raises the permissible minimum exit gas temperature. The operating temperature requirements of emissions control equipment such as SCR and flue gas desulfurization systems place additional constraints on the whole system. Specifically, for regenerative air heaters, used very commonly on fossil fuels fired boilers, corrosion-resistant and enameled heating surfaces may be installed to allow a lower design exit gas temperature. Around 10^oC reduction in exit gas temperature would improve the net plant efficiency by approximately 0.3% points [18].

1.7.4   Excess air ratio

Besides the exit gas temperature, another operating parameter with direct effect on the stack heat loss is the level of excess air used. The excess air increases the boiler exit gas mass flow and, hence, the waste gas heat loss. At a given stack temperature, a reduction in air flow rate will reduce the heat carried out through the stack. Ideally, to release the full heating value of the fuel, one would like to supply only that air

which is required for complete combustion of the fuel: that is, zero percent excess air or an air ratio of 1.0. Because of heterogeneous mixing of the combustible and oxygen molecules and other fuel and combustion-related conditions, an excess supply of air is provided to promote complete combustion of the fuel. Therefore, the optimal excess air level is a compromise between stack heat losses and combustion inefficiency losses as measured by unburned carbon in the ash and further indicated by CO emissions. Improved combustion technologies permit lowering the excess air ratio without sacrifing completeness of combustion. An optimal excess air for the efficiency loss balance described above will typically fall in the 15% (1.15 air excess ratio) range. Compared to the conventional 20% excess air level for bituminous coals (1.2 air excess ratio), this could result in a 0.05% point benefit in combustion efficiency, plus the incremental savings in air and gas fan power consumption [18].

1.7.5 Unburned carbon

The unburned carbon in the fly ash is the reason of the chemical enthalpy loss in the case of the coal combustion. In order to reduce the unburnt, the combustion should be effective and intensive and the residence time of the coal particle should be long enough to ensure completely burnout.

1.8 Pulverized coal (PC) boilers for power generation

Apart from the turbine-generator set, the boiler is a key component in modern, coal fired power plants. Its concept, design and integration into the overall plant considerably influence costs, operating behavior and performance of the power plant. In pulverized coal (PC) boilers, coal is milled into fine particles and then injected with air through a number of burners into the lower part of a combustion chamber. The fuel burns in suspension and release heat which is transferred to water tubes in the combustion chamber walls. The water absorbs heat and changes into the steam. The evaporation process takes place inside the tubes of combustion chamber walls. Then, steam is introduced into the superheater which is located in the region where the combustion gas has the higher temperature, at the exit of the combustion chamber. Further, steam is fed into the turbine-generator set to produce electricity. The steam cycle can be operated with single steam heating or with double steam heating. In the second case, after the High Pressure (HP) step of the turbine, steam is reversed to the reheater and heated up to the reheat temperature. Such a prepared steam is supplied into the Intermediate Pressure (IP) step of the turbine. The flue gas enthalpy is utilized for the water preheating in the economizer and for

the combustion air preheating in the air preheater. A typical configuration of the heat transfer surfaces in the standard PC boiler is presented in Fig. 1.9. This standard PC boiler consists of two passes: the first one, where superheater is located (the radiative part of the boiler) and the second one, where reheater, economizer and air preheater are located (the convective part of the boiler).
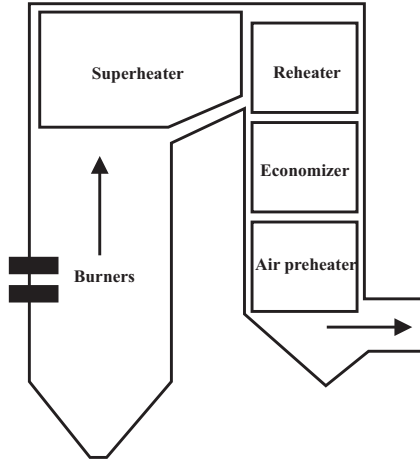
Figure 1.9: Configuration of the heat transfer surfaces in the standard PC boiler

The burner block can be located in different positions inside the PC boiler. The most common solutions are depicted in Fig. 1.10 [13]. In both the opposed (Fig. 1.10, left) and wall fired (Fig. 1.10, right) configurations burner blocks are located on the side walls of the boiler. It is not a good solution from the air-fuel mixing point of view. In order to improve mixing conditions, the tangential location of the burners was proposed (Fig. 1.10, center). The above boiler designs are called up-fired because the flame is fired from the bottom to the top of the boiler. Only very special boilers (for example, fired with anthracite) are built as down-fired type (the direction of the flame is from the top of the boiler to the bottom).

1.8.1 Drum type boilers

Drum boilers are restricted to subcritical pressures. In subcritical pressure units, the steam is generated in systems of natural or forced circulation depending on the level of the steam pressure. At lower pressures natural circulation can be used. As steam pressure approaches the critical point of water, the density difference between liquid and vapor phases which is the driving force for natural boiler circulation, diminishes. Therefore, a forced circulation or a once-through steam generator circuitry system must be utilized [14, 15].
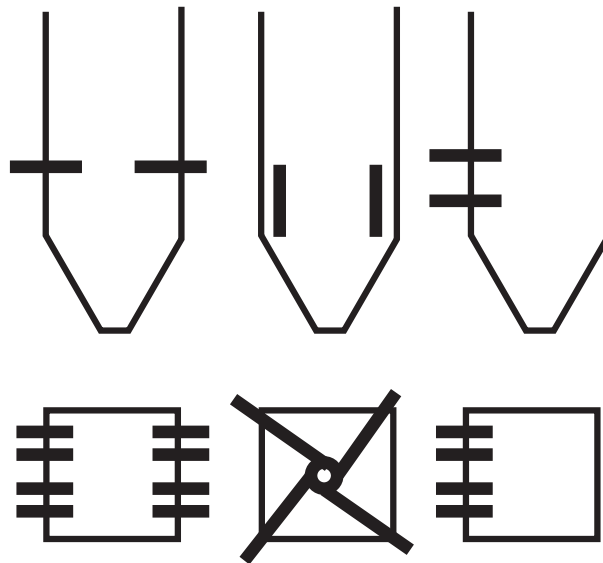
Figure 1.10: Typical burner location in the standard PC boiler: opposed walls (left), tangential (center) and single wall (right) firing

Steam is separated from the water inside a drum. Water at saturation temperature flows from the boiler-drum through unheated downcomer tubes, outside the boiler, and steam water mixture rises to the boiler drum through steam generating tubes that cover the fire side of furnace walls. In the drum type boilers water circulate continually inside the installation. The drum type boiler installation is shown in Fig. 1.11, left. For many years, the subcritical drum boiler has been the most popular boiler design worldwide. This well proven technology is a low cost one but does not have the potential for efficiency improvement inherent in supercritical cycles. Additionally, the drum type boilers have long start-up time and are very responsive to the load changes [38].

1.8.2   Once-through type boilers

In high-pressure subcritical boilers and in supercritical once-through boilers there is no boiler drum and therefore there is no water circulation. Instead the boiler consists of a bundle of parallel tubing through which water is pumped. Along the length of the tubes the water gradually forms steam and is getting superheated at the outlet of the tubes. Because of the lack of circulation, the tube length participating in the heat transfer has to be increased. The transition from evaporation to superheating is not fixed in location and can take place at any point in the upper section of the furnace. This enables dimensioning of the furnace without restrictions on the water/steam side [12]. The once-through type boiler installation is shown in Fig. 1.11, right.
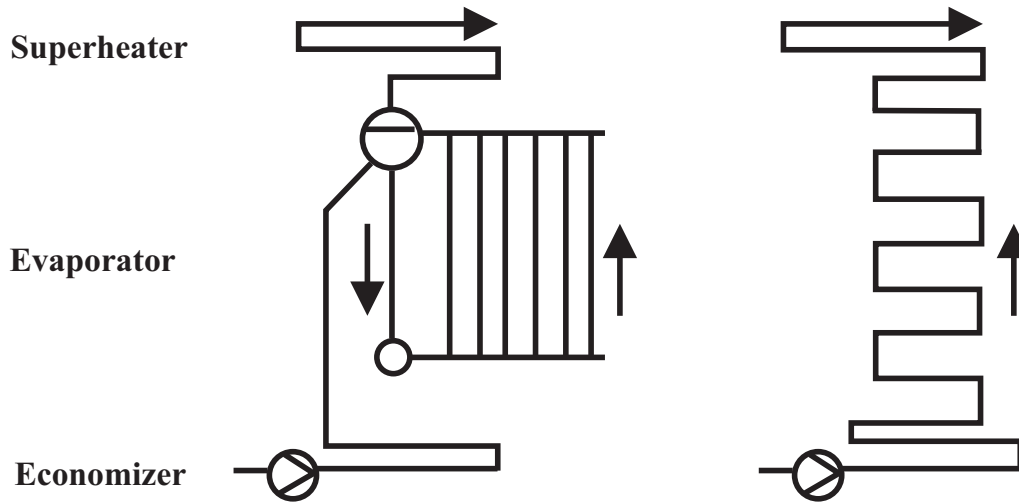
Figure 1.11: Types of the water circulation installation in the boiler: drum type boiler installation (left) and once-through boiler installation (right)

Once-through units require high water purity because of the lack of a boiler drum with blow down capability of the accumulated impurities. They also demand very well controlled and uniform volumetric heat release in the combustion chamber because the cooling of boiler tubes occurs at lower heat transfer rates than that by nucleate boiling in subcritical steam [18, 17].

Once-through boilers have been favored in many countries for more than 30 years. A once-through boilers could be operated at both subcritical and supercritical pressures. They can be operated with a pressure of 30 MPa or more without significant constructional changes. However, wall thicknesses of the tubes and headers however need to be designed to match the planned pressure level. At the same time, the heavy drum of the drum type boiler can be eliminated. Since once-through boilers can be operated at any steam pressure, variable pressure operation was introduced into power plants to make the operation of plants easier [39]. In fact once-through boilers are better suited to frequent load variations than drum type boilers since the drum is a component with a high wall thickness, requiring controlled heating. This limits the load change rate to 3% per minute while once-through boilers can step-up the load by 5% per minute. This makes once-through boilers more suitable for fast start-up as well as for transient conditions. A general problem for the once-through boiler is to ensure an effective cooling of the membrane walls in the burner zone where the radiation heat flux is high. Several solutions for this have been seen over time. Currently, two types of supercritical tube boiler furnace designs are in use and both requiring high mass flow per tube for cooling. One operates either at a constant fluid pressure in the furnace and utilizes vertical tubes or allows

the fluid pressure to vary with changing loads and utilizes a spiral tube design of the boiler walls. The vertical tube design have additional benefits over the spiral design that include a lower fabrication cost, 45% lower furnace pressure drop because of less feed pump power needed [40]. The spiral membrane wall feature very uniformly distributed heat fluxes. However, the spiral tube design is more complicated to manufacture than the vertical one. Both tube configurations are shown in Fig. 1.12.
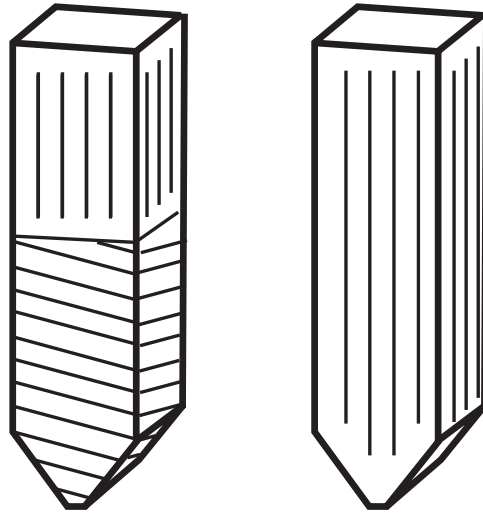
Figure 1.12: Types of tube designs in the boiler combustion chamber: spiral (left) and vertical (right)

The ideal furnace design for once-through boilers would allow the operating flexibility of the variable pressure furnace including on/off cycling and minimal low load pressure drop while using a conventional vertical tube arrangement to minimize cost. To accomplish this a tube with optimized characteristics that allows a low mass flow per tube and promotes natural circulation characteristics to enhance tube protection in areas of high heat flux is needed.

Once-through boilers are designed and constructed in two basic arrangements as the two-pass or is the single-pass (tower) type. Both perform equally well [12]. Typical boiler arrangements of these two main styles are shown in Fig. 1.13. Some particular advantages of the two-pass design are: lower cost construction, more optimized heating surface size because of decoupling back-pass from furnace section, smaller stack height requirement, dimensioning of convection section independent of furnace and low building height. The single-pass arrangement also has certain advantages. They are: small plant footprint, especially if fitted with SCR, lower flue gas velocity and erosion potential, no temperature differences between adjacent wall systems, simple construction of membrane walls and small building area. Single-pass design compared to two-pass boilers has 15-20% additional height. Approximately 10% of material consumption is reduced and penthouse

is not necessary. All together, the tower boiler design was found to be economical and technical feasible and the design has been improved over the years [41].
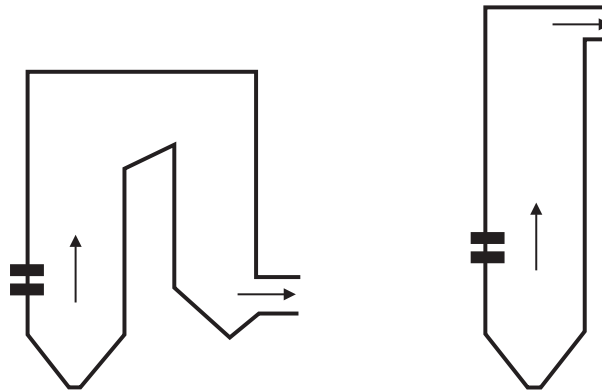
Figure 1.13: Configurations of the once-through boiler: the two-pass (left) and single-pass (right) design

Summarizing, the ability to realize supercritical steam conditions and the associated high plant efficiencies is a main advantage of the once-trough boiler technology. Further important advantages are as follow: a high plant efficiency even at part load, an enhanced fuel flexibility, short start-up times, a sliding-pressure operation with high load transients. These features of once-trough boiler technology cause that today thousands of these units are operated worldwide and continuous further development of this technology takes place. The boiler proposed in this work is dedicated as an once-trough boiler operated at ultra-supercritical parameters.

Chapter 2

Overview of HTAC technology

HTAC is a promising technology to decrease pollutants emissions and to improve the combustion efficiency. The main feature of this technique is a combination of air preheating and fuel dilution with combustion products to keep the oxygen concentrations low. To achieve this goal, preheated air and fuel are gradually mixed with large amounts of recirculated combustion products. High Temperature Air Combustion (HTAC or HiTAC) [42] is named also as: Excess Enthalpy Combustion (EEC) [43], FLameless OXidation (acronym FLOX)[1] [44], MILD (Moderate and Intensive Low-oxygen Dilution) combustion [45]. For the author all these names are synonym.

In this Chapter development, state of the art and challenges of HTAC technology are reviewed. Then, progress in modeling of HTAC technology is briefly described. Furthermore, fundamentals of this technology are explained. Additionally, there seem to exist only two publications attempting to develop a concept for HTAC application to boilers. These two are reviewed at the end of this Chapter.

2.1   Development of HTAC technology

Oil crisis in the $70s$ focused research in combustion science and technology on the fossil fuel saving. Preheating the combustion air was found as one of the most effective methods of achieving this goal. This principle of the technology, which later on was named HTAC, was presented as Excess Enthalpy Combustion by Weinberg [43] in conjunction with combustion of low calorific fuels. In EEC part of the thermal energy released during the combustion process is fed back to the fresh reactants.

---

[1]The name FLOX is registered name by WS Wärmeprozesstechnik GmbH referring to a particular type of burner

In the United Kingdom at British Gas and later at Hotwork International [46, 47] both regenerative and recuperative systems were intensively researched as pioneering methods of heat recovery at the burner. The recuperators were able to achieve relatively low preheat level (the air was preheated to a temperature of about 600^oC typically). The regenerative systems were able to reach about 1200^oC air preheat with an exit furnace temperature around 1400^oC. Ceramic balls were used in the regenerator to preheat the combustion air with the gases exiting from the furnace. With the increase of air preheat, the amount of nitric oxides emissions also increased and this tempered industrial applications of regenerative burners.

The work on fundamentals of EEC was initiated in Japan on the initiative of Mr. R. Tanaka at the early $90s$. Efforts made by Nippon Furnace Kyogo Kaisha Ltd. (NFK) focused on the process efficiency and minimization of pollutants emissions. The goal was to reduce pollutants emissions, save energy and increase furnace efficiency together with reducing the size of the equipment using Excess Enthalpy Combustion principles. This technology, named as HTAC [42, 48], used a honeycomb regenerator to maximize the air preheat. The honeycomb regenerator is much more compact than a bed packed with ceramic balls and features a low pressure drop [49, 50, 51]. In relation of ceramic honeycomb, a high cycle regenerative combustion system (HRS) burner was developed [52]. The thermal recirculation in HRS burner provides the stable combustion even at low oxygen concentrations, created by the exhaust gas recirculation. Furthermore, the flame temperature is decreased due to the lower oxygen concentration which results in low NO_x emissions. The largest available HRS burners are of 6-8 MW power [53].

In all the above described developments, NFK was assisted by the University of Maryland (USA). Gupta et al. [54, 55, 56] undertook research on the effect of combustion air temperature and oxygen concentration on flame color, visibility and thermal emission spectra. Gaseous fuels, such as methane, propane, LPG, carbon monoxide, hydrogen and acetylene were used in laboratory scale experiments. Formation of pollutants, including nitric oxide was taken into consideration.

NFK initiated also a cooperation with the Royal Institute of Technology (KTH) in Sweden. A semi industrial furnace equipped with regenerative burners were used to run several experiments, using liquefied propan gas (LPG). Single gas jet, as well as whole furnace domain were researched in details. Flame size, visibility, color, lift-off distance, flow structure were observed and measured by Lille et al. [57].

A very successful research and development program was undertaken at the International Flame Research Foundation (IFRF). In 1991, at IFRF in IJmuiden (Holland), a project called Scaling 400 was initiated [58, 59]. A family of burners spanning

the thermal input range from 30 kW to 12 MW was developed. The burners had a central air injector and individual fuel injectors located on a circumference around the central injector. A reduction of NO_x emissions of about 80% was reported at 12 MW thermal input. Moreover the level of NO_x achieved at high fuel staging was independent of the preheat. It was observed that in the staged flames the radiative heat flux was about 20% higher than the heat flux of the un-staged (baseline flame). Relying on the Scaling 400 project observations and based on the promising experiments in Japan, in 1997 the IFRF and NFK decided to test a NFK burner that used two natural gas injectors separated from the combustion air stream. A series of experiments were performed at IFRF using natural gas as fuel [60, 61, 62]. These trials were called HTAC 97. The success of these experiments prompted similar experiments using light and heavy oils (HTAC 98) [63, 53] and coal (HTAC 99) [64, 65]. Details of HTAC 99 trial are given in Chapter 4.

Independently of the Japanese investigations, Wünning [66] started investigating possibilities of NO_x reduction in natural gas firing utilizing high air preheat. In 1989, a surprising phenomenon was observed during experiments with a self recuperative burner. At 1000^oC furnace temperatures and 650^oC air preheat temperature, no flame could be seen and no UV-signal could be detected. Despite that, the fuel was completely burnt and the carbon-monoxide content in the exhaust was below 1 ppm. The NO_x emissions were in the single digits range what was first thought to be a malfunction of the NO-analyzer. The combustion was stable and smooth and this condition was called flameless oxidation, in short FLOX, and later on registered as a trade mark name [44]. Further experiments and numerical simulations were carried out to determine the essential conditions for FLOX [67, 68]. There are several versions of the FLOX burners commercially available and their thermal input is typically not larger than 200-300 kW [53].

An important development, based on the Scaling 400 technology, took place in Canada where the Canadian Gas Research Institute Burner (CGRI) was designed [69]. The idea was similar: the gas and air were injected separately so as to increase the entrainment of inert gas.

Recently, Cavaliere et al. [45] have examined the applicability of the existing chemical reaction schemes to combustion of hydrocarbons in high temperature air. The authors tried to develop a definition for this new combustion mode and proposed to call it MILD combustion.

2.2 Current investigations and challenges of HTAC technology

Although HTAC is already applied commercially, research on fundamental of this combustion method is still needed. Several companies, universities and research institutes are continually developing HTAC technology. Most of the previous research activities have been focused on gaseous fuels such as methane and propane. HTAC technology has significant potential for utilizing of various kinds of gaseous fuels (biogas, syngas, low BTU gas) as well as liquid, solid and waste fuels for applications to many technical processes.

In 2001, a research consortium comprising the IFRF Research Station, Corus Research Development & Technology and Gasunie Research commenced testing of HTAC technology, internally known as High Efficiency Combustion (HEC) [70]. The objective of this test was to enhance knowledge, gain experience and verify the potential benefits of HEC technology for industrial application in general and steel slab reheating furnaces in particular. The semi industrial tests with HEC technology have confirmed the high thermal efficiency, relatively low NO_x emission and high uniformity of the heat transfer. It was decided to do the next step in this research, namely full scale industrial test.

Masson et al. [71] have carried out an experiment at a laboratory scale. The gas burner consisted of two methane injectors and of the central air injector. Combustion air was preheated up to 873 K using an electric heater. In a first step, the parametric study of the air preheating temperature, the excess air ratio and combustion chamber dimensions were performed. The input/output measurements were carried out only. In the second step of these investigations, several in-flame measurements techniques were applied [72]. Reaction zone structures were revealed by OH^* chemiluminescence imaging. Fine wire thermocouples were used to determine local temperature in the furnace, and velocity fields were obtained by Particle Image Velocimetry (PIV). The obtained results were similar to the previous observations [60, 61, 62].

Experimental study on HTAC combustion of natural gas was performed also by Lupant et al. [73] and Murer et al. [74] in order to obtain more detailed information on this combustion process. In-flame temperature and species concentration measurements and UV-imaging were performed on a 200 kW natural gas furnace equipped with a self regenerative burner FLOX-REGEMAT.

In parallel to the IFRF experiments on combustion of light and high oils under HTAC conditions [63, 53], Shimo [75] and Chang et al. [76] also investigated oil combustion. It was found that HTAC technology with oil was able to work correctly.

Low emission of NO_x was obtained but very high emission of soot was observed. Further investigations on HTAC application for oil combustion shown that in order to decrease soot formation oil atomization should be improved [77]. Recently Wilk et al. [78, 79] performed experiments on oil combustion in HTAC technology. The combustion chamber of 100 kW was built at Silesian University of Technology. The research focused on the oil burner construction. Measurements of the radiative heat fluxes, temperature, soot, PAH, CO as well as NO_x were conducted. It was concluded that it was possible to operate furnaces in HTAC mode with similar effect as for the gaseous fuels.

The use of high temperature, low oxygen content air for pulverized coal combustion was examined by Kiga et al. [80]. Laboratory scale tests were conducted in a drop tube furnace to investigate the performance of such a combustion system. NO_x formation and combustion efficiency of the furnace were measured for various air preheat temperature, excess air ratio and oxygen concentration. The measurements indicated that increasing air preheat resulted in an increased combustion efficiency and reduced NO_x emission whereas decreasing the oxygen content led to a substantial reduction in combustion efficiency, accompanied with a slight increase in NO_x. It was concluded that high temperature diluted air was not suited for pulverized coal combustion.

The International Flame Research Foundation (IFRF) carried out perhaps the first experiment on applicability of the MILD combustion concept to pulverized coal firing [64, 65, 53]. A high volatile coal (1.4% N) was combusted with high temperature air and the lowest NO_x emissions were in the range 160-175 ppm (at 3% O_2) indicating high NO_x reduction potential of this technology also for nitrogen containing fuels (for details see Paragraph 4).

A pulverized coal FLOX burner is currently under development in the frame of an EU project [81]. The tests have been carried out in a drop tube furnace, in a bench-scale reactor (5-8 kW) at the University of Stuttgart and in a pilot-scale rig (40-60 kW) at RWTH Aachen [82, 83]. The burner combines the FLOX technique together with air staging. The primary air and pulverized coal are injected into the furnace via a central pipe. The secondary air is provided through nozzles located on the circumference of the primary jet while the tertiary (burnout) air is injected downstream. Under optimized firing conditions, the NO_x concentrations were below 200 $\frac{mg}{m^3}$ (at 6% O_2) and the carbon monoxide concentrations were around 30 $\frac{mg}{m^3}$ (at 6% O_2). While firing Lausitz lignite a high degree of burnout (carbon in ash < 0.3%) has been measured; burnout problems have occurred for hard Budryk and Kleinkopje coals (carbon in ash < 18.9%) [82, 83].

Coal behavior under MILD combustion conditions has also being researched at the Ruhr-University Bochum [84, 85] to gain a better understanding of NO_x formation and

reduction mechanisms. The data on volatile matter release, volatiles composition, and char were determined by flash pyrolysis investigations.

MILD combustion of pulverized coal was experimentally investigated by Suda et al. [86]. Flame stability, ignition delay, char burnout, and NO_x emission were examined using a 250 kW furnace. The combustion air was preheated to a temperature of either 623 K or 1073 K. The authors concluded that the ignition delay decreased dramatically with increasing air temperature. Stable combustion was obtained even for an anthracite. The peak temperature of the flames remained unaltered when the air preheat was increased from 623 K to 1073 K. NO_x emissions of 1000 ppm and 400 ppm were measured for the 623 K and 1073 K air temperature, respectively. Thus, a 40% NO_x emissions reduction was observed when the combustion air temperature increased. However, the absolute NO_x emissions were substantially larger than these obtained in the IFRF experiment [64].

Gases from landfills as well as exhausts from gas purification systems often have low calorific values (LCV) and are not anymore burnable in conventional systems. Schmid et al. [87] tested combustion of gases with LCV below 2.5 $\frac{MJ}{m^3}$. It was concluded that these gases can be burned safety even at moderate or low preheat temperatures applying flameless oxidation (FLOX) technology. In experiment of Suphansomboon et al. [88] low calorific value gases were burned with combustion air preheated up to 900^oC. The temperature profile and gaseous emissions were measured. The results showed that the higher the preheated combustion air temperatures the higher average flame temperatures and peak flame temperatures. Fuel savings were observed together with decreasing of NO_x emission.

Combustion of solid fuels like biomass and wastes in HTAC conditions has not been investigated as comprehensively as combustion of gaseous fuels. Ponzio et al. [89] performed experiments with wood pellets in a small scale batch reactor. Mass loss (as function of time), ignition time and the appearance of the flame were investigated as a function of oxidizer temperatures (600-1000^oC) and oxygen concentrations (5-21%). It was concluded that high oxidizer temperatures promoted fast mass loss. Oxygen concentrations have limited influence on the mass loss rate. Ignition time was strongly dependent on the oxygen concentration only at 600^oC. At 800 and 1000^oC, a very fast ignition occurred at all considered oxygen concentrations.

Derudi et al. [90] concluded that HTAC combustion can be effectively used for a wide range of low-BTU fuels with an inert gas content higher than 90%. Possibility of using both natural gas and biogas in HTAC combustion was assessed and operative parameter maps (in terms of average furnace temperature versus recycle ratio) were provided. It

was found that HTAC combustion is effective not only in reducing NO_x emissions (values larger than 15 *ppm* at 3% O_2 have never been observed) but also in preventing soot and PAH formation in fuel rich conditions.

Recent efforts of Gupta et al. [91, 92] have concentrated on high temperature gasification of wastes, biomass and low grade fuels to convert them to clean fuel medium heating value gas with high hydrogen content. High preheated air or steam were used as an oxidizer in the gasification process. It was found that high temperature gas generator works well for gasification of biomass or solid waste. The optimum thermal and gas recirculation conditions were obtained together with homogenized temperature distribution and low NO_x emissions. The applications of high temperature air/steam gasification in the various processes were studied.

The development in the conventional oxyfuel combustion led to the advent of the new generation burners that use internal flue gas recirculation exhibit flameless combustion and can be called flameless oxyfuel combustion- REBOX-W (Linde AG) [93]. The burner design was based on the findings of the IFRF OXYFLAME project [23]. This burner uses oxygen as oxidizer and maintain HTAC combustion mode in the furnace. The high velocity of oxygen at the exit of the nozzles causes excellent internal mixing and accounting for the flameless combustion. The salient features of this burner are extremely simple construction, operation and very small size. The NO_x emissions were the lowest for High Temperature Air Combustion with oxygen enhancement, NO_x decreased with an oxygen concentration increase (for the range of oxygen enrichment between 0-8%).

Leicher et al. [94] studied the phenomenon of HTAC combustion in order to evaluate its applicability to gas turbine combustors. HTAC combustion process was simulated using a chemical progress variable in conjunction with tabulated chemistry data provided by CHEMKIN. It was investigated whether FLOX burners can be used under gas turbine conditions with regard to flame stability and pollutant formation. Flamme [95, 96] described the experimental project on HTAC combustion technology which was investigated under gas turbine conditions using FLOX burner. The main objective of the project was to show that with the new combustion systems based on HTAC concept the following improvements can be achieved: elimination of pulsation in gas turbine combustion chambers, increase of the stability of the combustion process in a wide range of excess air ratio, suppression of high pollutant emissions at part load, increase in the efficiency of gas turbines and possible use of different fuels (natural gas and fuel oil). FLOX burner technology was investigated under gas turbine conditions also by Wünning [96]. It was concluded that it is applicable to gas turbine conditions for example, high pressure and overall lean conditions in conjunction with improved operational

performance compared to lean premixed combustion burner. Szlęk et al. [97, 98, 99, 100] proposed completely different application of HTAC technology in gas turbines. A new method of the isothermal expansion in a gas turbine were numerically investigated. This isothermal expansion is achieved by continuous supply of the fuel to the expanding oxidizer having the temperature higher than the fuel self-ignition temperature. It was concluded that this new gas turbine cycle provides a substantial increase in turbine performance keeping also the other advantages of HTAC technology.

2.3 Modeling of HTAC technology

The first CFD modeling of HTAC technology effort originated from Japanese industry where Ishii et al. [101, 102, 103] carried out simulations of an experimental continuous slab reheating furnace with emphasis on NO_x formation. The authors showed that the numerical code was able to describe the main characteristics in terms of the flow and temperature fields and could be used to identify the best low-emissions furnace configuration. The predicted slab temperature distribution and energy flow rates in the experimental furnace agreed well with the experimental data. They showed that one of the key points for this kind of combustion was the momentum of the air jets: the higher the momentum, the lower the NO emissions. Moreover, at constant air velocity, the NO_x reduction increased with the increase of the fuel jet velocity. However, the results of their simulations showed that their NO_x models required improvements to describe properly the NO formation under low-temperature conditions: the calculated NO level was found to be an order of magnitude lower than the observed one during the experiments.

Also the simulations carried out by Guo et al. [104] highlighted that the combustion in preheated air and flue gas recirculation improved the combustion efficiency and decreased NO_x emissions. Unfortunately, the simulations did not evaluate correctly the temperature uniformity and the contributions of thermal NO and prompt NO emission were not predicted.

Wünning [67] concluded that with the exception of the region near the burner the temperature and the flow conditions in the combustion chamber were similar for experiment and measurements. FLOX-A test furnace was designed and built to study flameless oxidation and to provide data sets for comparison with result from computer simulations. The burner was operated in lifted flame and FLOX modes. It was observed that NO_x and noise are substantially higher in flame mode compared to the FLOX mode. CFD calculations were performed using simple sub-models: $k - \varepsilon$ for turbulence, one step Arrhenius approach for chemistry and a flux model for radiation.

In 1997 the IFRF [61, 60, 62] generated a comprehensive set of the measurement data: the velocity, temperature field as well as main species compositions, the heat flux and the pollutants emissions. The data were used by Orsino et al. [105] to develop and validate models for predicting the flow field (including jet entrainment), temperature field and chemistry field (O_2, CO_2, CO, H_2O, unburned hydrocarbons). The authors demonstrated that the radiative heat fluxes could be predicted with a good accuracy due to the uniformity of both the in-furnace temperatures and CO_2 and H_2O concentrations. In another publication Mancini and Weber [106] focused exclusively on predicting NO_x emissions and concluded that the NO_x post-processors predicted very well the complex dependence of NO_x emissions on the temperature. A good agreement was found despite the inability of predicting correctly the temperature and the species in the weak natural gas jet. In more recent work Mancini et al. [107] analyzed further the IFRF experiments. They compared several turbulence models and have shown, using also an approach based on a network of reactors, that the failure in predicting the entrainment in the weak fuel jet is not related to any chemistry model. Further analysis was performed by Mancini [108]. He concluded that the prompt mechanism was responsible for 60% of the NO formed and no specific NO mechanisms were observable in HTAC flame. He pointed out that for HTAC technology the available models for NO_x formations need improvements mainly in relation to the reburning path and to the calculation of radicals.

Coelho and Peters [109] carried out numerical simulations of FLOX burner that operated at a 10 kW thermal input with a relatively low level of air preheat (500^oC). The experimental furnace was operated at a rather low temperature of 1000^oC, resulting in NO_x emissions of around 10 ppm. Coelho and Peters argued that the steady flamelet library was unable to correctly describe the formation of NO which is a chemically slow process.

Laser-optical investigations of HTAC systems with strong exhaust gas recirculation performed by Plessing et al. [110] showed that numerical models were able to predict the flow field and the heat transfer in the furnace fired in FLOX mode. The authors found that in order to predict HTAC combustion in a furnace environment, extinction at the base of the flame by the shear motion of the high velocity inlet air must be modeled.

Weihong and Blasiak [111, 112, 113] studied numerically the combustion of a single propane gas jet in the HTAC furnace of KTH. Common sub-models were used in this work: the $k-\varepsilon$ model for turbulence, Discrete Ordinates (DO) for radiation and the EDC concept with multi step chemical reactions for combustion. It was found that the benefits of HTAC technology are quantitatively demonstrated by mathematical models. They are: a lower peak temperature, a large flame volume, uniform thermal field and higher heat

transfer. Mathematical modeling of NO formation was also performed. The results showed that NO formed by the N_2O-intermediate mechanism was of paramount importance under HTAC conditions. Finally, it was concluded that numerical simulation results were very encouraging and could be used as an analytical or a design tool of industrial furnaces. Dong and Blasiak [114] reported on the modeling of the IFRF experiments on natural gas combustion with preheated air. Their numerical simulation showed globally good results, but the need for further model improvements was highlighted. Moreover, Dong and Blasiak [115] carried out a simulation of a single fuel jet flow in high temperature diluted air combustion. It was found that advanced turbulent models, such as Large Eddy Simulation (LES) and Reynolds Stress Model (RSM) gave small differences in the near field when predicting the flow.

Pasenti et al. [116] undertook a task of simulating a 200 kW FLOX burner operated under cyclic (unsteady state) conditions. The furnace exit temperature was varied in the range 1090-1330^oC (using a heat sink of a variable surface area) resulting in NO_x emissions that increased with the furnace exit temperature from 4 to 40 ppm (at 3% O_2). The steady state numerical simulations resulted in good quality predictions of the total radiative heat flux. The NO_x emissions were substantially under-predicted although the dependence of the NO_x emissions on the furnace exit temperature was correctly represented in the predictions.

Tobacco et al. [117] simulated a combustion chamber equipped with a FLOX WS-Rekumat C-150 B burner. The validation of FLUENT code sub-models was carried out using the measurements performed at ENEA (Italian National Agency for New Technology Energy and Environment). In the experiments three values of the air temperature were considered: 950^oC, 1050^oC and 1150^oC. In the calculations the $k - \varepsilon$ RNG model was used as the turbulence model and the following two chemical schemes were tested: a PDF model with the chemical equilibrium assumption and an EBU model with the one-step methane combustion. They found that the PDF method was not able to predict correctly the ignition point for the two lower temperatures, showing a high temperature peak just downstream the burner. The EBU 1-step model was instead able to predict correctly the temperature in the near burner region but at the end of the furnace the temperature was over-predicted by about 100 K.

Cavaliere and de Joannon [118] studied MILD combustion from the chemistry point of view. They performed measurements in a well-stirred reactor at low oxygen concentrations. The results were also numerically analyzed solving the stiff chemical equations for complex mechanisms. The authors investigated the different paths of MILD combustion of methane. They found that for reactor temperatures between 1000 and

1500 K the gas temperature reached super-adiabatic values due to the presence of unreacted radicals. More recently [119, 120] the group analyzed the dynamic behavior of the same well-stirred reactor. The dynamics of the reactors were also studied using numerical methods. The authors used two reaction mechanisms and both were able to predict the region of the flame oscillations as well as their shape but both mechanisms failed to reproduce the amplitude and the frequency, mainly at high temperatures.

Also Porcheron et al. [121] simulated a test furnace fired using NFK burners. They used the EBU model together with several global combustion mechanisms. They compared this model with a model based on PDF equilibrium but they found the first one superior. The NO furnace emissions were strongly under predicted.

Semi industrial test conducted by Corus RD&T [70] was also supported by mathematical modeling [122, 123]. FLUENT standard sub-models were used for these calculations. Since the average velocities were well predicted by the standard k-ε turbulence model, and they govern the turbulent mixing, there was good confidence for the CFD modeling of the reacting flow. Three combustion models have been analyzed in these numerical simulations. These were the PDF (Probability Density Function)- equilibrium model, PDF-flamelet model and the Eddy Break Up model (two equations). The radiation has been modeled using the Discrete Ordinates radiation model. The conclusion was drawn that all analyzed models qualitatively predicted well the air and fuel jet behavior with the corresponding chemical reactions and diffusion processes, but quantitatively there was room for improvements.

The experiment carried out by Lupant et al. [73] was also modeled using sub-models available in the CFD FLUENT code. The turbulence was modeled using the standard $k - \varepsilon$ model, with standard wall functions. Radiative heat transfer was modeled using the Discrete Ordinates (DO) approach. Two different models were tested for turbulent combustion modeling: a PDF model and a Finite Rate/Eddy-Dissipation Model. NO formation was predicted as a post-processing computation, using the standard thermal and prompt NO models implemented in FLUENT. The models were validated by comparison of the following computed and measured data: heat fluxes, fields of temperature and species content and NO emission level. The numerical simulations provided quite similar results outside the mixing zone for all the combustion models tested. The overestimation of temperature in the near burner zone obtained with the standard PDF was reduced with the Finite Rate/Eddy-Dissipation model. The authors concluded that computed NO values reproduce well the measurements although temperature field used for NO computation was substantially different from the measured values.

All the papers previously reviewed were concerned with combustion of gaseous fuels. However, CFD modeling of HTAC technology has also been applied to oil and coal combustion. A combustion chamber fired with oil operated under HTAC conditions was simulated by Misztal [124] using the CFD FLUENT code. Two chemical schemes were tested by the author: a 4-steps algorithm and a 42-steps n-heptane algorithm [125] and these were implemented in the EDC model. The standard $k - \varepsilon$ model for turbulence and the Discrete Ordinates (DO) model for radiation were used. Special emphasis was given to NO_x formation. It was concluded that the used models describing correctly oil combustion under HTAC conditions. However, only the 42-steps n-heptane algorithm was able to predict well the NO_x formation.

Numerical studies of MILD coal combustion were performed by He et al. [126] who modeled Suda's experiments [86]. The goal was to study NO_x formation and destruction mechanisms. The free jet theory was used to describe the flow field. It was assumed that during pyrolysis the coal nitrogen was released to volatiles as HCN or remained in the char. The thermal mechanism of NO_x formation was also considered. The model incorporated three NO destruction paths: the reactions with HCN, char and soot. It was concluded that 90% of the NO_x emissions were formed through the fuel path and the remaining 10% through the thermal route.

The experiment on MILD coal combustion under high pressure (3 bar) conditions was carried out by Heil et al. [127] and modeled by Erfurth et al. [128] using the CFD FLUENT code. Three dimensional steady-state simulations of a 1/6-sector of the furnace were performed for lignites and bituminous coals. Standard sub-models implemented in the FLUENT code were used; the Eddy Dissipation Concept with two global reactions for turbulence- chemistry interaction modeling and P1 or Discrete Ordinates models for radiation. A Lagrangian description for the solid phase was used. Very simple empirical sub-models were used for devolatilization (constant rates) and char burnout (diffusion-kinetics limited). This simple mathematical model was able to predict well the flow field and the recirculation inside the combustion chamber. The temperatures were over-predicted in comparison with the experimental data while the species concentrations differed substantially from the measured values. Needs for detailed sub-models for devolatilization and char burnout became apparent.

The IFRF experiments on MILD coal combustion technology [64] were simulated by Kim et al. [129, 130]. The objective was to investigate the ability of the CFD AIOLOS code to predict the nitrogen oxide levels. Three dimensional simulations of a quarter of the furnace were performed under steady-state conditions. The coal combustion was modeled including primary and secondary pyrolysis, volatile combustion, and char burnout, using

sub-models described by Förtsch [131, 132]. All the gas phase reactions were calculated using global mechanisms. The pyrolysis gas was represented by CH_4 while the tar was approximated as $C_xH_yO_z$. The secondary reactions of tar were modeled by three competing reactions yielding soot, hydrogen, light hydrocarbons, and carbon monoxide. The pyrolysis products were predicted using the Functional Group-Depolymerization Vaporization Cross linking (FG-DVC) model [133] which allowed for predictions of both the yield and the composition of products of primary pyrolysis. The NO_x formation modeling included fuel and thermal mechanisms. The release of volatile nitrogen was assumed to follow the rate of primary pyrolysis and HCN and NH_i were the primary N-containing species of the pyrolysis gas. The release of char nitrogen was enhanced in the initial stages of char combustion and char nitrogen was released not only as intermediate NH_i but also directly as NO, depending on a mechanism factor defined by Förtsch [131]. The char-NO production was proportional to the rate of CO formation in char oxidation. The interaction between chemistry and turbulence was modeled using the Eddy Dissipation Concept. Turbulence was calculated using the standard $k-\varepsilon$ model while radiative heat transfer by a Discrete Ordinates method. An Eulerian description for the solid phase was used. Generally, good agreement between experimental data and simulation results was achieved. However, the carbon monoxide concentrations were strongly over-estimated inside the combustion chamber and at the furnace exit. Throughout the furnace and at the furnace exit too high oxygen concentrations were computed while the carbon dioxide concentrations were under-estimated. The numerical model slightly under-estimated the NO_x values within the combustion zone. The authors concluded that there was a need for the development of detailed coal combustion models.

2.4 Basic implementations of HTAC technology

High Temperature Air Combustion technique is probably the most important achievement of the combustion technology in recent years. Within a decade or two, it has been developed from laboratory tests to industrial applications which seems to be an extraordinary fast progress as for an energy technology. In HTAC chemical reactions take place in almost the entire volume of the combustion chamber. Consequently, very uniform both temperature and species concentrations fields are characteristics of this technology. Moreover, the technology features very low NO_x and CO emissions and high and uniform heat fluxes. HTAC combustion gives very high energy utilization efficiency, thus low CO_2 emissions per tones of product. This combustion regime is characterized often by the lack of a visible flame and very low emissions of flame generated noise.

There are different methods of realization of HTAC technology. However, two of them seem to be widely applied and they are presented in Fig. 2.1.
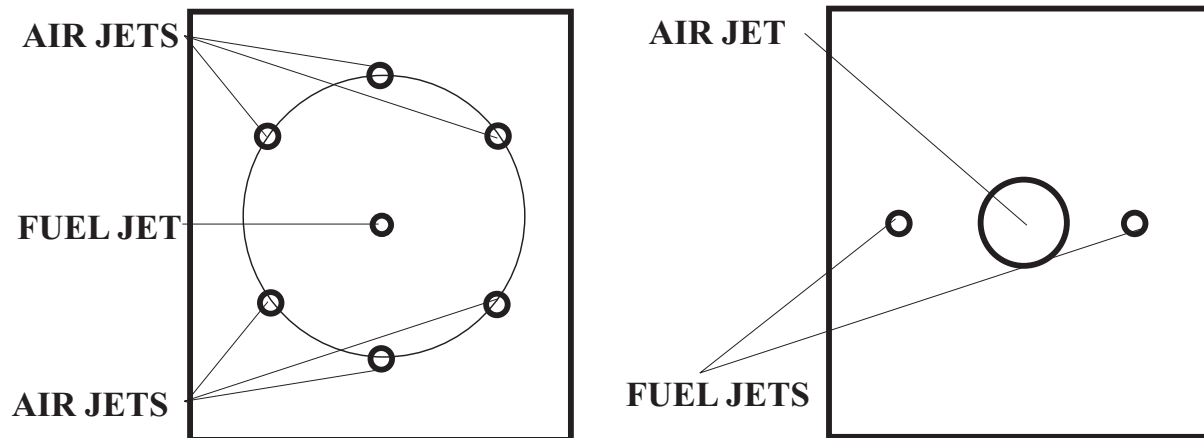
Figure 2.1: HTAC technology: FLOX burner (left) and NFK/IFRF burner (right)

Firstly, the FLameless OXidation (FLOX) [44] burner (Fig. 2.1, (left)) possesses a central jet of natural gas and a number (typically six or twelve) of air jets supplying preheated combustion air. The combustion air jets are spaced around the central jet of natural gas. In the NFK/IFRF design [42, 60, 63, 64], preheated air is supplied through a central jet, whereas natural gas is provided by several injectors located on the circumference of the burner (Fig. 2.1, (right)). The natural gas injectors are positioned away from the air jet so as to inject the fuel into hot combustion products that contain 1-2% of oxygen. The natural gas jets do not mix with the air stream until further downstream in the furnace and by that distance the fuel jets are substantially diluted with combustion products. In both flameless oxidation burners and in combustion systems with fuel injectors positioned away from the air jet, the fuel is oxidized in an environment that contains a substantial amount of inert gases (N_2, CO_2, H_2O) and some oxygen, typically not more than 5%. In this respect both modes of combustion are similar.

The specific kind of mixing pattern, shown in Fig. 2.2, is the key issue of HTAC technology. The internal recirculations of combustion products are generated by injecting preheated air jets into the combustion chamber with very high momentum. Both the air and fuel jets entrain combustion products and the oxygen concentrations in these jets decrease.
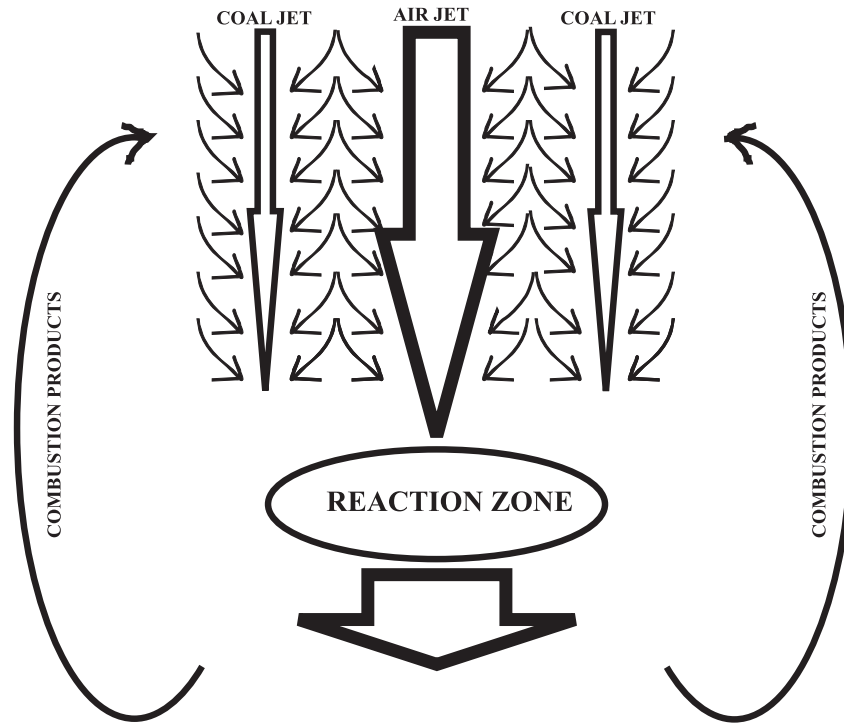
Figure 2.2: Mixing pattern in NFK/IFRF design

This specific recirculation of the combustion products inside the combustion chamber and the entrainment of the combustion products inside the jets bring several characteristics of HTAC technology. First of all, temperature and gas composition fields are uniform inside the whole volume of the combustion chamber. Secondly, ignition takes place in diluted oxygen environment which results in low peak of temperature. Low oxygen concentrations is obtained by recirculation of the combustion products into the incoming combustion air and fuel jets. Furthermore, due to this recirculation, combustion process is very stable over a wide range of fuel/air ratios and a large chemical reactions zone is obtained. Moreover, HTAC combustion offers high values of total heat fluxes and radiative heat fluxes along the combustion chamber with their uniform distribution compared to conventional combustion technologies.

2.5   Application of HTAC technology in furnaces

So far, HTAC technology was implemented mainly in industrial furnaces fired either with gaseous fuels or light oils. In most of industrial applications, the technology is combined with heat recovery systems and such a combination typically results in substantial fuel savings. Though the technology has been known for not a long time,

there are now over several hundreds of industrial furnaces all over the world which utilize the HTAC principle. In these furnaces, combustion air is highly preheated which leads to reduced specific fuel consumption. At the same time, high-efficiency heat recuperators or regenerators cause that outlet physical loss is lower. As an effect, the efficiency of HTAC furnaces is by circa 30% higher than that of conventional furnaces with moderate recuperation temperature. Additionally, there are very low emissions of harmful substances, including also NO_x [134] although a high air preheated is used. The conventional furnaces use either ambient temperature air or air preheated using recuperative heat exchangers. The maximum temperature of the air in the standard industrial furnaces is typically not higher than 500^oC. The concept of HTAC is based on a very efficient, high preheat of the combustion air to temperatures above the self-ignition point (greater than 850^oC for natural gas). The fuel consumption in industrial furnaces represents a major amount of the operational costs of the furnaces. Significant reductions in fuel consumption have been reported after installation of HTAC technology. These fuel energy savings directly relate to reduction of CO_2, NO_x and other pollutants emissions to the environment. Due to high heat fluxes in this combustion method the size of the furnace can be decreased up to about 20% [135]. Several burner designs to realize HTAC technology became a regular serial product for a variety of applications. Most of the burners were installed in heating and heat treating furnaces of the metal and steel industry, ceramic industry and chemical industry [136, 137, 138, 70].

2.6 Application of HTAC technology in boilers

Although most of current applications are limited to industrial furnaces, HTAC technology is expected to provide significant advantages when applied also to the power station boilers fired with pulverized coals. The foreseen advantages are as follows:

- An increase in radiative heat fluxes that may lead to a reduced size of the boiler

- More compact and smaller boilers can be built using a high quality steel so that the cycle thermal efficiency is improved due to increased (superheated) steam parameters

- A simple design of the burners and a very stable combustion process open up the possibility of using low rank coals

- Improved mixing of the fuel and oxidizer together with uniform temperature and oxygen concentration fields should minimize the coal burnout problems

- Increased particle residence time is likely to improve char burnout

- The technology can be operated with a relatively low excess air ratio

- The technology offers low NO_x emissions

In a coal or other fossil fuel fired boiler, it could be difficult to apply the conventional honeycomb type regenerator since the ash-containing flue gas at such a high temperature can cause plugging of the regenerator. Commercial boilers are usually of a large capacity and thus the flow rate of combustion air is significant. Heating up a big amount of combustion air to a high temperature in a short time period is technically not easy. Thus, it is a need to find in the future a way to utilize the enthalpy of the boiler exhaust gas to heat up the combustion air. A typical conventional boiler is composed of the radiative heat transfer section and the convective heat transfer section. An air preheater and an economizer are often used to recover the waste heat of flue gas. On the other hand, in the high temperature air combustion boiler, the adiabatic flame temperature is much higher than that of a conventional boiler and the heat transfer inside the boiler is dominated by radiative heat transfer. With this feature, it is possible to design a boiler without the convective heat transfer section and yet maintain the same thermal output. The removal of the convective heat transfer region will certainly lead to a significant reduction of boiler size and cost.

Several authors have postulated application of HTAC technology to power generation [99, 100, 139] but up to now there have been only two attempts to apply this technology to power boilers fired with pulverized coal. A new concept boiler where fuel could be efficiently combusted in high temperature preheated air was proposed by Kawai et al. [140]. It was perhaps the first attempt to develop a conceptual design of HTAC boiler. It was realized that a new construction of the entire boiler was needed. The proposed boiler was very similar to the industrial furnaces with regenerative burners. Low-BTU syngas was combusted with high temperature preheated air and the thermal energy contained in generated combustion gas was delivered to water/steam in boiler tubes mainly by radiative heat transfer. Then the combustion products of 1200^oC temperature passed through a honeycomb bed to be cooled down to about 150^oC and was exhausted to atmosphere. This boiler was equipped with two burners containing each a fuel injector and an air channel equipped with an regenerator. The first burner was located at the top wall of the boiler and the second one at the bottom wall of the boiler. The burners worked in a transient mode: when the first burner fired, the second worked as an outlet of the boiler and the regenerator recovered a substantial part of the exhaust gas energy. After the switching period (about 30 s) the role of two burners reversed. The

combustion air of 1000^oC temperature and the fuel of 25^oC were injected at a velocity of 30 and 11 $\frac{m}{s}$, respectively. The maximum thermal input examined during experiment was equal to 120 kW. Only output and input measurements were carried out without any detailed in-flame measurements. It was concluded that some design changes inside the combustion zone were needed in order to improve the mixing between the gas and the high temperature air. Finally, it was concluded that the proposed boiler was suitable for low BTU syngas derived from gasification process of coal and wastes with no dioxin emission and the boiler was characterized by the following features: uniform heat flux field, augmentation of heat transfer, reduction of combustion noise level, suppression of NO_x emission and compactness.

Zhang et al. [141] proposed a boiler equipped with PRP burner (PRP stands for primary air enrichment and preheating). The authors implemented the PRP burner as HTAC technology because both processes were similar in their application. The PRP burner was used to preheat the combustion air. It was equipped with a preheating chamber with one end connected with the ambient combustion air and the other end opened to the furnace. Inside the chamber, gas recirculation was effectively established. Low volatile petroleum coke and an anthracite coal were used as fuels in industrial scale (12 MW_{th}) test facility. In this approach PRP burner was installed at the side wall of the standard boiler. Beside the new burner construction no further modifications to the boiler were required. On the side wall of the furnace along the jet flow three rows of observation windows were arranged. Through these windows flame appearance was recorded with a video camera and flame brightness and temperature were measured by the color pyrometer. Flame temperature was also measured in the furnace nearly along the centerline of the chamber by using a S-type thermocouples with stainless steel sheath. The variations of the temperature inside and out of chamber were used to analyze the mechanisms of ignition, flame stabilization and NO_x formation. The flue gas properties including O_2, CO, NO_x, SO_2 and unburned carbon were measured at the exit of the furnace. It was concluded that the PRP burner was able to create a two-stage hot gas recirculation inside and outside of the preheating chamber. The rapid heating of the combustible mixture in the chamber facilitated pyrolysis, volatile matter release processes for the fuel particles, suppressing ignition delay and enhancing combustion stability. Moreover, compared with the results measured in the same facility but with a conventional low-NO_x burner, NO_x concentrations at the furnace exit were at the same level while petroleum coke was used as a fuel, and 50% lower while anthracite was used as a fuel.

Chapter 3

Mathematical model

Fluid dynamic is a field of engineering which studies the physical laws governing the flow of fluids under various conditions. Great effort has gone into understanding the governing laws and the nature of fluids themselves, resulting in a theoretically strong field of research. Computational Fluid Dynamics (CFD) involves the numerical solutions of fluid dynamic governing equations. The complex set of partial differential equations is solved in a geometrical domain divided into small volumes. CFD methodology consists of three main elements:

- A pre-processor which is used to create the geometry of the problem, to generate the grid, to define the flow parameters as well as the boundary conditions

- A solver which is used to compute the governing equations of the flow

- A post-processor which is used to analyze the data and to show the results in a graphical and easy to read format

All numerical simulations in this work were performed using GAMBIT (version 2.1) [142] as pre-processor and FLUENT (version 6.2.16 and 6.3) [143] as solver and post-processor. In this Chapter, both the governing differential equations for Computational Fluid Dynamic approach and their averaging method are given. Furthermore, the set of mathematical sub-models describing coal combustion process under HTAC conditions is specified and finally, all used sub-models are briefly described. A specially emphasis is given to devolatilization and char burnout models.

3.1   The governing partial differential equations

The mathematical modeling of the fluid flow is based on a set of coupled conservation equations of mass, momentum, energy, and chemical species [144, 145]. Properties of

fluid (the density, the viscosity, the specific heats, the molecular diffusivity, the thermal conductivity, the radiation properties etc.) have to be given as a function of the state variables.

3.1.1 The continuity equation

The continuity equation is a mass balance stating that the overall mass of the gaseous phase system is conserved. The gas phase conservation equation of mass can be written as [1]:

$$\frac{\partial \rho}{\partial t} + \frac{\partial}{\partial x_i}(\rho u_i) = S_m \tag{3.1}$$

where S_m is the mass source in the system. The source term S_m accounts for the mass transfer from solids (or liquid) phase to the gas phase.

3.1.2 The Navier-Stokes equation

The Navier-Stokes equation is the momentum conservation equation. The conservation equation of momentum can be written as:

$$\frac{\partial}{\partial t}(\rho u_i) + \frac{\partial}{\partial x_j}(\rho u_i u_j) = -\frac{\partial p}{\partial x_i} + \frac{\partial \tau_{ij}}{\partial x_j} + \rho f_i \tag{3.2}$$

where f_i is the sum of external forces (in our case it is only gravity) and τ_{ij} is the viscous stress tensor which is given by the Newton law:

$$\tau_{ij} = \mu(\frac{\partial u_i}{\partial x_j} + \frac{\partial u_j}{\partial x_i}) - \frac{2}{3}\mu\delta_{ij}\frac{\partial u_l}{\partial x_l} \tag{3.3}$$

where the molecular viscosity μ is introduced, depending on the fluid properties and δ_{ij} is the Kronecker symbol.

3.1.3 The conservation equation of chemical species

The conservation equation of chemical species can be written as follows:

$$\frac{\partial}{\partial t}(\rho Y_a) + \frac{\partial}{\partial x_i}(\rho u_i Y_a) + \frac{\partial J_{a,i}}{\partial x_i} = S_a \tag{3.4}$$

where n species have indicies $a = 1, ..., n$ and $J_{a,i}$ is the molecular diffusive flux of the species a. Species molecular diffusivities are generally described using the Fick law:

$$J_{a,i} = -\frac{\mu}{Sc_a}\frac{\partial Y_a}{\partial x_j} \tag{3.5}$$

---

[1]all equations are written using the Cartesian coordinate system and Einstein's notation is apllied

where Sc_a is the Schmidt number of the species a, defined as:

$$Sc_a = \frac{\mu}{\rho D_a} \tag{3.6}$$

and D_k is the molecular diffusivity of the species a relative to the major species.

3.1.4 The energy equation

The conservation equation of energy can be written as:

$$\frac{\partial}{\partial t}(\rho h) + \frac{\partial}{\partial x_i}(\rho u_i h) - \tau_{ij}\frac{\partial u_i}{\partial x_j} + \frac{\partial q_i}{\partial x_i} = \rho u_i f_i + S_h \tag{3.7}$$

where h is the total specific enthalpy and for a multicomponent medium it takes the following form:

$$h = \sum Y_i h_i \tag{3.8}$$

where Y_i is the mass fraction of species i in the mixture and h_i is the total enthalpy defined by:

$$h_i = h^0_{Tref,i} + \int_{T_{ref}}^{T} Cp_i(T)dT \tag{3.9}$$

where h^0 is the enthalpy of formation, T_{ref} is the reference temperature and $Cp_i(T)$ is the specific heat at a constant pressure.

3.1.5 The equation of state

The relationship between the pressure, the temperature and the fluid density is provided through the equation of state. The perfect gas Clapeyron equation is given as:

$$\rho = \frac{p}{R \cdot T \cdot \sum \frac{Y_a}{M_a}} \tag{3.10}$$

where $R = 8.314\frac{kJ}{kmol \cdot K}$ is the universal gas constant while M_a and Y_a stand for the molecular mass and the mass fraction of a-species, respectively.

3.1.6 The general governing differential equation

The conservation equations described in Sections 3.1.1-3.1.4 can be transformed into a general transport equation of dependent variable ϕ, written as follows:

$$\underbrace{\frac{\partial}{\partial t}(\rho\phi)}_{\text{unsteady term}} + \underbrace{\frac{\partial}{\partial x_j}(\rho\phi u_j)}_{\text{convective term}} = \underbrace{\frac{\partial}{\partial x_j}(\Gamma_\phi\frac{\partial\phi}{\partial x_i})}_{\text{diffusion term}} + \underbrace{S_\phi}_{\text{source term}} \tag{3.11}$$

where Γ_ϕ and S_ϕ are the diffusion coefficient and the source term, respectively and these are specific to a particular meaning of ϕ as shown in Tab. 3.1.

Equation	ϕ	Γ_ϕ	S_ϕ
Continuity	1	0	0
Momentum	u	μ	$\rho g_i + \frac{\partial p}{\partial x_i}$
Species	Y_a	$\frac{\mu}{Sc_a}$	Sc_a
Energy	h	$\frac{k}{c_p}$	S_h

Table 3.1: Comburent composition and properties

3.2 Averaging of the governing partial differential equations

Turbulent flow results when instabilities in a flow are not sufficiently damped by viscous action and the fluid velocity at each point in the flow exhibits random fluctuations [146]. The following is a list of the approaches that can be used in turbulence flow calculations:

DNS - Direct Numerical Simulation   In this approach the Navier-Stokes equation is solved without an approximation or closure modeling for the turbulence. All the scales in the eddy cascade are resolved from the macroscopic scale to the Kolmogorov scale. The simulations based on this model are extremely time consuming.

LES - Large Eddy Simulation   In this approach only the largest scales are spatially resolved and time dependent simulated. These scales are strongly affected by the macroscopic geometry and therefore it is difficult to create a model valid for all the physical situations and for all the geometries. The smallest scales are less dependent on a macroscopic geometry and are not resolved but modeled. Even this model is time consuming.

RAM - Reynolds Average Models   In this approach all the variables are split in two parts: the average value and its fluctuation. In Section 3.2.2 the equations for the average values are given.

PDF - Probability Density Function   In this approach, the variables are considered as stochastic fields and the methods of stochastic analysis are used. For each variable, its PDF function of time and space, can be derived from Navier-Stokes equations.

For most engineering applications, the time-averaged or spatial filtered properties of the flow are of interest, thus the time-averaged transport equations, such as the Reynolds averaged Navier-Stokes (RANS) equations, are established. However, time-averaged equations are unfortunately not closed and thus additional closure methods corresponding to different turbulence models have to be developed. As mentioned above, the full numerical solution of the instantaneous balance equations is possible only using DNS but it is too computational expensive. To overcome this difficulty, an additional term is introduced by averaging the conservation equations to describe only the mean flow field. Local fluctuations and turbulent structures are integrated in mean quantities and these structures have no longer to be described in the simulation.

3.2.1   Reynolds averaging

Reynolds averaging refers to the process of averaging a variable or an equation in time [147, 148]. By using Reynolds decomposition approach, an instantaneous flow variable ϕ can be decomposed into the mean value $\bar{\phi}$ and the fluctuation ϕ'.

$$\phi(t) = \bar{\phi}(t) + \phi'(t) \tag{3.12}$$

The mean quantity is defined as follow:

$$\bar{\phi}(t) = \langle \phi(t) \rangle \tag{3.13}$$

where $\langle \rangle$ stands for an averaging operator. If the modeled process is stationary, it makes sense to define the averaging operator in the following way:

$$\langle \phi(t) \rangle \equiv \bar{\phi}(t) = \frac{1}{\Delta t} \int_{t+\Delta t}^{t} \phi(t) d\tau \tag{3.14}$$

The averaged variable is not dependent on the time t but only on the fluctuating part $\phi'(t)$. This kind of averaging operators (called Reynolds averaging operators) are useful in the case of constant density only. Such an averaging procedure produce new terms in the Navier-Stokes equation. In order to achieve a closure, relations between these additional terms have to be constructed and this process increases the complexity of the problem.

3.2.2   Favre averaging

Time averaged equations can further be simplified for compressible flows by using Favre (density or mass) averaging procedure. In turbulent flames, fluctuations of density are observed because of the thermal heat release, and Reynolds averaging is therefore not

applicable. Instead, a Favre (density weighted) average is introduced. Each quantity is decomposed into:

$$\phi(t) = \bar{\phi}(t) + \phi'(t) \tag{3.15}$$

where the mean quantity is defined as follow:

$$\bar{\phi}(t) = \frac{\langle \rho\phi \rangle}{\bar{\rho}} \tag{3.16}$$

The Favre averaging operator has slightly different properties than the Reynolds operator. The most important one is that the Favre averaging allows for decoupling between the average of the density and the average of the other variables. This Favre operator is defined as below:

$$\langle \phi(t) \rangle \equiv \bar{\phi}(t) = \frac{1}{\bar{\rho}} \langle \frac{1}{\Delta t} \int_{t+\Delta t}^{t} \rho\phi'(t)d\tau \rangle \tag{3.17}$$

The Favre averaged fields have no physical meaning. The Favre averaging is a mathematical definition only that allows a more suitable formulation of the conservation equations. In other words, Favre averaging is only a mathematical simplification. It eliminates the density fluctuation from the time-averaged equations.

The Favre averaged conservation partial differential equations are as follow:

- The continuity equation

$$\frac{\partial \langle \rho \rangle}{\partial t} + \frac{\partial}{\partial x_i}(\langle \rho \rangle \langle U_i \rangle) = \langle S_m \rangle \tag{3.18}$$

- The Navier-Stokes equation

$$\frac{\partial}{\partial t}\langle \rho \rangle \langle U_i \rangle + \frac{\partial}{\partial x_j}\langle \rho \rangle \langle U_i \rangle \langle U_j \rangle + \frac{\partial}{\partial x_j}\langle \rho \rangle \langle U_i U_j \rangle = \frac{\partial}{\partial x_i}\langle \rho \rangle + \frac{\partial}{\partial x_j}\langle \tau_{ij} \rangle + \langle \rho \rangle \langle f_i \rangle \tag{3.19}$$

- The conservation equation of chemical species

$$\frac{\partial}{\partial t}\langle \rho \rangle \langle Y_a \rangle + \frac{\partial}{\partial x_j}\langle \rho \rangle \langle Y_a \rangle \langle U_j \rangle + \frac{\partial}{\partial x_j}\langle \rho \rangle \langle U_j Y_a \rangle = \frac{\partial}{\partial x_j}\langle J_{a,j} \rangle + \langle S_a \rangle \tag{3.20}$$

- The energy equation

$$\frac{\partial}{\partial t}\langle \rho \rangle \langle H \rangle + \frac{\partial}{\partial x_j}\langle \rho \rangle \langle H \rangle \langle U_j \rangle + \frac{\partial}{\partial x_j}\langle \rho \rangle \langle U_j H \rangle = \frac{\partial}{\partial x_j}\langle q_j \rangle + \rho\langle U_i \rangle \langle f_i \rangle + \langle \frac{\partial U_i}{\partial x_j}\tau_{i,j} \rangle + \langle S_r \rangle \tag{3.21}$$

The FLUENT code uses the Favre averaged conservation equations and these equations are closed with appropriate sub-models.

3.3 Set of the mathematical sub-models

Commonly used and widely accepted models available in the FLUENT code have been applied for the description of the turbulence, the gaseous combustion and the radiative energy exchange. In all calculations throughout this thesis the following models have been used:

- turbulence - the k-ε model

- interaction between chemistry and turbulence - EDM (Eddy Dissipation Model)

- Lagrangian particle tracking - DPM (Discrete Phase Model)

- devolatilization - CPD (Chemical Percolation Devolatilization) model

- char burnout - intrinsic model

- radiative heat transfer - DO (Discrete Ordinates) model

3.4 Turbulence

Computations of stationary turbulent flows require that the continuity equation (Eq. 3.1) and the momentum transport equation (Eq. 3.2) be accompanied by a model of turbulence that relates the Reynolds stresses $\rho\overline{u_i u_j}$ to known or calculable quantities. In all presented simulations, the $k-\varepsilon$ turbulence model according to Launder and Spalding [149] is used. It is the most common model due to its simplicity and due to its capability in predicting several turbulent flows. In the $k-\varepsilon$ model, the turbulent stresses $\rho\overline{u_i u_j}$ are assumed to be proportional to the mean rate of strain.

$$\rho\overline{u_i u_j} = -\mu_t\left(\frac{\partial U_i}{\partial x_j} + \frac{\partial U_j}{\partial x_i}\right) \tag{3.22}$$

The eddy viscosity μ_t is constructed from a turbulent length scale and a turbulent velocity scale which both are built up from the turbulent kinetic energy k and its turbulent viscous dissipation rate ε.

$$\mu_t = \rho c_\mu \frac{k^2}{\varepsilon} \tag{3.23}$$

$$k = \frac{1}{2}\overline{u_i u_i} \tag{3.24}$$

$$\varepsilon = \frac{\mu}{\rho}\overline{\frac{\partial u_i}{\partial x_j}}\,\overline{\frac{\partial u_j}{\partial x_i}} \tag{3.25}$$

The two turbulence quantities k and ε are solved for by means of two transport equations:

$$\frac{\partial}{\partial x_i}(\rho k U_i) - \frac{\partial}{\partial x_i}\left(\frac{\mu_t}{Pr_k}\frac{\partial k}{\partial x_i}\right) = P - \rho\varepsilon \tag{3.26}$$

$$\frac{\partial}{\partial x_i}(\rho\varepsilon U_i) - \frac{\partial}{\partial x_i}\left(\frac{\mu_t}{Pr_\varepsilon}\frac{\partial\varepsilon}{\partial x_i}\right) = C_{\varepsilon 1}\frac{\varepsilon}{k}P - C_{\varepsilon 2}\rho\frac{\varepsilon^2}{k} \tag{3.27}$$

In the above two transport equations, the turbulent kinetic energy production rate P defined by:

$$P = -\rho\overline{u_i u_j}\frac{\partial U_i}{\partial x_j} \tag{3.28}$$

is approximated by:

$$P = \mu_t\left(\frac{\partial U_i}{\partial x_j} + \frac{\partial U_j}{\partial x_i}\right)\frac{\partial U_i}{\partial x_j} \tag{3.29}$$

The constants (Tab. 3.2) and the Prandtl numbers (Tab. 3.3) for the turbulent kinetic energy and the turbulent viscous dissipation rate are given as:

$C_{\varepsilon 1}$	$C_{\varepsilon 2}$	C_μ
1.44	1.92	0.09

Pr_k	Pr_ε
1.0	1.3

Table 3.2: $k - \varepsilon$ model constants

Table 3.3: $k - \varepsilon$ model Prandtl numbers

3.5   Turbulent gas combustion

In the theory of combustion, two idealized cases are distinguished. In the first case, the reactants are completely mixed before some reaction takes place. This is the case of premixed (kinetic) flames. In the second case, the reactants mix and react at the same time and one speaks of non-premixed (diffusion) flames. These two cases of combustion are quite different and are treated separately. There are many situations that are not close to either limit. This is the case of partially premixed flames. Following the characteristic of the flow field, the chemically reacting flows can be laminar or turbulent. In practical combustion systems, the flow is almost always turbulent and the effect of turbulence in these flows is of a primary importance [146]. In this work, all computed flames are treated as turbulent diffusion flames.

Turbulent reacting flows can be characterized by several non-dimensional numbers. The most important one is the Damköhler number. The Damköhler number compares the turbulent (τ_t) and the chemical (τ_c) time scales:

$$Da = \frac{\tau_t}{\tau_c} \tag{3.30}$$

When the Damköhler number is large ($Da \gg 1$), the chemical time is short comparing to the turbulent one, corresponding to a thin reaction zone distorted and convected by the flow field. The internal structure of the flame is not strongly affected by turbulence and may be described as a laminar flame element called as a flamelet. The turbulent structures wrinkle and strain the flame surface. The burning rate may be quantified in terms of turbulent mixing. The reaction rate is limited by turbulent mixing, described in terms of scalar dissipation rates. The small scale dissipation rate of turbulence controls the mixing of the reactants and, accordingly plays a dominant role in combustion modeling, even for finite rate chemistry. When the Damköhler number is low ($Da \ll 1$), the chemical time is long compared to the turbulent one, corresponding to slow chemical reactions. Reactants and products are mixed by turbulent structures before reactions take place. In this perfectly stirred reactor, the mean reaction rate may be expressed from Arrhenius laws using mean mass fractions and temperature. In turbulent flames, as long as quenching does not occur, the most practical situations correspond to high or medium values of the Damköhler numbers.

Another important number in turbulent combustion is the Karlovitz number. The Karlovitz number is defined as a ratio of chemical time scale τ_c to a smallest turbulent time scale (Kolmogorov) τ_k.

$$Ka = \frac{\tau_c}{\tau_k} \tag{3.31}$$

If $Ka \ll 1$ the chemical reactions occur much faster than turbulent mixing at Kolmogorov scale. Turbulence does not alter the flame structure and the chemical region is in laminar conditions. If the gaseous combustion reactions proceed fast in comparison to the time of turbulent mixing the overall reaction rate is determined by the mixing himself and the reaction takes place as soon as the reactants (fuel and oxidizer) are mixed on the molecular scale (infinitely fast chemistry). The smallest eddies in the turbulent spectrum are responsible for the mixing at the molecular level. Inside these eddies (called fine structures) the gas is well mixed and the structure can be viewed as a well stirred reactor. Inside the fine structures the turbulence has no limiting effect. When the fine structure is destroyed by the turbulence, then the mixture inside them is released into the surrounding fluid. This is a convenient assumption in turbulent diffusion combustion models which are described and used in this thesis.

In the fine structures each chemical reaction is written in the following way:

$$\sum_i \nu_i R_i = \sum_j \nu_j' P_j \tag{3.32}$$

where R_is are the reactants and P_js are the products, ν_i and ν_j' are the stoichiometric coefficients.

The rate of formation or destruction of each species is :

$$\Re_i = k_{f,i} \prod_i [R_i]^{\nu_{j,i}} - k_{b,i} \prod_j [P_j]^{\nu'_{j,i}} \tag{3.33}$$

where $k_{f,i}$ and $k_{b,i}$ are the rate constants for the forward and backward reactions respectively, and $[R_i]$ and $[P_j]$ are mole concentration of reactants and products, respectively. The forward and the backward reaction rate constants are linked through the equilibrium constant:

$$\frac{k_f}{k_b} = \left(\frac{P}{RT}\right)^{\Delta\nu} exp\left(\frac{\Delta S^o}{R} - \frac{\Delta H^o}{RT}\right) \tag{3.34}$$

where $\Delta\nu = \sum_j \nu'_j - \sum_i \nu_i$

In chemical species equation (Eq. 3.4) the effect of the chemical reactions appears in the source term S_a only. The part due to chemical reaction is given by:

$$S_a = \mu_a \sum_j \nu_{ji} R_j \tag{3.35}$$

The source term in the species equation takes into account the rate of formation or destruction of each species. As discussed previously in this Chapter, the source term has to take in consideration effects of the turbulence. This term is very complicated to calculate and therefore sub-models are needed. Some approaches are described in the following Sections.

3.5.1 Turbulence-chemistry interaction models

The interaction between turbulence and chemistry is assumed to be well described using the concept of Spalding [150] - Eddy Break-Up Model (EBU), and developed further by Magnussen and Hjertager [151] - Eddy Dissipation Model (EDM). Both models assume that mass is exchanged between Kolmogorov eddies (fine structure) and surroundings. No detailed chemistry can be applied and only global mechanisms are used in these models. The Eddy Dissipation Concept (EDC) is an extension of Magnussen [152, 153, 154] to the Eddy Dissipation Model (EDM) that include detailed chemical mechanisms occurring in turbulent flows.

3.5.2 Eddy Break Up Model

Spalding [150] related the microscale mixing to the breakup of large eddies of unburned fluid into successively smaller ones until the surface of the lumps becomes significant and turbulent kinetic energy is dissipated. The model assumes that the

reactions are completed at the moment of mixing, so that the reaction rate is completely controlled by turbulent mixing. At every location, the gas mixture is supposed to comprise fully-burned and fully-unburned gases. Combustion is then described by a single step global chemical reaction. The reaction rate is:

$$\Re_i = A_{mix}\rho\langle\frac{\varepsilon}{k}\rangle\sqrt{Y_F'^2} \tag{3.36}$$

$$A_{mix} = A\langle\frac{k^2}{\varepsilon\nu}\rangle^{-B} \tag{3.37}$$

where A and B are the model parameters derived from experiments and are equal to 23.66 and 0.25, respectively. The EBU model was found attractive because the reaction rate is simply written as a function of known quantities without an additional transport equation. The modeled reaction rate does not depend on chemical characteristics and assumes a homogenous and isotropic turbulence.

3.5.3 Eddy Dissipation Model

Magnussen and Hjertager derived the Eddy Dissipation Model (EDM) [151] which is based on the EBU model. In diffusion flames both the fuel and the oxygen occur in separate eddies. Because the chemical reactions in most cases are very fast, it can be assumed that the rate of the combustion is determined by the rate of intermixing on the molecular level of fuel and oxygen eddies, in other words, by the rate of dissipation of the eddies. Because both the fuel and the oxygen appear as fluctuating intermittent quantities there is a relationship between the fluctuations and the mean species concentration. Consequently, the rate of dissipation can be expressed by the mean concentration of the reacting species.

The EDM is apparently closely related to the EBU model. However, it differs from the latter in relating the dissipation of eddies to the mean concentration of intermittent quantities instead of the concentration fluctuations. This is a great advantage, especially when taking into consideration the lack of the certainty with which concentration fluctuations of reacting species can be determined. However, the simplifications of the proposed model are only possible for quantities that appear intermittent.

Practically, the equations in both approaches are the same, but in EDM, as mentioned above, the reaction rate (and mixing also) is not dependent on the concentration fluctuations, hence mixing parameter A_{mix} is not calculated. It is empirically determined and it is a constant. The reaction rate for a single reaction is then given by smaller of the two expressions below:

$$\Re_{i,r} = \nu_{i,r}'M_{w,i}A\rho\left(\frac{\varepsilon}{k}\right)min\left(\frac{Y_R}{\nu_{R,r}'M_{w,R}}\right) \tag{3.38}$$

$$\Re_{i,p} = \nu'_{i,r} M_{w,i} AB\rho \left(\frac{\varepsilon}{k}\right) min \left(\frac{\sum\limits_{P} Y_P}{\sum\limits_{j}^{N} \nu''_{j,r} M_{w,j}}\right) \qquad (3.39)$$

where A and B are two model constants and that are equal 4 and 0.5, respectively. Y_P is the mass fraction of the product species (P) and Y_R is the mass fraction of the particular reactant (R); $\nu'_{i,r}$ is the stoichiometric coefficient for species i in reaction r; k and ε are the turbulent kinetic energy and the turbulent dissipation derived from the $k - \varepsilon$ model.

3.5.4 Eddy Dissipation Concept

The Eddy Dissipation Concept (EDC) is an extension of the EBU and EDM models as described by Magnussen et al. [152, 153, 154]. It is a reactor concept which identifies a reactor related to the fine structure in turbulence. This reactor is treated as a homogeneous reactor exchanging mass and energy with the surrounding fluid, thus allowing a complete treatment of the chemistry for the reactor. Everywhere, the gas mixture is supposed to comprise of mean mixture and fine structures. These both (as at the previous two models) exchange mass due to the destruction of the fine structures by the turbulence. Chemistry reactions are active only inside the fine structures, supposed to be mixed at the molecular level by the turbulence at the Kolmogorov scale. The reaction rate is given by:

$$\Re_i = \frac{\gamma^*}{\tau^*}(Y_i^0 - Y_i^*) \qquad (3.40)$$

where γ^* is the mass fraction of the fine structure inside the control volume and is described as follow:

$$\gamma^* = C_\gamma \left(\frac{\nu\varepsilon^{\frac{3}{4}}}{k^2}\right) \qquad (3.41)$$

where C_γ is the time scale constant and is equal 9.7687. The destruction time of the fine structure is indicates as τ^* and is given as:

$$\tau^* = C_\tau \left(\frac{\nu^{\frac{1}{2}}}{\varepsilon}\right) \qquad (3.42)$$

where C_τ is the time scale constant and is equal 0.4082. This model is more general than the EBU and EDM because it can be coupled with detailed kinetics since the fine structure can be considered as a well stirred reactor.

3.6 Particle behavior

Pulverized coal flame is modeled as two-phase turbulent flow system consisting of both a gaseous and a solid phase. In discrete phase modeling, coal particles of known

size distributions and properties are injected into the combustion chamber and tracked in a Lagrangian fashion throughout the computational domain. Heat and mass transfer to/from particles is calculated along each trajectory and it is used as the coupling mechanism between the gas phase and the solid phase. In others words, discrete phase model uses an Eulerian approach to calculate the continuous phase and a Lagrangian particle tracking to calculate the discrete phase. The coupling between the phases and its impact on both the discrete phase trajectories and the continuous phase flow is included.

A major assumption in the Lagrangian discrete phase model is that there is no interaction between solid particles. As a result this approach is only applicable to dilute fluid-particle flows where the solid phase volume fraction is low. Flows considered in this thesis have this characteristic.

3.6.1 Trajectory calculations

The trajectory of a discrete phase particle is predicted by integrating the force balance on the particle. The particle inertia must be equal to the forces acting on the particle, and the resulting equation can be written for x-direction in Cartesian coordinates in the following form:

$$\frac{du_{p,x}}{dt} = \underbrace{F_D(u - u_p)}_{\text{drag force}} + \underbrace{\frac{g_x(\rho_p - \rho)}{\rho_p}}_{\text{gravity and buoancy}} + \underbrace{F_x}_{\text{additional forces}} \tag{3.43}$$

where the drag force is defined:

$$F_D = \frac{18\mu}{\rho_p d_p^2} \frac{C_D Re_p}{24} \tag{3.44}$$

All forces in the force balance equation are given per unit of particle mass. The particle Reynolds number Re_p is defined in terms of the relative velocity between solid and fluid phase:

$$Re_p = \frac{\rho d_p |u_p - u|}{\mu} \tag{3.45}$$

where: u- fluid phase velocity, u_p- particle velocity, μ- molecular viscosity of the fluid, ρ- fluid density, ρ_p- density of the particle, d_p- particle diameter, C_D- drag coefficient. For the two other Cartesian directions analogous equations can be written.

In turbulence flows, the effect of turbulent dispersion is taken into account. The velocity fluctuations are assumed to be described by a Gaussian probability distribution. When the flow is turbulent, the trajectories of particle are predicted using the mean fluid phase velocity $\overline{u}$. In the stochastic particle tracking in turbulent flow, the instantaneous value of the fluctuating gas velocity $u = \overline{u} + w$ is used to predict the dispersion of the

particle due to turbulence. A stochastic method (in FLUENT- Discrete Random Walk (DRW) model) is implemented to determine the instantaneous gas velocity. The particle tracking procedure used in this work was developed at the beginning of the eighties at the University of Sheffield [155, 156] and later on it was implemented into the FLUENT code.

3.6.2 Heat and mass transfer calculations

The changes of momentum, mass and enthalpy during the particle trajectory calculations is computed for every control volume and appears as a source term in the equation for the fluid phase; this is a two way coupling between the solid and fluid phase. The following processes are taken into account:

- inert heating/cooling

- devolatilization phase

- char burnout

and they will be explained in details in next Paragraphs.

Inert heating or cooling

The inert heating or cooling is applied when the particle temperature is lower than the offset of devolatilization temperature (T_{dev}), and after the volatile fraction of a particle ($f_{v,0}$) has been released. These conditions may be written as:

- Inert heating

$$T_p < T_{dev} \tag{3.46}$$

- Inert cooling

$$m_p \leqslant (1 - f_{v,0})m_{p,0} \tag{3.47}$$

where T_p is the particle temperature, $m_{p,0}$ is the initial mass of the particle, and m_p is its current mass. During heating or cooling of particles, heat transfer is only due to convection and radiation at the particle surface:

$$m_p c_p \frac{dT_p}{dt} = hA_p(T_\infty - T_p) + \varepsilon_p A_p \sigma(\theta_R^4 - T_p^4) \tag{3.48}$$

where: m_p- mass of the particle, c_p- heat capacity of the particle, A_p- surface area of the particle, T_∞- local temperature of the continuous phase, h- convective heat transfer coefficient, ε_p- particle emissivity, σ- Stefan-Boltzmann constant, θ_R- radiation temperature. During heating and cooling, particles do not exchange mass with the continuous phase and do not participate in any chemical reactions.

Devolatilization phase

When the particle has reached an offset temperature for devolatilization T_{dev} volatile matter release begins:

$$T_p \geqslant T_{dev} \tag{3.49}$$

and remains in effect untill the mass of the particle, m_p, exceeds the mass of the nonvolatiles in the particle:

$$m_p > (1 - f_{v,0})m_{p,0} \tag{3.50}$$

The change of particle mass depends on the devolatilization model applied. The details of this model are presented in Section 3.7.1.

Heat transfer to the particle during the devolatilization process includes contributions from convection, radiation, and latent heat of devolatilization:

$$m_p c_p \frac{dT_p}{dt} = hA_p(T_\infty - T_p) + \frac{dm_p}{dt}h_{\text{fg}} + A_p \varepsilon_p \sigma(\theta_R{}^4 - T_p{}^4) \tag{3.51}$$

Char burnout

After the volatile component of the particle is completely evolved, a surface reaction begins which consumes the combustible fraction, f_{comb}, of the char particle. Char combustion is activated after the volatiles are evolved:

$$m_p < (1 - f_{v,0})(1 - f_{w,0})m_{p,0} \tag{3.52}$$

and it remains active until the combustible fraction in the char is consumed:

$$m_p > (1 - f_{v,0} - f_{comb})(1 - f_{w,0})m_{p,0} \tag{3.53}$$

When the combustible fraction, f_{comb}, has been consumed, the combusting particle may contain residual ash that reverts to the inert cooling phase (described previously). The surface reaction consumes the oxidant species in the gas phase; it supplies a (negative) source term during the computation of the transport equation for this species. Similarly, the surface reaction is a source of species in the gas phase: the product of the heterogeneous surface reaction appears in the gas phase as a chemical species. The change of the coal particle mass describes the char burnout model which is presented in details in Section 3.7.3.

The particle heat balance during surface reaction is

$$m_p c_p \frac{dT_p}{dt} = hA_p(T_\infty - T_p) - f_h \frac{dm_p}{dt}H_{reac} + A_p \varepsilon_p \sigma(\theta_R{}^4 - T_p{}^4) \tag{3.54}$$

where H_{reac} is the heat released by the surface reaction. Note that only a portion $(1 - f_h)$ of the energy produced by the surface reaction appears as a heat source in the gas-phase energy equation: the particle absorbs a fraction f_h of this heat directly.

3.7 Pulverized coal combustion

Coal is a compact, aged form of biomass (plant debris) containing combustibles, moisture, intrinsic mineral matter originating from salts dissolved in water and extrinsic ash [157]. Most coal combustion sub-models use simplified combustion and devolatilization steps because of the limitation of present day computational methods and particularly because of the limitation due to the lack of knowledge of the detailed coal combustion processes. As mentioned in Section 3.6.2, the combustion of coal is modeled according to the following steps: heating, devolatilization process, volatile combustion and char burnout. Coal particle is heated in a hot atmosphere by radiation and convection. Devolatilization process is fast and it can be completed within 10-100 ms. Burnout of char can take up to a few seconds. The successive stages of coal combustion are illustrated in Fig. 3.1.
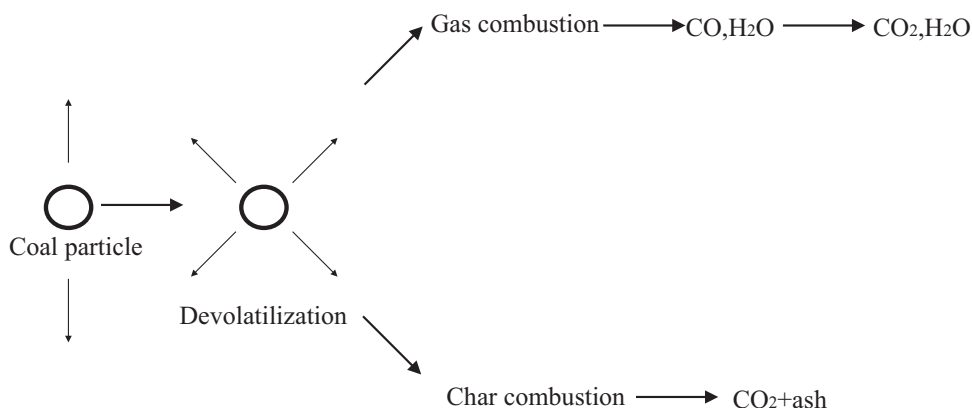
Figure 3.1: Diagram of the coal combustion stages

In practice, the coal is milled to give particles in 5-400 μm diameter range. The coal particles are pneumatically transported to the burner.

3.7.1 Coal devolatilization

Coal is a complex polymer consisting of C, H, N, O and minerals. Heating of coal results in the evolution of gases during pyrolysis and the formation of char. The process of evolution of combustible gases due to the thermal decomposition of the coal is referred to pyrolysis. Coal typically consists of 10 to 50% volatile matter (which is the fraction of solid fuel that can be released in the form of combustible gases) depending on its age or rank [157].

Typically a bituminous coal pyrolyzes at about 700 K, and the pyrolyzes is completed for most pulverized fuels within a time scale of 100 ms. Pyrolysis products

range from lighter volatiles such as CH_4, C_2H_4, C_2H_6, CO, CO_2, H_2 and H_2O to heavier tars. Tars thermally crack to form CH_4, C_2H_4, C_2H_6, C_3H_6, C_2H_2 and CO above 1000 K and are responsible for soot formation. The devolatilization model used in this work calculates the amount of tar and gas together. Tars produced from coal may occur in the form of liquids that vaporize if sufficient heat is supplied. If vaporization does not occur, tars can undergo repolymerization (or primary cracking) to produce lighter volatiles and char. The mixture of gases or volatiles can usually be represented by an overall empirical chemical formula $C_xH_yN_zO_tS_w$ where the subscripts x, y, etc. represent the number of atoms in volatiles for carbon, hydrogen, etc.

Coal can swell upon heating, resulting in a larger particle size. This effect is stronger in an inert environment or under reducing conditions. The swelling factor, that is the ratio of the larger swollen coal particle to its original dimension, can range from 1.3 (under oxidative conditions) to 4 (in an inert environment). Swelling introduces thin-walled cenospheres, which can produce a sudden decrease in the particle size when burned and a density increase during burn off.

CPD model   In contrast to the empirical devolatilization models (for example single rate model [158] and Kobayashi model [159]), the Chemical Percolation Devolatilization (CPD) model [160, 161, 162] characterizes the devolatilization behavior of rapidly heated coal particle, based on the description of physical and chemical transformation of the coal structure. During pyrolysis, the fragmentation from breaking up of aromatic clusters results in light volatile gas and precursors of tar with higher molecular weight. The latter remain within the particle for a longer time and can reattach to the coal lattice (crosslinking). These compounds together with the residual lattice are referred as metaplast. The softening behavior of a coal particle is determined by the quantity and nature of the metaplast generated during devolatilization. The portion of the lattice structure that remains after devolatilization is comprised of char and mineral-compound based ash.

Summarizing, during coal pyrolysis, the labile bonds between the aromatic clusters in the coal structure lattice are cleaved, resulting in two general classes of fragments. One set of fragments has a low molecular weight and escapes from the coal particle as a light gas. The other set of fragments consists of tar gas precursors that have a relatively high molecular weight and tend to remain in the coal for a long period of time during typical devolatilization conditions. During this time, reattachment with the coal lattice (which is referred to crosslinking) can occur.

The CPD model uses above described percolation theory and has the capability of predicting total volatiles and tar yields on the base of heating rate, temperature, pressure and coal type. The CPD model consists of five principal components:

- a description of the parent coal structure

- a bridge reaction mechanism with associated kinetics

- percolation lattice statistics to determine the relationship between bridge breaking and detached fragments (these fragments are tar precursor)

- a vapor-liquid equilibrium mechanism to determine the fraction of liquids that vaporize

- a cross-linking mechanism for high molecular weigh tar precursors to reattach to the char

Modeling the cleavage of the bridges and the generation of light gas, char, and tar precursors is then considered to be analogous to the chemical reaction scheme shown in Fig. 3.2.
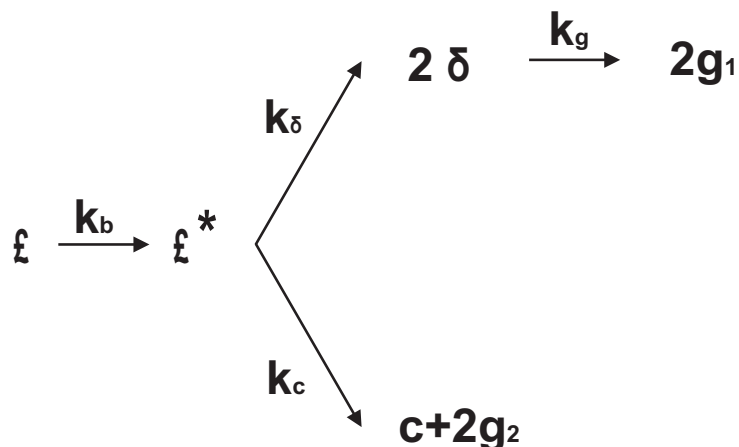
Figure 3.2: Scheme of the coal behavior during devolatilization process as a simplified network of chemical bridges [161]

The variable $\pounds$ represents the original population of labile bridges in the coal lattice. Upon heating, these bridges become the set of reactive bridges. For the reactive bridges $\pounds^*$, two competing paths are available. In one path, the bridges react to form side chains δ. The side chains may detach from the aromatic clusters to form light gas g_1. As bridges between neighboring aromatic clusters are cleaved, a certain fraction of the coal becomes detached from the coal lattice. These detached aromatic clusters are the heavy molecular

weight tar precursors that form the metaplast. The metaplast vaporizes to form coal tar. While waiting for vaporization, the metaplast can also reattach to the coal lattice matrix (crosslinking). In the other path, the bridges react and become a char bridge c, with the release of an associated light gas product g_2. The total population of bridges in the coal lattice matrix can be represented by the variable p, where $p = £ + c$. Given this set of variables that characterizes the coal lattice structure during devolatilization, the following set of reaction rate expressions can be defined for each, starting with the assumption that the reactive bridges are destroyed at the same rate at which they are created $\frac{\partial £^*}{\partial t}$:

$$\frac{d£}{dt} = -k_b £ \tag{3.55}$$

$$\frac{dc}{dt} = k_b \frac{£}{\rho + 1} \tag{3.56}$$

$$\frac{d\delta}{dt} = [2\rho k_b \frac{£}{\rho + 1}] - k_g \delta \tag{3.57}$$

$$\frac{dg_1}{dt} = k_g \delta \tag{3.58}$$

$$\frac{dg_2}{dt} = 2\frac{dc}{dt} \tag{3.59}$$

where the rate constants for bridge breaking and gas release steps, k_b and k_g, are expressed in Arrhenius form with a distributed activation energy:

$$k = Ae^{-(E \pm E_\sigma)/RT} \tag{3.60}$$

where A, E, and E_σ are, respectively, the pre-exponential factor, the activation energy, and the distributed variation in the activation energy; R is the universal gas constant, and T is the temperature. The ratio of rate constants, $\rho = k_\delta/k_c$, is set to 0.9 in this model based on experimental data.

Given the set of reaction equations for the coal structure parameters, it is necessary to relate these quantities to changes in coal mass and the related release of volatile products. To accomplish this, the fractional change in the coal mass as a function of time is divided into three parts: light gas (f_{gas}), tar precursor fragments (f_{frag}), and char (f_{char}). This is accomplished by using the following relationships, which are obtained using percolation lattice statistics:

$$f_{gas}(t) = \frac{r(g_1 + g_2)(\sigma + 1)}{4 + 2r(1 - c_0)(\sigma + 1)} \tag{3.61}$$

$$f_{frag}(t) = \frac{2}{2 + r(1 - c_0)(\sigma + 1)} [\Phi F(p) + r\Omega K(p)] \tag{3.62}$$

$$f_{char}(t) = 1 - f_{gas}(t) - f_{frag}(t) \tag{3.63}$$

The variables Φ, Ω, $F(p)$, and $K(p)$ are the statistical relationships related to the cleaving of bridges based on the percolation lattice statistics, and are given by the following equations:

$$\Phi = 1 + r \left[\frac{\pounds}{p} + \frac{(\sigma - 1)\delta}{4(1 - p)} \right] \tag{3.64}$$

$$\Omega = \frac{\delta}{2(1 - p)} - \frac{\pounds}{p} \tag{3.65}$$

$$F(p) = \left(\frac{p'}{p} \right)^{\frac{\sigma+1}{\sigma-1}} \tag{3.66}$$

$$K(p) = \left[1 - \left(\frac{\sigma + 1}{2} \right) p' \right] \left(\frac{p'}{p} \right)^{\frac{\sigma+1}{\sigma-1}} \tag{3.67}$$

where r is the ratio of bridge mass to site mass, m_b/m_a, where

$$m_b = 2M_\delta \tag{3.68}$$

$$m_a = M_{cl} - (\sigma + 1)M_\delta \tag{3.69}$$

where M_δ and M_{cl} are the side chain and cluster molecular weights respectively; $\sigma + 1$ is the lattice coordination number which is determined from solid state Nuclear Magnetic Resonance (NMR) measurements related to coal structure parameters, and p' is the root of the following equation in p (the total number of bridges in the coal lattice matrix):

$$p'(1 - p')^{\sigma-1} = p(1 - p)^{\sigma-1} \tag{3.70}$$

In accounting for mass in the metaplast (tar precursor fragments), the part that vaporizes is treated in a manner similar to flash vaporization, where it is assumed that the finite fragments undergo vapor/liquid phase equilibration on a time scale that is rapid with respect to the bridge reactions. As an estimate of the vapor/liquid that is present at any time, a vapor pressure correlation based on a simple form of Raoult's Law is used. The vapor pressure treatment is largely responsible for predicting pressure dependent devolatilization yields. For the part of the metaplast that reattaches to the coal lattice, a cross-linking rate expression given by the following equation is used:

$$\frac{dm_{cross}}{dt} = m_{frag}A_{cross}e^{-(E_{cross}/RT)} \tag{3.71}$$

where m_{cross} is the amount of mass reattaching to the matrix, m_{frag} is the amount of mass in the tar precursor fragments (metaplast), and A_{cross} and E_{cross} are rate expression constants.

Detailed information about CPD model parameters used in this work to describe the devolatilization of Guasare coal are given in Section 4.3.

3.7.2 Combustion of volatiles

Combustion of the volatiles has been simplistically represented by two overall reactions:

$$C_{1.2}H_{4.48}O_{0.44} + 1.5O_2 \longrightarrow 1.2CO + 2.24H_2O \tag{3.72}$$

$$CO + 0.5O_2 \longrightarrow CO_2 \tag{3.73}$$
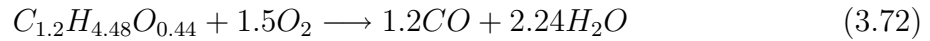
whose rates are calculated using the Eddy Dissipation Model (EDM) [151]. The reaction rate of production or consumption of species i is then given by the smallest of the two expressions: Eqs. 3.38 and 3.39.

3.7.3 Char combustion

Char particles produced from rapid pyrolysis are microporous solids whose properties can be described by their size, true and apparent density, porosity, pore volume distribution and surface area distribution. The rate of char oxidation is controlled by sequential or parallel processes of boundary layer diffusion, chemical reaction and pore diffusion. The three zone theory [163, 164] postulates the existence of the three different temperature regimes in which one or more control the overall reaction rate. In zone I, which occurs when chemical reaction is slow compared to diffusion (at low temperature and/or for small particles), chemical reaction is the rate-determining step. In zone II, the overall reaction rate is controlled by both chemical reaction and pore diffusion. Zone III, which occurs at high temperatures, is characterized by mass-transfer limitations in the boundary layer of the particle [165]. It should be noted that the theory idealizes and simplifies the actual variation rate with temperature. The difficulty comes in practice in exactly defining in which zone combustion occurs; generally, this takes place in inter-zone territory [166]. In other words, char oxidation rate is typically influenced by all three processes: boundary layer diffusion, pore diffusion, and chemical kinetics. Furthermore, the three-zone theory applies only to m-*th* order kinetics. Moreover, the three-zone theory assumes that the combustion rate contributed from the external surface area is negligible compared to the rate contributed from the internal surface area. This assumption is true for most cases, since the internal surface area is typically much larger than the external surface. However, the external surface area can become important under some conditions, these being favored by low internal surface area (typically in highly ordered carbons) or severe pore diffusion limitations which lead to an extremely low effectiveness factor.

Intrinsic model   Char burnout models can be classified into two main categories: global models and intrinsic models [167]. Global models consider char particles impervious to pore diffusion effects or else lump intraparticle diffusion effects into the chemical reaction rate constants. These models are highly empirical, basing the reaction rate on the particle external surface area and on the oxidizer concentration at the external surface. In contrast, intrinsic models relate char oxidation rate to the active surface area involved in the reaction and consider the non-uniform oxidizer profile within the particle. Intrinsic models rely on pore structure models to describe gaseous diffusion through complex pore structures and to model the local oxidizer concentration at the active surface area. Thus the intrinsic model approach has a high potential of providing coal-general kinetic rate constants instead of the coal-specific and condition-specific constants used in the global models [168].

Intrinsic models vary in levels of sophistication and can be classified into two subcategories: macroscopic and microscopic. Macroscopic models use average properties of the particle to estimate the effective diffusivity in the porous structures in the char particle, and usually do not model the evolution of pore structure with burnout. Microscopic models involve the development of a reaction model for a single pore and then the prediction of the overall particle reactivity by an appropriate statistical description of the pore size distribution [169]. If the pore structure is not allowed to change with conversion, and properties of the particle are assumed to be uniform, then the microscopic approach becomes equivalent to the macroscopic approach.

Char particles produced from rapid pyrolysis are microporous solids whose properties can be described by their size, true and apparent density, porosity, pore volume distribution and surface area distribution. The rate of char oxidation is controlled by sequential or parallel processes of oxygen boundary layer diffusion, chemical reaction and pore diffusion. The intrinsic model for char burnout used in this work is based on the Smith's [167] macroscopic pore model which assumed that the char oxidation reaction:

$$C(s) + O_2(g) = CO_2(g) \tag{3.74}$$

is of the first order. The overall surface reaction rate includes the effect of bulk diffusion and chemical reaction. The diffusion coefficient D_0 is computed via:

$$D_0 = C_1 \frac{[(T_p + T_\infty)/2]^{0.75}}{d_p} \tag{3.75}$$

The chemical rate is expressed in terms of the intrinsic chemical and pore diffusion rates:

$$\mathcal{R} = \eta \frac{d_p}{6} \rho_p A_g k_i \tag{3.76}$$

where: d_p- particle diameter, η- effectiveness factor, T_p- particle temperature, T_∞- bulk temperature, ρ_p- apparent density of the char, A_g- specific internal surface area of the char particle, k_i is the intrinsic reactivity. The effectiveness factor η is calculated as:

$$\eta = \frac{3}{\phi^2}(\phi \coth \phi - 1) \tag{3.77}$$

where ϕ is the Thiele modulus:

$$\phi = \frac{d_p}{2}\left[\frac{S_b \rho_p A_g k_i p_{\text{ox}}}{D_e \rho_{\text{ox}}}\right]^{1/2} \tag{3.78}$$

and ρ_{ox} is the density of oxidant in the bulk gas, S_b is the stoichiometric coefficient in Reaction (3.74) in $\frac{kg_{O_2}}{kg_{char}}$ and D_e is the effective diffusion coefficient in the particle pores. Assuming that the pore size distribution is unimodal and the bulk and Knudsen diffusion proceed in parallel, D_e is given by:

$$D_e = \frac{\theta}{\tau^2}\left[\frac{1}{D_{\text{Kn}}} + \frac{1}{D_0}\right]^{-1} \tag{3.79}$$

where D_0 is the bulk molecular diffusion coefficient and θ is the porosity of the char particle:

$$\theta = 1 - \frac{\rho_p}{\rho_t} \tag{3.80}$$

with ρ_p and ρ_t being, respectively, the apparent and true char densities and τ is the tortuosity of the pores. A typical value for τ is $\sqrt{2}$ which corresponds to an average intersecting angle between the pores and the external surface of 45°. The Knudsen diffusion coefficient D_{Kn} is calculated as:

$$D_{\text{Kn}} = 97.0 \bar{r}_p \sqrt{\frac{T_p}{M_{w,\text{ox}}}} \tag{3.81}$$

where T_p is the particle temperature, $\bar{r}_p$ is the mean pore radius of the char particle, and $M_{w,\text{ox}}$ is the oxygen molecule weight. The specific internal surface area (A_g) of the char particle is assumed in this model to remain constant during char combustion. The intrinsic reactivity (k_i) is of Arrhenius form:

$$k_i = A_i e^{-(E_i/RT_p)} \tag{3.82}$$

where A_i is the pre-exponential factor and E_i is the activation energy.

Detailed information about intrinsic model parameters used in this work to describe the char combustion of Guasare coal are given in Section 4.3.

3.8 Radiative heat transfer

Energy transfer due to radiation is taken into consideration through a source term in the energy equation. The Radiative Transfer Equation (RTE) for an absorbing, emitting and scattering medium at position $\overrightarrow{r}$ in the direction $\overrightarrow{s}$ is:

$$\frac{dI(\overrightarrow{r}, \overrightarrow{s})}{ds} + (a + \sigma_s)I(\overrightarrow{r}, \overrightarrow{s}) = an^2 \frac{\sigma T^4}{\pi} + \frac{\sigma_s}{4\pi} \int_0^{4\pi} I(\overrightarrow{r}, \overrightarrow{s'})\Phi(\overrightarrow{s} \cdot \overrightarrow{s'})d\Omega' \tag{3.83}$$

where $\overrightarrow{r}$- position vector, $\overrightarrow{s}$- direction vector, $\overrightarrow{s'}$- scattering direction vector, s- path length, a- absorption coefficient, n- refractive index, σ_s- Stefan- Boltzmann constant, I- radiation intensity, T- local temperature, Φ- phase function, Ω'- solid angle. If the scattering is neglected ($\sigma_s = 0$) and the gas is assumed to have the refractive index $n = 1$, then Eq. 3.83 simplifies notably:

$$\frac{dI(\overrightarrow{r}, \overrightarrow{s})}{ds} + aI(\overrightarrow{r}, \overrightarrow{s}) = a\frac{\sigma T^4}{\pi} \tag{3.84}$$

Discrete Ordinates (DO) [170, 171] radiation model is used to solve radiative heat transfer equation. The DO radiation model solves the Radiative Transfer Equation (RTE) for a finite number of discrete solid angles, each associated with a vector direction $\overrightarrow{s}$ fixed in the global Cartesian system (x, y, z). The DO model solves for as many transport equations as there are directions $\overrightarrow{s}$. When the solution for the RTE is known, the energy source term for energy equation is calculated using the radiation flux q_r:

$$S_{rad} = -\nabla q_r \tag{3.85}$$

The absorption coefficient in prescribed a value of 1.5 m^{-1}, see Paragraph 4.3.

3.9 Nitric oxides

In this work the fuel, thermal, prompt and N_2O paths as well as NO reburning have been considered, as shown in Fig. 3.3. The transport equations for nitric oxide (NO) and for intermediate species (HCN) have been solved while the N_2O and N-radical concentrations are calculated using the partial equilibrium assumption (see below). The sources for HCN and NO have been calculated averaging the instantaneous source term ($S_i = f(T)$) over the temperature fluctuations:

$$\langle S_i \rangle = \int_{T_0}^{T_{max}} P(T)S_i(T)dT \tag{3.86}$$

using a PDF-β function. The single-variable probability density function (PDF) approach used in our work was originally proposed by Hand et al. [172], extended by Peters and Weber [173] and finally implemented into the FLUENT code. T_0 is the reference temperature of the system, T_{max} is the adiabatic temperature of the flame. The NO calculations have been performed in post-processing.
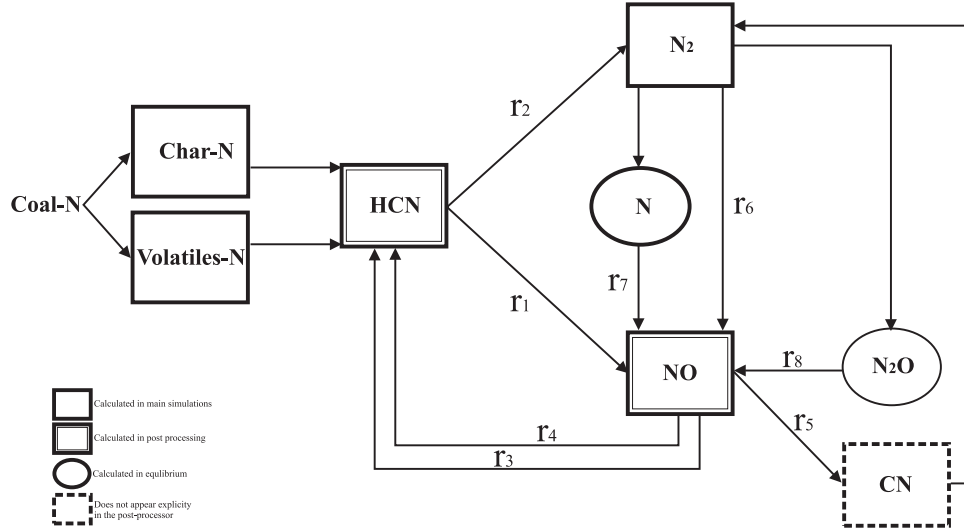
Figure 3.3: Path of NO formation and reburning

Fuel path It is assumed in this work that all fuel nitrogen, both from volatiles and char, is converted into HCN that can undergo reduction or formation of NO, as shown in Fig. 3.3.

$$\text{coal-N} \longrightarrow HCN \tag{3.87}$$

$$HCN + O_2 \longrightarrow NO + ... \tag{3.88}$$

$$HCN + NO \longrightarrow N_2 + ... \tag{3.89}$$
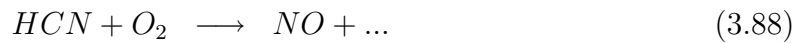
The HCN release rates are given by Eqs. 3.90 and 3.91, where $\dot{m}_{char}$ and $\dot{m}_{vol}$ are the combustion rates of char and volatile matter (in kg/s) respectively; $\dot{m}_{char}$ is delivered by the char combustion model (the intrinsic model) and $\dot{m}_{vol}$ is calculated using the CPD devolatilization model; V is the cell volume.

$$S_{HCN,char} = \frac{\dot{m}_{char} \cdot w_{N,char} \cdot M_{HCN}}{M_N \cdot V}, \qquad [\frac{kg}{m^3 s}] \tag{3.90}$$

$$S_{HCN,vol} = \frac{\dot{m}_{vol} \cdot w_{N,vol} \cdot M_{HCN}}{M_N \cdot V}, \qquad [\frac{kg}{m^3 s}] \tag{3.91}$$

The HCN depletion rates are given by De Soete [174] expressions:

$$r_1 = k_4 X_{HCN} X_{O_2} exp(-\frac{E_4}{RT}) \cdot \frac{p}{RT}, \qquad\qquad [\frac{mole}{m^3 s}] \qquad (3.92)$$

$$r_2 = k_5 X_{HCN} X_{N_2} exp(-\frac{E_5}{RT}) \cdot \frac{p}{RT}, \qquad\qquad [\frac{mole}{m^3 s}] \qquad (3.93)$$

where: $k_4 = 3.5 \cdot 10^{10} \frac{1}{s}$, $k_5 = 3.0 \frac{1}{s}$, $E_4 = 280.5 \frac{kJ}{mol}$, $E_5 = 251.2 \frac{kJ}{mol}$. The instantaneous source term S_{HCN} reads then:

$$S_{HCN} = S_{HCN,vol} + S_{HCN,char} - (r_1 + r_2) \cdot M_{HCN} \cdot 10^{-3}, \qquad\qquad [\frac{kg}{m^3 s}] \quad (3.94)$$

and is averaged over the temperature fluctuations using Eq. 3.86.

The NO source term from fuel nitrogen is expressed as follows:

$$S_{NO,fuel} = (r_1 - r_2) \cdot M_{NO} \cdot 10^{-3}, \qquad\qquad [\frac{kg}{m^3 s}] \qquad (3.95)$$

Prompt path De Soete [174] proposed a roughly estimated chemical reaction rate for prompt NO formation:

$$r_6 = f \cdot A \cdot [O_2]^b [N_2][C_x H_y] exp(-\frac{E_a}{RT}) \cdot V, \qquad\qquad [\frac{mole}{m^3 s}] \qquad (3.96)$$

where the exponent b may vary between 0 and 1, and depends on the conditions in the flame, namely the local mole fraction of oxygen $[O_2]$:

$$b = \begin{cases} 1.0, & [O_2] \leqslant 4.1 \cdot 10^{-3} \\ -3.95 - 0.9 \ln [O_2], & 4.1 \cdot 10^{-3} \leqslant [O_2] \leqslant 1.11 \cdot 10^{-2} \\ -0.35 - 0.1 \ln [O_2], & 1.11 \cdot 10^{-2} < [O_2] < 0.03 \\ 0, & [O_2] \geqslant 0.03 \end{cases}$$

The constant A and activation energy E_a take the following values: $A = 6.4 \cdot 10^6 (\frac{RT}{p})^{b+1}$, $E_a = 303.5 \frac{kJ}{mole}$. The prompt factor f accounts for the type of fuel and is calculated in the following way:

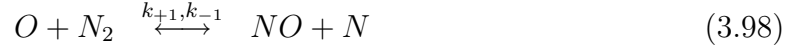$$f = 4.75 + 0.0819 \cdot c - 23.2 \frac{1}{\lambda} + 32 \frac{1}{\lambda^2} - 12.2 \frac{1}{\lambda^3}$$

where c is the number of carbon atoms per molecule of fuel and is assumed to be $c = 1.2$ for the volatile matter of the Guasare coal and λ is the air excess ratio.

The NO source term for prompt path reads then:

$$S_{NO,prompt} = r_6 \cdot M_{NO} \cdot 10^{-3}, \qquad\qquad [\frac{kg}{m^3 s}] \qquad (3.97)$$

Thermal path The extended Zeldovich mechanism incorporates the following reactions:

$$O + N_2 \xrightleftharpoons{k_{+1},k_{-1}} NO + N \tag{3.98}$$

$$N + O_2 \xrightleftharpoons{k_{+2},k_{-2}} NO + O \tag{3.99}$$

$$N + OH \xrightleftharpoons{k_{+3},k_{-3}} NO + H \tag{3.100}$$

where k_{+1}, k_{+2}, k_{+3} stand for the forward and k_{-1}, k_{-2}, k_{-3} for the backward rate constants corresponding to Reactions 3.98, 3.99 and 3.100. Under the assumption of partial equilibrium for N-radical, the NO formation rate can then be calculated as:

$$r_7 = 2k_{+1}[O][N_2] \frac{1 - \frac{k_{-1}k_{-2}[NO]^2}{k_{+1}[N_2]k_{+2}[O_2]}}{1 + \frac{k_{-1}[NO]}{k_{+2}[O_2]+k_{+3}[OH]}} \cdot V, \qquad [\frac{mole}{m^3 s}] \tag{3.101}$$

The O and OH radical concentrations are calculated by assuming equilibrium of the following reactions:

$$O_2 + H \longleftrightarrow OH + O \tag{3.102}$$

$$O_2 + M \longleftrightarrow M + O + O \tag{3.103}$$

Finally, the NO source term for thermal path reads:

$$S_{NO,thermal} = r_7 \cdot M_{NO} \cdot 10^{-3}, \qquad [\frac{kg}{m^3 s}] \tag{3.104}$$

N_2O **path** In low temperature combustion (below 1500 K) of lean mixtures of hydrocarbons (or at pressures higher than the atmospheric) a mechanism, in which the N_2O molecule is the intermediary, becomes important [175]. The concentration of N_2O is assumed to be in a quasi-steady state:

$$[N_2O] = \frac{k_{n1}[N_2][O][M] + k_{n2}[NO]^2}{(k_{n2} + k_{n3})[O] + (k_{n4} + k_{n5})[H]} \tag{3.105}$$

Assuming that the N_2O is converted to NO the rate of NO formation is:

$$r_8 = 2[N_2O]\,(k_{n2}[O] + k_{n4}[H]) \cdot V, \qquad [\frac{mole}{m^3 s}] \tag{3.106}$$
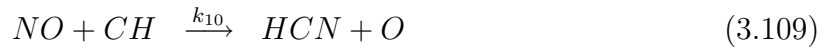
where

$$[M] = 1.4 \cdot [O_2] + 3.0 \cdot [CO_2] + 1.7 \cdot [N_2] + 12 \cdot [H_2O]$$

Then, the NO source term for N_2O path is calculated as:

$$S_{NO,N_2O} = r_8 \cdot M_{NO} \cdot 10^{-3}, \qquad [\frac{kg}{m^3 s}] \tag{3.107}$$

Reburning in gaseous phase Following the work of Chen et al. [176, 177] the major reburning reactions are:

$$NO + CH_2 \xrightarrow{k_9} HCN + OH \tag{3.108}$$

$$NO + CH \xrightarrow{k_{10}} HCN + O \tag{3.109}$$

$$NO + C \xrightarrow{k_{11}} CN + O \tag{3.110}$$

and in this work it is assumed that the volatile matter is the reburning agent, so the global NO reduction rates are:

$$r_4 = 4 \cdot 10^{-4} \cdot (k_9 + k_{10})[C_{1.2}H_{4.4}O_{0.44}][NO], \qquad [\frac{mole}{m^3 s}] \tag{3.111}$$

$$r_5 = 4 \cdot 10^{-4} \cdot k_{11}[C_{1.2}H_{4.4}O_{0.44}][NO], \qquad [\frac{mole}{m^3 s}] \tag{3.112}$$

where: $k_9 = 5.30 \cdot 10^9 \cdot T^{-1.54} \cdot exp(-\frac{27977}{RT})$, $k_{10} = 3.31 \cdot 10^{13} \cdot T^{-3.33} \cdot exp(-\frac{15090}{RT})$, $k_{11} = 1.356 \cdot 10^{12} \cdot T^{-2.64} \cdot exp(-\frac{144090}{RT})$.

Then, the source term for NO reburning is calculated as:

$$S_{NO,hom.\ reburn} = -(r_4 + r_5) \cdot M_{NO} \cdot 10^{-3}, \qquad [\frac{kg}{m^3 s}] \tag{3.113}$$

Reburning on char particles The heterogeneous reduction of NO on the char surface is modeled following the work of Levy et al. [178]:

$$r_3 = -k_6 \cdot X_{NO} \cdot p \cdot exp(-\frac{E_6}{RT}) \cdot c_s \cdot A_g, \qquad [\frac{mole}{m^3 s}] \tag{3.114}$$

where A_g is the (BET) specific surface area and c_s is the solid matter concentration and: $k_6 = 2.27 \cdot 10^{-3} \frac{mol}{Pa \cdot m^2}$, $E_6 = 142.7 \frac{kJ}{mol}$.

The source term for NO-reburning on the char particles is expressed as follows:

$$S_{NO,het.\ reburn} = r_3 \cdot M_{NO} \cdot 10^{-3}, \qquad [\frac{kg}{m^3 s}] \tag{3.115}$$

Thus, considering the above mentioned mechanisms of NO formation and destruction, the instantaneous source term for the NO transport equation is evaluated as

$$S_{NO} = S_{NO,fuel} + S_{NO,prompt} + S_{NO,thermal} + S_{NO,N_2O} + S_{NO,hom.\ reburn} + S_{NO,het.\ reburn} \tag{3.116}$$

Obviously, the above source term is then averaged over temperature fluctuations using Eq. 3.86.

Chapter 4

Model validation

In 1999 the IFRF (International Flame Research Foundation) carried out semi industrial scale trials called HTAC 99 [64] that revealed a high potential for HTAC technology also for the combustion of solid fuels. In this Chapter numerical simulations of pulverized coal flames generated during the IFRF trials are undertaken in order to examine if the combustion of coal under HTAC conditions can be predicted using the numerical code. Description of the experimental setup, measurements and validation procedure of the used sub-models against the IFRF measurements are provided in the following Sections.

4.1 Experimental equipment

4.1.1 Furnace

The experiments were executed in a refractory lined IFRF furnace No. 1 which is presented in Fig. 4.1. The furnace has $2 \, m$ times $2 \, m$ square cross section and its length is $6.25 \, m$. It consists of 11 water-cooled segments. For each segment the wall temperatures were monitored using thermocouples located at the top wall and at the side wall of the furnace. The furnace heat extraction was monitored measuring the volumetric flow rate and the temperature rise of the cooling water circulating in each segment. Measurements were carried out using the ports located on both sides of each segment. A pressure transducer was mounted on segment five to monitor the furnace pressure. In order to avoid air ingress, the furnace was kept in overpressure.
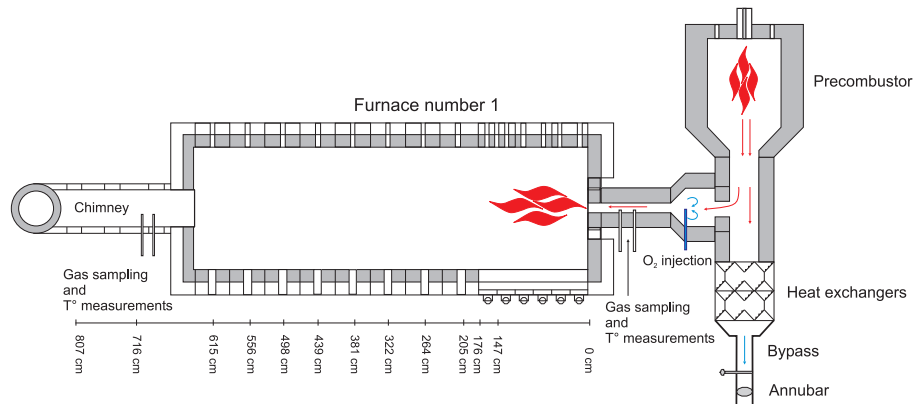
Figure 4.1: Experimental IFRF furnace together with precombustor

4.1.2 Precombustor

The regenerative air (other names: comburent or vitiated air) simulates the preheated air of the excess enthalpy combustion process. The regenerative air was generated using a precombustor which is shown in Fig. 4.1. The precombustor was operated using natural gas as a fuel. Oxygen was added to the flue gas in precombustor in order to keep the oxygen level to 19.5% vol. wet. After the oxygen addition the comburent was injected into the furnace. Both temperature and composition of the comburent were monitored using a suction pyrometer and gas sampling probe, respectively and they are listed in Tab. 4.1.

composition	value	unit
O_2	19.5	vol. % wet
CO_2	6.4	vol. % wet
N_2	59.1	vol. % wet
H_2O	15.0	vol. % wet
NO_x	100	vol. ppm wet
properties		
Molecular weight	28.31	$\frac{kg}{kmol}$

Table 4.1: Comburent composition and properties

Figure 4.2: The detailed geometry of the burner

4.1.3   Burner block

The experimental burner, shown in Fig. 4.2 operates at 0.58 MW fuel input and a high air preheat. The vitiated air is supplied through the central channel at an injection velocity of 65 $\frac{m}{s}$. Two coal guns are located at a 280 mm distance on both sides of the centerline.

4.2   Measurements

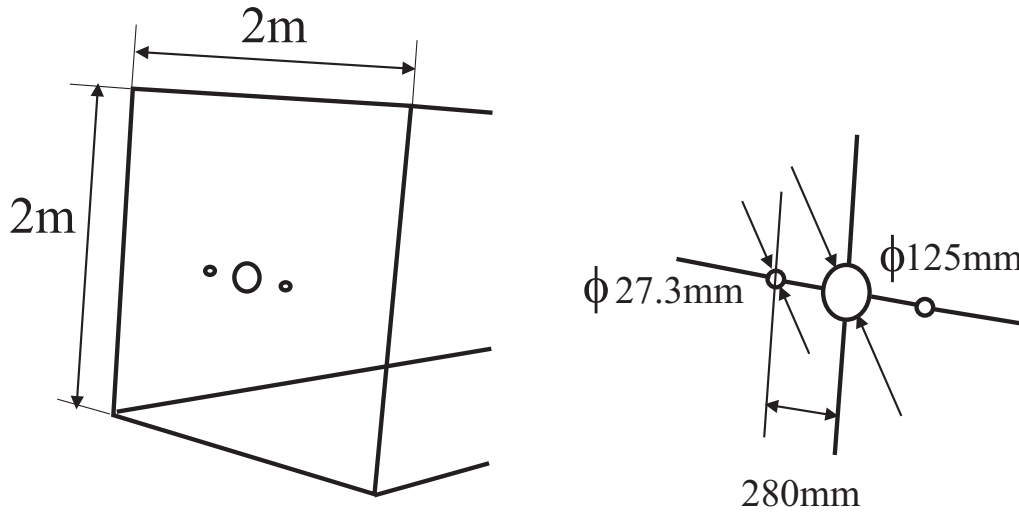The experiments consist of detailed in-flame measurements and input/output measurements. The measurements were taken at several traverses at several distances from the burner. The traverses were taken in the plane crossing both the coal and the comburent jets, as can be observed in Fig. 4.1, and in more details in Fig. 4.7.

In-flame measurements include both mean and rms (root mean square) axial velocities, gas temperature, gas composition (CO_2, O_2, CO, NO_x, C_nH_m), solid concentration, total radiance and total radiative fluxes at the furnace wall. In the input/output measurements the furnace flue gas temperature, gas composition (CO_2, O_2, CO, NO_x, C_nH_m) and burnout were measured.

Velocity measurements (mean velocity and rms) were performed using the IFRF water cooled Laser Doppler Velocimetry (LDV) probe. In-flame temperatures were measured using a suction pyrometer equipped with a type B thermocouple (Pt6%Rh/Pt30%Rh). Local in-flame gas compositions were measured using a gas sampling probe. Measurements of total radiance and total radiative heat fluxes were

performed using standard IFRF narrow angle radiometer and ellipsoidal radiometer probes, respectively. Solid sampling was performed using the IFRF static solid sampling probe. A detailed description of these measurements can be found in [64] and [65].

4.3   Coal characterization

The Venezuelan bituminous Guasare coal was combusted [64]. According to the ASTM classifications it is a high volatile bituminous A coal. The proximate and ultimate analysis of Guasare coal are given in Tab. 4.2 and 4.3, respectively.

composition	wt%
moisture ($105^o C$)	2.9
volatile matter	37.1
fixed carbon	56.7
ash	3.3
LCV	31.74 $\frac{MJ}{kg}$

Table 4.2: Guasare coal proximate analysis

composition, wt% daf	coal	char	volatiles
C	81.6	92.6	72.51
H	5.5	1.3	9.10
N	1.5	1.7	1.3
O	10.7	4.0	16.3
S	0.6	0.4	0.8

Table 4.3: Guasare coal ultimate analysis (dry, ash free basis)

The coal was milled to give a particle size distribution of 80%<90 μm. The Rosin-Rammler distribution function with the mean diameter of 42 μm and the spread of 1.36 represents nicely the measured data, as shown in Fig. 4.3. In the CFD predictions of this work, the 10-300 μm size range has been divided into twenty size classes and around 750 particles are injected per class, each time the particle tracking procedure is activated.

There are five coal-specific parameters of the CPD model: the average molecular weight per aromatic cluster (M_{cl}), the average molecular weight per side chain (M_{del}), the average number of attachments per cluster, referred to as the coordination number
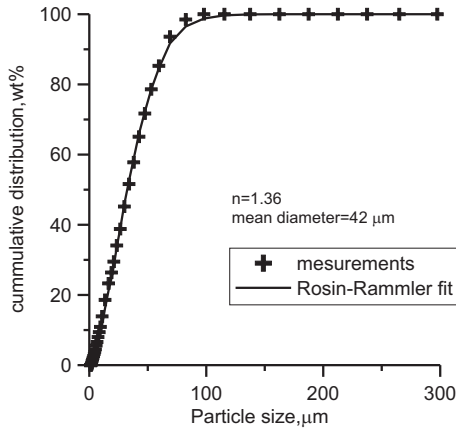
Figure 4.3: Guasare coal particle distribution (left) and distribution parameters (right)

$(\sigma+1)$, the fraction of attachments that are bridges (p_0) and initial fraction of char bridges (c_0), as shown in Tab. 4.4. The question is how to determine these five parameters for the considered coal? To this end other IFRF experimental data [179] on characterization of both devolatilization and char combustion of Guasare coal were used. Fig. 4.4 (left) shows the devolatilization curve obtained using the IFRF Isothermal Plug Flow Reactor (IPFR) operated at a 1200^oC temperature. The particle heating rate of these experiments is in the range $10^5 \div 10^6 \frac{K}{s}$ depending on the particle size. Under such rapid heating conditions a 55-75% high temperature yield is measured as opposed to 37% ASTM volatiles. The CPD devolatilization model has been run using as input the eight experimentally determined yields, shown in Fig. 4.4, left. The initial fraction of char bridges has been fixed to zero which is a typical value for bituminous coals. The obtained values of the other CPD parameters are listed in Tab. 4.4 while the CPD model devolatilization curve is shown in Fig. 4.4, left using a solid line. The volatiles are represented in the CFD predictions as $C_{1.20}H_{4.48}O_{0.44}$ which provides the stoichiometric coefficient of 1.5 (see Eq. 3.72).

Now one is facing the question of adapting the above char combustion model to the Guasare coal. To this end there are again used the IFRF measurements [179] of Guasare char burnout as a function of time for temperatures of 950^oC, 1300^oC and 1400^oC, see Fig. 4.4, right. These measurements were carried out at 4% oxygen volume fraction. The measured char morphology data were: the apparent char density equal to $339 \frac{kg}{m^3}$ and porosity equal to 74%. Fixing the mass diffusion-limited rate constant (C_1) at a value of $5 \cdot 10^{-12} \frac{m^3}{K^{0.75} \cdot s}$, the char porosity at the 74%, and the specific surface area at $2.5 \cdot 10^4 \frac{m^2}{kg}$ the values of both kinetic parameters A_i and E_i were selected to obtain a proper fit to the IFRF data, as shown in Fig. 4.4, right. The obtained values are given in Tab. 4.5.
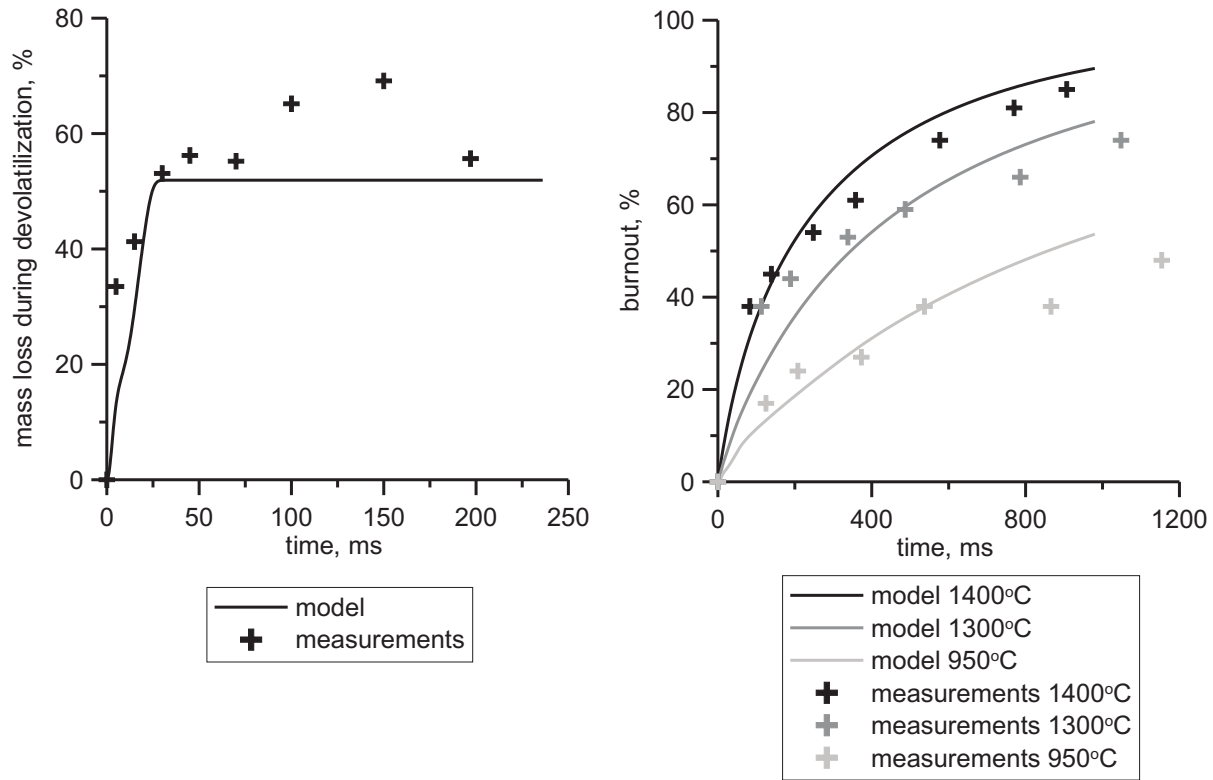
Figure 4.4: Devolatilization and burnout measurements [179] with the CPD (left) and the intrinsic (right) model fittings for Guasare coal

parameter	symbol	value	unit
Initial Fraction of Bridges in Coal Lattice	p_0	0.5	-
Initial Fraction of Char Bridges	c_0	0	-
Lattice Coordination Number	$\sigma + 1$	5	-
Cluster Molecular Weight	M_{cl}	300	$\frac{kg}{kmol}$
Side Chain Molecular Weight	M_{del}	30	$\frac{kg}{kmol}$

Table 4.4: The parameters for the CPD devolatilization model of Guasare coal

Thus, in the CFD predictions presented in this work, the initial particle diameter remains unaltered through the char combustion processes while the rate of char oxidation is calculated using Eq. 3.76. The char density is changing during the char burnout process according to the following equation:

$$B = \frac{(1 - \frac{\rho}{\rho_0})}{(1 - a_0)} \qquad (4.1)$$

where ρ_0 is the initial density of char particle, a_0 is the initial ash content and B is the burnout.

parameter	symbol	value	unit
Mass Diffusion-Limited Rate Constant	C_1	$5 \cdot 10^{-12}$	$\frac{m^3}{K^{0.75} \cdot s}$
Pre-exponential Factor	A_i	$1 \cdot 10^{-3}$	$\frac{kg}{m^2 s}$
Activation Energy	E_i	$5 \cdot 10^7$	$\frac{J}{kmol}$
Char Porosity	Θ	0.74	-
Mean Pore Radius	$\overline{r_p}$	$1 \cdot 10^{-7}$	m
Specific Internal Surface Area	A_g	$2.5 \cdot 10^4$	$\frac{m^2}{kg}$
Tortuosity	τ	$\sqrt{2}$	-

Table 4.5: The parameters for the intrinsic char combustion model of Guasare coal

During the devolatilization process, macromolecules break up and formation of tar and gases can lead to swelling of the particle. In our model the swelling coefficient (C_{sw}) takes a value of 2.

Figure 4.5: The coal combustion model used in this work
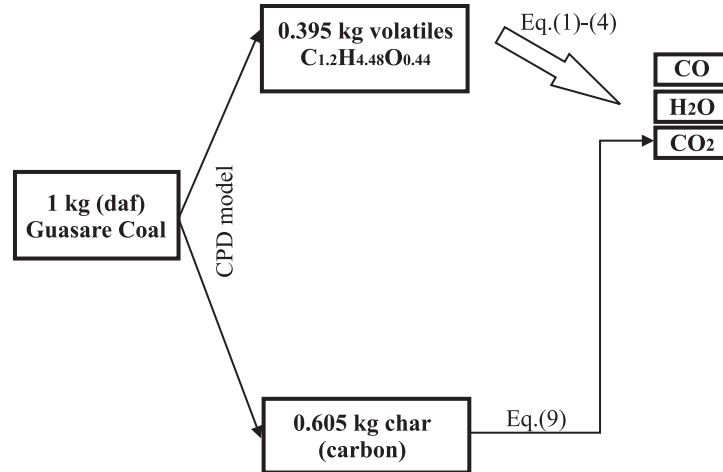
In summary of this Section one refers to Fig. 4.5 which shows the coal combustion models used in the simulations. The devolatilization is modeled using the CPD model with the model parameters listed in Tab. 4.4. The volatile matter combustion is calculated using Eqs. 3.72-3.39 while for the char combustion rate there is used Eq. 3.76 with the parameters listed in Tab. 4.5.

4.4   Numerical modeling

4.4.1   Model geometry and calculation procedure

A quarter of the furnace has been modeled only taking advantage of the symmetry. An unstructured mesh consisting of 700,000 cells has been used with the small cell size being around 2 mm and the largest around 75 mm. For numerical representation of the central jet inlet area 600 cells have been used while the small fuel jet inlet area has been represented by 150 cells. Convergency has been achieved after performing around 50,000 iterations. A grid sensitivity study was performed and two grids consisting of 700,000 and 1,500,000 cells were tested. Predictions using both grids were very similar and the smaller grid has been used for all simulations presented below.

Operating and boundary conditions are shown in Fig. 4.6 and in Tab. 4.6, respectively.
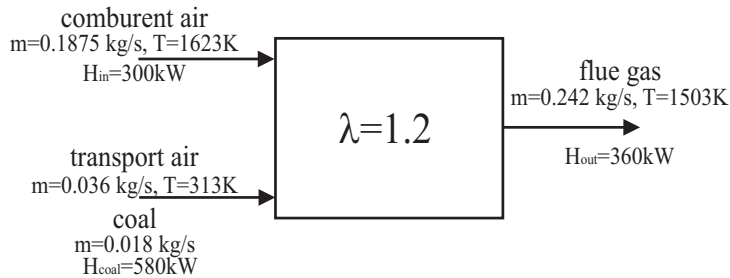
Figure 4.6: Operating conditions in the IFRF experiment

name	type	num.	settings
Comburent air inlet	mass flow inlet	1	$wt_{O_2} = 0.22$, $wt_{H_2O} = 0.095$, $wt_{CO_2} = 0.125$, $wt_{NO} = 8.9 \cdot 10^{-5}$, $\dot{m} = 0.1875 \frac{kg}{s}$, $T = 1623K$
Transport air inlet	mass flow inlet	2	$wt_{O_2} = 0.23$, $wt_{N_2} = 0.77$, $\dot{m} = 0.036 \frac{kg}{s}$, $T = 313K$
Coal inlet	injection	2	$\dot{m} = 0.018 \frac{kg}{s}$, $u = 26 \frac{m}{s}$, $T = 313K$
Outlet	outflow	1	$\varepsilon = 0.6$, $T_{rad} = 1200K$
Walls	wall		$\varepsilon = 0.6$, $T = 1523K$

Table 4.6: Boundary conditions in the numerical simulations
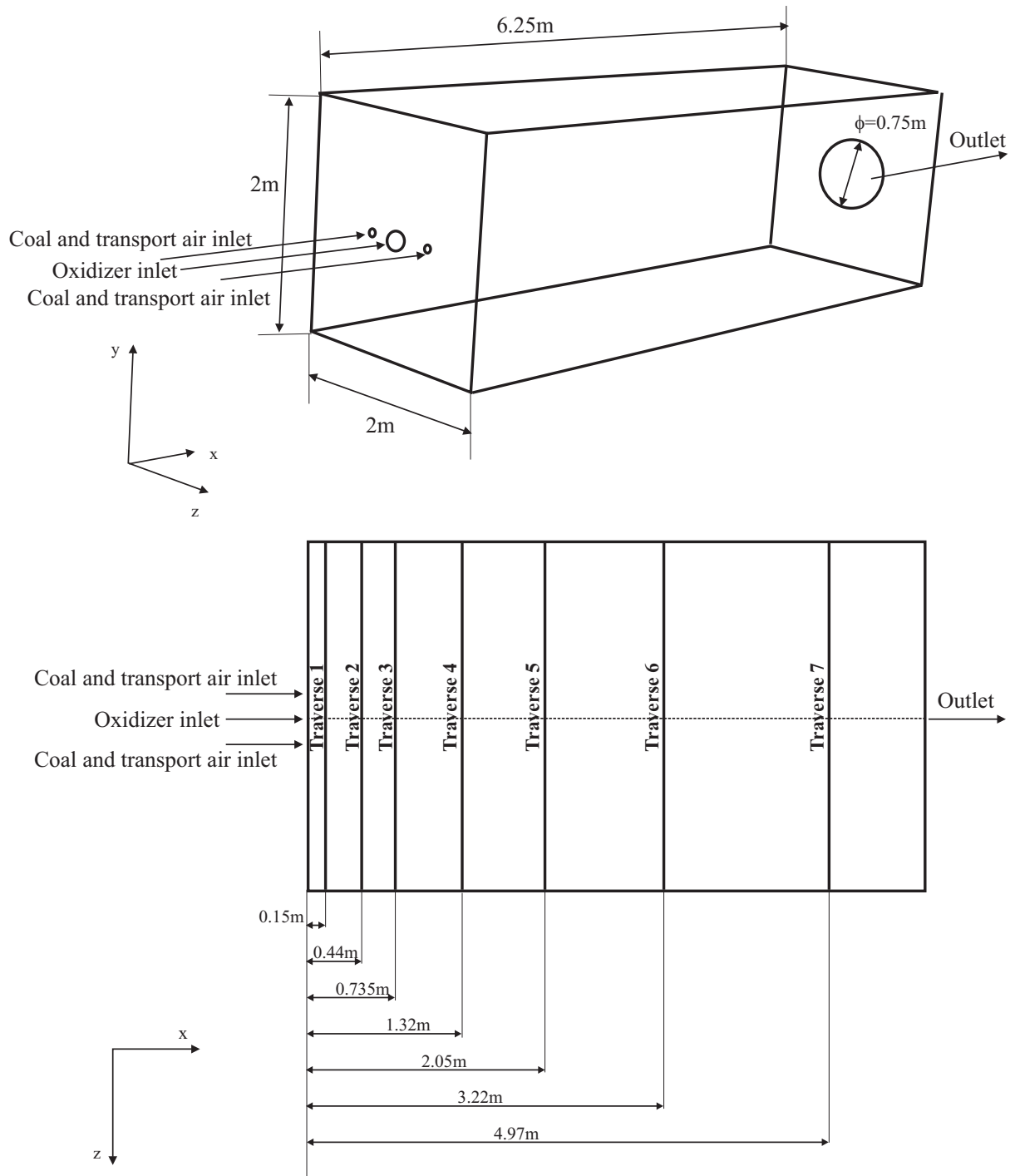
Figure 4.7: Geometry of the simulated IFRF furnace

4.4.2 Flow field and recirculation

In Fig. 4.8, left, the measured and calculated velocities along the seven traverses are shown. At the first traverse the computed values correspond well with the measured velocities except for the comburent centerline velocities which were measured about $20\frac{m}{s}$ lower than the calculated values. Here the measured values are obviously incorrect. For a 128 mm diameter jet of 65 $\frac{m}{s}$ inlet velocity, at $\frac{x}{d} = 1.2$ which is in the jet potential core [148], the velocity must be still around 65 $\frac{m}{s}$. At the first two traverses the comburent jet can be clearly distinct from the coal jet. The coal jet merges into the comburent jet near the third traverse. Downstream of the third traverse both jets merge and form one stream that can be observed at the next traverses. At a distance of 2 m downstream of the furnace front wall (from the fifth traverse onwards) the velocity profile is flat. As shown in Fig. 4.8, left the size of the recirculation region formed in the furnace and its low magnitude (negative) velocities are well reproduced in the computation. Generally, the velocity predictions (the flow field together with the recirculation) are in good agreement with the measurements.

4.4.3 Temperature field and radiative heat fluxes

The temperature profiles along the traverses are given in Fig. 4.8, right. No substantial difference between the model predictions and the measurements can be seen with exception of the fuel jet at the first traverse. The temperature level, as well as the temperature peaks are reproduced very well by the simulations. Ignition of the fuel jet takes place somewhere between the first and the second traverse so that the peak temperature of around 1800 K occurs between the second and third traverses. This feature is again well reproduced in the numerical simulations. From the fourth traverse downwards the temperature profile is flat since slow combustion proceeds downstream in the furnace and the temperature level is everywhere around 1600 K. Generally, the agreement between the temperature predictions and the measurements is quite satisfactory.

To obtain such a good accuracy of the temperature predictions it is imperative that the value of the absorption coefficient appearing in Eq. 3.83 is properly selected. Following the method of Lallemant et al. [180] and Sayre et al. [181] the narrow angle radiance measured at the fifth traverse (2.05 m) is here used. Fig. 4.9 shows that using a value of 1.5 m^{-1} which accounts for the CO_2/H_2O radiation as well as for soot and particles radiation, the predicted and measured radiation intensities are in good agreement. The ultimate verification of the correctness of the radiative heat transfer procedure is demonstrated in Fig. 4.10 showing very good agreement between the measured and the
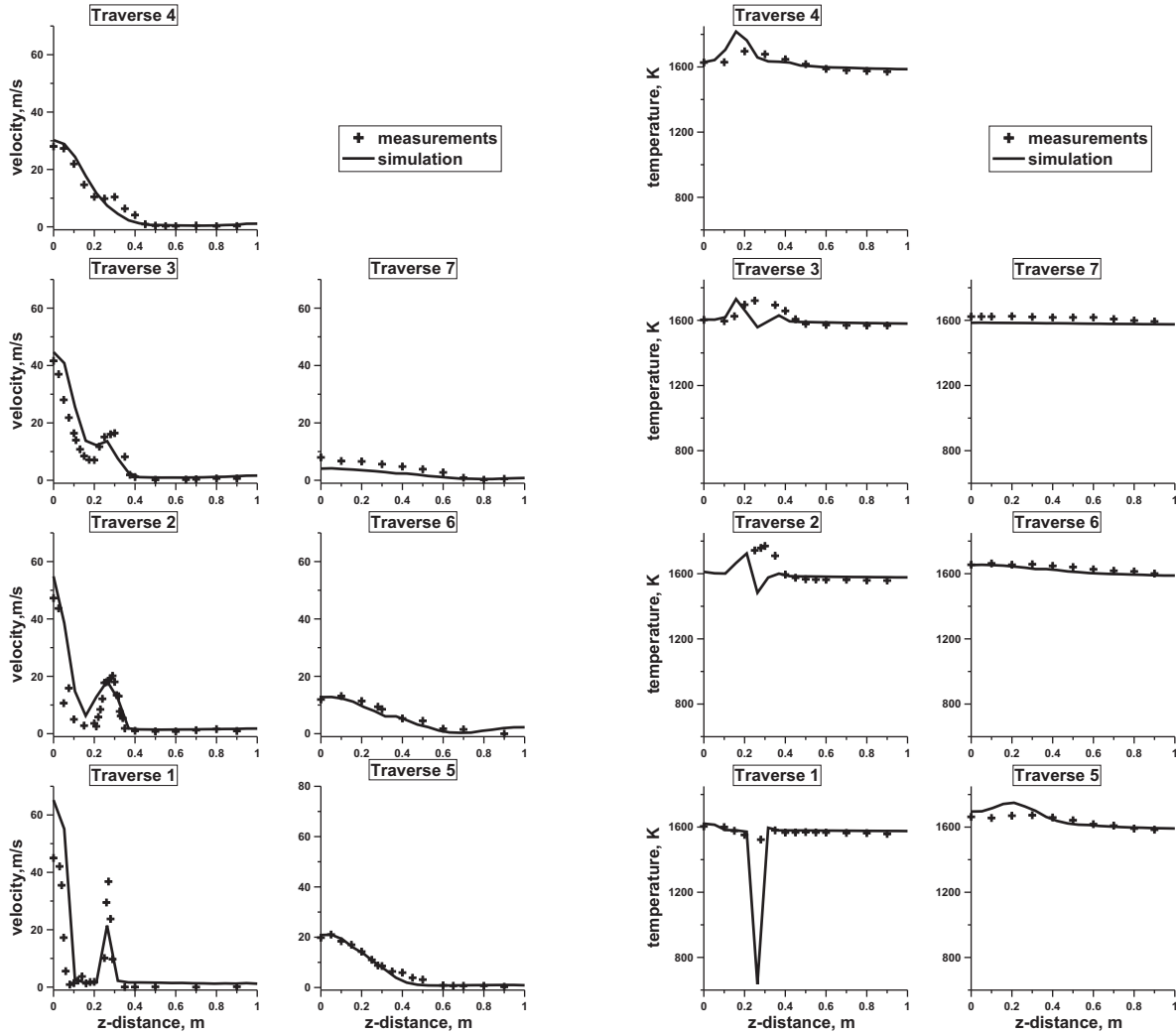
Figure 4.8: Velocity (left) and temperature (right) profiles along the measurement traverses. The measured values taken from [64]. For location of the measurement traverses see Fig. 4.7

predicted total incident heat flux at the furnace wall. Flatness and high values of the radiative heat flux are characteristics of HTAC combustion [62, 61].

4.4.4   Oxygen and carbon dioxide concentrations

In Fig. 4.11, left, the profiles of oxygen concentration are shown. No major differences between the measurements and calculated values can be observed. However, the oxygen concentrations near the coal nozzle are too low in comparison with the experimental values which is consistent with the temperature predictions in this region, see Fig. 4.8, right. It is interesting to note that the same model deficiency was already observed in numerical simulations of the natural gas combustion [61] and it was related to inaccurate predictions of the entrainment of the fuel jet [107]. Downstream of the fourth traverse the oxygen concentration is uniform and practically everywhere in the furnace
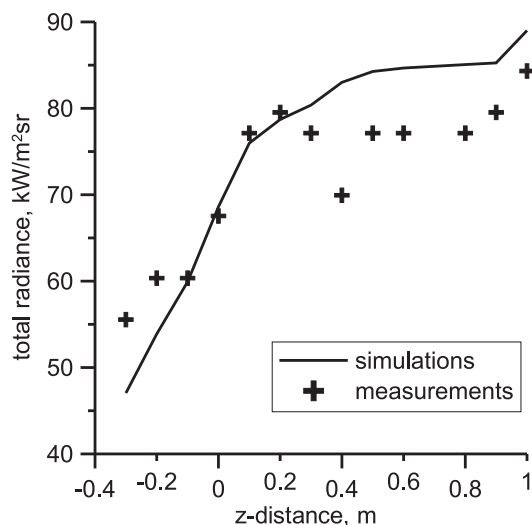
Figure 4.9: Measured [64] and calculated total radiation intensity for a=1.5 m^{-1}
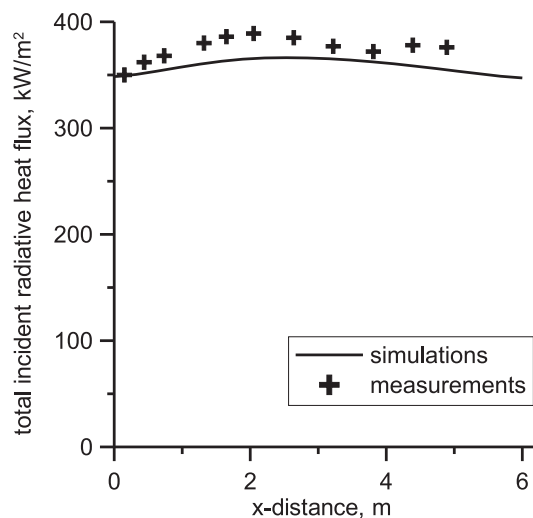
Figure 4.10: Measured [64] and calculated total incident radiative heat flux

is about 3%. Altogether, the numerical predictions of oxygen concentration and the measurements are in good agreement. Carbon dioxide profiles are given in Fig. 4.11, right. The calculated values are very close to the measured values along all traverses.

4.4.5 Carbon monoxide concentration

Carbon monoxide profiles are illustrated in Fig. 4.12, left. In our simulations carbon monoxide is generated from the combustion of volatiles only. If oxygen is available it can be further oxidized to carbon dioxide. It is formed mostly within the coal jet up to the fourth traverse. The highest concentration of CO is about 6% and it is located at the third traverse. The prediction of its peak value agrees perfectly with the measurement. Downstream of the fifth traverse no considerable amount of carbon monoxide is detectable. Although the carbon monoxide predictions are in very good agreement with the measured values, this agreement is regarded as coincidental for several reasons. The carbon monoxide is formed and oxidized in a number of sequential and parallel reactions. It is released as a component of the volatiles, as a product of the volatiles oxidation, and as a product of char combustion. The carbon monoxide is oxidized by OH radicals as well as by O radicals, although with much lower a rate. Furthermore, the water gas shift reaction alters CO concentrations. None of these processes are taken into account in our modeling. Thus, from the fundamental point of view, the works of Kim et al. [129, 130] are superior since their attempt to take these CO-involving reactions into account although the CO-predictions in Kim's simulations depart from the measured values.

Figure 4.11: Oxygen (left) and carbon dioxide (right) concentration profiles along the measurement traverses. The measured values taken from [64]. For location of the measurement traverses see Fig. 4.7

4.4.6 Volatiles concentration

The computed concentration of volatiles is plotted together with the measured concentrations of unburned hydrocarbons in Fig. 4.12, right. Obviously, the released volatile matter does not only contain hydrocarbons but also hydrogen, carbon monoxide, water vapor and tar. Thus, the predicted concentrations of volatiles exceed by far the measured concentrations of the hydrocarbons. The region where the volatiles are released is predicted to be located between the first and the fifth traverse and it agrees well with the measurements. The peak of the volatiles concentration is calculated at the second traverse. Downstream of the fifth traverse no volatiles are detectable.
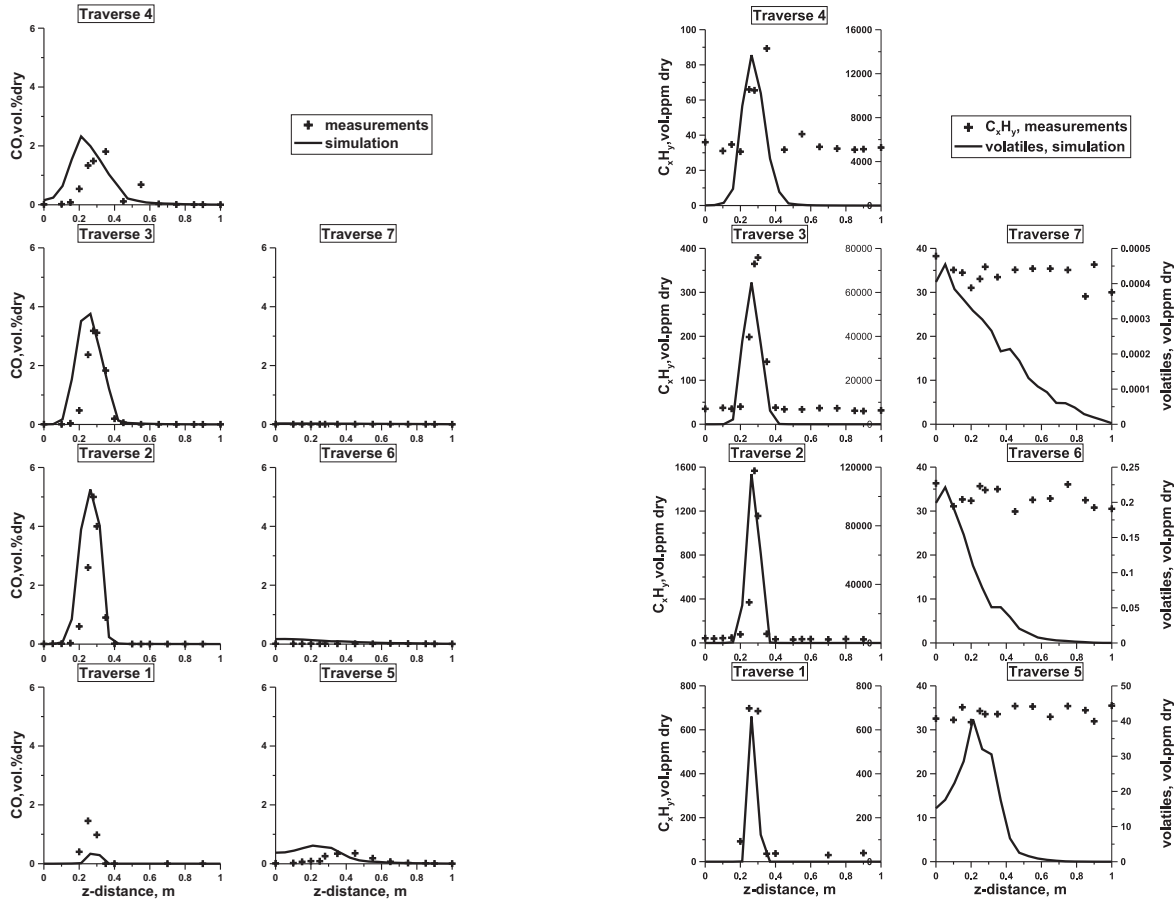
Figure 4.12: Carbon monoxide profiles (left). Measured C_xH_y concentrations and predicted concentrations of volatiles (right). The measured values taken from [64]. For location of the measurement traverses see Fig. 4.7

4.4.7 Nitric oxide concentration

Nitric oxide concentration profiles are given in Fig. 4.13, left showing that the concentrations of NO are well predicted by the model, not only qualitatively but also quantitatively. It can be observed that the NO formation begins upstream of the first traverse, however most of the NO is formed upstream of the third traverse in the volatiles released zone. At the second traverse the highest peak of 900 ppm has been measured. This peak is also well reproduced in the calculations. Downstream of the fourth traverse the nitric oxide profile is flat and of a low level (around 300 ppm). At the outlet 333 ppm NO was calculated and this value agrees very well with the measurements (320 ppm).

Among the six terms which appear in Eq. 3.116 for the net NO formation rate only the fuel-NO source (Eq. 3.95), the homogenous NO-reburning source (Eq. 3.113) and heterogenous NO-reburning source (Eq. 3.115) are significant and there are plotted in Fig. 4.13 (right). The fuel-NO source, $S_{NO,fuel}$, is of the order of $0 \div 7.8 \cdot 10^{-4} \frac{kmol}{m^3 s}$ while the homogenous NO-reburning rate, $S_{NO,hom.reburn}$, is in the range of $-2.7 \cdot 10^{-4} \div 0 \frac{kmol}{m^3 s}$
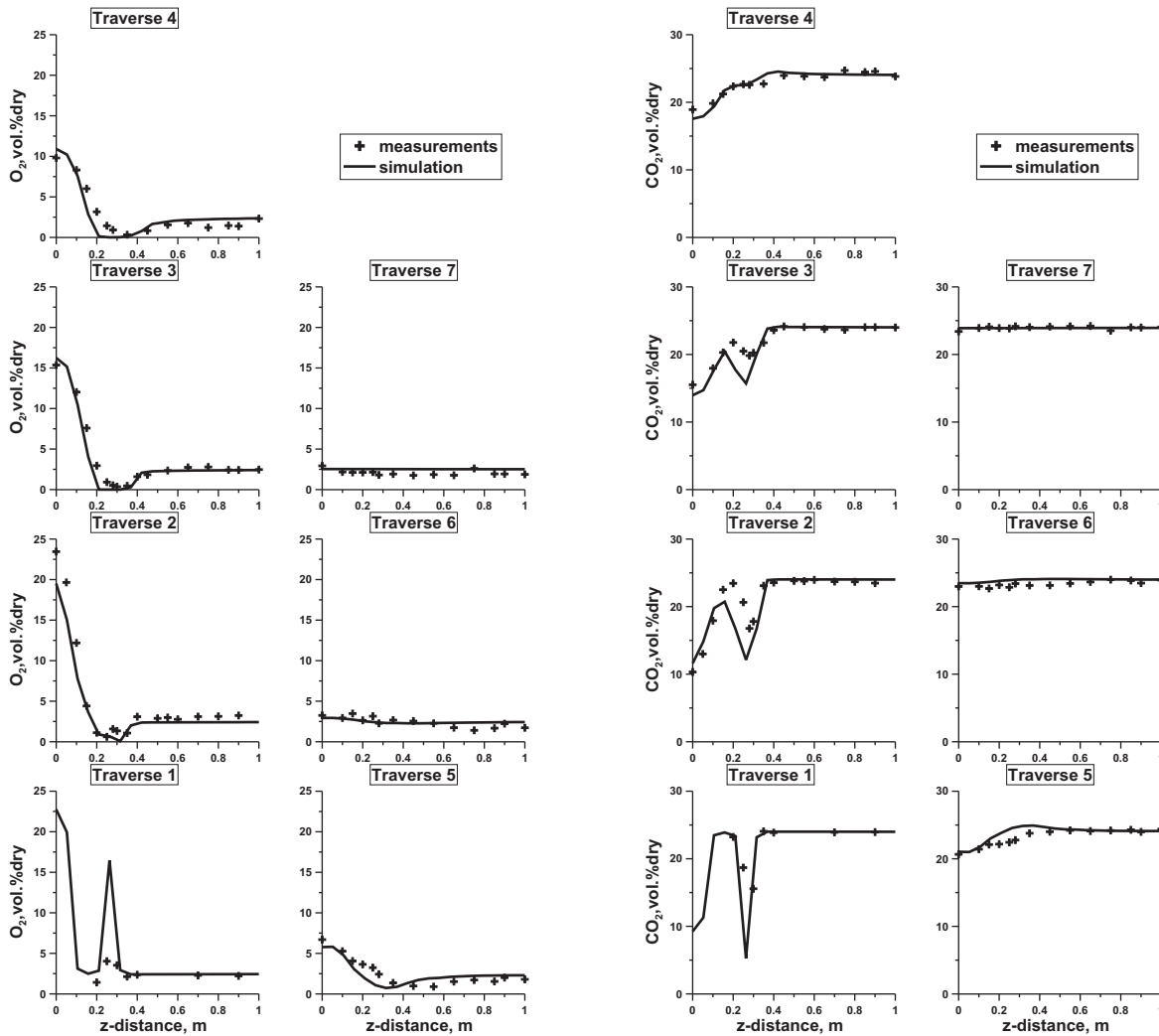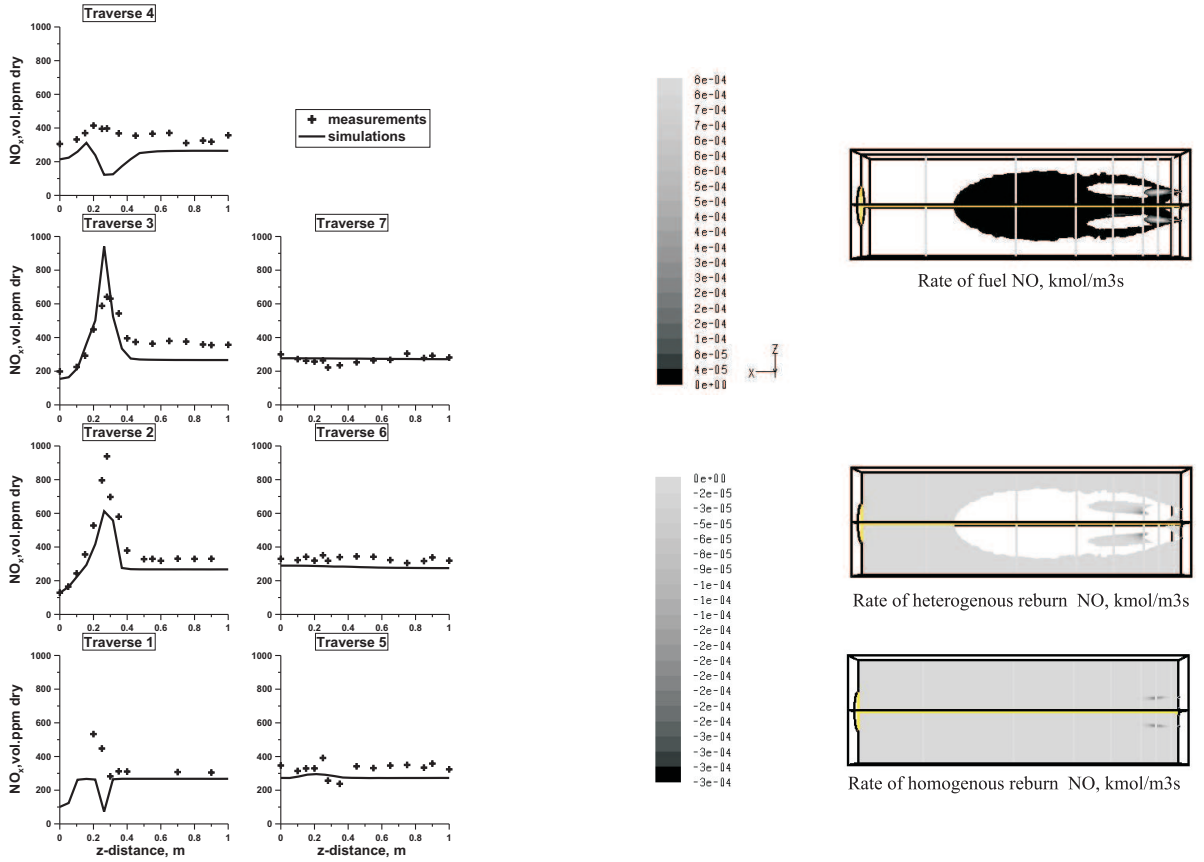
Figure 4.13: Nitric oxide (left) concentration profiles along the measurement traverses. The measured values taken from [64]. For location of the measurement traverses see Fig. 4.7. Sources in the NO balance equation (right). From the top to the bottom: $S_{NO,fuel}$-Eq. (3.95), $S_{NO,het.\ reburn}$-Eq. (3.115), $S_{NO,hom.\ reburn}$-Eq. (3.113)

and the heterogenous NO-reburning rate, $S_{NO,het.reburn}$, is in the range of $-2.0 \cdot 10^{-4} \div 0 \ \frac{kmol}{m^3 s}$. Thus, these three sources are of the same order of magnitude and the in-flame NO-concentrations are determined by their balance which is then altered due to the NO advection and diffusion. The NO post-processor predicts a rapid reburning occurring already in the fuel jet where NO is formed directly from HCN decomposition. Examining the NO predictions in the fuel jet, see Fig. 4.13, left, one can observe that the NO reburning rate seems to be over-estimated. Here is recalled that in the used model the entire volatile matter is involved in the NO-reburning (see Eqs. 3.111 and 3.112) which may be questionable. The second reason is related to the lack of oxygen in the fuel jet obtained in our predictions while in the measurements still around 2% of oxygen can be observed. The oxygen concentration affects strongly the NO-fuel formation path (see Eq. 3.92). For the sake of completeness we report that the thermal-NO source (Eq. 3.104), the prompt-NO source (Eq. 3.97) and the N_2O-NO source (Eq. 3.107) are in the range of $0 \div 6.6 \cdot 10^{-8} \ \frac{kmol}{m^3 s}$, $0 \div 1.6 \cdot 10^{-6} \ \frac{kmol}{m^3 s}$, $0 \div 4.6 \cdot 10^{-9} \ \frac{kmol}{m^3 s}$, respectively. Integration of

the NO sources over an entire furnace volume provides a further insight into the NO-mechanisms. The overall NO production rate through the fuel mechanism is calculated to be $18.5 \cdot 10^{-6} \frac{kg_{NO}}{s}$ (see Tab. 4.7). The NO reburning rate is $11.5 \cdot 10^{-6} \frac{kg_{NO}}{s}$ so that the net NO production rate in the furnace amounts to $7 \cdot 10^{-6} \frac{kg_{NO}}{s}$. The difference between the amount of the NO at the furnace exit $(11 \cdot 10^{-6} \frac{kg_{NO}}{s})$ and at the furnace inlet $(4 \cdot 10^{-6} \frac{kg_{NO}}{s})$ amounts exactly to $7 \cdot 10^{-6} \frac{kg_{NO}}{s}$. Thus, only two terms in the overall NO-balance are significant; the NO generation via the fuel mechanism and the NO reburning mechanism.

$M_{NO,in},\ \frac{kg_{NO}}{s}$	$4.0 \cdot 10^{-6}$
$M_{NO,out},\ \frac{kg_{NO}}{s}$	$-11.0 \cdot 10^{-6}$
$M_{NO,fuel},\ \frac{kg_{NO}}{s}$	$18.5 \cdot 10^{-6}$
$M_{NO,reburn},\ \frac{kg_{NO}}{s}$	$-11.5 \cdot 10^{-6}$

Table 4.7: Mass balance of NO

4.4.8 Char burnout

Fig. 4.14 shows both the measured and predicted char burnout along the centerline of the fuel jet. The char burnout predictions are in good agreement with the measured data up to 80% burnout. For higher degrees of burnout the model over-predicts the char oxidation rates and at the furnace outlet a complete burnout is predicted (see Tab. 4.8). This is a consequence of the fact that the parameters of the char combustion model have been derived using the measured data (Fig. 4.4, right) that extend up to 85% burnout. As can be seen in Fig. 4.4, right, an extrapolation of the char model predictions to residence times of 5-6 seconds results in complete burnout. In order to predict the last stages of burnout, corrections to the char model are needed to slow down the rate as the char oxidation proceeds (see for example [182, 183]).

4.4.9 Furnace outlet

The temperature, oxygen, carbon oxides and nitric oxide concentrations as well as char burnout at the outlet of the furnace for calculations and measurements are summarized in Tab. 4.8. The furnace exit temperature is very close to the measured value and the difference is about $50\ K$ which corresponds to 2.37% of the furnace thermal input.
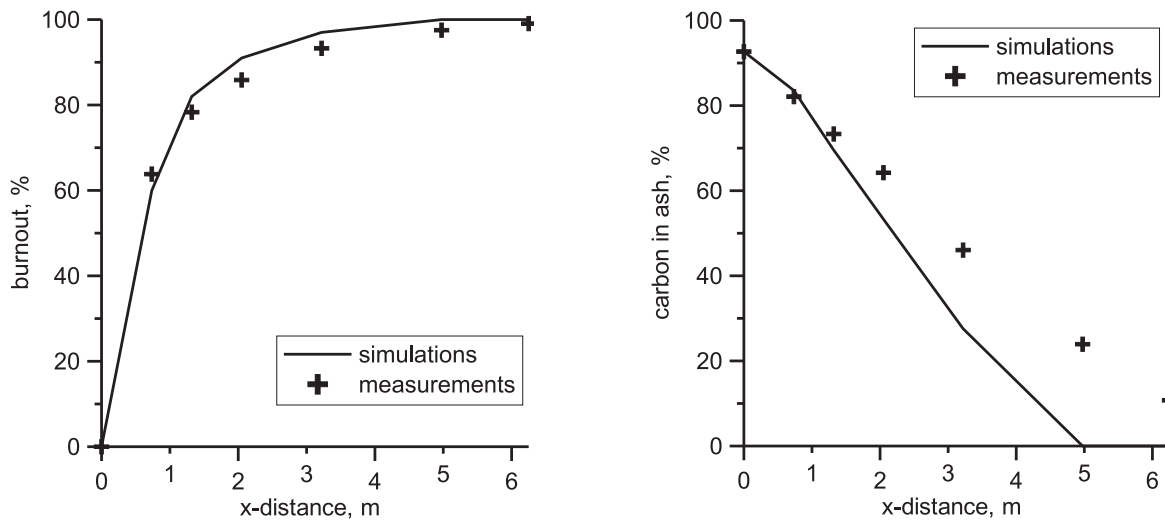
Figure 4.14: Char burnout (left) and carbon in ash (right) along the centerline of the fuel jet. The measured values taken from [64]

parameter	unit	experiment [64]	predictions, this work
T	K	1503	1555
O_2	vol. % dry	3.1	2.52
CO	vol. ppm dry	<50	10
CO_2	vol. % dry	25.50	23.93
NO_x	vol. ppm dry	320	333
Char burnout	%	99.4	100
Carbon in ash	%	14.95	none

Table 4.8: Computed and measured values at the furnace exit

4.5 Findings

The mathematical model has been validated against the IFRF experimental data in order to evaluate sub-models describing the coal combustion under HTAC conditions. It was found that the gas composition and temperature trend to be a uniform all over the furnace. The combustion is slow and takes place beyond the zone where the fuel jets are diluted by the entrainment of hot combustion products. The maximum temperature, as well as all temperature field are predicted accurately as compared with the measured values. The oxygen concentration, except in the near fuel jets region, agrees with the measured values. The carbon monoxide concentrations, although the relative simple turbulence-chemistry model (EDM) is used, are very close to the measured values.

Prior to performing the numerical simulations of HTAC 99 trials, substantial efforts have been allocated to an accurate modeling of combustion of Guasare coal which was used in the IFRF experiments. To this end both the Chemical Percolation Devolatilization (CPD) model and the char combustion intrinsic reactivity model have been tuned to represent the coal in question. To ensure accurate predictions of radiative transfer an appropriate value of the local absorption coefficient appearing in the Radiative Heat Transfer equation has been derived using the measured data. Subsequently performed numerical simulations of the HTAC 99 experiments have demonstrated that the CFD FLUENT code predicted both the in-furnace measured data and the furnace exit parameters with good accuracy. Such a validated model has then been used in the boiler design studies.

Chapter 5

Design of the HTAC boiler

HTAC combustion process is different from conventional combustion. Therefore there is a need for an innovative design of boilers utilizing this technology. Several particular boiler concepts have been analyzed in the context of the following three key points: existence of an intensive in-furnace recirculation, homogeneity of both the temperature and the chemical species fields, and uniformity of heat fluxes.

The Venezuelan bituminous Guasare coal is used as fuel in all the simulations. Its composition and parameters are reported in Tab. 4.2 and 4.3 (see Section 4.3). The set of mathematical sub-models representing combustion of this coal is given in Chapter 4. A hypothetical 130 MW_{th} ultra-supercritical boiler producing 20 $\frac{kg}{s}$ steam at parameters: pressure equal to 30 MPa and temperature up to 700 ^oC has been developed. The combustion air is preheated to 1200 K. The boiler is operated at air excess ratio of 1.2.

In this Chapter several simulations have been performed in order to find the shape of the boiler and its dimensions, to optimize both the distance between burners and location of the burner block. Results obtained by the numerical modeling of analyzed boilers are presented and discussed in the following Sections. At the end of each Section the findings are briefly summarized.

5.1   Shape of the HTAC boiler

To the best of author's knowledge, no research on HTAC technology application to power station PC boilers has been carried out, with the aim of developing a completely new configuration of the boiler (see Section for details 2.6). In this thesis a new approach is presented. In contrast to previous investigations on boilers operating under HTAC conditions, in this work it is claimed that the key point of the HTAC technology implementation in power boilers is an original construction of the entire combustion

chamber, not only the burner. Consequently, the first challenge of this part of work is to find a shape of the boiler appropriate for HTAC technology. To realize this goal, a first series of numerical calculations is performed.

Three boiler geometries shown in Fig. 5.1 have been considered. Calculations have been prepared for two-dimensional model using a structured grid in the whole computational domain.
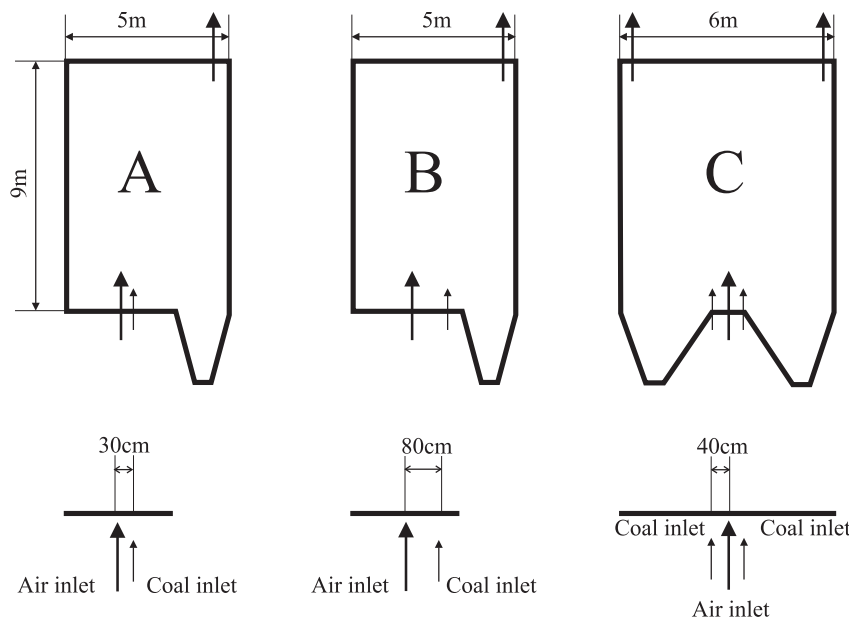
Figure 5.1: Illustration of the considered combustion chamber forms with 30 *cm* separation distance (left), with 80 *cm* separation distance (center) and symmetric configuration with 40 *cm* separation distance (right)

Each boiler is 9 *m* high and has either a 5 *m* (boiler A and B, see Fig. 5.1) or a 6 *m* (boiler C, see Fig. 5.1) width. These dimensions are chosen in order to keep the value of the firing density (ratio of thermal input to furnace volume) similar to that of the radiative section of the standard PC boilers (around 240 $\frac{kW}{m^3}$). Each boiler is equipped with one burner only. The burner is located at the bottom wall of the boiler. In boilers A and B (see Fig. 5.1), the combustion air injector is situated on the left hand side of the coal injector. These two burners differ in the distance between the air and the coal nozzles which is either 30 *cm* in boiler A or 80 *cm* in boiler B, as shown in Fig. 5.1. In boiler C (see Fig. 5.1), the burner consists of a central injector of the combustion air and two coal injectors situated on both sides of the central air injector and separated by a distance of 40 *cm*.

The shapes of boiler A and B are derived so as to resemble standard PC boilers. Design C is an original concept of the author. By examination designs A and B the

intention is to check whether in conventional PC boilers firing conditions needed for HTAC can be created. Furthermore, one examines the impact the distance between the coal and the combustion air nozzles on the in-furnace recirculation. The symmetric boiler is invented to create proper internal recirculation of the combustion products.

5.1.1 Results and discussion
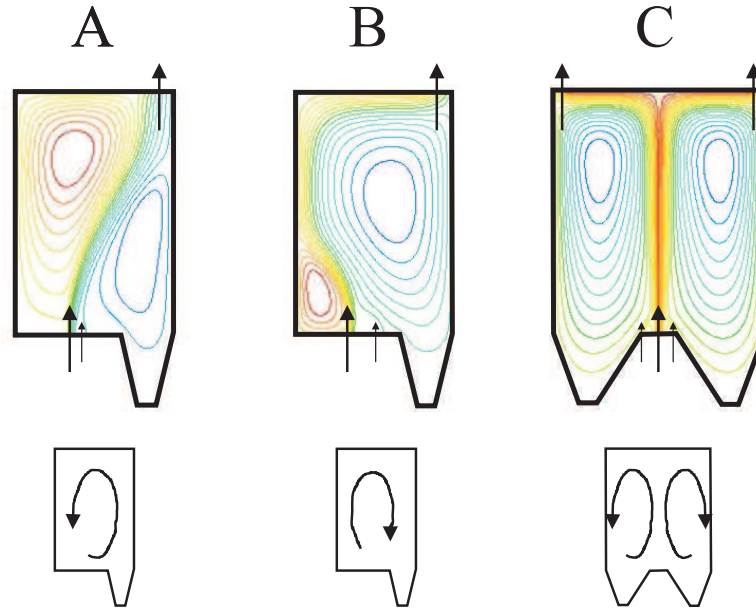
Figure 5.2: Recirculation inside the combustion chamber for A (left), B (center) and C (right) boiler designs

The recirculation patterns inside the three examined boilers are presented in Fig. 5.2. Boiler A (see Fig. 5.2, left) features a weak recirculation. The flow pattern inside this boiler rotates in the anti-clockwise direction and a substantial amount of the combustion products leaves the boiler without participating in the in-furnace recirculation zones. The flow behavior in boiler B (see Fig. 5.2, center) is different. The recirculation direction is clockwise and the path of the combustion gases is longer than inside boiler A. It can be observed that the symmetric geometry (boiler C) is the best in relation to the recirculation. This boiler design results in the most intensive recirculation and the dead zones are smaller than in the other configurations. It can be noticed that in boilers A and B the dead zones are large in volume. The whole combustion chamber volume of boiler C participates in the combustion process. It results in a good heat exchange due to uniform temperature field (see Fig. 5.3) and in a complete combustion (see Fig. 5.5).

Figure 5.3: Temperature field inside the combustion chamber for A (left), B (center) and C (right) boiler designs

Figure 5.4: Oxygen concentrations field inside the combustion chamber for A (left), B (center) and C (right) boiler designs
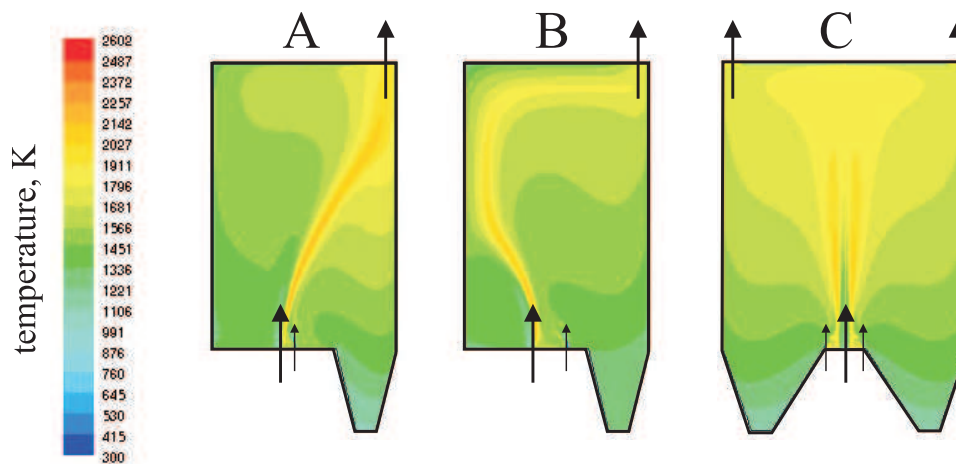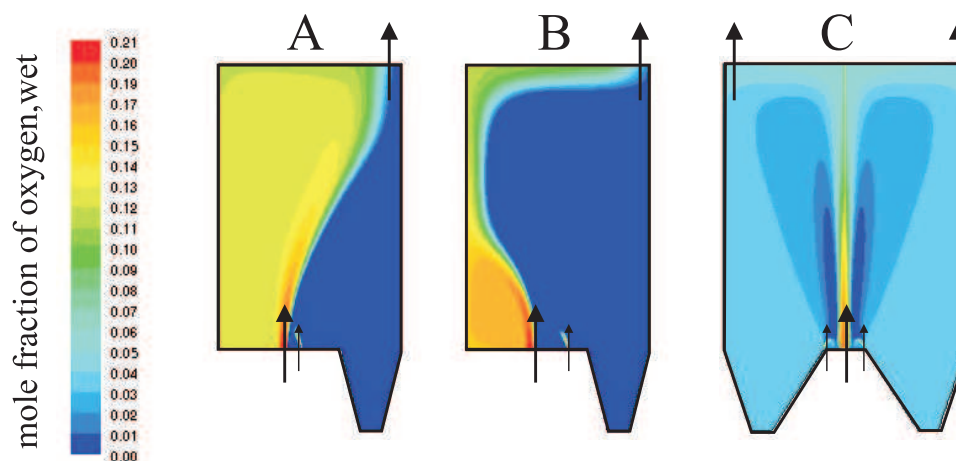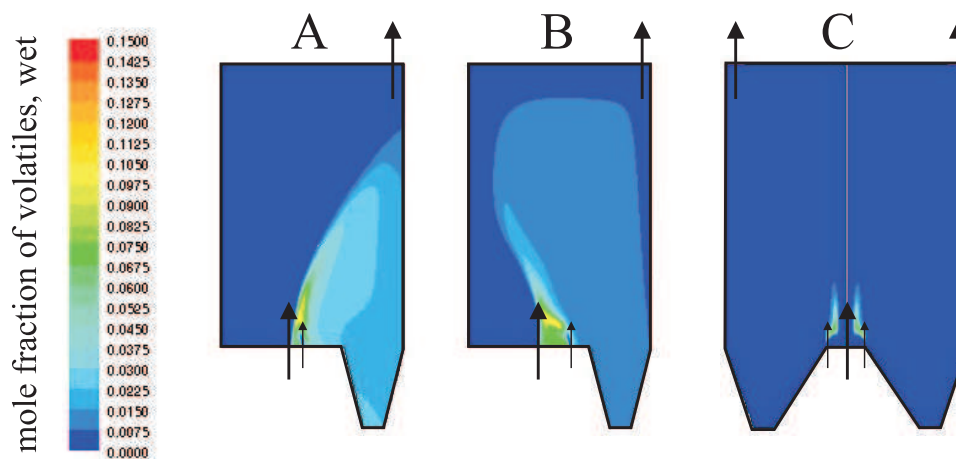

Figure 5.5: Volatiles concentrations field inside the combustion chamber for A (left), B (center) and C (right) boiler designs

HTAC technology is characterized also by the uniform temperatures in the whole combustion chamber and by low temperature peaks. These both features have been provided by the symmetric boiler geometry. In boiler C the temperature peak is the lowest (T_{max}=2106 K) among the three examined geometries (T_{max}=2602 K for boiler A, and T_{max}=2405 K for boiler B) and the temperature field is the most uniform. The impact of the distance between the fuel and the combustion air nozzles on HTAC combustion is also visible. Due to a too small distance between the air and the coal nozzles these jets mix very quickly, before the air and the fuel streams are diluted by the recirculated combustion products. It results in higher temperature values in boilers A and B than in boiler C. Due to an intense recirculation of the combustion products, the oxygen concentrations are low (about 3-5%) and homogenous inside boiler C (see Fig. 5.4). Thus, the combustion is stable and takes place in the whole volume of the boiler. In Fig. 5.5 it can be observed that volatiles are released and burned mostly in the region between the air and the fuel injectors. In this region, the oxygen values are consequently the lowest. Only in boiler C a complete burnout of the combustible gases (volatiles and CO) is achieved. At the outlet of boiler C no volatiles exist while for boilers A and B figures of 0.053% and 0.019%, respectively. The CO concentration is 0% in boiler C while in boiler A is 1.5% and in boiler B is 0.9%. The char burnout at the outlet is complete only in boiler C (100%). In boiler A the char burnout is equal to 97% and in boiler B to 99%. As a consequence, the thermal efficiency for boiler A is 20% lower, and for boiler B is 5% lower than the efficiency for boiler C. It is concluded that the best configuration has boiler C (the symmetric one).

5.1.2   Findings

This first calculation series has been performed to optimize the boiler shape for HTAC technology. Both, the geometry of the boilers and the configuration of the inlets determine the recirculation pattern and the flame stability. The intensive recirculation created in boiler C results in a more uniform temperature field, moderate oxygen concentrations, lower temperature peaks and completely burnout of the combustible gases and char. As a result of the simulations, symmetric boiler C has been found to be optimized among the three considered designs. Therefore, the symmetric boiler will be used for further investigations. This configuration is shown in Fig. 5.6.

To summarize, the optimized [1] boiler is symmetric; it is 9 m high and 6 m width. It is equipped with one burner consisting of a central injector of the combustion air issuing

---

[1]According to the New Encyclopedia Britannica (15th Edition, Vol.8, pp.972) optimization is a field of applied mathematics consisting of a collection of principles and methods used for the solution of quantified problem in many disciplines: physics, biology, engineering, economics and other. In this thesis
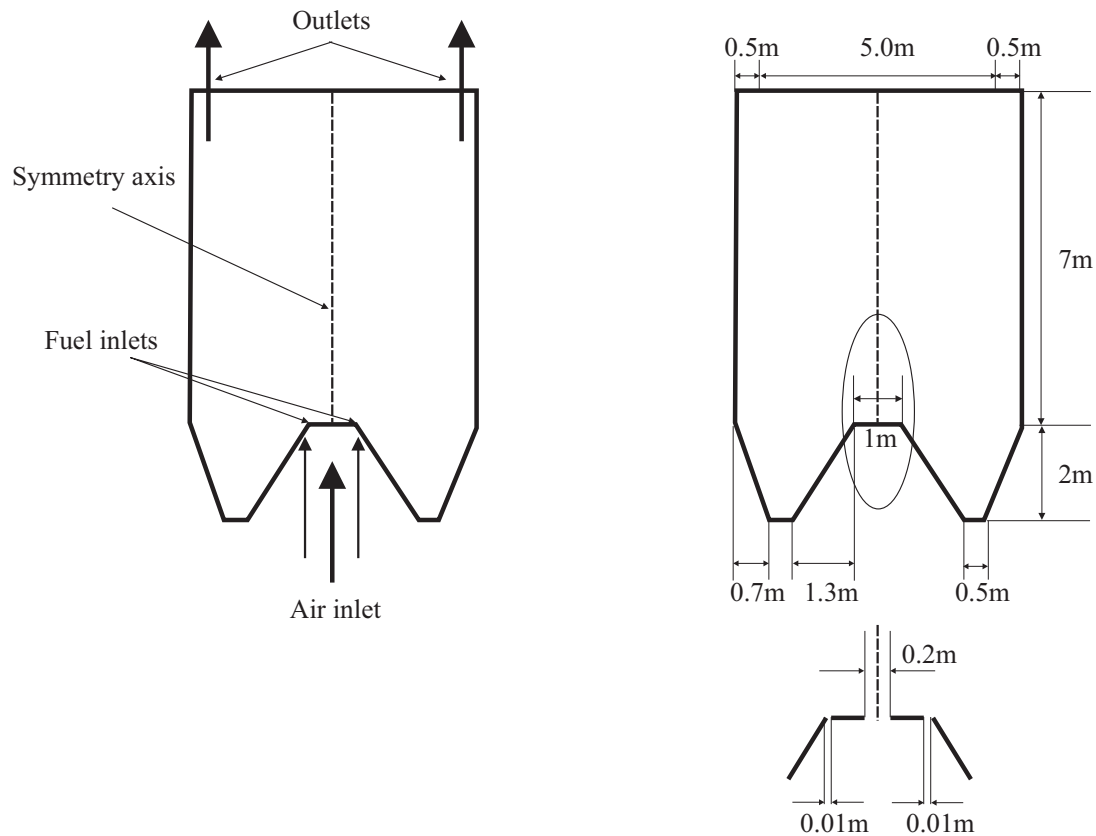
Figure 5.6: Optimized boiler shape

at a high velocity and two coal injectors. The burner is located at the bottom wall of the boiler. Two coal guns supply the fuel at 40 *cm* distance from the central air jet. This distance is important design parameter because mixing between both the fuel and the combustion air streams has to be delayed until the proper dilution of both jets with recirculated combustion products occur. The boiler outlets are positioned at the top wall of the boiler.

5.2 Distance between individual burners

Burners used in the numerical simulations presented in Section 4 resemble the NFK/IFRF design [60, 63, 64], see also Fig. 2.1. The NFK/IFRF burner has a very simple construction: there is no air staging, there is no flame stabilizer or swirl commonly used in commercial pulverized coal burners. The crucial point in the proposed burner construction is the distance between the central air nozzle and the coal nozzles. It allows

no mathematical optimization procedure is applied. The word "optimized" is therefore used in the context of a change that brings an improvement

to achieve the mixing appropriate for HTAC technology (see Section 2.4). In order to keep this mixing conditions, scaling the distance between individual burners is the key issue. On the other hand, the interrelation between the burner and the combustion chamber geometry is also important. It will be examined in this Section. An optimization of the distance between the burners and its relation to the combustion chamber is the goal of the second calculation series.
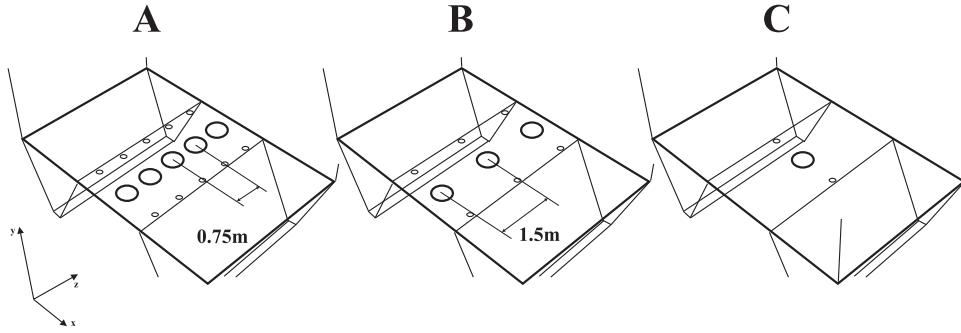
Figure 5.7: Geometry of the examined boilers: with five burners (left), with three burners (center) and with one burner (right)

The calculations have been performed using the three dimensional model with an unstructured grid in the whole domain. The geometry of the model is based on the symmetric shape of the boiler (see Fig. 5.6) found in the previous simulation series (see Section 5.1). Three different configurations of the burners are tested (see Fig. 5.7): the boiler with five burners (distance between successive burners 0.75 m), the boiler with three burners (distance between successive burners 1.5 m), and the boiler with one burner only. The thermal input of boiler A is equal to 130 MW_{th} (100%, nominal load), it means that each of the five burners is operated at 26 MW_{th}. In boiler B two burners are switched off. It results in an decrease of the thermal input to 78 MW_{th} (60% of the nominal load). In boiler C four burners are switched off and the thermal input is equal to 26 MW_{th} (20% of the nominal load). During this simulation series the boiler flexible operation (with decreasing load) is also examined. The air excess ratio is kept constant for each computational run and it is equal to 1.2.

5.2.1 Results and discussion

In this discussion considerations are given to the primary mixing which controls the dilution of both jets with combustion products and to the secondary mixing controlled by global combustion gases recirculation. For given injector velocities the primary mixing is

determined by the distance between the nozzles. The shape and dimensions of the whole combustion chamber determine the secondary mixing.
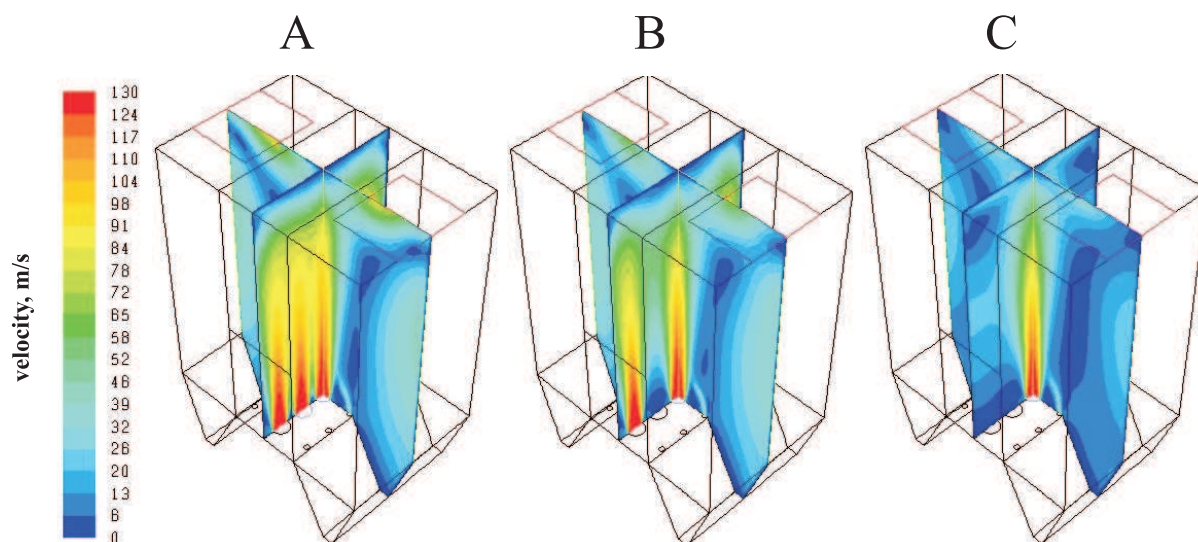
Figure 5.8: Velocity field inside the boiler operated with five burners (left), three burners (center) and one burner (right)
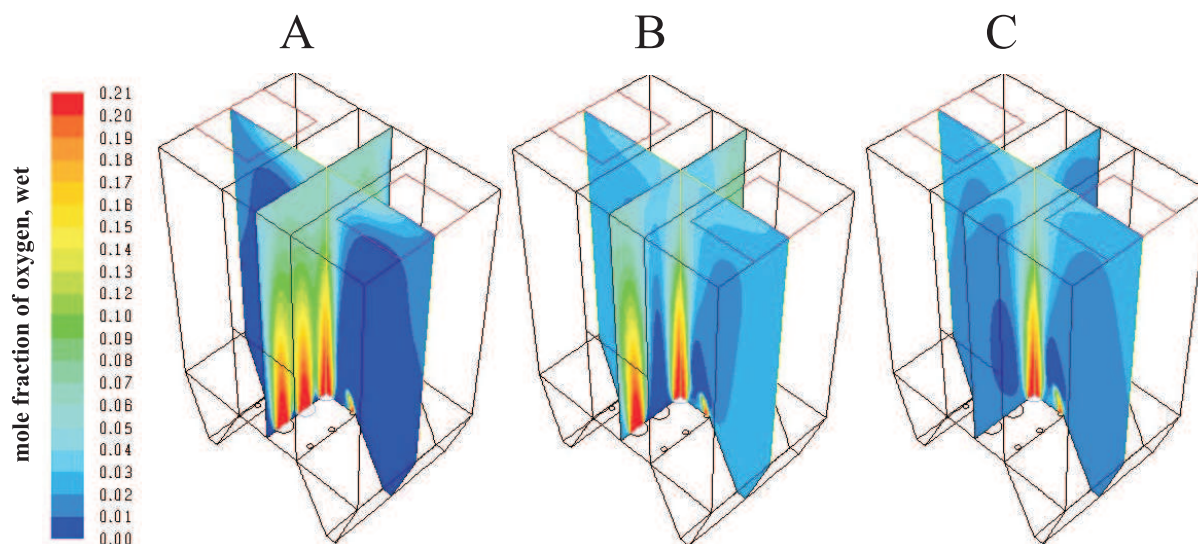
Figure 5.9: Oxygen concentration field inside the boiler operated with five burners (left), three burners (center) and one burner (right)

In Fig. 5.8 the velocity fields inside the considered boilers are shown. In boilers A (Fig. 5.8, left) and B (Fig. 5.8, center) very intense recirculation of the combustion products can be observed. The velocity fields obtained in boilers A and B are qualitatively very similar. The biggest difference occurs when the boiler is equipped with one burner (Fig. 5.8, right). Only one burner in the combustion chamber is not able to create an

intense mixing conditions. There are several regions where there is almost no movement (the velocity is zero) and the insufficient mixing of the combustion products inside the chamber occurs. As a consequence, the uniformity of both the temperature and the species concentration fields disappear (see Fig. 5.9, right).

Although in boilers A and B the global recirculation works correctly, problems with the air and fuel streams dilution (and subsequently with the low and uniform oxygen concentration) seem to occur. In boiler A there is not enough space between the neighboring burners to ensure the correct dilution of both the air and the fuel streams with combustion products in y-symmetry plane. The entrainment works correctly only in the x-symmetry (due to a sufficient separation between the air and coal nozzles). In the considered boiler, y-symmetry plane cuts through the combustion air inlets, and x-symmetry plane cuts through the central burner, perpendicularly to the y-symmetry plane. The oxygen concentration fields are presented in Fig. 5.9. The oxygen concentrations in boiler A are in some regions near zero and in some regions around 12%. These are too large variations as for HTAC technology. As mentioned above, the desired oxygen concentration in HTAC combustion process is about 3-5% in the whole chamber. This substantial non-uniformity in the oxygen concentration of boiler A makes this design unsuitable for HTAC.

5.2.2 Findings

The second calculation series has been carried out in order to optimize distance between single burners. This distance affects the mixing conditions inside the boiler, especially of the air and the fuel jets dilution with the combustion products. The single burner boiler produces unsatisfactory global recirculation while the boiler with five burners features wrong entrainment conditions. Therefore for further investigations the burner spacing of 1.5 m is chosen and five burners are still used in order to keep the assumed thermal input of 130 MW_{th}. This arrangement results in an increase of the boiler depth up to 6 m. Summarizing, as a result of these calculations the optimized distance between successive burners was found and it will be used in the forthcoming simulations.

The performance of the HTAC boiler under partially load conditions has been also examined. Operation with varies loads is very important for power station boilers because of the continuously changing demand for steam. It would be optimal if the boiler could rapidly responde to variations in power demand. In the present simulation series three values of the load were tested: 130 MW_{th}- the nominal load (100%), 78 MW_{th}- 60% of the nominal load and 26 MW_{th}- 20% of the nominal load. The conclusion is that the HTAC

boiler works stable with the load decreasing to about 20% of maximal load. It means that the proposed boiler is very flexible in comparison with the standard PC boilers that usually operate in the 60-100% nominal load range [12].

5.3   Location of the burner block

A boiler can be designed with the burner block positioned either at the top of the boiler or at the bottom. These configurations are called down- and up-fired, respectively. In the up-fired boiler the combustion substrates (air and fuel) are delivered at the bottom and the flame (combustion) direction is upwards. In the down-fired boiler the opposite is applicable. The standard PC boilers are usually designed as the up-fired boilers with the burners located at a side wall. In Section 5.1 and 5.2 only up-fired boiler construction was considered with the burner located at the bottom wall. PC boilers typically experience slagging/fouling problems. The risk of the ash overhang downfall exists in the pulverized coal boilers. These overhangs can weight from few hounders kilograms up to few tons in the standard PC boiler and their downfall could destroy completely the burner block. In order to avoid this situation the down-fired configuration was taken into the consideration. In the third calculation series down-fired configuration of the HTAC boiler has been tested and compared with the up-fired design.
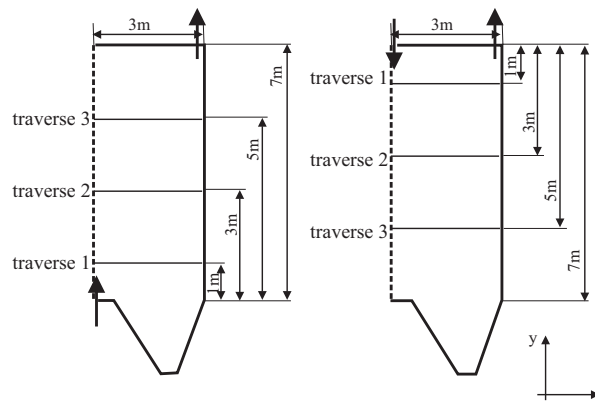
Figure 5.10: Geometry and position of the traverses inside the up-fired boiler (left) and down-fired boilers (right)

The calculations have been performed using a two-dimensional model meshed with fully structured grids. Identical geometry of the combustion chamber and the same burner construction were used in both computational runs (for details see Fig. 5.6). The boiler has 130 MW_{th} thermal input and it is operated at the air excess ratio equal to 1.2. Two different burner locations are examined: at the bottom wall- corresponding to an up-fired

boiler, Fig. 5.10, left and at the top wall- corresponding to an down-fired boiler, Fig. 5.10, right. To facilitate a comparison the predictions are plotted along three traverses located at the distance 1, 3, 5 m downstream of the burner, as shown in Fig. 5.10.

5.3.1   Results and discussion

In Fig. 5.11 the recirculation of the combustion products inside the boiler is illustrated. It can be seen that in the up-fired configuration the circulated gas has a shorter path between the inlets and the outlets. It results in a shorter residence time (average 1.78 s) of the gas in the up-fired boiler than in the down-fired boiler (average 3.97 s). Further, in the up-fired boiler some combustion products leave through the outlets without being recirculated in the combustion chamber. This adversely affects the heat transfer and the outlet temperature of the flue gas in the up-fired boiler is around 200 K higher than in the down-fired one. The longer residence time of the combustion products together with an intensive in-furnace recirculation increase the heat exchange in the boiler. Consequently at the same thermal input, more heat can be transferred to the steam in the down-fired boiler than in the up-fired one. The thermal efficiency of the down-fired boiler is 7% higher than of the up-fired one.
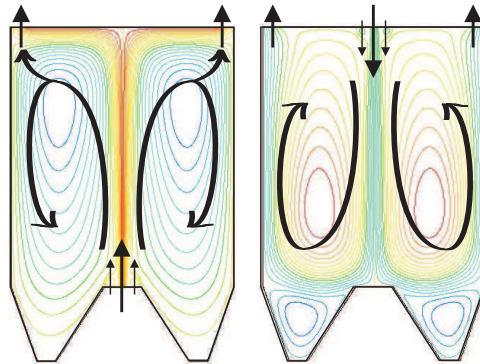
Figure 5.11: Recirculation inside the up-fired boiler (left) and down-fired boiler (right)

The results of the numerical simulation are plotted as profiles along traverses 1, 2 and 3 in Fig. 5.10. In Fig. 5.12, left, the y-velocity profiles are plotted. Negative values of the velocity indicate a recirculating stream. In the down-fired boiler the amount of the recirculating combustion products is larger than in the up-fired boiler. It is so since the substantial part of the hot combustion products leaves the up-fired boiler and does not recirculate. In Fig. 5.12, right, the temperature profiles along traverses 1, 2 and 3 are shown. It can be noticed that the temperatures in the down-fired boiler are higher than in the up-fired one. In the down-fired configuration hotter combustion product

are entrained into the fresh reactants jets than in the up-fired configuration. In the down-fired boiler the coldest gas near the walls leaves the boiler. Most of the still hot combustion products recirculates back to the furnace. Thus, the temperature of the down-fired configuration is lower.
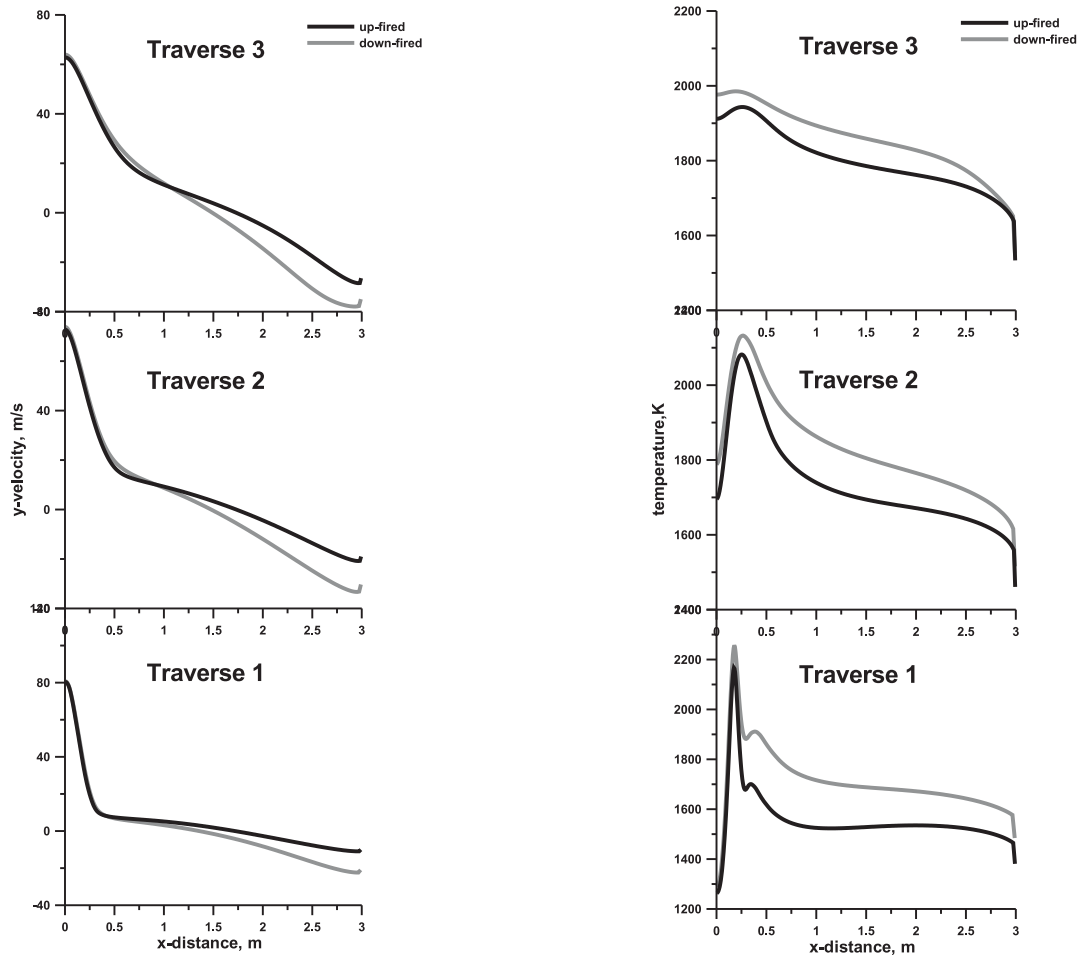
Figure 5.12: Velocity (left) and temperature (right) profiles along traverses; comparison of the up- (black line) and down-fired (grey line) boilers

In Fig. 5.13, the heat fluxes along the height of the up- and down-fired boilers are plotted. It can be noticed that the heat fluxes are more uniform for the down-fired configuration than for the up-fired one. The range of the total heat fluxes along the height of the up-fired boiler is between 120 and 400 $\frac{kW}{m^2}$ and for the down-fired between 250 and 310 $\frac{kW}{m^2}$. Almost constant value of the heat flux along the boiler walls is a feature of HTAC technology and this is also an advantage because of the required steel quality. The obtained higher maximum temperature (and at the same time high heat fluxes) demand expensive materials. Both, the up- and down-fired solution have similar mean heat flux; 250 $\frac{kW}{m^2}$ for up-fired, and 280 $\frac{kW}{m^2}$ for down-fired. However, they differ in the maximum heat flux values; for the up-fired configuration the temperature peak (and at the same time the heat fluxes) is significantly higher than for the down-fired configuration. This peak values demand a high quality steel.
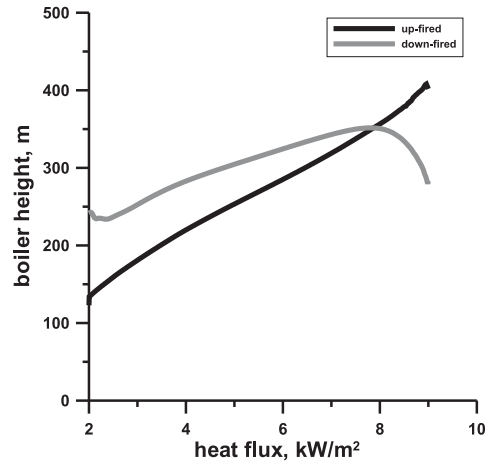
Figure 5.13: Heat fluxes along the height of the boiler; up-fired (black line) and down-fired (grey line) boilers

5.3.2 Findings

The down-fired boiler configuration has been tested in the third calculation series. Several advantages of the down-fired boiler have been identified; the recirculation path is longer resulting in an intensified heat transfer. So, lower flue gas temperatures are observed. Furthermore, the down-fired configuration features more uniform heat fluxes. Therefore, the down-fired configuration has been selected for further investigations.

5.4   Dimensions of the HTAC boiler

One of the most important advantages of HTAC applications are high heat fluxes. In a standard PC boiler these are around 150 $\frac{kW}{m^3}$ with the peak value up to 450 $\frac{kW}{m^3}$ [13]. For the whole volume of the HTAC combustion chambers a figure of 300$\frac{kW}{m^3}$ is applicable. This high heat fluxes allows to build HTAC combustion chambers very compact so the investment capital can be lowered. In order to keep high values of the heat fluxes in the HTAC boiler, the dimensions of the combustion chamber need to be scaled. On the other hand, the combustion chamber has to be big enough to ensure an efficient heat exchange between the combustion products inside the chamber and the medium inside the tubes. In order to optimize dimensions of the combustion chamber a fourth series of the simulations has been performed.

This series of calculations has been performed using the three-dimensional model with an unstructured grid in the whole domain. Three different dimensions sets are tested and they are called as the small boiler, the medium size boiler and the large boiler, as shown in Fig. 5.15.
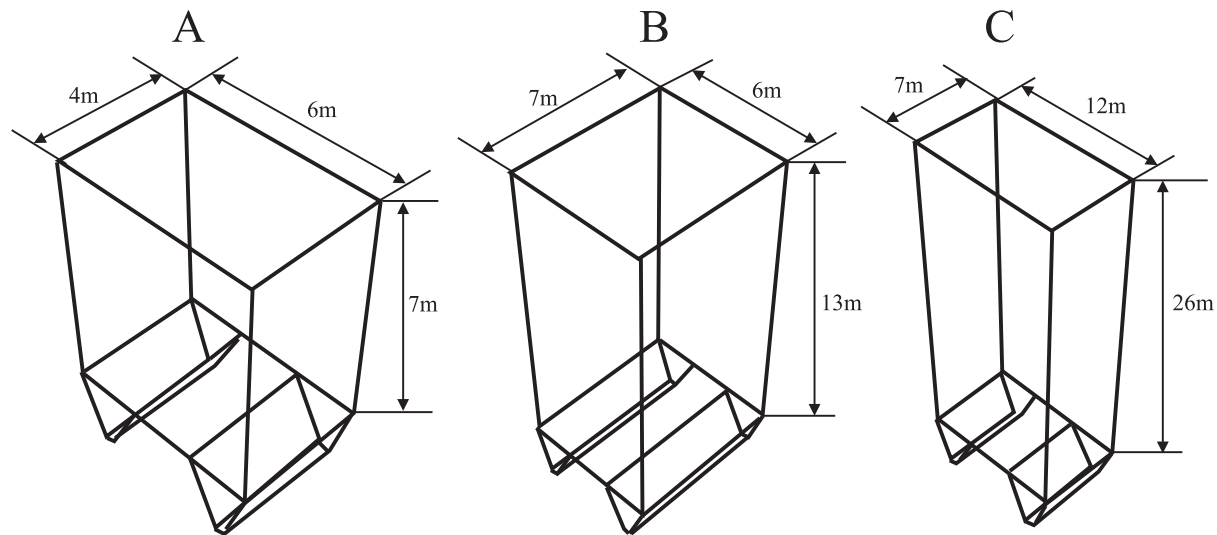
Figure 5.14: Geometry of the examined boilers: small boiler (left), medium size boiler (center) and large boiler (right)

5.4.1   Results and discussion

The attention is focused on the heat exchange in the considered three boilers. Thermal input is kept constant for each computational runs and it is equal to 130 MW.

The firing density together with the combustion chamber dimensions and the volume are listed in Tab. 5.1.

Obviously the highest firing density of 770 $\frac{kW}{m^3}$ corresponds to boiler A. In this boiler the thermal input is too high in comparison with the boiler volume and the energy released during the combustion cannot be utilized. It could result in a too high temperature of the flue gas and at the same time, a high physical outlet loss. On the other hand, the firing density of boiler C is very low (60 $\frac{kW}{m^3}$). It means that the combustion chamber is too big and some of the boiler heat transfer areas are not efficiently used. The firing density of boiler B (240 $\frac{kW}{m^3}$) seems to be the best one. It is significantly higher than in a typical PC boiler.

type	unit	boiler A	boiler B	boiler C
x-length	m	6	6	12
y-length	m	4	7	7
z-length	m	7	13	26
Volume	m^3	168	546	2184
Firing density	$\frac{kW}{m^3}$	770	240	60

Table 5.1: Boiler dimensions and firing density
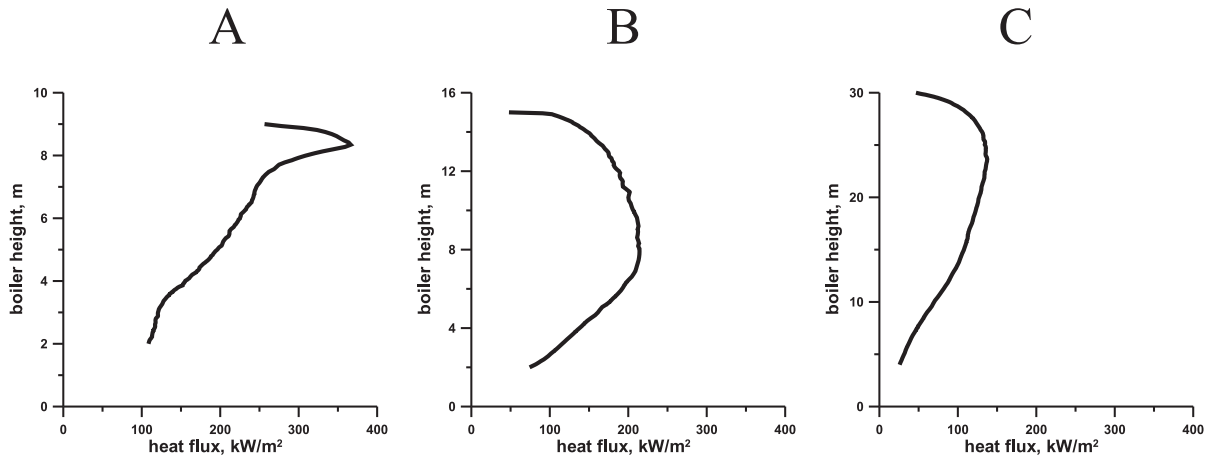
Figure 5.15: Heat fluxes along height of the boilers: small (left), medium (center) and large (right) boiler

The heat fluxes along the height of the boiler for three investigated boilers are shown in Fig. 5.15. The heat is transferred to the water/steam mixture and the boiler geometry should be large enough to ensure a high efficiency of this process. The feature of HTAC technology is homogenous heat fluxes along the whole chamber. It can be seen in Fig. 5.15 that the most uniform heat fluxes profile is for boiler B. Boiler A is too short

and the high temperatures region occurs at the top part of this boiler. It results in the high enthalpy of the flue gas and a decrease of the boiler efficiency. In boiler C the values of heat fluxes are uniform but two times lower than in the medium size boiler. Extremely low value of the firing density and the low heat fluxes show that this boiler is too big.

5.4.2 Findings

The fourth calculation series has been carried out in order to find the combustion chamber dimensions which can, on one hand, ensure an efficient heat exchange between the combustion products and water/steam mixture and on the other hand, provide a high value of the firing density. Medium size boiler (boiler B) is chosen for further investigations.

Chapter 6

Final HTAC boiler design

The investigations presented in Chapter 5 have been carried out to determine the final geometry of the combustion chamber, the configuration of the burners, the location of the burner block as well as the dimensions of the boiler. Obviously the find design incorporates findings of the previous Chapter. In this Chapter details of the final boiler design, as well as its operating and boundary conditions are presented. Again the recirculation, the temperature and the chemical species concentration fields, as well as coal particles behavior and heat transfer are analyzed.

The simulation has been performed for the three-dimensional model meshed with an unstructured grid. Since the boiler is symmetric in two directions the calculations have been performed for a quarter of the domain only. The boiler is 13 m high and has 7 m times 6 m cross section, see Fig. 6.1. It is equipped with a burner block that consists of 5 identical burners located at the top wall thus the boiler is down-fired. The flue gas outlets are also located at the top wall of the boiler and they are symmetrically positioned on both sides of the burner block. The outlets have a quadrate form with lateral length of 1 m. The advantage is that the outlets are located near the burner block and the eventual heat exchanger between flue gas and combustion air could be built there. Each of five burners is equipped with a central injector of the hot air and two coal guns positioned on both sides of the air injector. Pulverized coal is introduced into the furnace by nozzles of 15 mm diameter and the combustion air with nozzles of 48 mm. The boiler is equipped with two ash hoppers. This specific boiler design, derived in Chapter 5, realizes HTAC technology. The details of the boiler construction are given in Fig. 6.1.
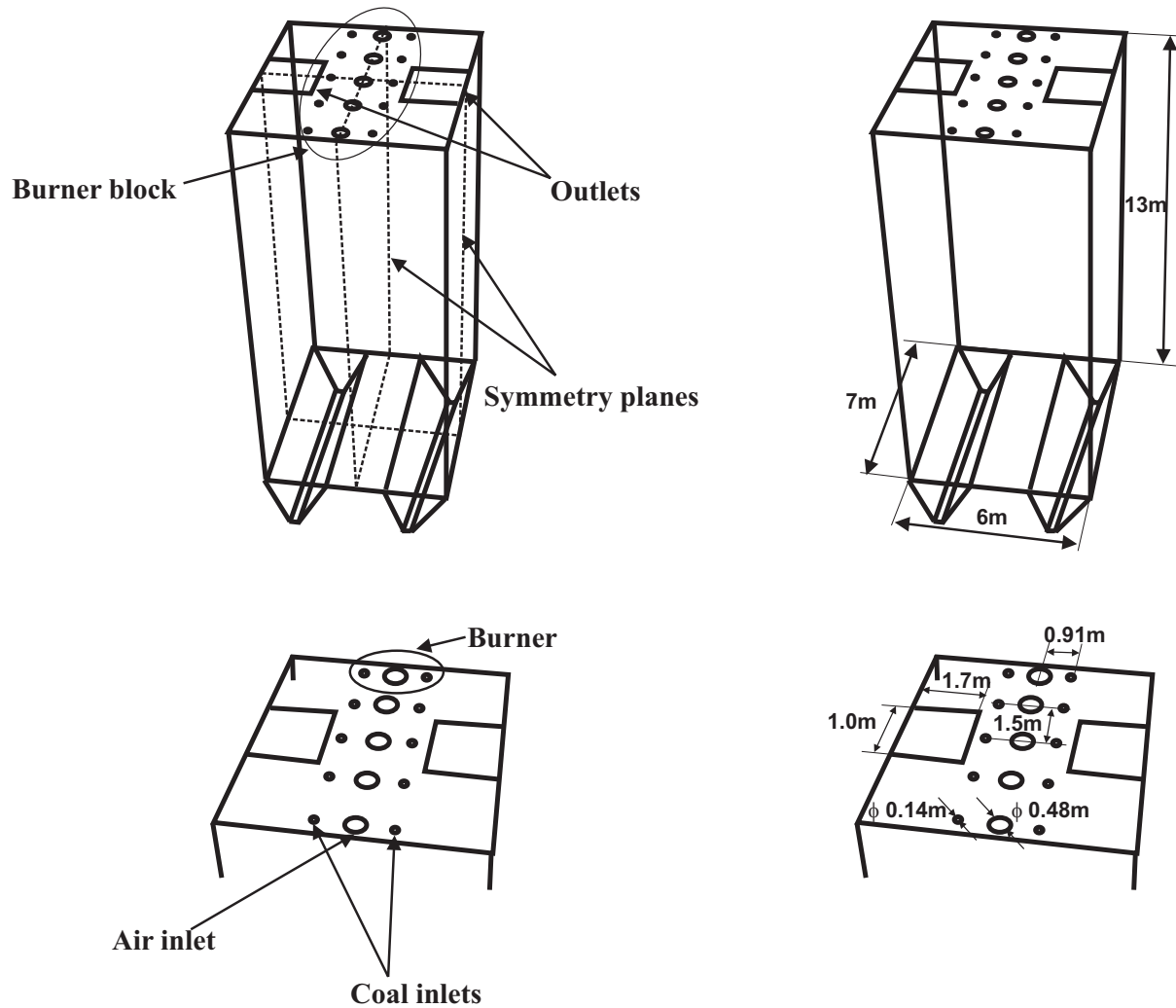
Figure 6.1: Final geometry of the HTAC boiler

The combustion air is preheated to 1200 K and the coal together with its transport air is supplied at ambient temperature (300 K). The combustion air should be heated using the enthalpy of the flue gas. However, a practical realization of such a heat exchanger is a very challenging task since it is very difficult to design heat exchangers operating with dusty flue gas at such a high temperature. The feeding rate of coal is 3.2 $\frac{kg}{s}$, and of its transport air almost twice as high (6.3 $\frac{kg}{s}$). The mass flow of combustion air is equal to 33.1 $\frac{kg}{s}$. The air jet is supplied at a high velocity (120 $\frac{m}{s}$) and coal jet has the velocity of 30 $\frac{m}{s}$. Such a high momentum of the main air flow is needed to create HTAC mixing conditions. The boiler is operated at 130 MW total thermal input. The fuel thermal input is equal to 100 MW so each burner operates at 20 MW fuel power. The already described boiler operating conditions are presented in Fig. 6.2.
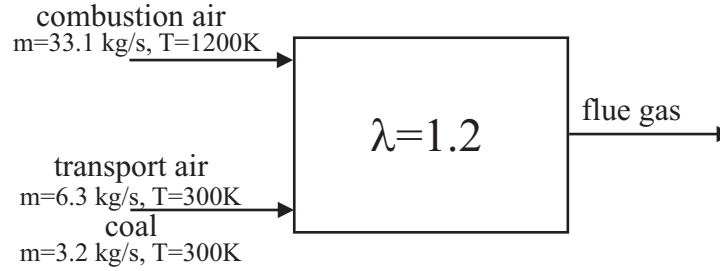
Figure 6.2: Operating conditions of the HTAC boiler

Both the combustion and the transport air streams contain 23% (by mass) oxygen and 77% (by mass) nitrogen. The wall emissivity is estimated to be 0.6 since this is a typical value for boiler tube steels. The wall temperature is constant in the final boiler design calculations and it is equal to 800 K. However, more detailed simulations to calculate the temperature profile along the boiler walls are performed in Chapter 10. The boundary conditions specified for the simulations of the final boiler design are summarized in Tab. 6.1.

name	type	numb.	settings
Combustion air inlet	mass flow inlet	5	$wt_{O_2} = 0.23$, $\dot{m} = 4.8\frac{kg}{s}$, $T = 1200K$
Transport air inlet	mass flow inlet	10	$wt_{O_2} = 0.23$, $\dot{m} = 0.8\frac{kg}{s}$, $T = 300K$
Coal inlet	injection	10	$\dot{m} = 0.4\frac{kg}{s}$, $w = 30\frac{m}{s}$, $T = 300K$
Outlet	outflow	2	$\varepsilon = 0.6$, $T_{rad} = 1200K$
Walls	wall		$\varepsilon = 0.6$, $T = 800K$

Table 6.1: Boundary conditions of the boiler simulation

6.1 Results and discussion

6.1.1 Velocity and recirculation

An intense recirculation in the combustion chamber plays an important role in HTAC technology. This recirculation affects in the combustion air and the fuel dilution with combustion products before both the air and fuel jets merge together. Furthermore, an intense recirculation generates uniform temperature and chemical species concentration fields.

Three different views of the velocity field inside the boiler are shown in Fig. 6.4 in order to give a good overview of the recirculation behavior. The combustion air is supplied through nozzles separated from the fuel (coal) injection position. This separation distance between the air and the fuel inlets is an important design parameter in the context of generating a correct flow field with an intensive recirculation and proper entrainment. It can be noticed that the boiler design leads to very intensive recirculation and the dead zones are small thus, the whole volume of the chamber participates in the combustion process. This flow pattern results in a high heat transfer rate and additionally, in uniform temperature fields and complete combustion. Moreover, problems related to the coal ignition should be reduced.
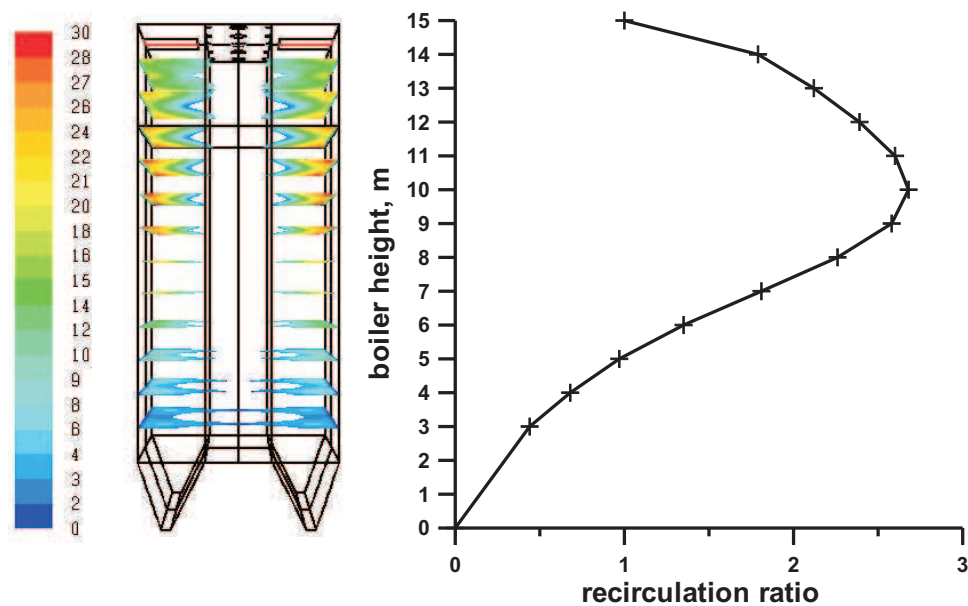
Figure 6.3: Recirculation contours in the successive planes (left), and graph of the recirculation ratio along the boiler height (right)

To quantify the recirculation a recirculation ratio, denoted as r, is introduced and this is a ratio between the mass recirculated and the total mass entering the boiler. The plains where the mass flow integration is performed are shown in Fig. 6.3, left. The distance between successive planes is equal to 1 m. In Fig. 6.3, right, the results of each integration are plotted. It can be observed that the maximum mass recirculated is 2.6 times larger than the mass flow rate into the boiler. This is a typical value achieved in HTAC technology. The maximum recirculation can be observed at the 5 m distance downstream of the burner wall. The whole volume of the boiler takes part in the recirculation of the combustion gas; although the lower part (ash hoppers) with a rather low intensity.

6.1.2 Temperature

The whole boiler is filled up with combustion products in a 1600-2000 K temperature range, as shown in Fig. 6.5. The peak temperature is suppressed in comparison with conventional combustion using so high preheated air, and it is around 2100 K. The furnace exit temperature is around 1400 K and the furnace exit gas has a substantial amount of enthalpy (see Tab. 6.2). This enthalpy must be recovered in a heat exchanger and utilized to preheat the combustion air. It should be realized that designing such a heat exchanger would require pushing the existing engineering practice to the limit. The energy balance components for the proposed boiler are listed in Tab. 6.2.

T_{inn}, K	$\dot{H}_{inn}, MW$	T_{out}, K	$\dot{H}_{out}, MW$	$\dot{Q}, MW$
1200	130	1400	65	65

Table 6.2: Components of the boiler energy balance

Summarizing, the total thermal enthalpy supplied to the boiler is equal to 130 MW. The enthalpy of the exhaust gas is equal to 65 MW so 65 MW is transferred to the steam. Thus, the boiler thermal efficiency is only 50%. However, in this work it is assumed that the enthalpy of exhaust gas is used to preheat the combustion air in an external heat exchanger.

6.1.3 Oxygen concentration

The oxygen field is also uniform and on average its concentration in almost the entire boiler is in a range of 3-5% vol. which is lower than in a conventional boiler. The oxygen concentration drops to almost zero in the coal devolatilization region. The oxygen concentration in flue gas is 3.4%. This uniform and low oxygen concentrations affect reducing temperature peaks.
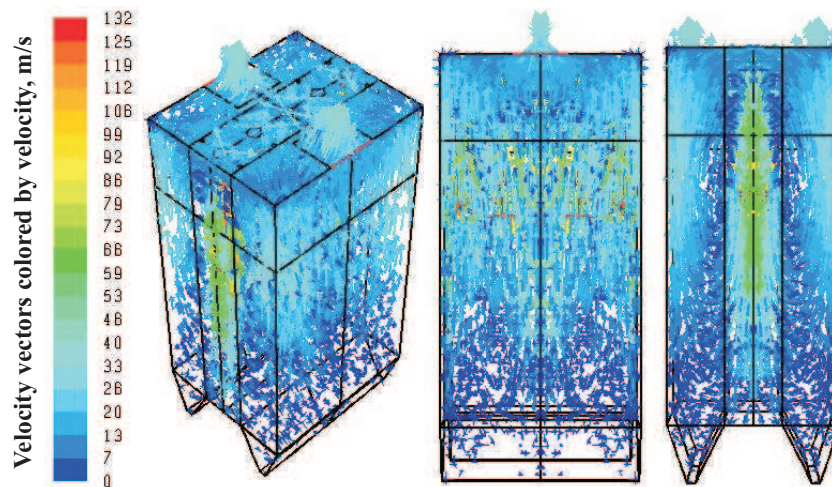
Figure 6.4: Velocity vectors inside the HTAC boiler: isometric (left), side (center) and front (right) views
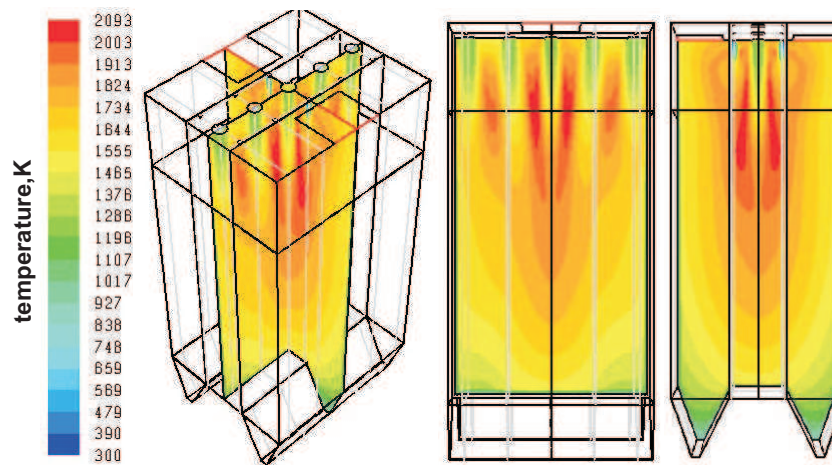
Figure 6.5: Temperature fields inside the HTAC boiler: isometric (left), side (center) and front (right) views
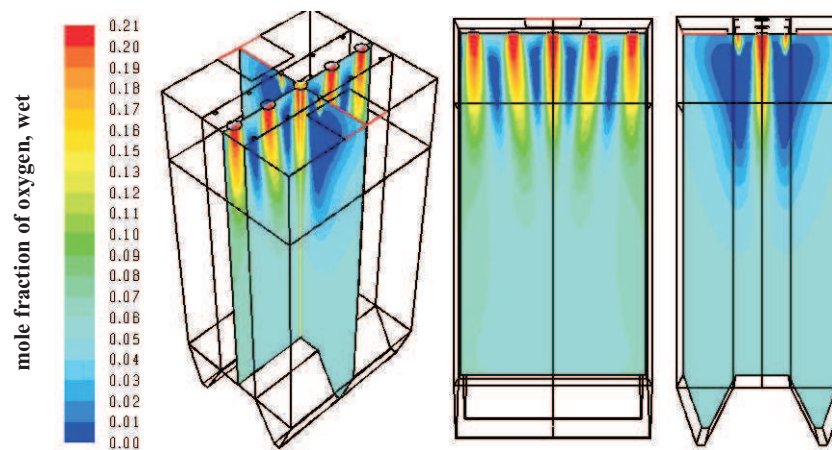
Figure 6.6: Oxygen concentration fields inside the HTAC boiler: isometric (left), side (center) and front (right) views

6.1.4 Coal particles behavior

Coal particle trajectories colored by the stage of the coal combustion process are shown in Fig. 6.7. The successive stages of the coal combustion are listed below:

- Particle law index number 1 represents the inert heating or cooling

- Particle law index number 2 represents the droplet vaporization (not used)

- Particle law index number 3 represents the droplet boiling (not used)

- Particle law index number 4 represents the devolatilization process

- Particle law index number 5 represents the char combustion

Steps number 2 and 3 are not relevant, so Fig. 6.7 shows the particle heating, the devolatilization phase and the char combustion.
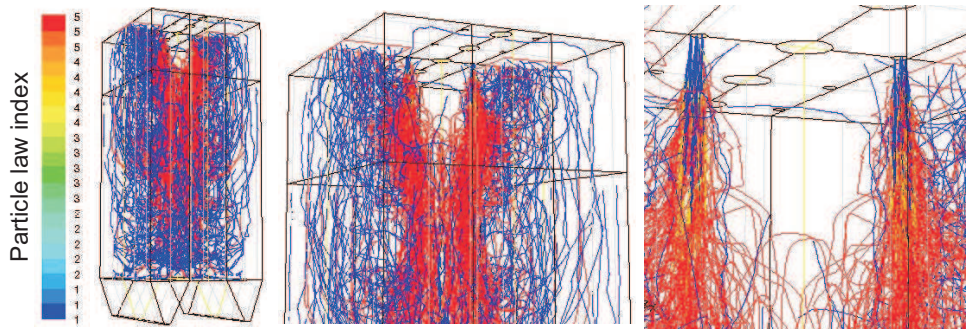
Figure 6.7: Particle tracking with coal combustion stages

As it can be seen in Fig. 6.7, the coal particles are completely burned before they leave the boiler. It can be also remarked that the devolatilization phase finishes before $1\ m$ downstream of the inlet. 1.5% ash of the coal input is trapped in ash hoppers while the rest leaves boiler together with the flow of exhaust gas.

In Section 2.4, the mixing pattern of HTAC technology was defined. The same mixing patterns can be observed in the simulated boiler (compare Fig. 6.8 with Fig. 2.2). Consider the region between the air and the coal inlets. In this region the coal jet has not merged yet into the central air jet. Before the mixing between the jets takes place, both the air and the fuel streams are diluted by the recirculated combustion products and the coal ignition takes place in a lower oxygen concentration environment. At two meters downstream of the inlets both the air and the coal flows merge together and create one strong stream of the combustion gas which recirculates intensively inside the combustion chamber.
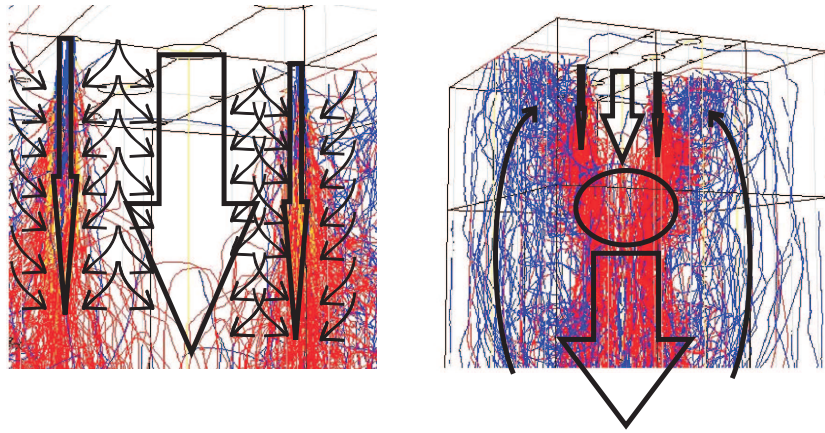
Figure 6.8: Mixing modes inside the HTAC boiler

Due to the internal recirculation of the combustion products the residence time of the coal particles is significantly longer in comparison with the standard PC boiler. In Fig. 6.9 a histogram of the particle residence time inside the boiler is given. It is depicted for 98% of the particles total mass.

Particle residence time, s
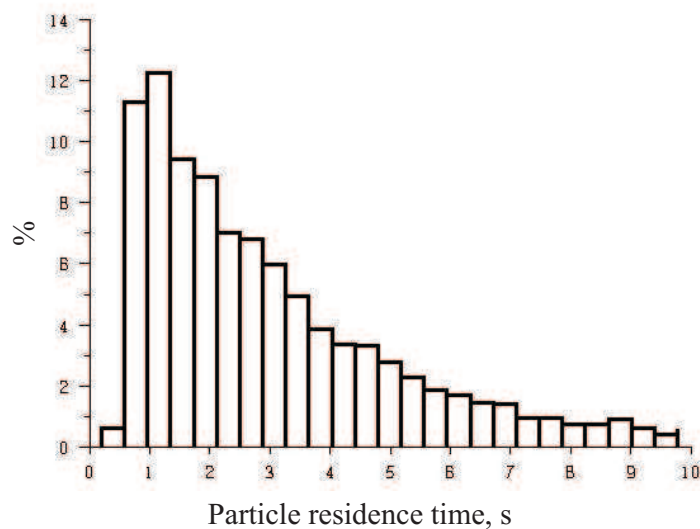
Figure 6.9: Histogram of the particle residence time inside the HTAC boiler

The mean residence time for the coal particles is relatively long and it is calculated to be around 3.5 s while in a standard PC boiler it is around 1.5 s [12]. It can be also observed that for 70% of the particles this time is much longer. Some of them stay inside the chamber and recirculate inside the boiler even up to infinity. Only 30% of the particles stay inside the boiler shorter than for a period of 3 s.

6.1.5 Heat transfer

As a result of the strong recirculation inside the combustion chamber and as a consequence of the uniform temperature and species concentrations fields, the heat fluxes are high and almost constant along the height of the boiler, as shown in Fig. 6.10, right. For the sake of comparison typical heat flux profiles for fluidized bed boilers (Fig. 6.10, left [184]), and for conventional wall-fired boilers (Fig. 6.10, center [184]), are also shown.
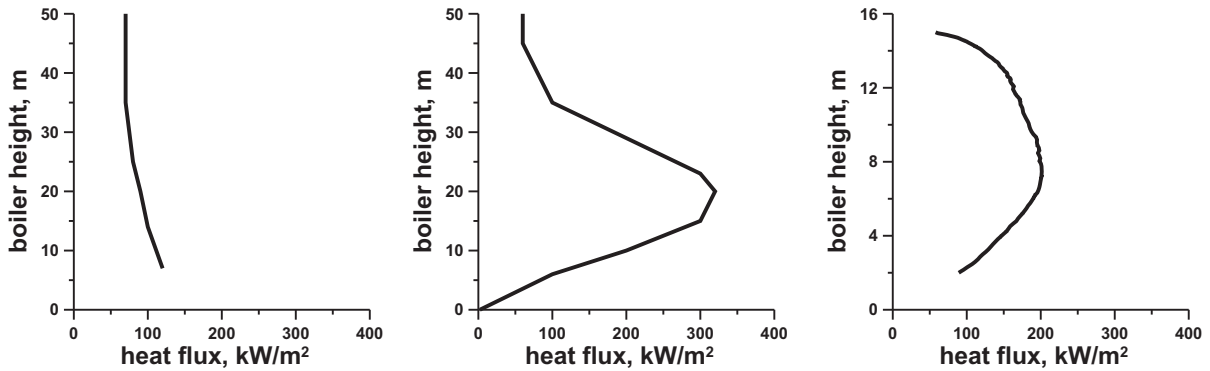
Figure 6.10: Heat flux along the height of a fluidized bed (left) boiler [184], conventional pulverized coal (center) boiler [184], and the simulated boiler (right)

The heat fluxes in the boiler operated in HTAC mode are two times larger if compared with fluidized bed technology and furthermore, the heat fluxes profile along the boiler height is flat. Thus, an intensive and uniform heat transfer occurs in the HTAC boiler. Non-uniformity of the heat fluxes is a feature of a conventional wall-fired boiler, see Fig. 6.10, center. This is due to a non-uniform temperature field; the maximum heat flux corresponds to the maximum temperature location.

Summarizing, the HTAC boiler has two advantages: the uniform heat fluxes along the boiler height (as in fluidized bed boilers) and high heat fluxes (as in pulverized coal boilers). Heat transfer due to radiation plays a dominant role in the HTAC boiler. Its value is 83% of the total heat transfer. The rest is due to the heat convection.

6.2 Findings

The presented final version of the boiler fired with pulverized coal possesses all the features required for HTAC technology. First of all, an intense recirculation inside the combustion chamber make both temperature and chemical substances concentration fields uniform. Further, due to dilution between combustion air and fuel jets the coal ignition takes place in low oxygen concentration environment, and therefore the temperature peak is suppressed. Then, high and uniform heat fluxes improve heat transfer in the boiler. Moreover, the intensification of radiative heat transfer results in an increase of firing density, and at the same time allows to reduce the size of the boiler. It can be economically justifiable to build this boiler from high quality steels and to increase the steam parameters. Long particles residence time, as well as recursively recirculation of the combustion products improve the char burnout. Very stable combustion process and simple burner construction offer the possibility of using low rank coals. Strong recirculation of the hot combustion products eliminates the problems related to coal ignition. The proposed boiler has a very simple construction of the combustion chamber, as well as of the burners in comparison with typical conventional PC boilers.

Chapter 7

Evaluation of the grid sensitivity

A grid sensitivity study has been performed to investigate the dependence of the numerical results on the computational grid used. Similar grid sensitivity tests have been performed for all the configurations analyzed in previous and next Chapters. Grid quality and independence will be presented based on the final configuration case (see Section 6) only.

The calculations are performed using unstructured grid. The meshed boiler geometry is presented in Fig. 7.1, left. The mesh near the burners and in the region where both the air and the coal flows merge together has the highest amount of cells, as can be observed in Fig. 7.1, right. Two grids were used to verify the solution independence: a reference mesh of 320,000 cells called coarse grid (Fig. 7.1), and refined mesh of 2,000,000 cells, called fine grid.
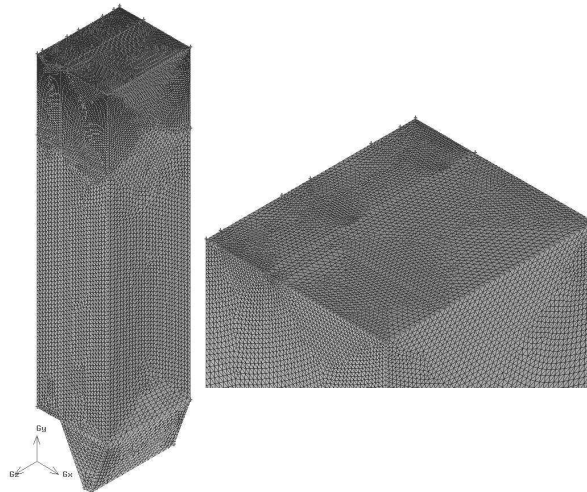
Figure 7.1: Numerical grid of the simulated boiler: the whole domain (left) and zoom on the burner region (right)

7.1 Grid independence

The comparison between the two tested meshes is performed to determine the effect of grid resolution on the accuracy of the present model solution. Since the temperature field and the gas composition are of special importance, profiles of temperature and oxygen concentration along the height of the boiler are presented in Fig. 7.2 and Fig. 7.3, respectively. For location of the traverses see Fig. 9.14.

The temperature and oxygen concentration profiles vary with the grid fines, however the differences are not too large. It can be concluded that the solution was not too sensitive to the griding level. Due to decreasing of computational time, the mesh of 320,000 cells was used for all calculations presented in this thesis.
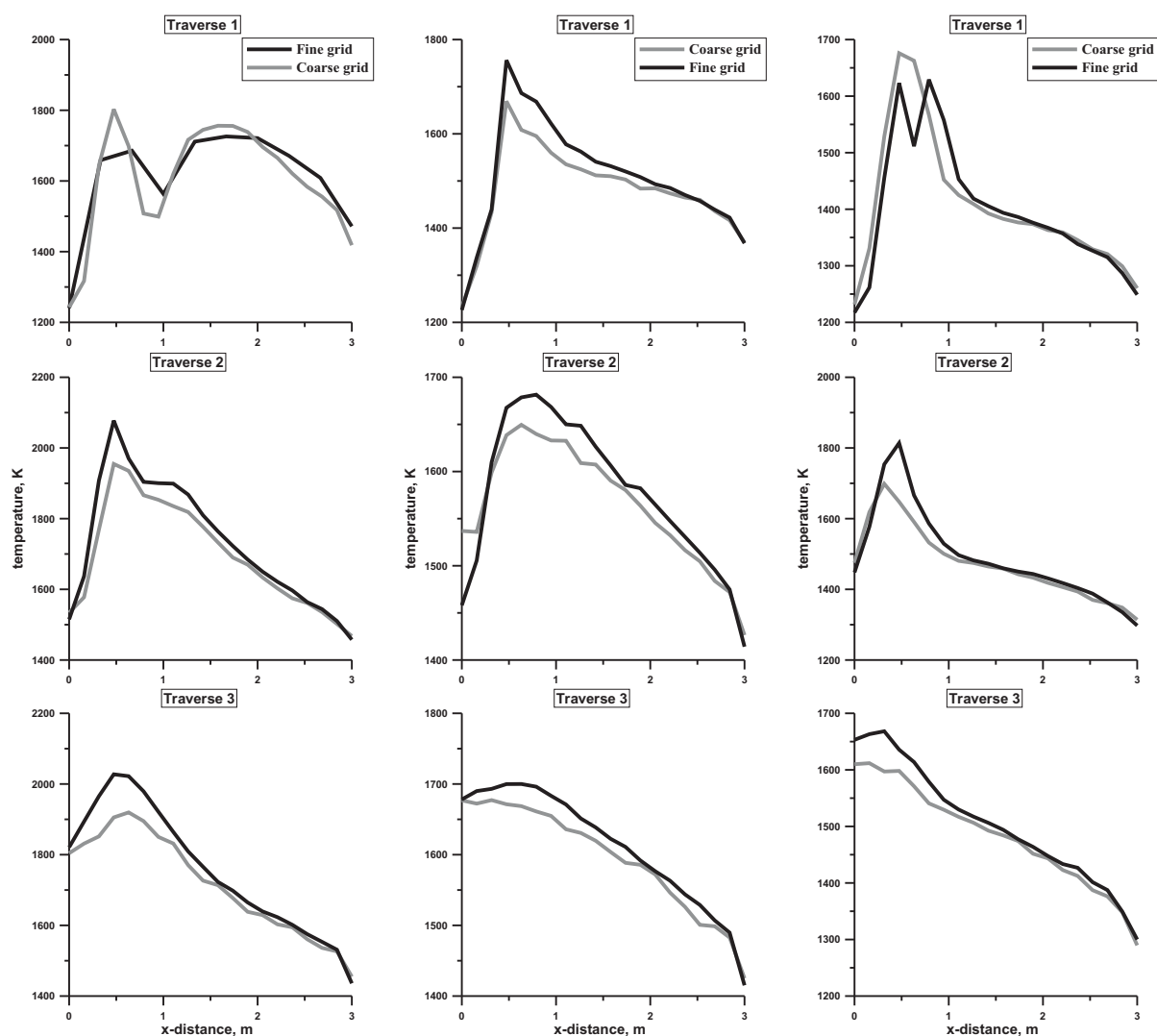
Figure 7.2: Temperature profiles for two different grids along burner 1 (left), burner 2 (center) and burner 3 (right)
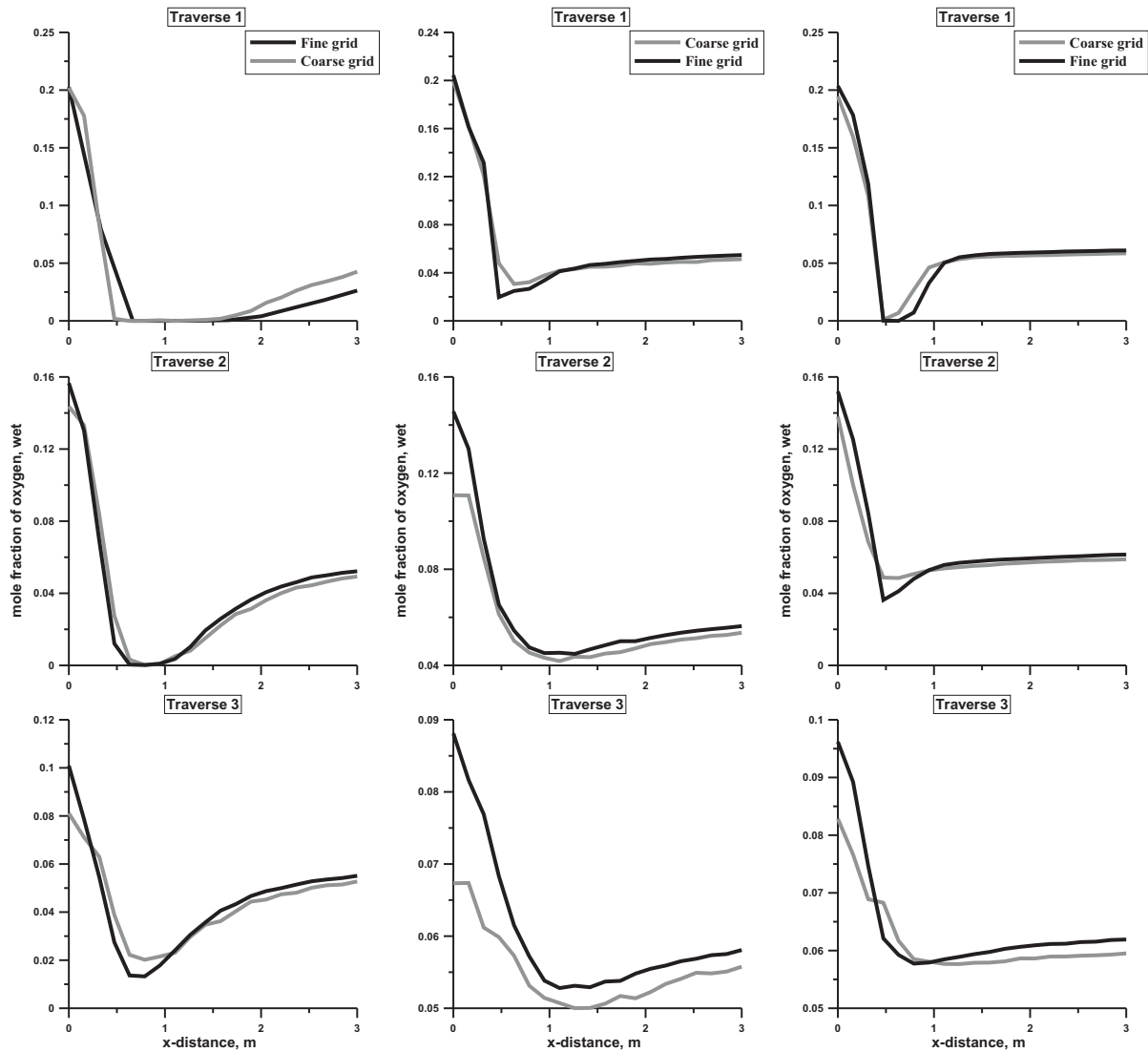
Figure 7.3: Oxygen concentration profiles for two different grids along burner 1 (left), burner 2 (center) and burner 3 (right)

7.2 Grid quality

The quality of the mesh plays an important role in the accuracy and in the stability of the numerical computation [144, 145, 185]. Therefore, three major attributes have been introduced in order to measure the quality of the numerical grid: node point distribution, smoothness and the cell shape. The quality of the grid is examined for the mesh containing 320,000 cells (coarse grid).

7.2.1   Node-point distribution

Since the continuous domain in the numerical simulations is defined discretely, the degree that the salient features of the flow (such as shear layers, separated regions, boundary layers) are resolved depends on the density and distribution of nodes in the mesh. In many cases, poor resolution in crucial regions can substantially alter the flow characteristic. The resolution of the boundary layer (mesh spacing near the wall) also plays a significant role in the accuracy of the computed wall shear stress and the heat transfer calculations. In regions of large gradients, the mesh should be fine enough to minimize the change in the flow variable from cell to cell. Unfortunately, it is very difficult to determine the locations of important flow features in advance. This particular attribute of mesh quality is satisfied by grid independence validation trials.

Distribution of the cell volume is presented in Fig. 7.4, left. The smallest cell volume is $2.91 \cdot 10^{-6} \ m^3$ and the biggest cell volume is $1.43 \cdot 10^{-3} \ m^3$. As can be further observed in Fig. 7.4, left, the smallest cells are located near the burner and in the mixing (and at the same time ignition) region because of their importance in the combustion process. The biggest cells are at the bottom part of the boiler, near the ash hoppers.
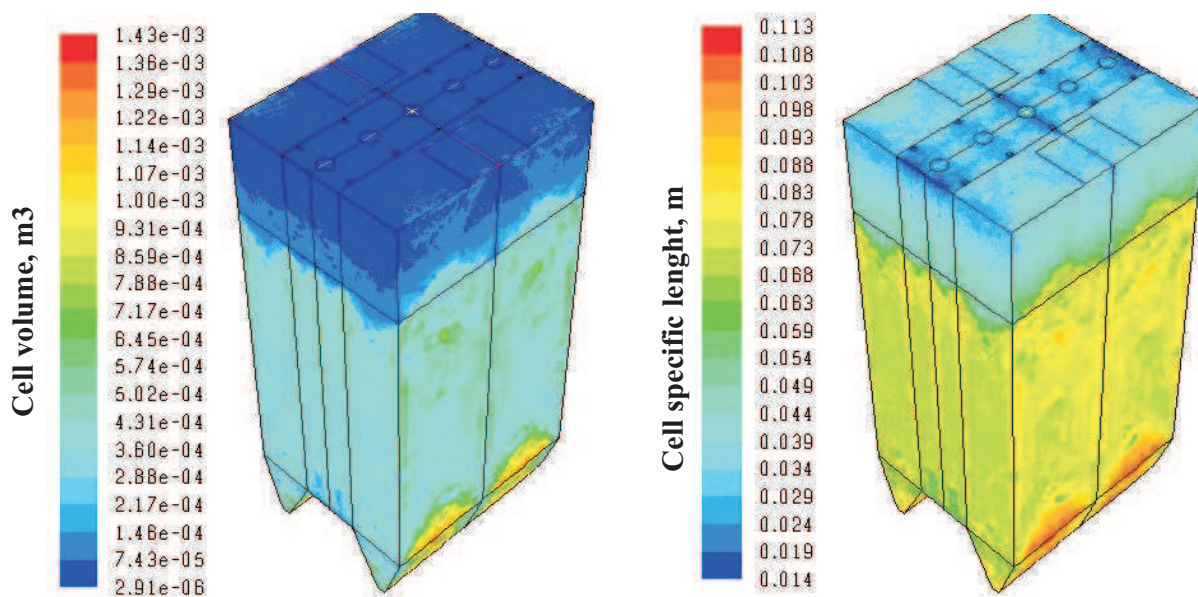
Figure 7.4: Cell volume (left) and cell specific length (right) for the boiler grid

7.2.2   Smoothness

Smoothness of the grid is defined as the ratio between adjacent cells. Smoothness is related to the truncation error which is defined as the difference between the partial

derivatives in the governing equations and their discrete approximations. Rapid changes in the cell volume between adjacent cells cause larger truncation errors. During meshing process main attention was placed on keeping small ratio between adjacent cells. The maximum volume ratio in the creating grid was forced to be 1.2.

7.2.3 Cell shape
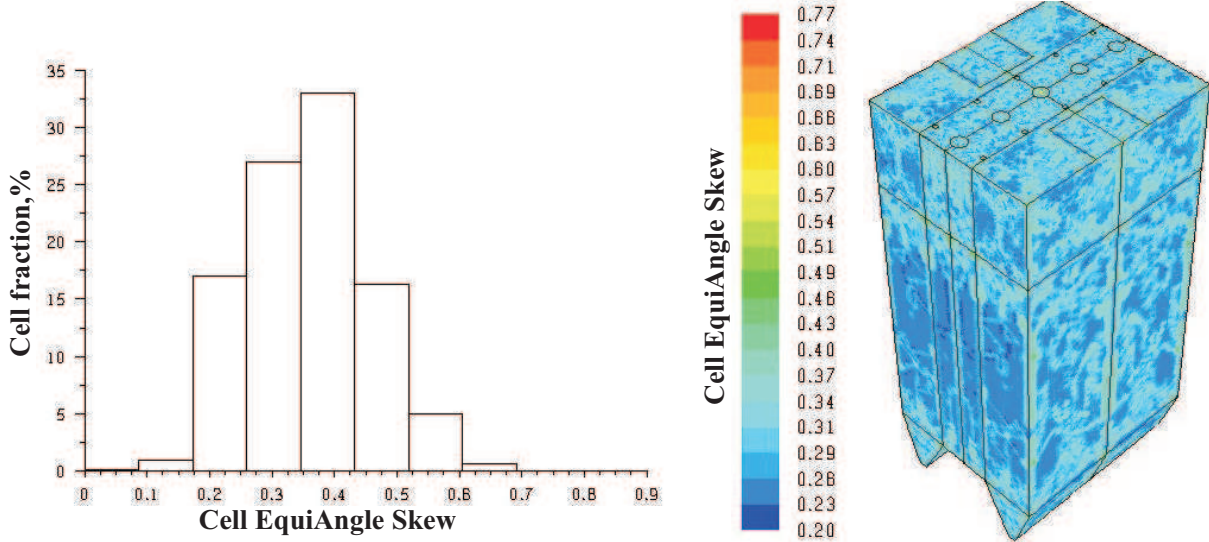
Figure 7.5: Histogram (left) and contours (right) of the cell skewness

The shape of the cells which includes its skewness and aspect ratio are defined as follow:

- Aspect ratio is a measure of the stretching of the cell. For highly anisotropic flows extreme aspect ratios may yield accurate results with fewer cells. In general aspect ratios larger than 5 should be avoided. In the computations performed in this thesis, aspect ratio is between 1-1.3 for 76% of total cell number, and between 1.3-1.6 for 16% of total cell number. The rest 8% of the cells has higher value. The maximum value is 3.6. The specific length of the cell associated with the ratio between the successive cells is presented in Fig. 7.4, right. The smallest cell is of 0.014 m length and the biggest on is 0.113 m. The specific length l of the cell is defined as follow:

$$l = \sqrt[3]{V}$$

where V is the cell volume.

- Skewness of the cell is the difference between the shape of the cell and the shape of an equilateral cell of equivalent volume. Highly skewed cells can decrease accuracy

121

and destabilize the solution. The EquiAngle Skew method provided by the GAMBIT package is used to examine the quality of the mesh [142]. Generally, the measure of EquiAngle Skew (EAS) is contained between 0 and 1, where $Q_{EAS}{=}0$ describes an equilateral element, and $Q_{EAS}{=}1$ describes a completely degenerate (poorly shaped) element. In general, high-quality meshes contain elements that possess average Q_{EAS} values of 0.1 (for 2-D geometry) and 0.4 (for 3-D geometry). In the analyzed mesh, the elements with the skewness up to 0.4 are 70% of total cell number, between 0.4 and 0.6 are 28% of total cell number. Only 2% of the cells are between 0.6 and 0.77. The detailed distribution of the skewness is presented in the histogram of Fig. 7.5.

Generally, it can be concluded that the meshes used in computations of this work are of good quality.

Chapter 8

Environmental issues

The use of coal in combustion to generate electricity creates a number of environmental challenges. The basic environmental issues related to the combustion of coal in power boilers are: nitric oxide formation and emission, as well as burnout of combustible gases and char. In this Chapter, the environmental issues of the HTAC boiler are discussed, with a special emphasis on nitric oxides emissions, carbon monoxide and volatiles emissions and char burnout.

8.1 Nitric oxides emissions

For a given coal, formation of NO_x depends mainly on local oxygen concentration and temperature. Due to a low peak of the temperature and uniform and low oxygen concentrations the nitric oxide formation should be significantly suppressed in the proposed HTAC boiler. The model used in this work for NO-formation and -reduction is described and discussed in details in Section 3.9.

The predicted nitric oxide concentrations inside the HTAC boiler are depicted in Fig. 8.1. The NO concentrations fields can be observed in three different views: isometric (left), side (center) and front (right) view. It can be observed that most of NO is generated in the region between the fuel inlets and the ignition region. Downstream of this position the concentrations of nitric oxide are low and they are in a range from 300 up to 400 ppm. The NO concentration peak is equal to 1195 ppm.
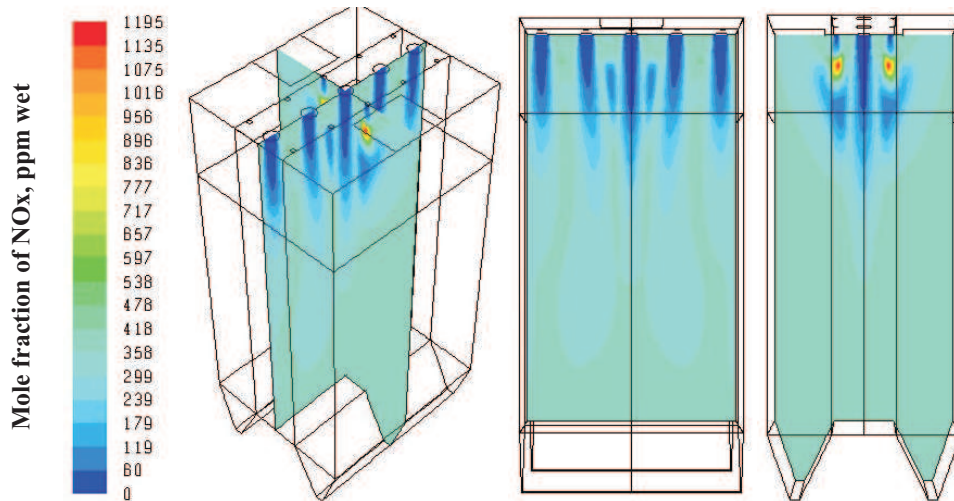
Figure 8.1: Concentrations of nitric oxide inside the HTAC boiler: isometric (left), side (center) and front (right) views

The formation rates for each NO-formation mechanism are shown in Fig. 8.2. The relative importance of the different paths of NO-formation (and destruction) can be judged by its corresponding formation rates taken from the computation. The highest peak of the formation rates ($R = 1.93 \cdot 10^{-03} \frac{kmol}{m^3 s}$) is due to the fuel mechanism near the inlets. All other mechanisms exhibit a lower peak. The rate of fuel NO is depicted in Fig. 8.2, top left. This is the dominant formation mechanism for the HTAC boiler and it occurs over a large volume. Most of the nitrogen oxide derived from the fuel path is formed in the volatiles release region. The thermal mechanism occurs only in the highest temperature region which is rather small in volume. Prompt formation route is also insignificant. The N_2O mechanism is also negligible since its formation rate is two orders of magnitude lowers than the other mechanisms. The nitric oxide reduction through reburning plays quite an important role in HTAC combustion process. Both the average and the maximum NO formation and destruction rates are listed in Tab. 8.1. The amount of the NO_x formation due to each path is given in % of the total NO_x formation rate.

In the HTAC boiler 78% of nitric oxide is formed via fuel mechanism. Both N_2O and prompt mechanisms of NO_x formation are of marginal importance. Thermal NO_x are 19% of the total NO_x. Reburning plays a significant role and this is affected by the strong combustion products recirculation; 30% of the previously formed NO_x is reburned inside the boiler. Thus, only two mechanisms in the overall NO-balance are significant; the NO generation via the fuel mechanism and the NO reburning mechanism.
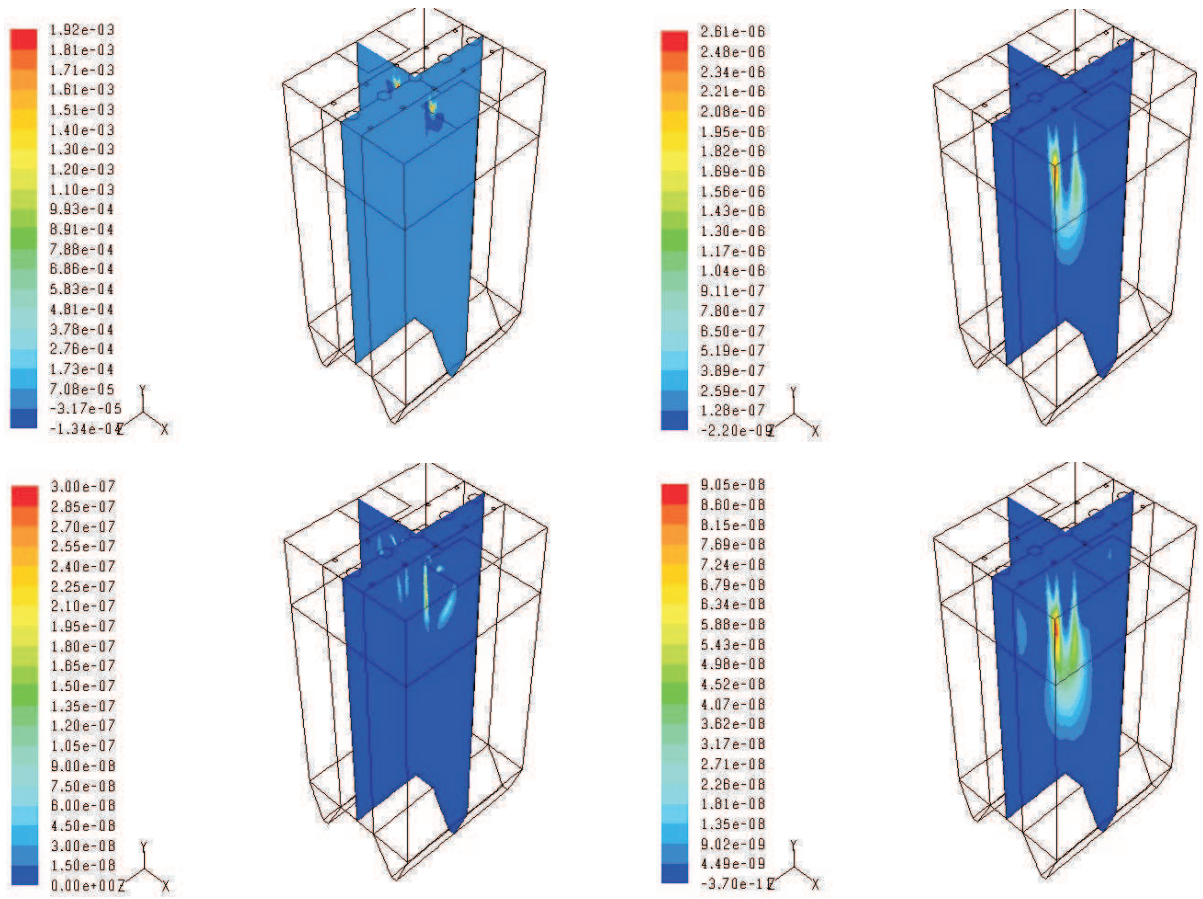
Figure 8.2: Formation rates of NO_x paths: fuel (top left), thermal (top right), prompt (bottom left) and via N_2O (bottom right)

mechanism	total rate of formation, $\frac{kmol}{s}$	%
fuel	$13.25 \cdot 10^{-5}$	78
prompt	$0.31 \cdot 10^{-5}$	2
thermal	$3.32 \cdot 10^{-5}$	19
N_2O	$0.09 \cdot 10^{-5}$	1
reburn	$-5.26 \cdot 10^{-5}$	30

Table 8.1: Nitric oxide formation paths

The predicted nitric oxide emissions at the boiler outlets are equal to 298 *ppm*. For the purpose of comparison of NO_x emission with the forthcoming legislation (see Tab. 1.1), the NO_x concentrations in the flue gas are recalculated to 6% oxygen content (Eq. 8.1), and then converted from the volume fraction in *ppm* to concentration in $\frac{mg}{m^3}$ (Eq. 8.2). The mole fraction of oxygen in the flue gas is equal to 3.75%, so that the conversion equations are as follows:

$$NO_x@6\%O_2 = NO_x(\frac{21-6}{21-3.75}) = 259ppm \tag{8.1}$$

$$NO_x@6\%O_2, \frac{mg}{m_n^3} = NO_x@6\%O_2, ppm\frac{10^{-6} \cdot M_{NO_2} \cdot 10^6}{22.4} = 508\frac{mg}{m_n^3} \tag{8.2}$$

The outlet NO_x concentration is equal to 508 $\frac{mg}{m_n^3}@6\%O_2$. It is worth to notice that this value is not higher than typical emissions of standard PC burners (that are usually in the range between 600 and 800 $\frac{mg}{m_n^3}@6\%O_2$ [13]) despite that the air is highly preheated.

8.2 Carbon monoxide and volatiles emissions

In the numerical model carbon monoxide is released exclusively from the combustion of the volatiles. It is formed mostly in the region, where combustion air and volatiles mix together. The highest CO concentration is equal to 6.5%. and appear where the oxygen concentration is the lowest.

The region where devolatilization takes place can be seen in Fig. 8.3, left. Volatile matter is released from the coal upon heating. The volatiles appear only in a small region inside the boiler and besides this region no considerable amount of the volatiles exists. The maximum peak of the volatiles concentration is equal to 14.5%. The burnout of volatiles is equal to 100% and no volatiles concentration is found at the outlet, just the model predicts no problems neither with carbon monoxide nor with volatiles burnout. However, one should realize that the volatile matter combustion sub-model and the CO-creation and oxidation mechanism are oversimplified in the numerical model. Thus, a deeper analysis of coal burnout issues is recommended.
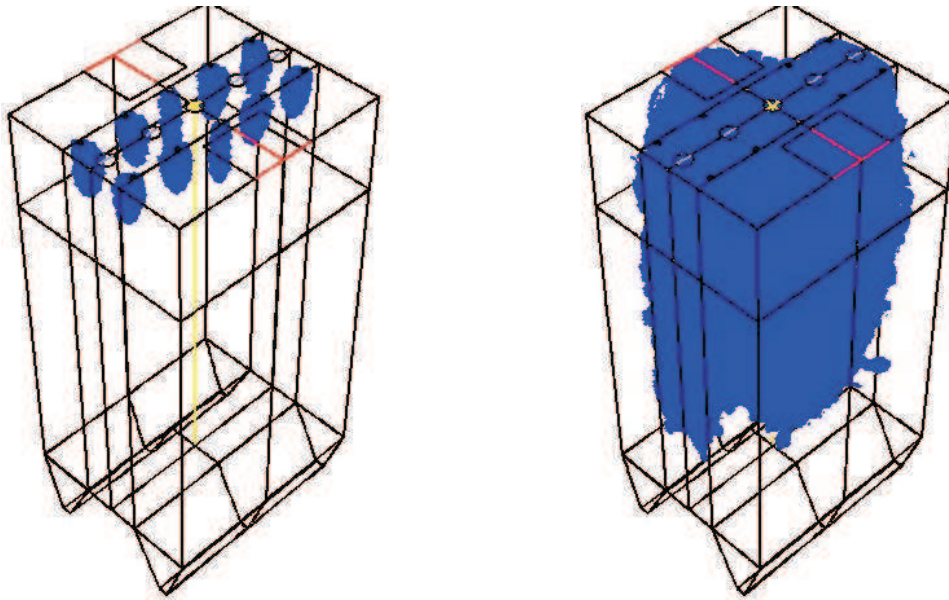
Figure 8.3: Devolatilization (left) and char burnout (right) regions inside the HTAC boiler

8.3 Char burnout

The char burnout is a concern of HTAC technology. The region where char burnout takes place is shown in Fig. 8.3, right. Although the predicted value of char burnout is equal to 99.9% at the outlet, the sub-model for char burnout used in this work is simple (for details see Sections 3.7.3 and 4.3). However, in HTAC technology complete burnout is expected due to intensive recirculation of the combustion gas and long particles residence time. Char burnout process should be taken into consideration in further investigations.

8.4 Findings

In this Chapter the environmental issues related to the HTAC boiler have been investigated. It was concluded that a low emission of NO_x is achieved in this boiler which allows to adhere to the forthcoming strict legislation of NO_x emissions from power plants without the need of a substantial capital investment. The complete burnout of the gaseous combustibles (CO and volatiles), as well as of the char probably allows the possibility of operating the proposed boiler at air excess ratio just a little bit higher than stoichiometric.

Chapter 9

Effects of selected operating parameters

The internal recirculation zones in HTAC combustion are generated by injecting combustion air jets of a high momentum into the combustion chamber. The HTAC combustion regime is characterized by a stable combustion over a wide range of fuel/air ratios. In this Chapter an impact of three important parameters: the combustion air preheat, the combustion air jet velocity and the air excess ratio on HTAC combustion mode has been tested in the context of the HTAC boiler designed in Chapter 5. Thus, for all calculations of this Chapter the final HTAC boiler geometry is retained (see Fig. 6.1). However, boiler operating conditions are different and these are going to be specified for each computational run. The final boiler design (see Chapter 6) is named here as the reference case.

9.1   Impact of the combustion air preheat

In a typical HTAC system, the combustion air is preheated to temperatures around 1000^oC using recuperative or regenerative heat exchangers. However, such a preheating process is difficult to implement in pulverized coal boilers. In a PC boiler the combustion air stream is preheated to a temperature typically not higher than 623 K. However, flames with highly preheated combustion air are significantly more stable and more homogeneous (both temporally and spatially) compared to conventional flames.

The possibility of operating the HTAC boiler at the ambient temperature air (300 K), at 600 K air preheat, and at 900 K air preheat are examined in this calculation series. The fuel input is kept constant for every simulation and it is equal to 100 MW. However, the total thermal input of the boiler decreases due to a decrease of the combustion air temperature. The combustion air which is preheated to the 1200 K has the enthalpy of 30 MW while the air at ambient temperature has the enthalpy

of 0 MW. The change of the combustion air temperature influences the inlet velocity. Therefore the air inlet diameter has been adjusted to keep the air injection velocity at the constant value of 120 $\frac{m}{s}$. The other operating conditions are analogous to the reference case. Operating conditions for each computational runs are compared in Fig. 9.1.
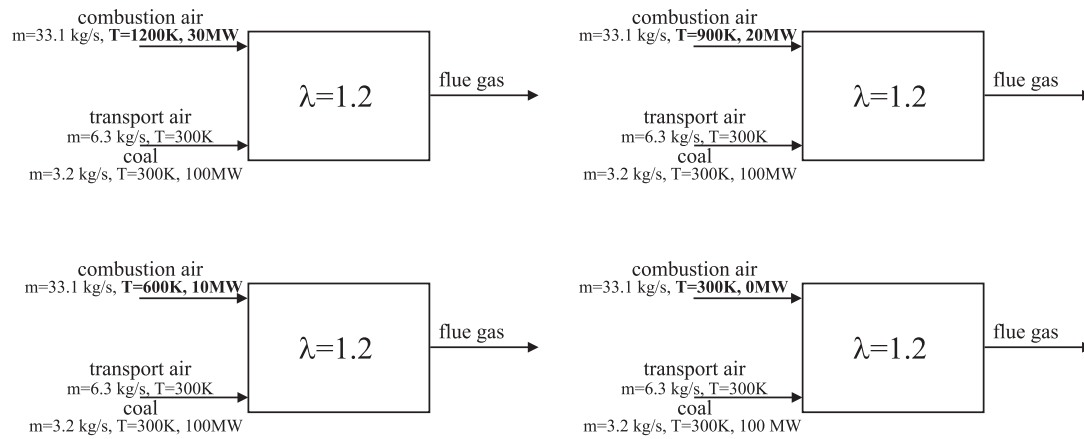
Figure 9.1: Operating conditions in the boilers: at 1200 K preheat temperature (top left), at 900 K preheat temperature (top right), at 600 K preheat temperature (bottom left) and at ambient temperature (bottom right)

9.1.1 Results and discussion

Results of the simulation series considered the impact of the combustion air temperature on the HTAC boiler operation are presented in the following graphs and compared with the reference case. Predictions of the field variables are presented along the traverses 1, 2, 3 which are located as shown in Fig. 9.2.
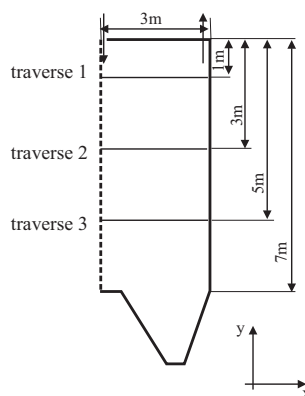
Figure 9.2: Location of the traverses inside the boilers
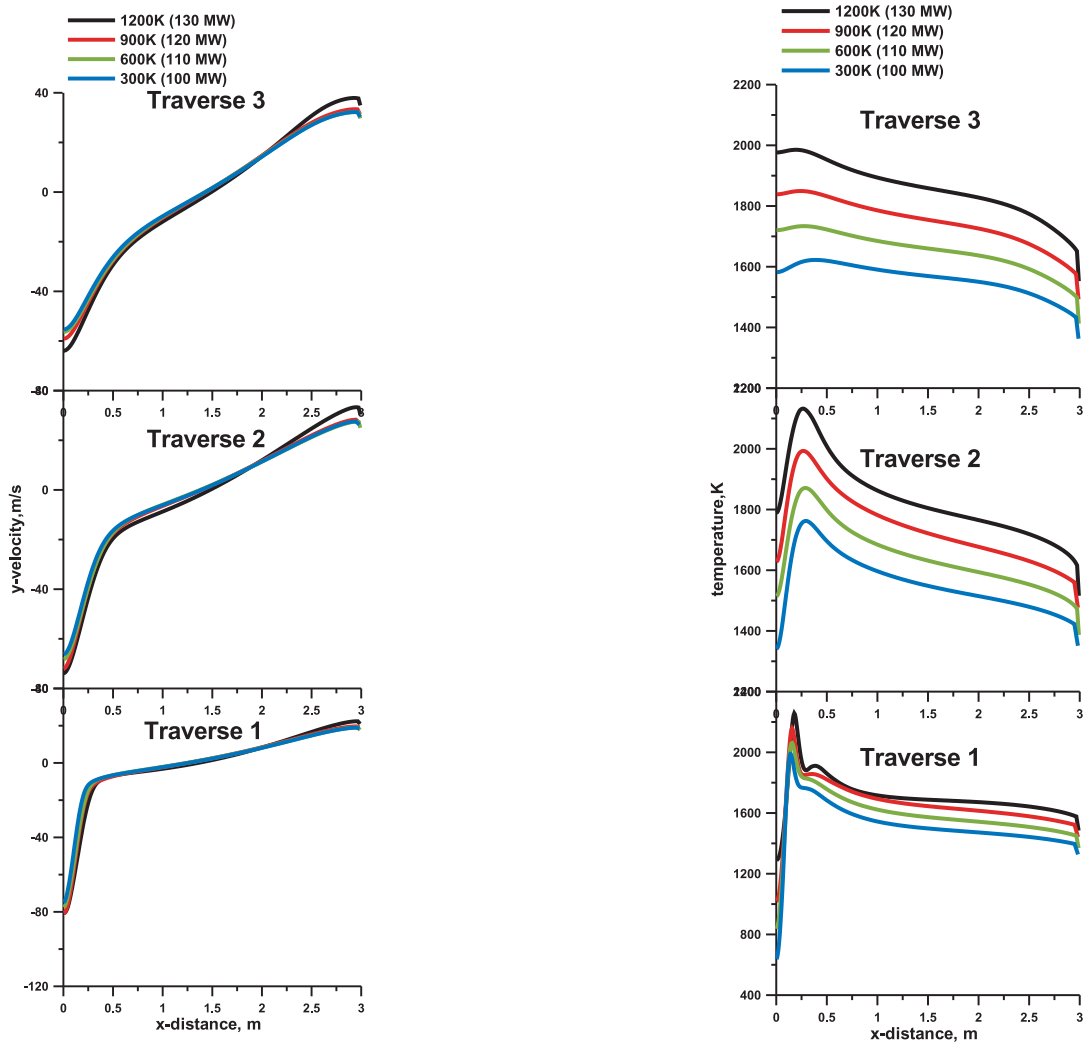
Figure 9.3: Velocity (left) and temperature (right) profiles along the traverses
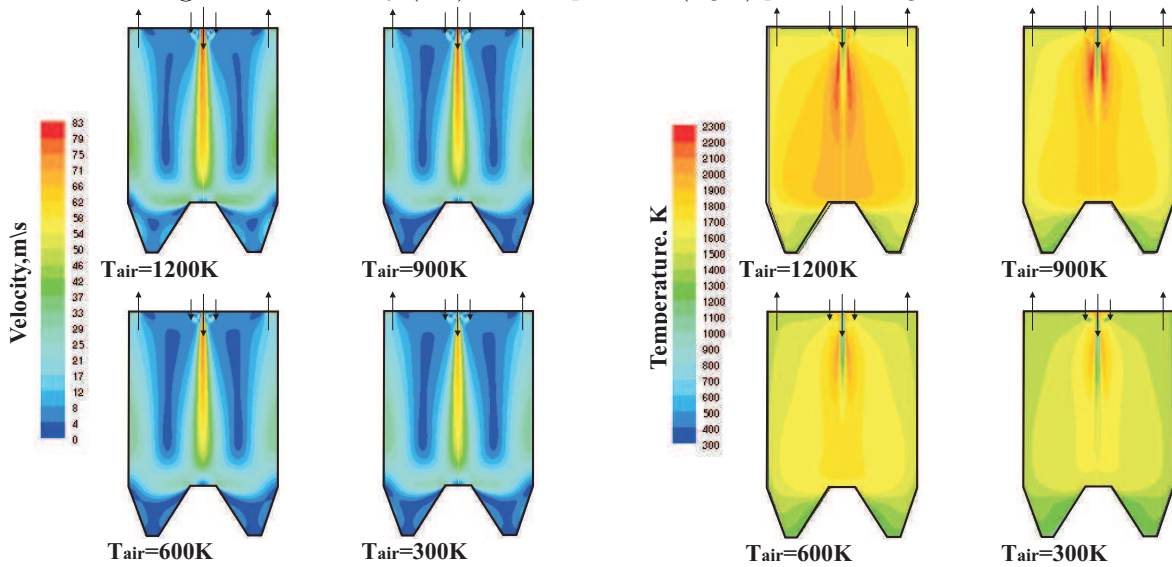
Figure 9.4: Velocity (left) and temperature (right) contours inside the examined boilers

Profiles of the y-velocity (left) and temperature (right) along three traverses are presented in Fig. 9.3. Contours of the velocity field (left) and the temperature field (right) are shown in Fig. 9.4. It is found that inside the HTAC boiler, regardless of the combustion air preheat, the recirculation of combustion products is almost identical (see Fig. 9.4, left). It can be concluded that HTAC conditions in the boiler are created due to high jet velocities, and as observed during the design procedure (see Chapter 5), the distance between air and coal inlets, burners location inside the combustion chamber, as well as shape of the combustion chamber, however they are independent on the combustion air temperature.

The combustion products recirculation is responsible for the uniformity of both the temperature and species concentration fields. As can be found in Fig. 9.4, right, the temperature fields for each boiler are homogeneous. The peak of the temperature is lower in each simulated boiler domain if compared to the standard PC boilers. The only difference is in the combustion temperature level achievable in individual boiler. Adiabatic combustion temperature is dependent on the combustion air temperature since the fuel flow and the air excess ratio are fixed. The adiabatic temperature increases together with increasing combustion air temperature. Thus, it can be observed that the highest temperatures in the boiler are obtained for the reference case with 1200 K air preheated. It can be concluded that independently of the air preheating the boiler operates in HTAC mode. However, a high temperature of the combustion air helps to ignite the coal and to maintain stable combustion. Unfortunately, with the model used in this work it is not possible to examine in details the coal ignition process. Although, due to the hot combustion products recirculation into the ignition zone no problems with coal ignition are expected.

No substantial differences are visible in the oxygen concentration profiles which can be found in Fig. 9.5, left. The oxygen concentration level is about 4-5% in the whole volume except the region near the burners. In this region the devolatilization occurs and therefore the lack of the oxygen is visible.

The carbon monoxide profiles are presented in Fig. 9.5, right. In the model carbon monoxide is generated during the combustion of the volatiles. In the graphs it can be seen that higher temperatures contribute to more intense devolatilization and subsequently higher carbon monoxide concentrations. Therefore, the maximal concentration of the carbon monoxide can be found for the highest preheated air temperature. However, the concentration of carbon monoxide at the boiler outlet is almost zero regardless of the air preheat.
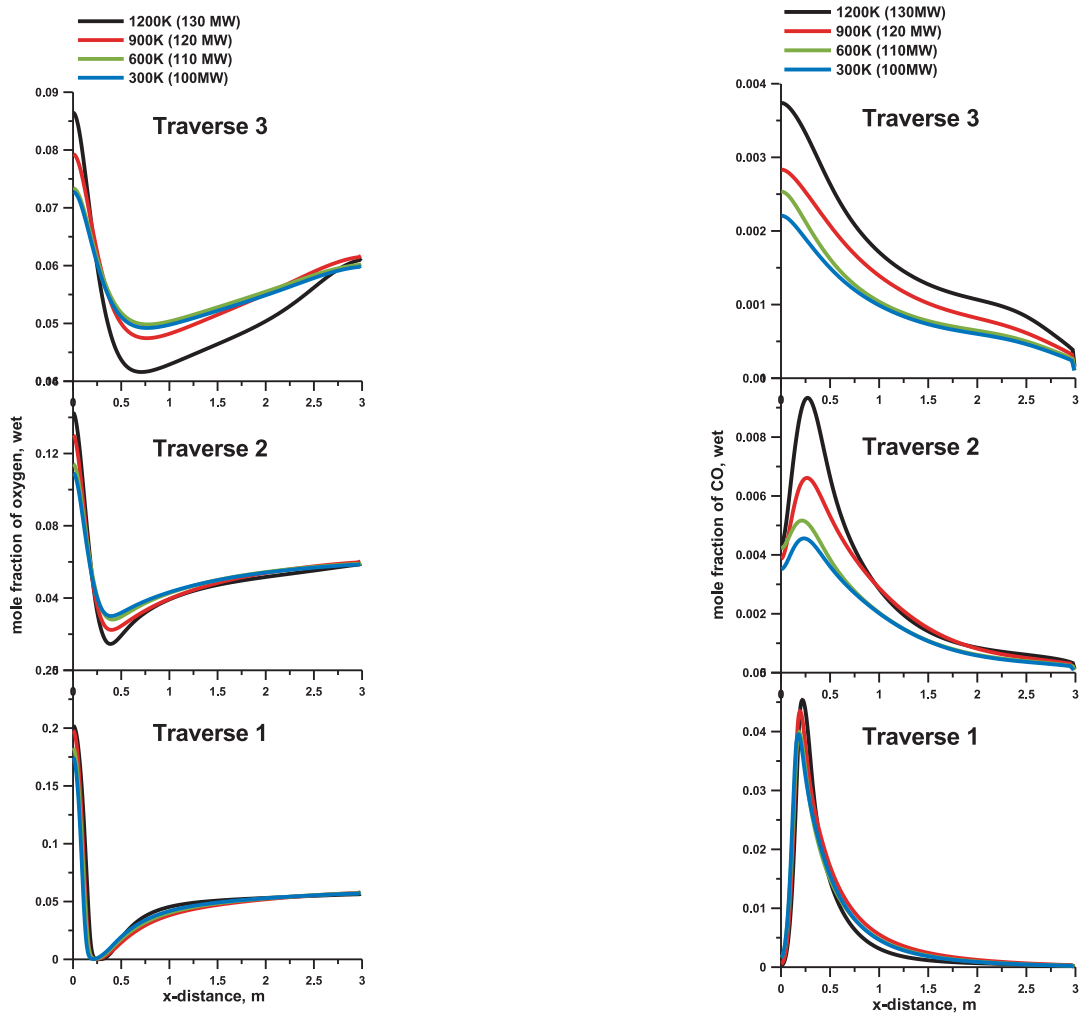
Figure 9.5: Oxygen (left) and volatiles (right) concentration profiles along the traverses
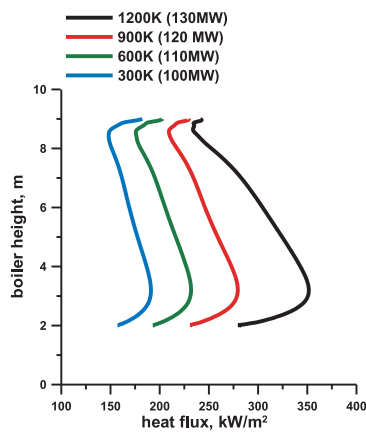
Figure 9.6: Heat flux along the height of the boilers

The calculated heat flux along the combustion chamber height is depicted in Fig. 9.6. It can be observed that the heat flux profiles have similar trend for each examined combustion air temperature. The difference is in the heat flux values. The highest values appear for the highest temperature of the combustion air (1200 K) and its average value is 320 $\frac{kW}{m^2}$. Further, the lowest heat fluxes are for the ambient temperature air and its average value is equal to 175 $\frac{kW}{m^2}$. The only reason of these differences is a decrease of the total thermal input.

9.1.2 Findings

This calculation series has been conducted to examine HTAC boiler operation at different combustion air temperatures of: 900 K, 600 K and at ambient temperature. It can be emphasized that HTAC technology can be realized independently of the combustion air temperature. Features of HTAC technology: a strong combustion products recirculation, dilution of the combustion air and fuel, uniformity of both the temperature and the species concentration fields and low temperature peaks, are obtained for each examined combustion air temperature. Proportionally with a decrease of the combustion air temperature (and subsequently a decrease of the thermal input) a decrease of the temperature level in the boiler (and subsequently a decrease of the heat fluxes) is predicted. However, operating HTAC boiler with either ambient combustion air or with the standard preheating temperature combustion air eliminates the need for a heat exchanger working between a dusty and hot exhaust gas and a combustion air. It can be concluded that the temperature of the combustion air has a limited impact on the correct performance of HTAC technology. Therefore, the HTAC boiler can be operated at different combustion air temperatures. Although due to hot combustion products recirculation in the region near the burners no problems with the coal ignition are observed, in the case of the ambient and standard combustion air temperature the ignition process should be examined in more details.

9.2 The HTAC boiler equipped with low-momentum burners

The key issue in realizing HTAC technology is a high velocity (and at the same time a high momentum) of the central air jet. This creates an intense internal recirculation which creates an homogenous distribution of all field variables inside the combustion chamber. However, high inlet velocity is obtained using a fan which needs electricity. An

estimated power needed to operate the fan at inlet velocity equal to $0 \frac{m}{s}$ and the required outlet velocity of $120 \frac{m}{s}$ is around $90 \ kW$ while assuming the outlet velocity of $60 \frac{m}{s}$ is around $10 \ kW$. Therefore, in this Section a possibility of operating the HTAC boiler with a low velocity central air jet ($60 \frac{m}{s}$) is examined.
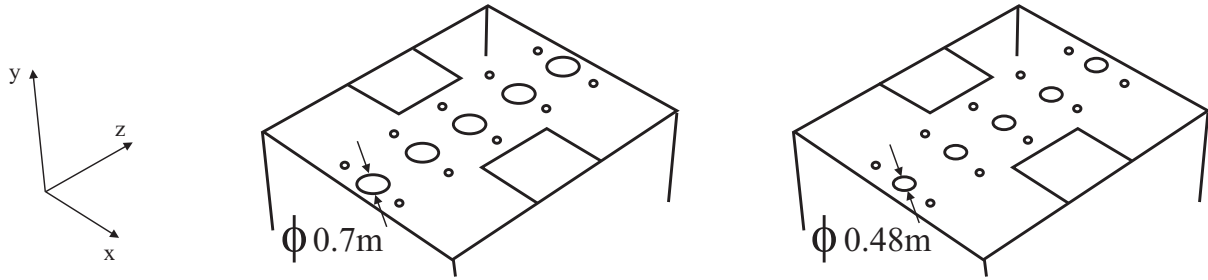
Figure 9.7: Air inlet geometry for the boilers with inlet velocity of $60 \frac{m}{s}$ (left) and $120 \frac{m}{s}$ (right)

The results are compared to the reference case (central air jet velocity equal to $120 \frac{m}{s}$). Air inlet geometry for both computational runs is presented in Fig. 9.7. The lower cental air jet velocity is obtained keeping the same combustion air mass flow as in the reference case HTAC boiler. Therefore, the combustion air inlet diameter was recalculated and it is equal to $0.7 \ m$ for the central air jet velocity of $60 \frac{m}{s}$ while the combustion air inlet diameter is equal to $0.48 \ m$ for the central air jet velocity of $120 \frac{m}{s}$.

The operating parameters for both the examined boiler and the base case boiler are presented in Fig. 9.8. As can be observed in Fig. 9.8, for both boilers the input power is equal $130 \ MW_{th}$, the firing density is kept constant, the air excess ratio is 1.2. The only difference is in the combustion air velocity (and the momentum). The high-velocity burner operates at the momentum of $752 \ N$ while the low-velocity burner operates at the momentum of $188 \ N$.
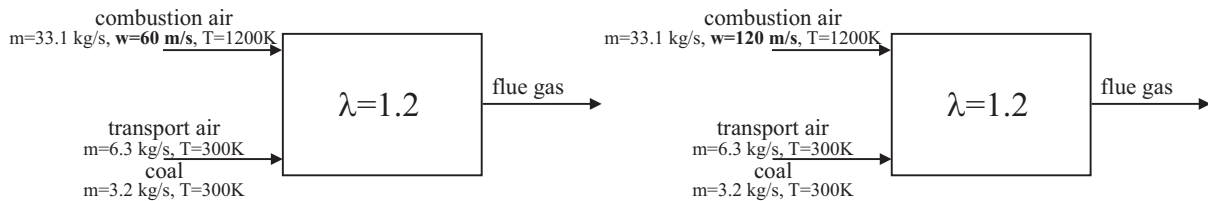
Figure 9.8: Operating conditions in the boilers: with the inlet velocities of $60 \frac{m}{s}$ (left) and $120 \frac{m}{s}$ (right)

9.2.1 Results and discussion

The predicted velocity field in the y-plane (see Fig. 6.1) is presented in Fig. 9.9 for the boiler operated at $60 \frac{m}{s}$ inlet velocity (left) and for the boiler operated at $120 \frac{m}{s}$ inlet

velocity (right). It can be observed that in the boiler operated at the low combustion air velocity (60 $\frac{m}{s}$) both the air and the coal jets merge together after shorter distance downstream from the inlet than in the boiler operated at the high combustion air velocity (120 $\frac{m}{s}$). Therefore, in the boiler operated at the low combustion air velocity no proper dilution of both the air and the fuel jets can be observed. In this boiler, a coal ignition takes place in a rich oxygen environment which is a characteristic of a conventional combustion: high temperature peaks occurs in this boiler and non-uniformity of the temperature and the oxygen concentration fields. It can be seen also that in the boiler operated at the low combustion air inlet velocity dead zones are bigger than in the boiler operated at the high combustion air inlet velocity. As a result, the combustion does not occur in the whole volume of the combustion chamber.

The predicted temperature field in the symmetry x-plane (see Fig. 6.1) is shown in Fig. 9.10. Improperly developed recirculation in the boiler operated at the low combustion air velocity results in a high non-uniformity of the temperature distribution inside this boiler. Due to the lack of both the space and the time for dilution of both the combustion air and the fuel stream, the temperature peak is substantially higher in the boiler operated at the low combustion air velocity (it is equal to 2260 K) than in the boiler operated at the high combustion air velocity (it is equal to 2100 K).

The predicted oxygen field in the symmetry x-plane is shown in Fig. 9.11. In the boiler operated at the low combustion air velocity the oxygen concentrations are strongly non-homogenous in the whole volume of the combustion chamber. The lack of oxygen is observed in the large region near the burners. However, in both cases the oxygen concentration at the boiler exit is around 4%. It can be concluded that in the boiler operated at the low combustion air inlet velocity (60 $\frac{m}{s}$) several characteristics of HTAC technology are not present: the dilution of both the air and the fuel, low temperature peaks, uniform distribution of both the temperature and the oxygen concentration fields, and volumetric combustion. As a result, combustion in the boiler operated with the low-momentum burner resembles combustion of conventional PC boilers.
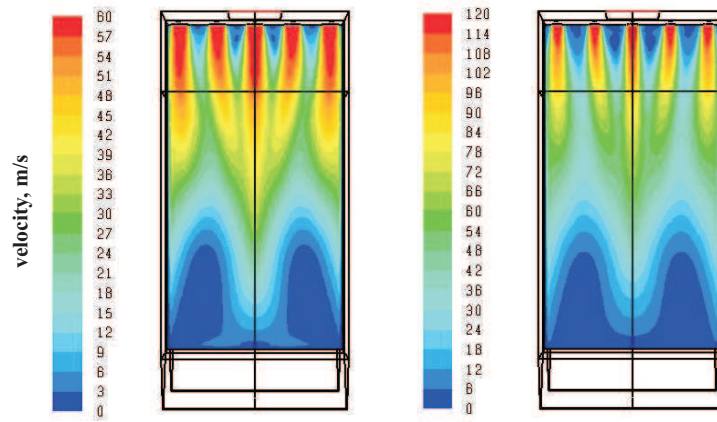
Figure 9.9: Velocity field inside the boilers at 60 $\frac{m}{s}$ (left) and 120 $\frac{m}{s}$ (right) combustion air inlet velocity
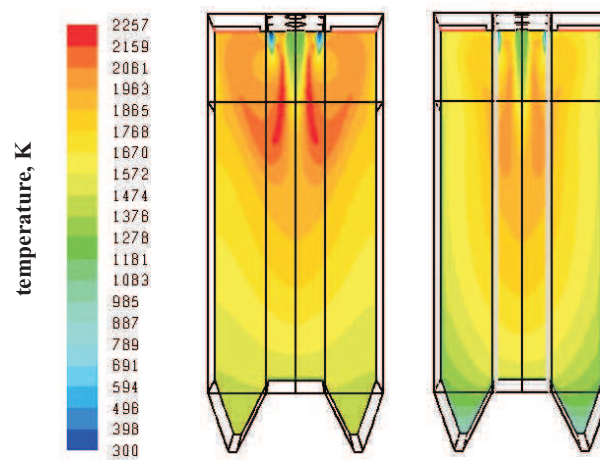
Figure 9.10: Temperature field inside the boilers at 60 $\frac{m}{s}$ (left) and 120 $\frac{m}{s}$ (right) combustion air inlet velocity
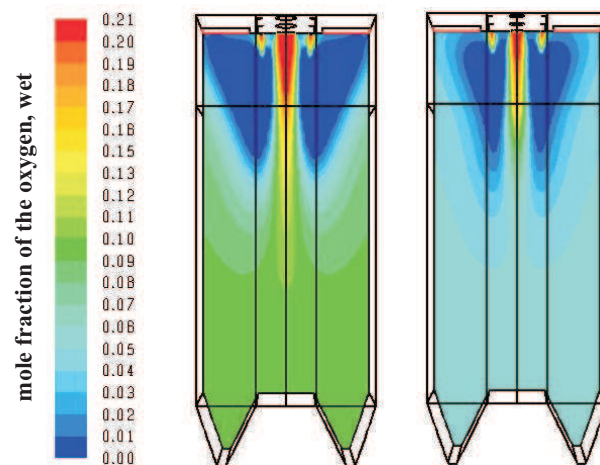
Figure 9.11: Oxygen concentration field inside the boilers at 60 $\frac{m}{s}$ (left) and 120 $\frac{m}{s}$ (right) combustion air inlet velocity
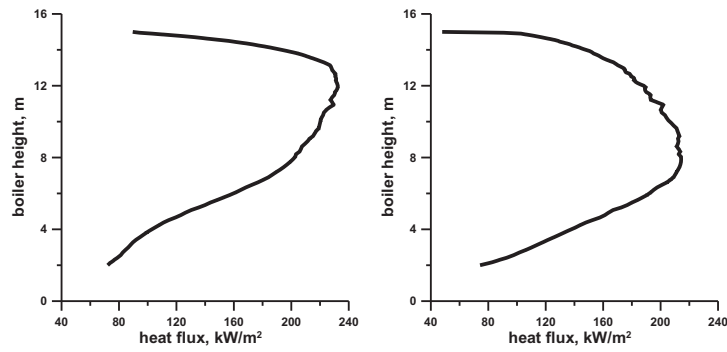
Figure 9.12: Heat flux along the height of the boilers at combustion air inlet velocities of 60 $\frac{m}{s}$ (left) and 120 $\frac{m}{s}$ (right)

The heat flux along the height of the boilers are presented in Fig. 9.12. Due to the absence of strong combustion products recirculation the heat transfer in boiler operated at the low combustion air inlet velocity (left) is not so intensive as in the case of the high combustion air inlet velocity (right). The heat fluxes profile along the boiler height is more uniform in the case of boiler operated at the high combustion air velocity than at the boiler operated at the low combustion air inlet velocity. In the boiler operated at the low combustion air inlet velocity, at the bottom part of the boiler small values of the heat fluxes can be observed while in boiler operated at the high combustion air inlet velocity along the boiler height the heat fluxes are of high and similar values. The thermal efficiency of the boiler operated at combustion air inlet velocity equal to 120 $\frac{m}{s}$ is 13% higher than of the boiler operated at combustion air inlet velocity of 60$\frac{m}{s}$.

9.2.2 Findings

This series of numerical simulations has been performed to test the HTAC boiler operated at a 60$\frac{m}{s}$ injection velocity of the combustion air. It has been confirmed that a high velocity (and at the same time a high momentum) of the combustion air jet is an essential feature to create a correct recirculation pattern inside the combustion chamber. If this injection velocity is reduced by half, insufficient recirculation is created. Both the combustion air and the fuel jets are not diluted by the combustion products and as a consequence the important characteristics of HTAC technology disappear: the homogeneity of both the temperature and the species concentration fields, low temperature peaks and uniformity of the heat fluxes profiles along the height of the boiler.

9.3 The HTAC boiler operated at nearly stoichiometric conditions

One of the important factors controlling combustion in a boiler chamber is an amount of the supplied air since an adequate amount of air is needed for complete combustion. Amount of the combustion air is defined using air excess ratio (λ) which is a ratio between the amount of the air present in the combustion process to the amount of the air needed for complete combustion. Operating a boiler at too low air excess ratio results in incomplete combustion (combustible gases in exhaust gas and carbon in ash). On the other hand, too high air excess ratio increases physical outlet loss. Modern power plant boilers fired with pulverized coal usually run at air excess ratio in a range between 1.15-1.3 [13].
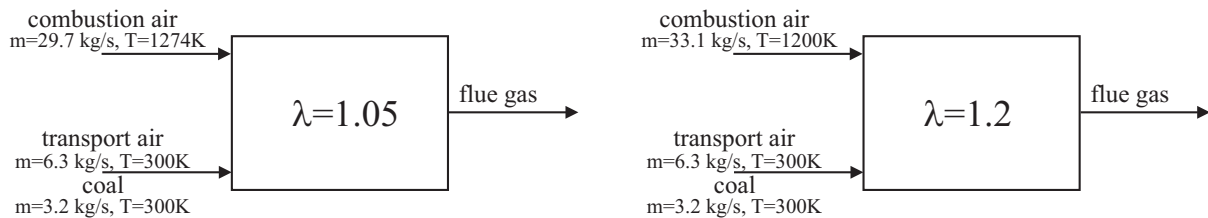
Figure 9.13: Operating conditions in the boilers operated at 1.05 (left) and 1.2 (right) excess air ratios

In this Section the possibility of the HTAC boiler operation at air excess ratio just above stoichiometric value (λ=1) has been examined and a special emphasis is given to the coal burnout. The series of the computations has been performed for the HTAC boiler operated at 1.05 air excess ratio. Therefore, the combustion air input into the boiler is slightly lower in comparison to the reference boiler (air excess ratio of 1.2). However, the same thermal input in preheated air and fuel is kept in both boilers (130 MW_{th}), increasing the combustion air temperature up to 1274 K in the boiler operated at 1.05 excess air (see Fig. 9.13). Other operating conditions are similar in both computational runs.

9.3.1 Results and discussion

Results of the numerical simulation of the boiler operated at λ=1.05 are compared with the results of the numerical simulation of boiler operated at λ=1.2 (reference case) in the following graphs. The profiles are plotted along traverses 1, 2, 3, as showing in Fig. 9.14.
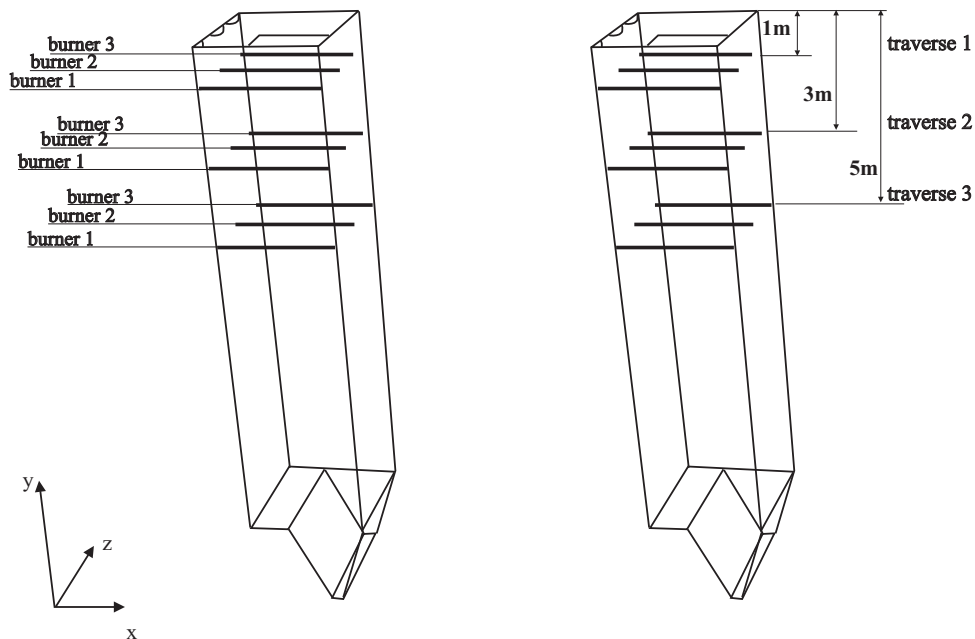
Figure 9.14: Location of the traverses inside the boilers

The predicted temperature profiles along the selected traverses and for each burner are plotted in Fig. 9.15. In the region of the first traverse, it can be seen that the combustion air jet and the coal jet are separated. In the region of traverse 2 both jets begin to merge together and to create one general flow. The peak of the temperature occurs in the region of the second traverse. It is about 2100 K in the boiler operated at λ=1.2 and about 2200 K in the boiler operated at λ=1.05. It can be noticed that the temperatures are higher in the boiler operated at λ=1.05 as expected.

The predicted oxygen concentration profiles plotted along three traverses for three burners are presented in Fig. 9.16. In the region of the first traverse for both tested excess air values the oxygen concentration profiles are similar; the lack of the oxygen can be seen. The difference between oxygen levels are visible beginning from the second traverse onwards up to the outlets. The oxygen concentration level is around 2% higher in the boiler operated at λ=1.2 than in the boiler operated at λ=1.05. However, the oxygen concentration profiles are similar. The highest predicted concentrations of the volatiles in the boiler operated at 1.2 air excess ratio is 10% and in the case of the boiler operated at 1.05 air excess ratio is 6% higher. However, the volatiles are completely burned before they reach the boiler outlets. No carbon monoxide concentrations were predicted at the outlets. The char burnout at the boiler outlets is equal to 99.9%.
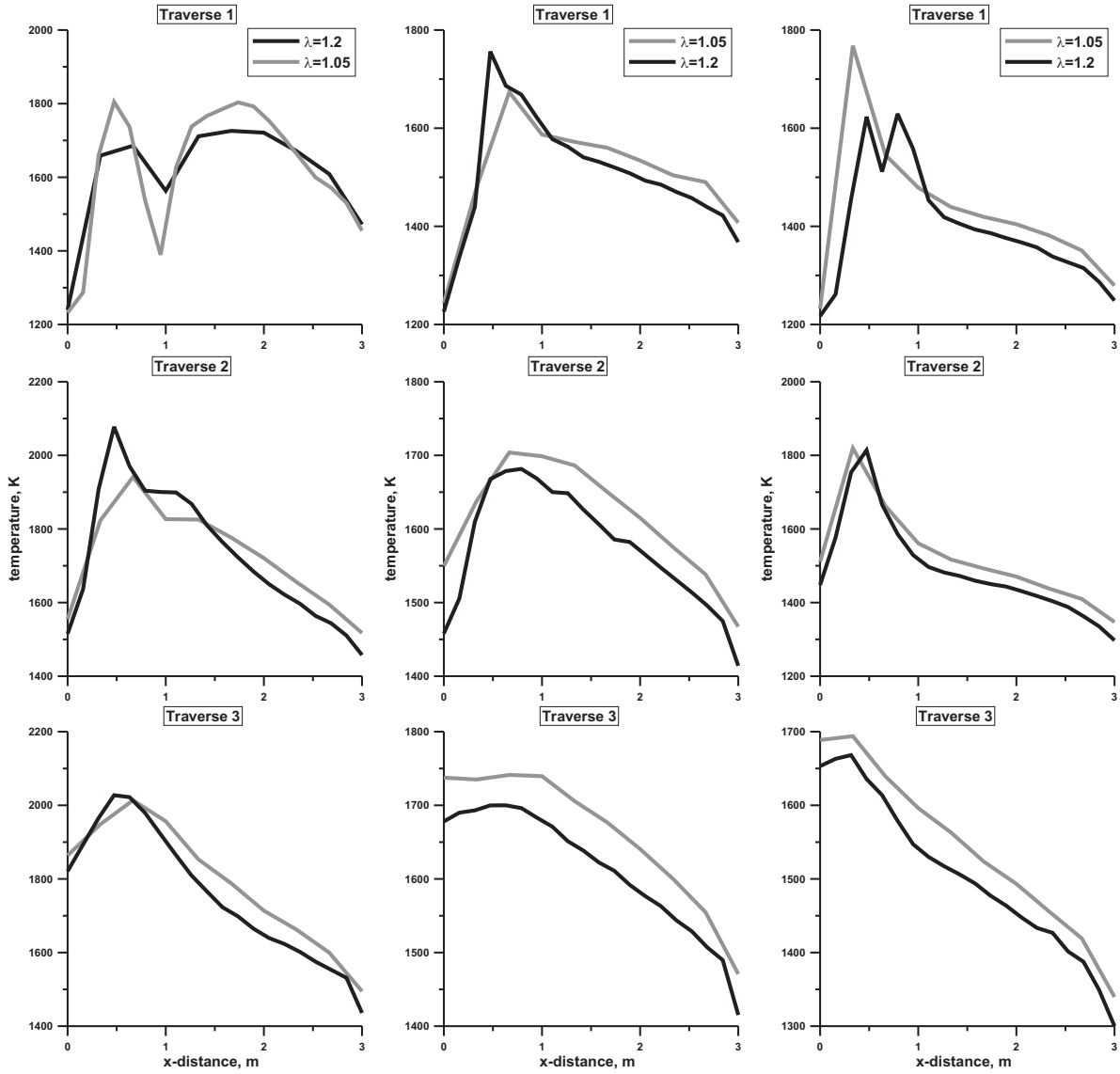
Figure 9.15: Temperature profiles along the traverses in the plane of: burner 1 (left), burner 2 (center) and burner 3 (right)

9.3.2   Findings

One of the challenges of the PC boilers construction is to reduce the boiler energy losses. The biggest loss is the physical outlet loss related to the exhaust gas enthalpy. On the other hand, a complete burnout has been ensured. In the HTAC boiler, due to very intensive recirculation of the combustion gas, the coal particles residence time is extended. Therefore, problems with char burnout may be eliminated. This opens up the possibility to operate the HTAC boiler at a low air excess ratio. This calculation series has been carried out for the HTAC boiler operated at 1.05 air excess ratio.
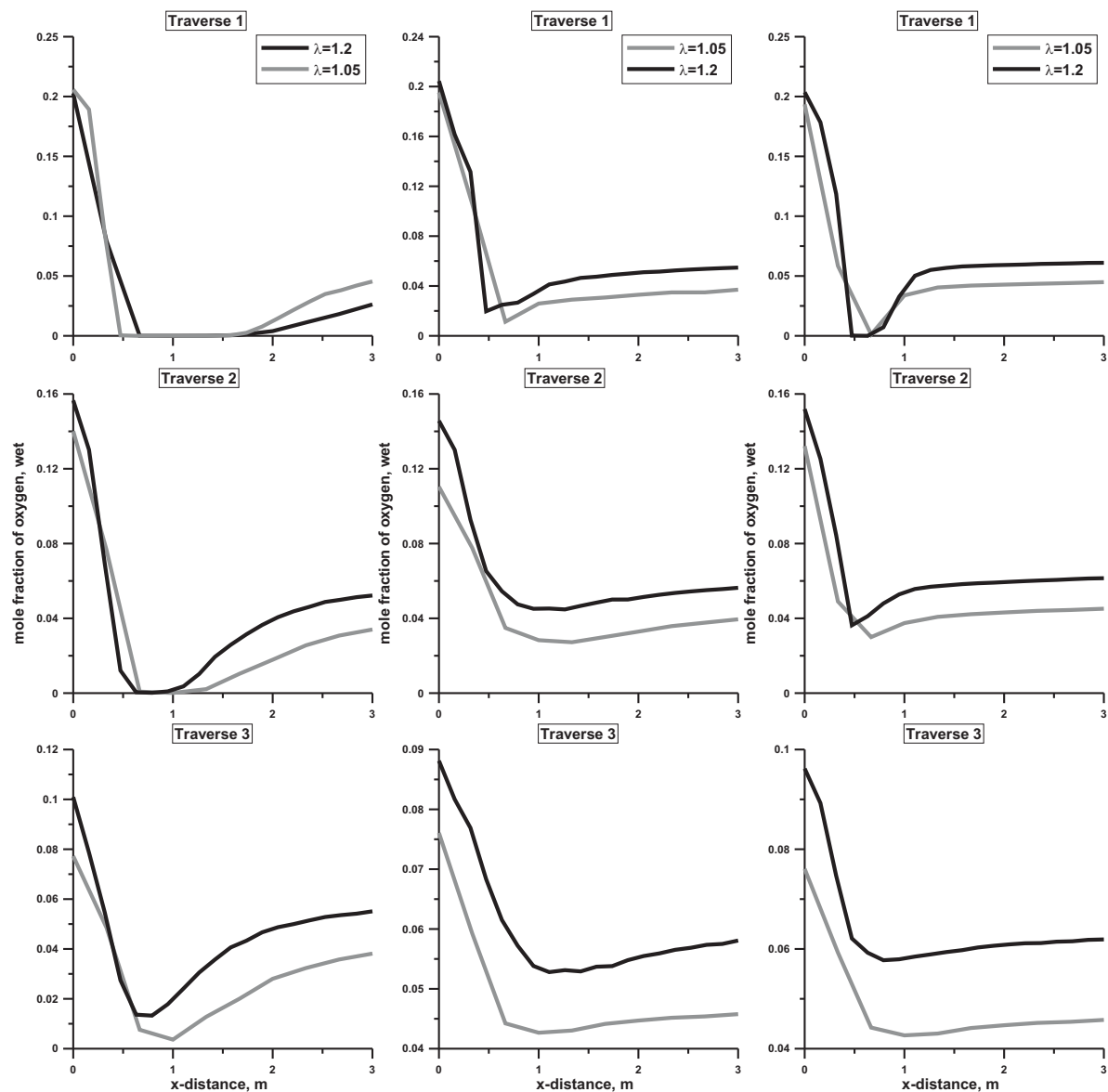
Figure 9.16: Oxygen concentration profiles along the traverses in the plane of: burner 1 (left), burner 2 (center) and burner 3 (right)

It is concluded that all features of HTAC technology are retained; 99.9% burnout of the char and 100% burnout of the combustible gas (carbon monoxide and volatiles) are predicted.

Chapter 10

Coupling between the HTAC boiler and the steam cycle

Boiler design procedure involves an examination of the combustion process as well as the steam cycle. Both issues are strongly coupled due to the heat transferred from the combustion products inside the chamber to the water/steam mixture inside the boiler tubes. In this Chapter the coupling between the HTAC boiler and the entire steam cycle is taken into consideration. The HTAC boiler is proposed as an ultra-supercritical boiler with the once-through type of the water circulation. Supercritical water/steam is considered as the working fluid. The pressure of the superheated steam at the end of the boiler tubes and its mass flow are assumed while the temperature of the superheated steam is computed. A subroutine implemented into the FLUENT code has been written to perform the calculations. In the calculations performed until now, the temperature of the boiler walls was assumed to be constant. In this simulation series, the wall temperature profiles are computed based on the heat transfer calculations. Finally, the thermal efficiency of the steam cycle coupled with the HTAC boiler is estimated.

As mentioned in Section 1.8, there are different types of boiler tubing and in this Chapter the most common used tubes configurations are examined, namely vertical and spiral tubes arrangements. Vertical tubing is tested for two designs: down-up (water is supplied from the bottom of the boiler and flows to the top) and the opposite situation up-down (water is supplied from the top of the boiler and flows to the bottom). These three considered configurations are illustrated in Fig. 10.1.
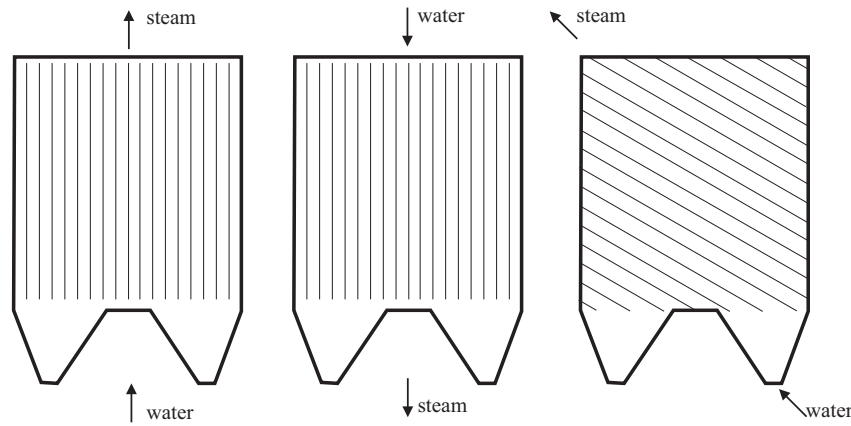
Figure 10.1: Arrangement of the tubing walls: vertical down-up (left), vertical up-down (center) and spiral (right)

A key factor in boiler design is the amount of energy needed to heat up the supercritical working fluid up to the required parameters. For the considered boiler, the supercritical water at T=300 K and p=30 MPa is converted into supercritical steam whose temperature is calculated. The temperature of the water supplied to this HTAC boiler is around 300-400 K lower than in a standard PC boiler where water is preheated in an economizer. Usually, in the economizer the combustion products are cooled from 2200 K to around 1300 K. The rest of the energy included in the flue gas is utilized in a heat exchanger preheating the combustion air. The flue gas temperature at the stack should be around 400 K. Heat transfer to the boiler walls is basically controlled by radiation. The furnace enclosure is made out of the tubes in a membrane construction (called membrane wall or panel). These are closely spaced tubes connected by bars continuously welded to each tube. The construction of the enclosure walls is presented in Fig. 10.2.
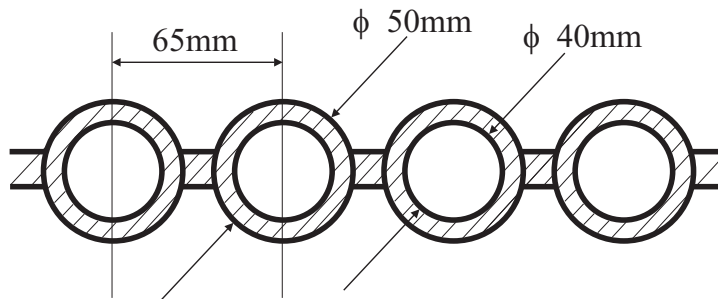
Figure 10.2: Construction of the enclosure walls of the boiler: view from the top and from the side

The following boiler tubing geometry is selected: outer diameter of each tube is equal to 0.05 m and inner diameter to 0.04 m. The spacing between successive tubes

is equal to 0.065 m. Each of the membrane wall consists of 800 tubes (consequently, in the simulations of the quarter of the combustion chamber 200 tubes are taken into consideration only). One side of the wall is exposed to the hot combustion products; at the other side an insulation and lagging (sheet metal) are provided to minimize heat losses.

In all previously performed simulations of the combustion chamber the temperature at the boiler walls was fixed at 800 K. In this Chapter, the temperature profiles at the boiler walls are calculated. The HTAC boiler is designed as one-through boiler which means that the medium flows only once through the tubes in boiler (see Section 1.8). A standard once-through system consists simply of one tube in which the working fluid is preheated, evaporated, and superheated while it flows through. In a real one-trough boiler, this tube is divided into several heating surfaces with many tubes in parallel, headers (collectors) at the inlet and outlet, and the pipes connecting the headers of the heating surfaces. In one-through boilers an increase of heat transfer coefficients is achieved by an increased mass flow rate. For a given steam generation rate (feeding water flow) this solution leads to a smaller tube diameter, a smaller number of tubes in parallel and a higher pressure drops in tubes.

In order to include the heat transfer between the combustion products and the supercritical working fluid into the FLUENT code a user define subroutine (UDF) has been written. The final HTAC boiler geometry as well as the operating and boundary conditions (see Chapter 6) are the starting point for these calculations. Three different tubing designs presented in Fig. 10.1 are considered. The vertical boiler walls are regarded as the heat transfer (tubing) surfaces, as shown in Fig. 10.3. The other faces of the boiler (as the ash hoppers, wall between burners, etc.) are assumed to be adiabatic.

The algorithm describing the calculation procedure is schematically shown in Fig. 10.4. The heat transfer rates per unit of height ($\dot{Q}_l$) of the membrane wall have been obtained in the CFD predictions of the combustion chamber. These values are the input data for the UDF subroutine. The heat is transferred to the boiler tubes and to the working fluid. The conduction heat transfer inside the tube walls is neglected. At the beginning of the process the working fluid is a supercritical water which is converted into an ultra-superheated steam. The working fluid consists of the one phase only because of supercritical conditions of the process.

The heat transfer rate between the combustion products and the working fluid is described by the following equation:

$$\frac{d\dot{H}}{dy} = \dot{Q}_l \tag{10.1}$$

Introducing into the above equation the mass flow of the medium one obtains:

$$\dot{m}\frac{dh}{dy} = \dot{Q}_l \qquad (10.2)$$

where $\dot{Q}_l$ is the heat transfer rate per meter of the tube height, $\dot{H}$ stands for the total enthalpy of the medium, h is the medium specific enthalpy and $\dot{m}$ is the mass flow rate of the medium while y is the distance in y direction (see Fig. 10.4).
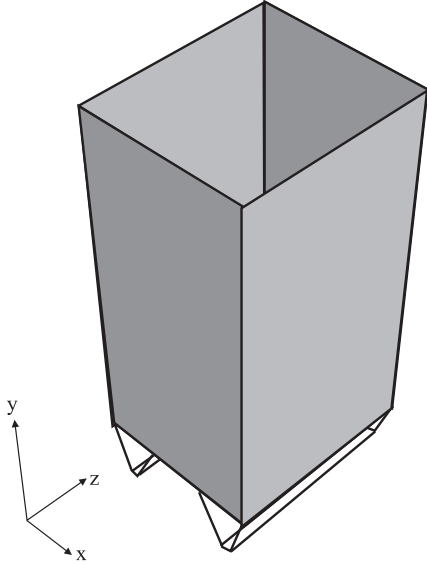
Figure 10.3: Heat transfer surfaces in the boiler
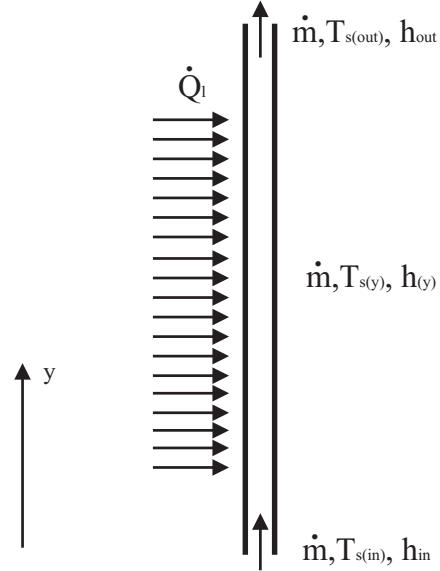
Figure 10.4: Algorithm of the boiler tube heat transfer

Using Eq. 10.2 the specific enthalpy of the medium, represented by $h(y)$ is calculated, as a function of y distance. Furthermore, the temperature of the working fluid, denoted as $T_s(y)$ is calculated using the steam tables [32]. This temperature shoud be lower than 750^oC which is assumed in this calculations as the maximum thermal resistance temperature of the steel material. The steam pressure is assumed to be p=30 MPa and water/steam mass flow is equal to 17 $\frac{kg}{s}$. Additionally, the convective heat transfer coefficient α is computed along the tube at the side of the supercritical working fluid. Nusselt function is calculated for the water/steam under supercritical conditions according to the formula of Yamagata et al. [186]. The efficiency of the fins is assumed to be equal to 1. The temperature profiles of the steam as well as the combustion products at the boiler walls are obtained.

10.1   Results and discussion

As a result of the heat transfer calculations, the temperature profiles along the boiler walls are obtained. The gas temperature at the boiler walls is indicated as T_1 and is shown

in Fig. 10.5 while contours of the working fluid temperature (T_2) are shown in Fig. 10.6. The temperature difference ΔT between the wall temperature at the gas side and the wall temperature at the working fluid side is also calculated as $\Delta T = T_1 - T_2$. Contours of this temperature are presented in Fig. 10.7.
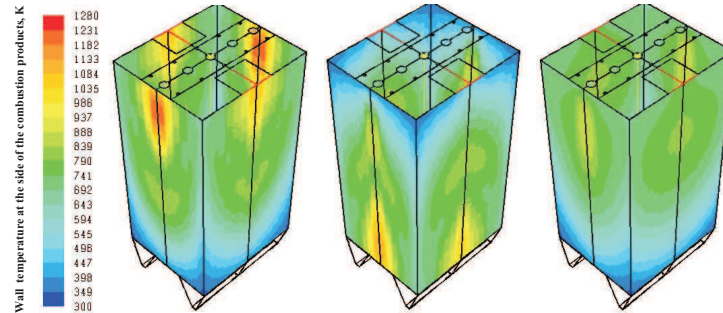
Figure 10.5: Wall temperature at the side of the combustion products for three tubes arrangements: vertical down-up (left), vertical up-down (center) and spiral (right)
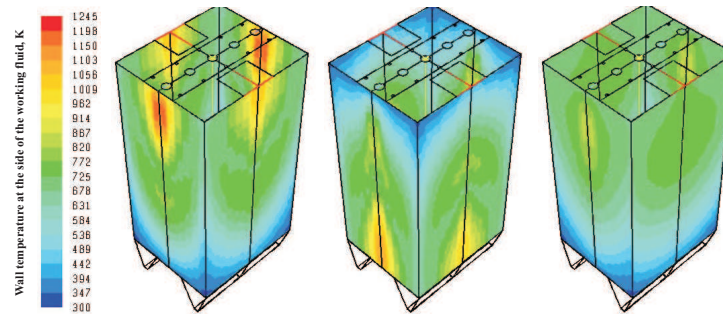
Figure 10.6: Wall temperature at the side of the working fluid for three tubes arrangements vertical down-up (left), vertical up-down (center) and spiral (right)
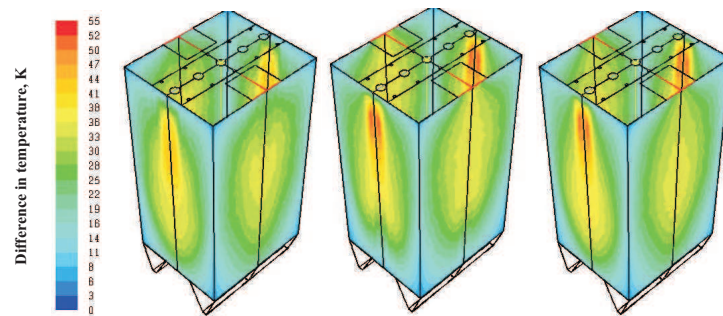
Figure 10.7: Temperature difference for three tubes arrangements: vertical down-up (left), vertical up-down (center) and spiral (right)

It can be observed that the temperature profile at the walls of the combustion side (inside the combustion chamber) as well as at the cooling side (inside the tubes) is generally uniform and almost of a constant level. The maximum difference between both temperatures is observed in the case of the vertical up-down type of the tubes construction and it is equal to $55\ K$. This maximum temperature occurs near the coal ignition region and this part of the tubes should be carefully cooled. In all considered tubes arrangements it can be noticed that the less utilized parts of each boiler are the corner regions, mostly these which are located at the bottom part of the boiler. Smaller temperature differences are observed in the corners located at the top part of the boiler. It could be suggested that the best shape of the boiler, from this point of view, could be a cylindrical boiler. Further investigations on the subject will be required but this question is not here addressed.

The temperature distribution along the boiler tubes for all three arrangements is shown in Fig. 10.8; the horizontal line in each graph marks the maximum thermal resistance temperature of the assumed steel material $(750^{o}C)$.
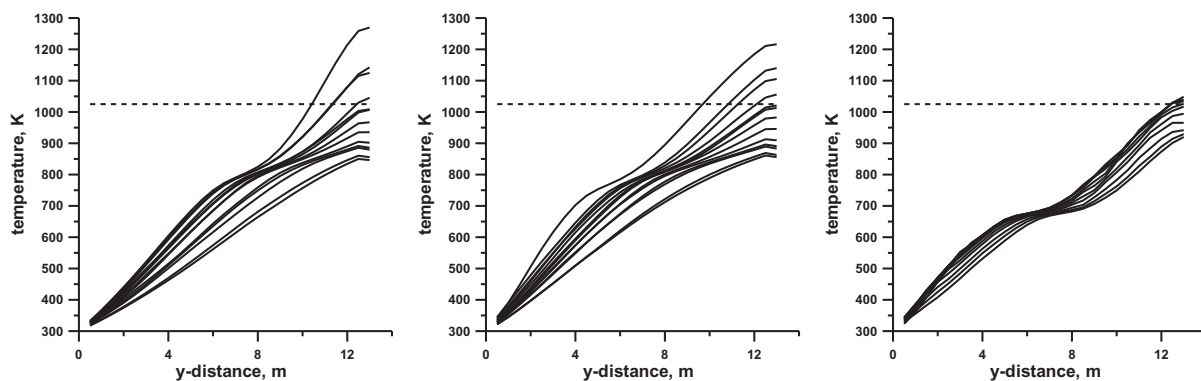
Figure 10.8: Temperature distribution along selected tubes for the simulated arrangements: vertical down-up (left), vertical up-down (center) and spiral (right)

The most uniform temperature profile can be found in the boiler with spiral tubing. It has to be noticed that despite the similar averaged steam temperature in all three tubes arrangements in both vertical configurations the temperature dispersion is significantly higher than in the spiral one. As an result, some tubes in vertical arrangements have the final temperature higher than the maximum available from the steel thermal resistance, as can be seen in Fig. 10.8. This problem does not occur in the spiral arrangement. According to this results the water/steam mass flow $(17\ \frac{kg}{s})$ has been selected as the minimum mass flow forcing in the spiral tube arrangement that none of the boiler tubes overrun the temperature limit. In order to keep the tubes temperature under the limit in both vertical arrangements, the water/steam mass flow has to be increased to $20\ \frac{kg}{s}$. As a consequence,

the averaged steam temperature decreases to 560^oC. That implies the reduction of the Rankine cycle thermal efficiency. Comparing two vertical tubes arrangements, it can be noticed that the up-down configuration is inferior to the down-up one. In the up-down configuration water is added from the top of the boiler and it achieves immediately the hottest region of the boiler while near this region the steam superheating process should take place. Therefore, better results are obtained with the down-up arrangement of the vertical tubing boiler.

The calculated averaged steam temperatures (after the steam of each tube is mixed in the collector) for each considered tubes arrangement are summarized in Tab. 10.1. It can be observed that the calculated steam temperature are of a similar level and only slightly differences can be observed. In both vertical tubes configurations the average steam temperature is around $965\ K$. The steam temperature in the spiral tubes design is equal to $973\ K$.

configuration	steam temperature, ^oC	steam temperature, K
down-up	692	965
up-down	693	966
spiral	700	973

Table 10.1: Calculated steam temperatures for considered tubes configurations

The uniform heat fluxes distribution at the boiler walls is the consequence of the uniform temperature field inside the HTAC boiler. The furnace wall heat flux profile for all tested tube designs is presented in Fig. 10.9.
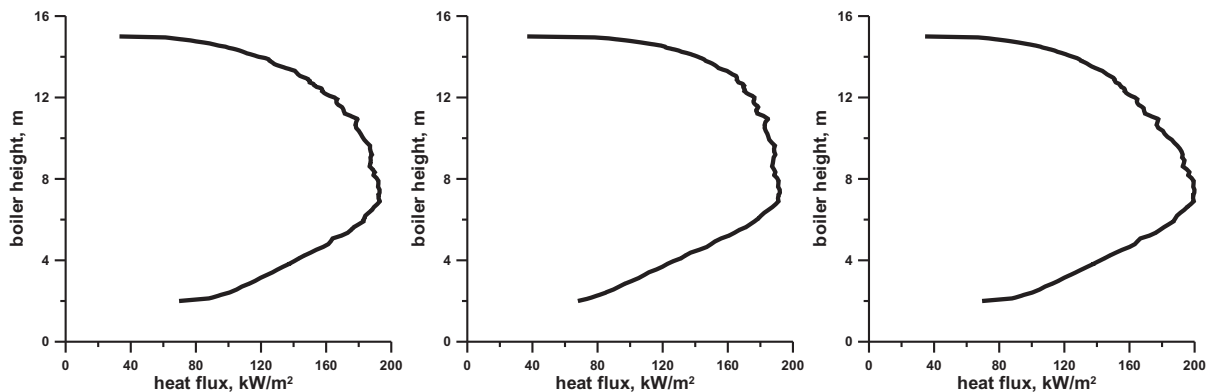
Figure 10.9: Heat flux along the height of the boiler for the simulated tubes arrangements: vertical down-up (left), vertical up-down (center) and spiral (right)

It can be noticed that all heat flux profiles are similar in both the shape and the heat flux values. However, it was concluded that not all of the proposed tubes arrangement are appropriate for the HTAC boiler designed as once-through supercritical boiler. The spiral arrangement seems to be the most suitable for the HTAC boiler due to the most uniform temperature distribution inside the boiler tubes.

10.2   Cycle efficiency

In this Paragraph, the thermal efficiency of the Rankine cycle is calculated using the steam parameters calculated previously. Since the implementation of the Rankine cycle is not a subject of this work, only the most basic approach of the Rankine cycle is taken into consideration in this calculations. According to Eq. 10.3, thermal efficiency of the HTAC boiler is calculated.

$$\eta_R = \frac{i_2 - i_3}{i_2 - i_1} \tag{10.3}$$

For these computations the following assumptions are made: the pumping work is negligible, the steam inside the turbine expands to p_3=0.008 MPa, and the expansion process in the turbine is isentropic. The pumping work is negligible. Rankine cycle in T-s diagram depicted for the calculated cycle is shown in Fig. 10.10.
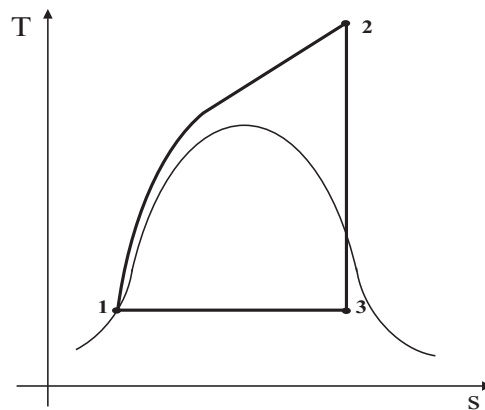
Figure 10.10: T-s diagram of the considered Rankine cycle

The enthalpies i_1, i_2 and i_3 which occur in Eq. 10.3 represent the state of the working medium before boiler, after boiler/before turbine and after turbine, respectively. The calculated values of enthalpies, as well as steam temperatures and pressures are presented in Tab. 10.2.

point	medium	temperature,K	pressure,MPa	enthalpy,$\frac{kJ}{kg}$
1	water	300	30	140
2	steam	973	30	3743
3	steam	302	0.004	2041

Table 10.2: Parameters for the Rankine cycle efficiency calculations

The efficiency of the Rankine cycle is dependent only on the steam parameters at the outlet of the boiler and at the outlet of the turbine and water parameters at the inlet of the boiler. The efficiency calculated for the simple Rankine cycle assumed in these computations is around 48%.

10.3 Findings

In this Chapter the heat exchange process between the combustion products inside the boiler and the working fluid inside the tubes has been considered. Thus, the temperature profiles at the boiler walls and along the boiler tubes has been calculated. Three commonly used configurations of the once-trough boiler tubes have been tested. The most uniform temperature profile along the tubes has been found in spiral tubes configuration. The temperatures peaks higher than the assumed thermal resistance of the steel has been avoided in this tubes arrangement. However, this configuration is the most complicated for manufacturing. It was concluded that the spiral tubes configuration is the most suitable for the HTAC boiler designed in this thesis. The obtained supercritical steam temperature is around 970 K in the spiral arrangement and slightly lower in the vertical tubing arrangement. The Rankine cycle efficiency of the steam cycle coupled with the HTAC boiler calculated for the parameters 30 MPa and 700$^o C$ is around 48%. It has to be emphasized that the Rankine efficiency is not depended on the boiler performance but is based on the temperature and the pressure of the supercritical steam. Each boiler of whatever principle reaching the same steam parameters obtains the same Rankine cycle efficiency. In has been proved that the HTAC boiler is able to reach the required steam parameters keeping the design of the boiler itself compact and simple.

Chapter 11

Conclusions and future works

Conclusions

This thesis presents a novel boiler concept that utilizes the principle of High Temperatures Air Combustion. Although the combustion with highly preheated air has substantially advanced over the last decade or so, there has been relatively little work undertaken to adapt it to coal combustion. The HTAC technology has already been successfully applied to a number of industrial furnaces. However, such applications are limited to either gaseous fuels or light oils. To the best of author's knowledge this thesis is the first attempt to design a HTAC boiler fired with pulverized coal. A hypothetical 130 MW_{th} supercritical boiler producing 20 $\frac{kg}{s}$ steam at parameters: pressure of 30 MPa and temperature up to 700 ^oC has been developed.

Realizing the advantages of High Temperatures Air Combustion technology a boiler of a high firing density has been designed with the combustion process proceeding in such a way as to provide the highest possible uniformity of the increased heat fluxes. To this end the NFK/IFRF burner concept which can be characterized by a central combustion air jet and two pulverized coal jets, has been carefully tailored into the optimized boiler shape (and volume). In order to achieve the required uniformity of the combustion process which efficiently proceeds over the entire boiler volume a thorough optimization of the following parameters has been carried out:

- number of burners and burner spacing

- distance between the coal jets and the central air jet

- the momentum (velocity) of the combustion air stream

- dimensions of the combustion chamber

Among the several geometries considered, the symmetrical boiler of a down-fired type equipped with a one-trough spiral arrangement of cooling tubes has proven to be superior. Such a design may result in the Rankine cycle efficiency exceeding 50%.

The study has indicated that such a boiler will possess several additional characteristics as follow:

- low NO_x emissions which for a coal containing around 1.5% N is around 260 *ppm* at $6\%O_2$

- flexible operation in terms of boiler turn-down

- improved fuel burnout due to enhanced coal ignition and long residence times

- simple burner constructions; without flame stabilization devices, swirl or air staging which are commonly used in conventional pulverized coal burners

- small boiler size in comparison with standard PC boilers

Although HTAC technology seems to be attractive for power boilers fired with pulverized coal there are still many open questions. The particulate concentration in the flue gas for the coal flame is probably too high to use this technique in conjunction with regenerative heat exchangers. There is a need to find a way to utilize the enthalpy of the boiler exhaust gas. The unresolved issues of the HTAC technology application to coal-fired boilers which have been identified in this work are:

- practical realization of preheating of combustion air using the flue gas

- the design may be prone to erosion

Overall, the present study confirmed that HTAC technology could be a practicable, efficient and clean technology for fossil fuel fired boilers. However, it has to be pointed out that the investigated boiler is still a concept only.

The study has been carried out for a Guasare high volatiles coal which in its properties is similar to many hard coals of Poland. However, before proceeding further with the boiler design optimization a comprehensive analysis of the effect of coal properties is needed to establish a range of coals suitable for this particular design.

Future works

The work has demonstrated the advantages of the HTAC boiler although it is prematurely to say that this new concept is complete. Research in the follow areas is still required:

Optimization procedure of the boiler. The developed HTAC boiler is only a concept; there are still several parameters which should be optimized. Probably, a cylindrical boiler could be advantages.

Boiler fired with natural gas or oil. The major obstacle of the proposed HTAC boiler is in the lack of a clear concept for utilization of the exhaust gas enthalpy for air preheating. High particles concentrations of the exhaust gas cause slagging and fouling of such devices. This problem does not occur when gaseous fuels or oils are combusted. Boilers fired with natural gas were not investigated in this work because of a low importance of natural gas in Poland. However, applications of HTAC technology to boilers fired with gaseous fuels or oils are extremely attractive.

FLOX configuration. In the present work only the NFK/IFRF concept of HTAC technology implementation has been studied. It could be interresting to examine also the German approach, namely FLOX burner application into the proposed boiler.

HTAC combustion under O_2/CO_2 atmosphere. Increase interest in CO_2 sequestration from large CO_2 sources such as fossil fuel power plants is forced through the anty-global warming polices. Several technologies for large scale CO_2 capture are under development. HTAC technology may be suitable for coal combustion under O_2/CO_2 atmosphere.

Laboratory, pilot and semi-industrial scale tests. Extra laboratory tests are needed to enhance the understanding of both the devolatilization and the char combustion under HTAC conditions. Furthermore, slagging, fouling, corrosion and errosion of metal surfaces under HTAC conditions is poorly understood. Together with a basic research, there is a need to increase the knowledge on applicability of HTAC technology to real power plant boilers. Before an eventual industrial application of this technology takes place, pilot tests, as well as semi industrial scale tests will be needed.

Nomenclature

Abbreviations

Symbol/Acronym	Description
AFBC	Atmospheric Fluidized Bed Combustion
ASTM	American Society for Testing and Materials
BTU	British Thermal Unit
CFD	Computational Fluid Dynamics
CG	Coal Gasification
CPD	Chemical Percolation Devolatilization
DNS	Direct Numerical Simulation
DO	Discrete Ordinates
EBU	Eddy Break Up
EDC	Eddy Dissipation Concept
EDM	Eddy Dissipation Model
EEC	Excess Energy Combustion
EU	European Union
FBC	Fluidized Bed Combustion
FGD	Flue Gas Desulphurization
FLOX	FLameless OXidation
HRS	High Regenerative Combustion
HTAC	High Temperature Air Combustion
IFRF	International Flame Research Foundation
IGCC	Integrated Gasification Combined Cycle
IGFC	Integrated Gasification Fuel Cells
LCV	Low Calorific Value
LDV	Laser Doppler Velocimetry
LES	Large Eddy Simulation
LPG	Liquefied Propan Gas

Symbol/Acronym	Description
MILD	Moderate and Intensive Low-oxygen Dilution
NFK	Nippon Furnace Kogyo
NMR	Nuclear Magnetic Resonance
PC	Pulverized Coal
PFBC	Pressurized Fluidized Bed Combustion
PFR	Plug Flow Reactor
RAM	Reynolds Avaraged Models
RANS	Reynolds Avaraged Navier Stokes Equation
R&D	Research and Development
SCR	Selectiv Catalytic Reduction
SNG	SyNtesis Gas
UNFCCC	United Nations Framework Convention on Climate Change
USA	United States of America
USC	Ultra Super Critical

Latine symbols

Symbol	Unit	Description
A	m^2	surface area
A, B		constants of EDM
a	$\frac{1}{m}$	absorption coefficient
C_μ		constant of the $k - \varepsilon$ model
c_p	$\frac{J}{kg \cdot K}$	specific heat at constant pressure
D	$\frac{m^2}{s}$	diffusion coefficient
d	m	diameter
Da		Damköhler number
F	N	force
H	J	total enthalpy
$\dot{H}$	kW	total enthalpy of the flow
h	$\frac{W}{m^2 \cdot K}$	convective heat transfer coefficient
I	$\frac{W}{m^2 \cdot sr}$	radiation intensity
J	$\frac{mol}{m^2 \cdot s}$	molecular diffusive flux of the species
Ka		Karlowitz number
k	$\frac{kg \cdot m^2}{s}$	kinetic energy
k	var	rate constant of reaction
M	$\frac{kg}{kmol}$	molar mass
m	kg	mass
$\dot{m}$	$\frac{kg}{s}$	mass flow
P		products
p	Pa	pressure
Pr		Prandtl number
$\dot{Q}$	kW	heat flux
R	$\frac{J}{kg \cdot K}$	universal gas constant
R		reactants
$\Re$	$\frac{mol}{m^3 \cdot s}$	reaction rate
Re		Reynolds number
S	$\frac{kg}{m^3 \cdot s}$	source term
s	m	path length
Sc		Schmidt number
T	K	temperature
t	s	time
u	$\frac{m}{s}$	velocity

Symbol	Unit	Description
U	$\frac{m}{s}$	Reynolds average velocity
x, y, z	m	cartesian coordinates
Y		mass fraction

Greek symbols

Symbol	Unit	Description
Γ		diffusion coefficient
γ		mass fraction inside the control volume
ε	$\frac{kg \cdot m}{s}$	dissipation of turbulent kinetic energy
ε		emissivity
η		effectiveness factor
θ	K	temperature difference
λ		air excess ratio
μ	$\frac{kg}{m \cdot s}$	dynamic viscosity
ν	$\frac{m^2}{s}$	kinematic viscosity
ν		stoichiometric coefficient
ρ	$\frac{kg}{m^3}$	density
σ	$\frac{W}{m^2 \cdot K^4}$	Stefan-Boltzmann constant
τ	$\frac{N}{m^3}$	stress tensor
Φ		phase function
ϕ		general variable
Ω	sr	solid angle

Superscripts

Symbol	Description
$\star$	fine structures

Subscripts

Symbol	Description
$a, b, ..$	chemical species
c	chemical
$comb$	combustion
dev	devolatilization
$i, j, ...$	variables
inn	at the inlet
m	mass
out	at the outlet
p	particle
R	radiation
t	turbulent
vap	vaporization
∞	continuous phase
0	initial

Bibliography

[1] *Key World Energy Statistics.* International Energy Agency, IEA, 2008. (`www.iea.org`).

[2] *Survey of Energy Resources.* World Energy Council, WEC, 2007. (`www.worldenergy.org`).

[3] *Deciding the Future: Energy Policy Scenarios to 2050.* World Energy Council, WEC, 2007. (`www.worldenergy.org`).

[4] J.P. Longwell, E.S. Rubin, and J. Wilson. Coal: energy for the future. *Prog. Energy Comb. Sci.*, 21:269–360, 1995.

[5] *International Energy Outlook.* Energy Inormation Administration, EIA, 2008. (`www.eia.doe.gov`).

[6] D. Scott and P. Nilsson. Competitivness of Future Coal-Fired Units in Different Countries. Coal Research Report. Technical Report CCC/14, IEA, January 1999.

[7] J.P. Longwell, E.S. Rubin, and J. Wilson. Fossil fuel power generation. State of the art. Technical Report Contract No. ENK5-CT-2002-20625, Report prepared by PowerClean R,D&D Thematic Network under the European Union Fifth Framework Energy R&D Programme, July 2004.

[8] *Directive 2001/80/EC of the European Parliament and of the Council of 23 October 2001 on the limitation of emission of certain pollutants into the air from large combustion plants.* Official Journal L 309, 27/11/2001 P. 0001-0021.

[9] *Standardy emisyjne zgodnie z Rozporządzeniem Ministra Środowiska z 4.08.2003 w sprawie standardów emisyjnych z instalacji.* Dz.U. Nr 163, poz.1584. (in Polish).

[10] *Dreizehnte Verordnung zur Durchführung des Bundes-Immissionsschutzgesetzes (Verordnung über Grossfeuerungs- und Gasturbinenanlagen, 13. BImSchV) Vom*

20. Juli 2004. Bundesgesetzblatt Jahrgang 2004 Teil I Nr. 37, ausgegeben zu Bonn am 23. Juli 2004, Seite 1717. (in German).

[11] *Kyoto Protocol to the United Nations Framework Convention on Climate Change.* United Nations, 1998. (`www.unfccc.int`).

[12] E.E. Khalil. *Power Plant Design.* Abacus Press/Gordon and Breach Science Publishers, 1990.

[13] S. Kakac, editor. *Boilers, evaporators and condensers.* John Wiley & Sons, Inc., 1991.

[14] P. Kiameh. *Power generation handbook. Selection, Applications, Operation, and Maintenance.* McGraw-Hill, 2003.

[15] T.C Elliot, K. Chen, and R. Swanekamp. *Standard Handbook of Powerplant Engineering.* McGraw-Hill, 1997.

[16] H. Termuehlen and W. Empsperger. *Clean and Efficient coal fired power plants.* ASME Press, 2003.

[17] M. Pronobis. *Modernizacja kotłów energetycznych.* Wydawnictwa Naukowo-Techniczne, Warszawa, 2002. (in Polish).

[18] J.M. Beer. High efficiency electric power generation: The environmental role. *Prog. Energy Comb. Sci.*, 33:107–134, 2007.

[19] E.S. Tavoulareas. Fluidized bed combustion technology. *Annu. Rev. Energy Environ.*, 16:25–57, 1991.

[20] M.L. Murphy. Fluidized Bed Technology Solution to Animal Waste Disposal. In *17th International Pittsburgh Coal Conference*, Pittsburgh, USA, 2000.

[21] B.J.P. Buhre, L.K. Elliott, C.D. Sheng, R.P. Gupta, and Wall T.F. Oxy-fuel combustion technology for coal-fired power generation. *Prog. Energy Comb. Sci.*, 31:283–307, 2005.

[22] K. Damen, M. van Troost, A. Faaij, and W. Turkenburg. A comparison of electricity and hydrogen production systems with CO_2 capture and storage. Part A: Review and selection of promising conversion and capture technologies. *Prog. Energy Comb. Sci.*, 32:215–246, 2006.

[23] D.M. Woycenko, W.L. van de Kamp, and P.A. Peters. Combustion of pulverized coal in mixtures of oxygen and recycled flue gas. Technical Report IFRF Doc. No. F98/y/1, IFRF Reaserch Report, IJmuiden, 1995.

[24] Y.R. Mao, M.X. Fang, and S.R. Wang. Current Development of Research on Air Separation Flue Gas Recycle Technology. *Boiler Technology J.*, 33:5–9, 2002.

[25] Y.R. Mao, Y.G. Zhang, and G.S. Zhang. Research on Technologies for CO_2 Emission Control Sequestration and Recovery from Coal-fired Power Plant. *Boiler Manufacturing J.*, 1:20–22, 2003.

[26] K. Littewood. Gasification: Theory and Application. *Prog. Energy Combust. Sci.*, 3:35–71, 1977.

[27] X.T. Lia, J.R. Gracea, C.J. Lima, A.P. Watkinson, H.P. Chen, and J.R. Kim. Biomass gasification in a circulating fluidized bed. *Biomass and Bioenergy*, 26:171–193, 2004.

[28] R.F. Geosits and L.A. Schmoe. IGCC- the challenges of integration. In *ASME Turbo Expo 2005: Power for Land, Sea and Air*, Reno-Tahoe, Nevada, USA, 2005.

[29] Gasification Plant Cost and Performance Optimization. Technical Report Contract No. DE-AC26-99FT40342, US Department of Energy National Energy Technology Laboratory (NETL), September 2003.

[30] R.D. Hottenshine, N.A. Phillips, and R.A. Dill. Developments plans for advanced fossil fuel power plants. Technical Report CS-4029, EPRI, 1985.

[31] The Federation of Power Companies of Japan. *Electricity Review Japan*, March 2007. (www.fepc.or.jp).

[32] J. Szargut. *Termodynamika*. Wydawnictwo Politechniki Śląskiej, 2000. (in Polish).

[33] DTI/IEA. *Supercritical Steam Cycles for Power Generation Applications*, January 1999.

[34] K. Yamamoto, I. Kaijgaya, and I. Umaki. Operational Experience of USC Steam Condition Plant and PFBC Combined Cycle System with Material Performance. *Materials at High Temperatures*, 20:15–18, 2003.

[35] J.E. Oakey, L.W. Pinder, R. Vanstone, M. Henderson, and Osgerby S. Review of status of advanced materials for power generation. Technical Report COAL R224 DTI/Pub URN 02/1509, 2003.

[36] S. Kjaer. The Advanced Supercritical $700^{o}C$ Pulverised Coal-Fired Power Plant. In *Power-Gen Europe 2001*, Brussels, Belgium, 2001.

[37] J. Hald and B. Nath. New High Temperature Steels For Steam Power Plants. In *Power-Gen Europe 1998*, Milan, Italy, 1998.

[38] K. Strauss. *Kraftwerkstechnik*. Springer Verlag, 2006. (in German).

[39] Z.L. Rataj and A.W. Walewski. Once-through Benson boiler system after 83 years permament development- optimal design for supercritical CFB (OTU) boilers. In *10th International Conference on Boiler Techniology 2006*, Szczyrk, Poland, 2006.

[40] D.K. Mc Donald and S.S Kim. Vertical Tube, Variable Pressure Furnace for Supercritical Steam Boilers. In *Power-Gen International*, Las Vegas, Nevada, USA, 2001.

[41] H.H. Poulsen. Advantages of Ultra Super Critical Technology in Power Generation. In *International Conference on Clean Coal Technologies for our Future*, Sardinia, Italy, 2005.

[42] M. Katsuki and T. Hasegawa. The Science and Technology of in Highly Preheated Air. *Proc. Combust. Inst.*, 27:3135–3146, 1998.

[43] F. Weinberg and D. Hardesty. Burners producing large excess enthalpies. *Combust. Sci. Tech.*, 8:201–214, 1974.

[44] J. Wünning. Flammenlose Oxidation von Brennstoff mit hochvorgewärmter Luft. *Chem.-Ing.-Tech.*, 63:1243–1245, 1991. (in German).

[45] A. Cavaliere and M.D. de Joannon. Mild Combustion. *Prog. Energy Combust. Sci.*, 30:329–366, 2004.

[46] M. Gettings. The regenerative burner in the metals industry. *Gaswärme International*, 35:292–296, 1986.

[47] J. Masters, R. Webb, and R. Davies. The use of modelling techniques in the design and application of recuperative burners. *J. Inst. Energy*, 52:196–204, 1979.

[48] H. Tsuji, A.K. Gupta, T. Hasegawa, M. Katsuki, K. Kishimoto, and M. Morita. *High Temperature Air Combustion: from energy conservation to pollution reduction*. CRC Press, 2003.

[49] T. Hasegawa. Environmentally Compatible Regenerative Combustion Heating System. In *2nd International Seminar on High Temperature Air Combustion*, Stockholm, Sweden, 2000.

[50] T. Hasegawa and S. Mochida. Highly Preheated Air Combustion Characteristic Development of a Combustion Diagnostic on Advanced Industrial Furnace Making. In *International Joint Power Generation Conference*, San Francisco, USA, 1999.

[51] T. Hasegawa and S. Mochida. Development of a Combustion Diagnostic Method on Advanced Industrial Furnaces Utilizing High Temperature Air Combustion. In *3rd HiTACG Symposium*, Yokohama, Japan, 2000.

[52] S. Mochida and Yasuda T. Review of HiTAC Development and Future Possibility. In *6th HiTACG Symposium*, Essen, Germany, 2005.

[53] R. Weber. Combustion of Natural Gas, Oil and Coal with Air Preheated to Temperatures in Excess of 1000^oC. In *13th IFRF Members Conference*, Noordwijkerhout, The Netherlands, 2001.

[54] A.K. Gupta. Flame Characteristics and Challenges with High Temperature Air Combustion. In *International Joint Power Generation Conference*, Miami Beach, Florida, USA, 2000.

[55] A.K. Gupta. Thermal characteristics of gaseous fuel flames using high temperature air. *ASME J. Eng. Gas Turbines Power*, 126:9–19, 2004.

[56] T. Hasegawa, S. Mochida, and A.K. Gupta. Development of Advanced Industrial Furnace using Highly Preheated Air Combustion. *J. Propulsion and Power*, 2:233–239, 2002.

[57] S. Lille, W. Blasiak, and M. Jewartowski. Experimental study of the fuel jet combustion in high temperature and low oxygen content exhaust gases. *Energy*, 30:373–384, 2005.

[58] R. Weber, J. Driscoll, and W. Dahm. Scalling characteristic of the aerodynamics and low NO_x properties of industrial natural gas burner. Technical Report GRI-93/0227, IFRF Reaserch Report, IJmuiden, 1993. The Scalling 400 Study.

[59] R. Weber, J. Dugué, A. Sayre, and H. Horsamnn. Scalling characteristics of the aerodynamics and low NO_x properties of industrial natural gas burner. Technical Report IFRF Doc. No. F40/y/9, IFRF Reaserch Report, IJmuiden, 1993. The Scalling 400 Study.

[60] A. Verlaan, S. Orsino, N. Lallemant, and R. Weber. Fluid flow and mixing in a furnace equipped with the low NO_x regenerative burner of Nippon Furnace Kyogo. Results of HTAC 97 trials. Technical Report IFRF Doc. No. F46/y/1, IFRF Reaserch Report, IJmuiden, 1998.

[61] R. Weber, A. Verlaan, S. Orsino, and N. Lallemant. On emerging furnace design methodology that provides substantial energy savings and drastic reductions in CO_2, CO and NO_x emissions. *J. Inst. Energy*, 72:77–83, 1999.

[62] R. Weber, A. Verlaan, S. Orsino, and N. Lallemant. Combustion of natural gas with high temperature air and large quantities of flue gas. *Proc. Combust. Inst.*, 28:1315–1321, 2000.

[63] A. Verlaan, G. Deus Vasquez, M. Kosters, S. Orsino, N. Lallemant, and R. Weber. Excess enthalpy combustion of light and heavy fuel oils. Results of HTAC 98 trials. Technical Report IFRF Doc. No. F46/y/2, IFRF Reaserch Report, IJmuiden, 1999.

[64] S. Orsino, M. Tamura, P. Stabat, S. Costantini, O. Prado, and R. Weber. Excess enthalpy combustion of coal. Results of HTAC 99 trials. Technical Report IFRF Doc. No. F46/y/3, IFRF Reaserch Report, IJmuiden, 2000.

[65] R. Weber, J. Smart, and W. Vd Kamp. On the MILD Combustion of Gaseous, Liquid, and Solid Fuels in High Temperature Preheated Air. *Proc. Combust. Inst.*, 30:2623–2629, 2005.

[66] J.G. Wünning. *Flammlose Oxidation von Brennstoff.* PhD thesis, Aachen University of Technology, 1996. (in German).

[67] J.A. Wünning and J.G. Wünning. Flameless Oxidation to Reduce Thermal NO-Formation. *Prog. Energy Combust. Sci.*, 23:81–94, 1997.

[68] J. Wünning. Flameless Oxidation. In *6th HiTACG Symposium*, Essen, Germany, 2005.

[69] A. Sobiesiak, S. Rahbar, and H.A. Becker. Performance characteristics of the new low NO_x CGRI burner for use with high air preheat. *Combust. and Flame*, 115:93–125, 1998.

[70] B.T. Burggraaf, B. Lewis, P.D.J. Hoppesteyn, N. Fricker, S. Santos, and B.K. Slim. Towards industrial application of High Efficiency Combustion. In *15th IFRF Members Conference*, Pisa, Italy, 2007.

[71] E. Masson, B. Taupin, L. Dampt, A. Boukhalfa, D. Honore, R. Hauguel, and L. Porcheron. Parametric study of flameless combustion regime in a laboratory-scale facility. In *6th HiTACG Symposium*, Essen, Germany, 2005.

[72] C. Rottier, C. Lacour, G. Godard, B. Taupin, A. Boukhalfa, D. Honore, L. Porcheron, and R. Hauguel. Velocity and temeprature measurements in a laboratory-scale facility operating in flameless (MILD) combustion regime. In *15th IFRF Members Conference*, Pisa, Italy, 2007.

[73] D. Lupant, B. Pesenti, P. Evrard, and P. Lybaert. Numerical and experimental characterization of a self-regenerative flameless oxidation burner operation in pilot-scale furnace. In *6th HiTACG Symposium*, Essen, Germany, 2005.

[74] S. Murer, B. Pesenti, and P. Lybaert. CFD modeling of flameless combustion of natural gas in a $30kW$ combustor. In *6th HiTACG Symposium*, Essen, Germany, 2005.

[75] N. Shimo. Fundamental Research of Oil Combustion with Highly Preheated Air. In *2nd International Seminar on High Temperature Air Combustion*, Stockholm, Sweden, 2000.

[76] R.C. Chang and W.C. Chang. Research of High Temperature Air Combustion Fired Heavy Oil. In *2nd International Seminar on High Temperature Air Combustion*, Stockholm, Sweden, 2000.

[77] R. Wilk, K. Malczyk, T. Misztal, A. Szlęk, and A. Zajdel. Liquid Fuel Combustion under HTAC Technology. In *4th HiTACG Symposium*, Rome, Italy, 2001.

[78] R. Wilk, T. Misztal, A. Szlęk, and K. Malczyk. Investigation of the NO emission during High Temperature Air Combustion of light oil. In *13th International Symposium on Combustion*, Chicago, USA, 2004.

[79] R. Wilk, T. Misztal, K. Malczyk, A. Szlęk, and A. Zajdel. Investigations of the NO formation during light oil combustion in highly preheated air. In *5th HiTACG Symposium*, Tokyo, Japan, 2002.

[80] T. Kiga, K. Yoshikawa, M. Sakai, and S. Mochida. Characteristics of Pulverized Coal Combustion in High-Temperature Preheated Air. *J. of Propulsion and Power*, 16:601–605, 2000.

[81] FLOX-coal development of a pilot scale flameless oxidation burner for ultra low NO_x combustion of pulverized coal. European Commission (Research Fund for Coal and Steel), RFCR-CR-2005-00010.

[82] D. Ristic, A. Schuster, G. Scheffknecht, H. Stadler, M. Foerster, Kneer R., and J.G. Wünning. Experimental Study on Flameless Oxidation of Pulverised Coal in Bench and Pilot Scale. In *23th German Flameday*, Berlin, Germany, 2007.

[83] D. Ristic, M. Schneider, A. Schuster, G. Scheffknecht, and J.G. Wünning. Investigation of NO_x formation for flameless coal combustion. In *7th HiTACG Symposium*, Phuket, Thailand, 2008.

[84] S. Löhr, M. Kretschmann, S. Wirtz, and V. Scherer. Pyrolyse und Flüchtigenabbrand von Kraftwerkskohlen bei niedrigen Sauerstoffkonzentrationen. In *23th German Flameday*, Berlin, Germany, 2007. (in German).

[85] Untersuchungen zur Schadstoffbildung bei der FLOX-Verbrennung von Kohlestaub. DFG (German Research Foundation), Gz.: SCHE 322/4-2, (in German).

[86] T. Suda, M. Takafuji, T. Hirata, M. Yoshino, and J. Sato. A study of combustion behavior of pulverized coal in high-temperature air. *Proc. Combust. Inst.*, 29:503–509, 2002.

[87] M.R. Schmid, J.G. Wünning, and R. Berger. New horizons for FLOX-technology for biomass fuels. In *6th HiTACG Symposium*, Essen, Germany, 2005.

[88] V. Suphansomboon, P. Suvarnakuta, S. Patumsawad, and S. Kerdsuwan. Investigation into Low Calorific Value Gas Combustion with High Temperature and Low-Oxygen Concentration Combustion Air. In *6th HiTACG Symposium*, Essen, Germany, 2005.

[89] A. Ponzio, S. Kalisz, J. Promelle, and W. Blasiak. Combustion of Wood Pellets in an Oxygen Diluted and High Temperature Environment. In *6th HiTACG Symposium*, Essen, Germany, 2005.

[90] M. Derudi, A. Effuggi, A. Villani, and R. Rota. Use of Methane-derived Fuel Mixtures, Natural Gas and Biogas, for MILD Combustion Applications. In *6th HiTACG Symposium*, Essen, Germany, 2005.

[91] A.K. Gupta and S. Mochida. Developments in High Temperature Air Combustion (Flameless Oxidation) and Fuel Reforming. In *6th HiTACG Symposium*, Essen, Germany, 2005.

[92] W. Cichonski and A.K. Gupta. Hydrogen Generation from Wastes using Ultra-High Temperature Steam Gasification. In *6th HiTACG Symposium*, Essen, Germany, 2005.

[93] N. Krishnamurthy, Y. Weihong, T. Ekman, and W. Blasiak. Combustion Characteristics of Flameless Oxyfuel and Oxygen Enriched -High Temperature Air Combustion. In *6th HiTACG Symposium*, Essen, Germany, 2005.

[94] J. Leicher, S. Wirtz, and V. Scherer. Simulating Flameless Oxidation Using a Progress Variable Approach. In *6th HiTACG Symposium*, Essen, Germany, 2005.

[95] A. Al-Halbouni and M. Flamme. New Burner Systems for Gas Turbines. In *6th HiTACG Symposium*, Essen, Germany, 2005.

[96] M. Flamme. New combustion systems for gas turbines (NGT). *Applied Thermal Engineering*, 24:1551–1559, 2004.

[97] R. Weber, A. Szlęk, and R. Wilk. A novel application of mild combustion technology to gas turbines that results in substantial increase of cycle efficiency. In *6th HiTACG Symposium*, Essen, Germany, 2005.

[98] A. Szlęk. Combustion of methane in a compressed, preheated and expanding air. In *31st International Symposium on Combustion*, Heidelberg, Germany, 2006. poster presentation.

[99] A. Szlęk, R. Weber, and R. Wilk. High Temperature Air Combustion Technology in Power Cycles. In *ECOS Conference*, Trondhaim, Norway, 2005.

[100] A. Szlęk, R. Wilk, K. Malczyk, and T. Misztal. On HTAC application in power generation. In *5th HiTACG Symposium*, Tokyo, Japan, 2002.

[101] Y. Hino, C. Zhang, and T. Ishii. Comparison of measurements and predictions of flame structure and NO_x emissions in a gas-fired furnace. In *AIAA/ASME Joint Thermophysics and Heat Transfer Conference*, Albuquerque, New Mexico, USA, 1998.

[102] T. Ishii, C. Zhang, and S. Sugiyama. Numerical analysis of NO_x formation rate in a regenerative furnace. In *Joint Power Generation Conference*, Denver, Colorado, USA, 1997.

[103] C. Zhang, T. Ishii, and S. Sugijama. Numerical modeling of the thermal performance of regenerative slab reheating furnaces. *Num. Heat Transf.*, 32:613–631, 1997.

[104] H. Guo, Y. Ju, and K. Mauta. Numerical investigations for NO_x emissions in high temperature air combustion. In *First Asia-Pacific Conference on Combustion*, Nagoya, Japan, 1997.

[105] S. Orsino, R. Weber, and U. Bollettini. Numerical simulation of natural gas combustion with high-tempeature air. *Combust. Sci. Tech.*, 168:1–34, 2002.

[106] M. Mancini and R. Weber. Formation and destruction of nitrogen oxides in combustion of natural gas with high temperature air. In *5th HiTACG Symposium*, Yokohama, Japan, 2002.

[107] M. Mancini, P. Schwöppe, R. Weber, and S. Orsino. On mathematical modeling of flameless combustion. *Combust. Flame*, 150:54–59, 2007.

[108] M. Mancini. *Analysis of mild combustion of Natural Gas with preheated air*. PhD thesis, Clausthal University of Technology, Faculty of Energy and Management, 2007.

[109] P. Coehlo and N. Peters. Numerical simulation of a MILD combustion burner. *Combust. Flame*, 124:503–518, 2001.

[110] P. Coehlo and N. Peters. Laseroptical investigation of highly preheated combustion with strong exhaust gas recirculation. *Proc. Combust. Inst.*, 27:3197–3204, 1998.

[111] S. Yang and W. Blasiak. Numerical study of fuel temperature influence on single gas jet combustion in highly preheated and oxygen deficient air. *Energy*, 30:385–398, 2005.

[112] S. Yang and W. Blasiak. Numerical simulation of properties of a LPG flme with high-temperature air. *International Journal of Thermal Sci.*, 44:973–985, 2005.

[113] S. Yang and W. Blasiak. Mathematical modelling of NO emissions from high-temperature air combustion with nitrous oxide mechanism. *Fuel Proc. Tech.*, 86:943–957, 2005.

[114] W. Dong and W. Blasiak. Numerical modeling of highly preheated air combustion in a $580kW$ testing furnace at IFRF. In *3rd CRST International Symposium*, Yokohama, Japan, 2000.

[115] W. Dong and W. Blasiak. Large Eddy Simulation of a single jet flow in highly preheated and diluted air combustion. *Archivum Combustionis*, 20:163, 2000.

[116] B. Pasenti, P. Evrard, and P. Lybaert. NO_x production and radiative heat transfer from an autoregenerative flameless oxidation burner. In *4th HiTACG Symposium*, Rome, Italy, 2001.

[117] D. Tobacco, C. Innarella, and C. Bruno. Theoretical and numerical investigation on flameless combustion. *Combust. Sci. Tech.*, 174:1–35, 2002.

[118] A. Cavaliere and M.D. de Joannon. Zero-dimensional analysis of diluted oxidation of methane in rich conditions. *Proc. Combust. Inst.*, 28:1639–1646, 2000.

[119] M. de Joannon, P. Saba, A. Tregrossi, and A. Cavaliere. Dynamic behavior of the methane oxidation in premixed flow reactor. *Combust. Sci. and Tech.*, 176:769–783, 2004.

[120] M. de Joannon, A. Cavaliere, T. Faravelli, E. Ranzi, and P. Sabia. Analysis of process parameters for steady operation of methane MILD technology. *Proc. Combust. Inst.*, 30:2605–2612, 2005.

[121] L. Porcheron, L. Ferrand, E. Masson, F. Aguile, A. Quinqueneau, D. Honore, and M. Boukhalfa. High Temperature Air Combustion burner: semi-industrial scale experiment and CFD simulation. In *6th HiTACG Symposium*, Essen, Germany, 2005.

[122] B.T. Burggraaf, B. Lewis, P.D.J. Hoppesteyn, N. Fricker, S. Santos, and B.K. Slim. Towards industrial application of High Efficiency Combustion. *IFRF Combustion Journal*, 200704, 2007.

[123] R. Hekkens and M. Mancini. CFD modeling for high efficiency combustion. In *14th IFRF Member Conference*, Noordwijkerhout, Netherlands, 2004.

[124] T. Misztal. *Badanie emisji NO podczas spalania oleju w warunkach wysokotemperaturowego podgrzewu powietrza spalania.* PhD thesis, Silesian University of Technology, Faculty of Environmental Protection Technology and Energy, 2005. (in Polish).

[125] M. Bui Pham and K. Seshadri. Comparison between Experimental Measurements and Numerical Calculations of the Structure of Heptane-Air Diffusion Flames. *Combust. Sci. and Tech.*, 79:293–310, 1991.

[126] R. He, T. Suda, M. Takafuji, T. Hirata, and J. Sato. Analysis of low NO emission in high temperature air combustion for pulverized coal. *Fuel*, 83:1133–1141, 2004.

[127] P. Heil, U. Renz, and R. Kneer. Experimentelle Untersuchung eines FLOX-Brenners bei Druckkohlenstaubfeuerungsbetrieb. In *4. Druckflamm Seminar*, Dortmund, Germany, 2004. (in German).

[128] J. Erfurth, D. Toporov, S. Tschunko, C. von Petry, and R. Kneer. Modellierung der Flammlosen Verbrennung in einer Druckkohlenstaubfeuerung. In *22th German Flameday*, Braunschweig, Germany, 2005. (in German).

[129] J.P. Kim, U. Schnell, G. Scheffknecht, and A.C. Benim. Numerical Modeling of MILD Combustion for Coal. *Prog. in Comput. Fluid Dynamics*, 7:337–346, 2007.

[130] J.P. Kim. *Numerical modeling of MILD combustion*. PhD thesis, University of Stuttgart, Faculty of Energy Technology, Process Engineering and Biological Engineering, 2008.

[131] D. Förtsch. *A Kinetic Model of Pulverised Coal Combustion for Computational Fluid Dynamics*. PhD thesis, University of Stuttgart, Faculty of Energy Technology, Process Engineering and Biological Engineering, 2003.

[132] D. Förtsch, F. Kluger, U. Schnell, H. Spliethoff, and H.R.G. Klaus. A kinetic model for the predtiction of NO emissions from staged combustion of pulverized coal. *Proc. Combust. Inst.*, 27:3037–3044, 1998.

[133] P.R. Solomon, T.H. Fletcher, and R.J. Pugmire. Progress in coal pyrolysis. *Fuel*, 72:587–597, 1993.

[134] D. Szewczyk, J. Sudoh, A. Świderski, and B. Forsberg. Over decade of the industrial experience in high temperature air combustion applied with HRS regenerative burners. In *6th HiTACG Symposium*, Essen, Germany, 2005.

[135] M. Mörtberg, W. Blasiak, and A.K. Gupta. Flameless Combustion of Methane Fuel Jet injected into Transverse High Temperature Air Flow. In *6th HiTACG Symposium*, Essen, Germany, 2005.

[136] J. Massingham. Evaluation of low NO_x burners for steel industry applications. In *2nd International Seminar on High Temperature Air Combustion*, Stockholm, Sweden, 2000.

[137] J. Wünning. Regenerative Burner Using Flameless Oxidation. In *IGRC*, Cannes, France, 1995.

[138] R. Weber, A.L. Verlaan, S. Orsino, and N. Lallemant. On emerging furnace design methodology that provides substantial energy savings and drastic reductions in CO_2, CO and NO_x emissions. In *2nd International Seminar on High Temperature Air Combustion*, Stockholm, Sweden, 2000.

[139] A. Saponaro. The Ansaldo Caldaie combustion research experience in HiTAC. In *6th HiTACG Symposium*, Essen, Germany, 2005.

[140] K. Kawai, K. Yoshikawa, H. Kobayashi, J.S. Tsai, M. Matsuo, and H. Katsushima. High temperature air combustion boiler for low BTU gas. *Energy Conversion and Management*, 43:1563–1570, 2002.

[141] H. Zhang, G. Yue, J. Lu, Z. Jia, J. Mao, T. Fujimori, T. Suko, and T. Kiga. Development of High Temperature Air Combustion technology in pulverized fossil fuel fired boilers. *Proc. Combust. Inst.*, 31:2779–2785, 2007.

[142] Fluent Inc. of ANSYS Inc. *GAMBIT 2.2 Documentation. User's Guide*, 2006.

[143] Fluent Inc. of ANSYS Inc. *FLUENT 6.3 Documentation. User's Guide*, 2006.

[144] J. Ferziger and M. Peric. *Computational Methods for Fluids Dynamics*. Springer Verlag, 1999.

[145] T.J. Chung. *Computational Fluid Dynamics*. Cambridge University Press, 2002.

[146] S.R. Turns. *An Introduction to Combustion. Concepts and applications*. McGraw-Hill, 2000.

[147] R.O. Fox. *Computational Models for Turbulent Reacting Flows*. Cambridge University Press, 2003.

[148] S.B. Pope. *Turbulent flows*. Cambridge University Press, 2000.

[149] B.E. Launder and D.B. Spalding. The numerical computation of turbulent flows. *Computer Methods in Applied Mechanics and Engineering*, 3:269–289, 1974.

[150] D.B. Spalding. Mixing and chemical reaction in steady confined turbulent flames. *Proc. Combust. Inst.*, 13:649–657, 1971.

[151] B.F. Magnussen and B.H. Hjertager. On mathematical modeling of turbulent combustion with special emphasis on soot formation and combustion. *Proc. Combust. Inst.*, 16:719–729, 1976.

[152] B.F. Magnussen. On the Structure of Turbulence and a Generalized Eddy Dissipation Concept for Chemical Reaction in Turbulent Flow. In *19th AIAA Meeting*, St. Louis, USA, 1981.

[153] B.F. Magnussen. Modeling of NO_x and Soot Formation by the Eddy Dissipation Concept. In *1st Topic Oriented Technical Meeting*, International Flame Research Foundation, Amsterdam, Holland, 1989.

[154] I.S. Ertesvag and B.F. Magnussen. The Eddy Dissipation Turbulence Energy Cascade Model. *Combust. Sci. and Tech.*, 159:213–235, 2000.

[155] F. Boysan, W.H. Ayers, and J. Swithenbank. Fundamental Mathematical Modelling Approach to Cyclone Design. *Trans. I. Chem. E.*, 60:222–230, 1982.

[156] R. Weber, F. Boysan, W.H. Ayers, and J. Swithenbank. Simulation of Dispersion of Heavy Particles in Confined Turbulent Flows. *AICHE J.*, 30:490–492, 1984.

[157] K. Annamalai and I.K. Puri. *Combustion Science and Engineering*. CRC Press Taylor & Francis Group, 2007.

[158] S. Badzioch and P.G.W. Hawksley. Kinetics of Thermal Decomposition of Pulverized Coal Particles. *Ind. Eng. Chem. Process Design and Development*, 9:521–530, 1970.

[159] H. Kobayashi, J.B. Howard, and A.F. Sarofim. Coal Devolatilization at High Temperatures. *Proc. Combust. Inst.*, 16:411–425, 1976.

[160] D.M. Grant, R.J. Pugmire, T.H. Fletcher, and A.R. Kerstein. Chemical Model of Coal Devolatilization Using Percolation Lattice Statistics. 3:175–186, 1989.

[161] T.H. Fletcher, A.R. Kerstein, R.J. Pugmire, and D.M. Grant. Chemical Percolation Model for Devolatilization: 2. Temperature and Heating Rate Effects on Product Yields. *Energy and Fuels*, 4:54–60, 1990.

[162] T.H. Fletcher and A.R. Kerstein. Chemical Percolation Model for Devolatilization: 3. Direct Use of ^{13}C NMR Data to Predict Effects of Coal Type. *Energy and Fuels*, 6:414–431, 1992.

[163] P.L.Jr. Walker, F.J. Rusinko, and L.G. Austin. Gas Reactions of Carbon. *Advances in Catalysis*, 11:133–140, 1959.

[164] D. Gray, J.G. Cogoli, and R.H. Essenhigh. Problems in Pulverized Coal and Char Combustion. *Advances in Chemistry Series*, 13:72–91, 1974.

[165] V. Banin, R. Moors, and B. Veefikind. Kinetic study of High-Pressure Pulverised Coal Char Combustion: Experiment and Modelling. *Fuel*, 76:945–949, 1997.

[166] A. Williams, M. Pourkashanian, and J.M. Jones. Combustion of pulverised coal and biomass. *Prog. Energy Comb. Sci.*, 27:587–610, 2001.

[167] I.W. Smith. The Combustion Rates of Coal Chars: A Review. *Proc. Combust. Inst.*, 19:1045–1065, 1982.

[168] H.E. Klimesh and R.H. Essenhigh. Non-Dissociative and Dissociative Adsorption of Oxygen on Carbon: A Theoretical Comparison with Prediction of Reaction Order. *Proc. Combust. Inst.*, 27, 1998.

[169] N.M. Laurendeau. Heterogeneous Kinetics of Coal Char Gasification and Combustion. *Prog. Energy Com. Sci.*, 4:221–270, 1978.

[170] W.A. Fiveland and A.S. Jamaluddin. Three-dimensional radiative heat transfer solutions by the discrete-ordinates method. *J. Thermophysics*, 2:309–316, 1988.

[171] J.S. Truelove. Three-dimensional radiation in absorbing-emitting-scattering in using the discrete-ordinates approximation. *JQSRT*, 39:27–31, 1988.

[172] G. Hand, M. Missaghi, M. Pourkashanian, and A. Williams. Experimental Studies and Computer Modeling of Nitric Oxides in a Cylindrical Natural Gas Fired Furnace. In *9th IFRF Members Conference*, Noordwijkerhout, the Netherlands, 1989.

[173] A.A.F. Peters and R. Weber. Modeling of a 2.25 MW_{th} Swirling Natural Gas Flame. Part I: Eddy Break-up Concept for Turbulent Combustion; Probability Density Function Approach for Nitric Oxide Formation. *Combust. Sci. Tech.*, 110-111:67–101, 1995.

[174] G.G. De Soete. Overall Reaction Rates of NO and N_2 Formation from Fuel Nitrogen. *Proc. Combust. Inst.*, 15:1093–1102, 1975.

[175] P. Malte and D. Pratt. Measurements of atomic oxygen and nitrogen oxides in jet stirred combustion. *Proc. Combust. Inst.*, 15:1061–1070, 1974.

[176] W. Chen, L.D. Smoot, T.H. Fletcher, and R.D. Boardman. Global Rate Expression for Nitric Oxide Reburning. Part II. *Energy & Fuels*, 10:1046–1056, 1999.

[177] W. Chen, L.D. Smoot, S.C. Hill, and T.H. Fletcher. A Computational Method for Determining Global Fuel-*NO* Rate Expressions. Part I. *Energy & Fuels*, 10:1036–1046, 1999.

[178] J.M. Levy, L.K. Chen, A.F. Sarofim, and J.M. Beer. *NO*/Char Reactions at Pulverized Coal Flame Conditions. *Proc. Combust. Inst.*, 18:340–343, 1981.

[179] M. Tamura. Data on characterization of Guasare coal, 2000. (unpublished).

[180] N. Lallemant, A. Sayre, and R. Weber. Evaluation of emissivity correlations for $H_2O - CO_2 - N_2/air$ mixtures and coupling with solution methods of the Radiative Transfer Equation. *Prog. Energy Combust. Sci.*, 22:543–574, 1990.

[181] A. Sayre, N. Lallemant, J. Dugué, and R. Weber. Effect of radiation on nitrogen emissions from non-sooty swirling flames of natural gas. *Proc. Combust. Inst.*, 25:235–242, 1994.

[182] A.A.F. Peters and R. Weber. Mathematical Modeling of a 2.4 MW_{th} Swirling Pulverized Coal Flame. *Combust. Sci. and Tech.*, 122:131–182, 1997.

[183] J. Haas. *Experimentelle Untersuchungen der Reaktivität von Kohlenkoks zur Modellierung seines Verbrennungsverhaltens in Staubfeurungen.* PhD thesis, Clausthal University of Technology, Faculty of Energy and Management, 1999. (in German).

[184] R. Lundquist, A. Schrief, P. Kinnunen, K. Myohanen, and M. Seshamani. A Major Forward- The Supercritical CFB Boiler. In *Power-Gen International 2003*, Las Vegas, USA, 2003.

[185] A. Saario and A. Oksanen. Effect of Computational Grid in Industrial-Scale Boiler Modeling. *Int. J. of Numerical Methods for Heat & Fluid Flow*, 19:93–117, 2009.

[186] K. Yamagata, K. Nishikawa, S. Hasegawa, T. Fuji, and S. Yoshida. Forced convective heat transfer to supercritical water flowing in tubes. *Int. J. Heat Mass Transfer*, 15:2575–2593, 1972.

Extended abstract

High Temperature Air Combustion (HTAC or HiTAC) is named also as: Excess Enthalpy Combustion (EEC), FLameless OXidation (acronym FLOX), MILD (Moderate and Intensive Low-oxygen Dilution) combustion. The most important feature of HTAC technology is an existence of an intense recirculation of combustion products inside the chamber. This recirculation causes that both the combustion air stream and the fuel stream being diluted before the ignition occurs. Therefore, the temperature peaks are suppressed. The second result of these specific mixing conditions is homogeneity of both the temperature and the species concentrations fields. Consequently, HTAC technology features low NO_x and CO emissions and high and uniform heat fluxes. So far, HTAC technology was implemented mainly in industrial furnaces fired either with gaseous fuels or light oils. In most of industrial applications, the technology is combined with heat recovery systems and such a combination typically results in substantial fuel savings. In this work, the application of HTAC technology in power boilers fired with pulverized coal has been investigated. The following advantages are expected:

- In HTAC furnaces, the radiative heat fluxes are significantly higher than in traditional ones. If the same could be achieved in boilers, then the size of the heat transfer area, and thus boiler investment costs, could be significantly reduced. The boiler could be build using high temperature alloys allowing an increase of superheated steam parameters to an ultra-supercritical level and, subsequently, an increase of the thermal efficiency of the entire cycle.

- The next advantage is in significant reduction of pollutants emissions, mainly nitric oxide which allows eliminating expensive flue gas cleaning installations.

Summarizing, application of HTAC technology to boilers fired with pulverized coal could be one of the future coal combustion technologies for the clean power generation. Technical and ecological aspects of such applications are analyzed and discussed in this thesis.

The main objective of this work is to investigate applicability of HTAC technology to power station boilers fired with pulverized coal for environmental friendly electricity production. In order to achieve this goal, several technical objectives have been formulated. The first objective is to examine how accurately HTAC combustion of coal can be predicted using numerical modeling methods. To this end the mathematical model has been validated against the IFRF measurements. The CFD-based simulations have been performed using FLUENT code. The mathematical model selected in the validation and verification process is then used in all subsequent investigations. The second objective is

to develop a conceptual design of a pulverized coal fired boiler utilizing HTAC technology. This involves determination of the combustion chamber shape, its dimensions, distances between individual burners and positions of the burner block. The third objective involves the examination of the environmental aspects of the HTAC technology implementation. Here one focuses on NO_x, CO, unburned hydrocarbons and char burnout. The fourth objective is to examine the HTAC boiler operation under different operating conditions like: low combustion air temperatures, low combustion air jet momentum and a low excess air ratio. The fifth objective is to investigate whole steam cycle in order to estimate the efficiency of electricity production using such a HTAC boiler.

The work on the HTAC boiler fired with pulverized coal has been presented starting with an overview on coal based technologies applied in power generation. Further, the fundamentals of the power station boilers construction have been provided. Then, a development, current status and challenges of HTAC technology have been briefly reviewed. Special attention has been given on the progress in modeling of combustion under HTAC conditions, especially using the solid fuels. In the next part of the work, the mathematical sub-models used in this work have been described. Here has been focused on both, the coal combustion and the nitric oxide formation and destruction sub-models.

In this part of the work, the mathematical model describing coal combustion in HTAC technology has been validated against the data generated during an IFRF experiment called HTAC 99. Several sub-models have been tested during the validation and verification procedure and as a result the following sub-models have been selected:

- $k - \varepsilon$ model for turbulence

- eddy dissipation model for interaction between chemistry and turbulence

- discrete phase model for description of particles behavior

- CPD model for devolatilization process

- intrinsic model for char burnout

- discrete ordinates model for radiation

- nitric oxides formation and destruction considering the fuel, thermal, prompt and N_2O paths, as well as NO reburning in the gaseous phase and on the char surface

It was concluded that the predicted values are, generally, in very good accordance with the measurements. Therefore, such a validated model has then been used in the boiler design studies.

HTAC combustion process is very different from conventional combustion. Therefore there is a need for an innovative design of boilers utilizing this technology. In this part of the work several particular boiler concepts have been analyzed in the context of the following three key points: existence of an intensive in-furnace recirculation, homogeneity of both the temperature and the chemical species fields, and uniformity of heat fluxes. Several simulations have been performed in order to find the shape of the boiler and its dimensions, to optimize both the distance between burners and location of the burner block.

Based on the previous investigations, the final configuration of the HTAC boiler was selected. The boiler is 13 m high and has a 7 m times 6 m cross section. It is equipped with a burner block that consists of 5 identical burners located at the top wall thus the boiler is a down-fired one. The flue gas outlets are also located at the top wall and they are symmetrically positioned on both sides of the burner block. The outlets have a quadrate form with lateral length of 1 m. Each of the five burners is equipped with a central injector of hot air and two coal guns positioned on both sides from the air injector. Pulverized coal is introduced into the furnace by nozzles of 15 mm diameter and the combustion air by 48 mm nozzles. The boiler is equipped with two ash hoppers.

The combustion air is preheated to 1200 K and the coal together with its transport air is supplied at ambient temperature (300 K). The feeding rate of coal is of 3.2 $\frac{kg}{s}$, and of its transport air almost twice a high. The mass flow of combustion air is equal to 33.1 $\frac{kg}{s}$. The air jet is supplied at a high velocity (120 $\frac{m}{s}$) and coal jet has the velocity of 30 $\frac{m}{s}$. The boiler is operated at 130 MW total thermal input. The fuel thermal input is equal to 100 MW so each burner operates at 20 MW fuel power. Both the combustion and the transport air streams contain 23% mass oxygen and 77% mass nitrogen. The wall temperature is constant in the final boiler design calculations and it is equal to 800 K. The final boiler design leads to the intensive recirculation and the dead zones are small. The whole volume of the chamber participates in the combustion process. The internal recirculation of the combustion products creates homogenous both the temperature and the chemical species concentration fields. Further, due to dilution of the combustion air and fuel jets the coal ignition takes place in low oxygen concentration environment, and therefore the temperature peak is suppressed. Strong recirculation of the hot combustion gas eliminates the problems related to the coal ignition.

The whole boiler is filled up with combustion products of 1600-2000 K temperatures. The temperature peak is substantially suppressed in comparison with conventional combustion using such high air preheat, and it is about 2100 K. The furnace exit temperature is around 1400 K, and the furnace exhaust gas has a high enthalpy. This

enthalpy must be recovered in a heat exchanger and utilized to preheat the combustion air. The oxygen concentration in almost entire boiler is in a range of 3-5% while in the flue gas is equal to 3.4%. Uniform and low oxygen concentrations result in the temperature peak reduction. The HTAC boiler has two advantages: uniform heat fluxes along the boiler height (as in fluidized bed boilers) and high heat fluxes values (as in wall fired pulverized coal boilers). Heat transfer due to radiation plays a dominant role. Its share is 83% of the total heat transfer. The rest is due to the convection.

Most of NO is generated in the region between the burners. The NO concentration peak is equal to 1195 ppm. Downstream of this region the nitric oxide concentrations are low and they are in a range from 300 up to 400 ppm. In the HTAC boiler, 98% of nitric oxide is formed via fuel mechanism. The NO reburning mechanism plays an important role. As a result, the nitric oxide concentrations at the boiler outlet are low and equal to 298 ppm. The long particles residence time and recursive recirculation of the combustion products improve the burnout of the CO and volatiles and of the char. Very stable combustion process and simple burner construction offer the possibility of using low rank coals.

In the next part of the work, an impact of three important parameters: the combustion air preheat, the combustion air jet velocity and the air excess ratio on the HTAC boiler performance have been tested. Thus, for all calculations the final HTAC boiler geometry is retained and the same boundary conditions are applied. However, boiler operating conditions are different and these are specified for each computational run. The final boiler design is the reference case. It was concluded that the HTAC technology in boilers can work correctly at different levels of the air preheating, as well as without air preheating. Further, it was confirmed that the high velocity (and at the same time high momentum) of the strong combustion jet is needed in order to realize HTAC technology. Additionally, it was noticed that could be possible to operate the HTAC boiler at the air excess ration near the stoichiometric values.

Boiler design procedures involve an examination of the combustion process as well as the steam cycle. Both issues are strongly coupled due to the heat transfer proceeding from the combustion products inside the chamber to the water/steam mixture inside the boiler tubes. In this part of the work, coupling between the HTAC boiler and the entire steam cycle is taken into consideration. The final boiler geometry as well as the operating and boundary conditions are the starting point for these calculations. User define subroutine implemented into FLUENT code has been written to perform the calculations. As a result of these calculations, the temperature profiles at the boiler walls are obtained. The HTAC boiler is proposed in this thesis as an ultra-supercritical boiler with the once-through type

of the water circulation. Three commonly used configurations of the once-trough boiler tubes were tested in this series of calculations: vertical down-up, up-down and spiral. The most uniform temperature profile can be found in the boiler with the spiral tubing; therefore it was concluded that the spiral tubes configuration is the most suitable for the HTAC boiler designed in this work. However, this configuration is technically most complicated. The Rankine cycle efficiency of the steam cycle coupled with the HTAC boiler is calculated to be above 50%.

Overall, the present study confirmed that HTAC technology could be a practicable, efficient and clean technology for pulverized coal fired boilers.

Summarizing, the most important advantages of the pulverized coal fired boiler operating under HTAC conditions are as following. Firstly, heat fluxes emitted during combustion process are high and uniform which results in the high firing density and consequently the small size of the boiler. Secondly, low NO_x emissions in comparison with the standard PC boilers. Then, burners have a very simple construction: without air staging, flame stabilizer or swirl which are commonly used in the commercial pulverized coal burners.

Although HTAC technology seems to be attractive for power boilers fired with pulverized coal, there are still many open questions. First of all, the particulate concentration in the flue gas for the coal flame is probably too high to use the technique in conjunction with regenerative heat exchangers. It is a need to find in the future a way to utilize the enthalpy of the boiler exhaust gas. However, it was proved that the boiler can be operated without air preheating even if the ignition mechanism has to be examined in more details. Secondly, it could be also a problem with erosion because of the strong recirculation and high velocity of the coal particles.

Obszerne streszczenie

Technologia HTAC (High Temperature Air Combustion) jest prawdopodobnie najważniejszym odkryciem w dziedzinie spalania w przeciągu ostatnich lat. Technologia HTAC znana jest także pod nazwą FLameless OXidation- FLOX lub MILD (Moderate and Intensive Low-oxygen Dilution) combustion. Najważniejszą cechą tej metody jest występowanie intensywnych recyrkulacji wewnątrz komory spalania, które powodują, że zarówno struga powietrza jak i paliwa ulegają rozcieńczeniu zanim wystąpi zjawisko zapłonu. W konsekwencji obniżone są maksymalne temperatury osiągane w procesie spalania. Drugim efektem, wynikającym z występowania intensywnych recyrkulacji, są równomierne pola temperatury oraz stężenia substancji chemicznych. W następstwie obserwuje się wyrównany profil strumieni ciepła na ścianach komory oraz niskie emisje substancji szkodliwych, szczególnie NO_x. Jak dotąd, technologia HTAC została zastosowana głównie w piecach przemysłowych opalanych paliwami gazowymi lub lekkim olejem. W większości zastosowań przemysłowych technologia ta jest zintegrowana z systemami regeneracji ciepła, co pozwala na znaczne zmniejszenie zużycia paliwa.

Zastosowanie technologii HTAC w kotłach energetycznych opalanych pyłem węglowym mogłoby być jedną z czystych technologii wykorzystywanych w przyszłości do wytwarzania energii elektrycznej. Nadrzędnym celem tej pracy jest analiza możliwości wykorzystania technologii HTAC w kotłach energetycznych opalanych pyłem węglowym w celu przyjaznego środowisku naturalnemu wytwarzania energii elektrycznej. Oczekuje się przy tym, że zastosowanie tej metody spalania do pyłu węglowego przyniesie następujące korzyści:

- W piecach przemysłowych pracujących w technologii HTAC radiacyjne strumienie ciepła są znacznie wyższe niż w konwencjonalnych piecach przemysłowych. Jeśli ten sam efekt zostanie osiągnięty w kotłach, wtedy powierzchnia wymiany ciepła, a tym samym nakład inwestycyjny na budowę kotła, mogą być znacznie obniżone. W takim przypadku ekonomicznie uzasadnione może być użycie lepszej jakości stali, co pozwoliłoby podnieść parametry pary świeżej do wartości superkrytycznych, a tym samym poprawić sprawność całego obiegu parowego.

- Obniżenie emisji substancji szkodliwych, głównie tlenku azotu i tlenku węgla, co pozwoliłoby uniknąć konieczności budowy kosztownych instalacji odazotowania spalin. Mniejsza emisja tlenków azotu wynika z ograniczenia temperatur w komorze spalania.

Na początku pracy przedstawiono przegląd aktualnych i przyszłościowych technologii węglowych stosowanych do produkcji energii elektrycznej, a następnie przybliżono podstawowe wiadomości z zakresu budowy i projektowania kotłów energetycznych zasilanych pyłem węglowym. W kolejnej części pracy zostały pokrótce zreferowane rozwój, stan aktualny oraz wyzwania stojące przed technologią HTAC. Skupiono się przede wszystkim na postępie dokonanym w dziedzinie modelowania numerycznego procesu spalania paliw stałych w tej technologii. Kolejny rozdział poświęcony został opisowi zastosowanych matematycznych modeli jednostkowych, w szczegolności tych dotyczących spalania pyłu węglowego oraz formowania i destrukcji tlenków azotu.

Dla realizacji postawionego nadrzędnego celu pracy sformułowano szereg celów szczegółowych. Pierwszym z nich było opracowanie wiarygodnego modelu spalania pyłu węglowego w warunkach HTAC. Dla realizacji tego zadania model matematyczny poddano weryfikacji korzystając z pomiarów przeprowadzonych w instytucie badawczym IFRF (International Flame Research Foundation, IJmuiden, Holandia). Symulacje oparte o numeryczną mechanikę płynów wykonano używając oprogramowania FLUENT. W procesie weryfikacji przebadano wiele różnych modeli jednostkowych i w rezultacie wybrano:

- $k - \varepsilon$ do opisu turbulencji,

- eddy dissipation model charakteryzujący interakcje pomiędzy reakcjami chemicznymi procesu spalania i turbulencjami,

- discrete phase model do opisu zachowania cząsteczek stałych,

- CPD model do charakterystyki procesu odgazowania węgla,

- intrinsic model do spalania koksiku,

- discrete ordinates model opisujący wymianę ciepła przez promieniowanie,

- model formowania i redukcji tlenków azotu uwzględniajacy mechanizm paliwowy, termalny, za pośrednictwem N_2O, szybki a także redukcję tlenków azotu zarówno w fazie gazowej jak i na powierzchni cząsteczki węgla.

Stwierdzono, że wyniki obliczeń numerycznych pozostają w zadowalającej zgodzie z wartościami pomiarowymi i w konsekwencji wybrany na tym etapie pracy model matematyczny został użyty w dalszych badaniach numerycznych nad opracowaniem projektu kotła pracującego w technogii HTAC i opalanego pyłem węglowym.

Proces spalania w warunkach HTAC jest diametralnie różny od standardowego procesu spalania. Z tego względu koniecznym było opracowanie nowej koncepcji kotła, co stanowiło drugi cel pracy. Wybrane geometrie kotłów przeanalizowane zostały ze względu na trzy kluczowe zagadnienia: występowanie intensywnych recyrkulacji w komorze spalania, równomierność rozkładu temperatury i stężenia tlenu, oraz wyrównanane i wysokie wartości strumieni ciepła wzdłuż wysokości komory spalania. Przeprowadzono szereg serii symulacji numerycznych w celu znalezienia kształtu komory spalania, jej wymiarów, konfiguracji bloku palników i jego lokalizacji w komorze spalania.

Opierając się na wynikach uzyskanych w poprzedniej części pracy opracowana została finalna konfiguracja kotła pyłowego pracującego w technologii HTAC. Kocioł ma wysokość 13 m i przekrój poprzeczny o wymiarach 6 na 7 m. Kocioł wyposażony jest w blok palników składający się z pięciu identycznych palników, położonych na górnej ścianie kotła. Wyloty spalin umiejscowione są również na górnej ścianie kotła, symetrycznie po obydwu stronach bloku palników. Wyloty spalin mają formę kwadratu o boku 1 m. Każdy z palników składa się z centralnie położonej dyszy wlotu powietrza i ulokowanych po obu jej stronach dyszy wlotu paliwa. Pył węglowy wraz z powietrzem transportującym doprowadzany jest przez dysze o średnicy 15 mm. Powietrze do spalania doprowadzane jest przez otwór o średnicy 48 mm. Kocioł wyposażony jest w dwa leje żużlowe. Powietrze do spalania podgrzane jest do temperatury 1200 K, podczas gdy pył węglowy wraz z powietrzem transportującym podawany jest w temperaturze otoczenia (300 K). Węgiel podawany jest w ilości 3.2 $\frac{kg}{s}$ natomiast ilość powietrza transportującego jest prawie dwa razy większa. Strumień masowy powietrza jest równy 33.1 $\frac{kg}{s}$. Powietrze do spalania podawane jest z prędkością wynoszącą 120 $\frac{m}{s}$, powietrze transportujące zaś- 30 $\frac{m}{s}$. Kocioł zaprojektowany jest na 130 MW_{th} nominalnego obciążenia cieplnego, z czego w paliwie doprowadzanych jest 100 MW_{th} reszta zaś dostarczana jest wraz z wysokopodgrzanym powietrzem do spalania. Każdy palnik pracuje z obciążeniem 20 MW_{th}. Zarówno powietrze do spalania jak i powietrze transportujące mają skład powietrza atmosferycznego (23% masowo tlenu i 77% masowo azotu). Temperatura ścian komory spalania została przyjęta na stałym poziomie w tej serii obliczeń i wynosi 800 K.

Opracowana konfiguracja kotła zapewnia powstawanie intensywnych recyrkulacji wewnątrz komory spalania, zaś strefy martwe są niewielkie. Proces spalania zachodzi w całej objętości komory spalania. Wewnętrzne recyrkulacje produktów spalania tworzą wyrównane pola temperatury i tlenu wewnątrz komory spalania. Ponadto, z powodu rozcieńczenia strug reagentów przez recyrkulujące produkty spalania, zapłon pyłu węglowego zachodzi w środowisku ubogim w tlen, co powoduje obniżenia maksymalnych temperatur. Silne recyrkulacje gorących gazów spalinowych w strefę spalania eliminują

problemy związane z zapłonem pyłu węglowego. Cała objętość komory spalania wypełniona jest gazami o temperaturze 1600-2000 K. Temperatura spalin opuszczających komorę spalania wynosi ok. 1400 K, w związku z czym spaliny posiadają znaczną entalpię, która musi zostać wykorzystana do podgrzewania powietrza. Koncentracja tlenu jest prawie w całej objętości komory spalania waha się w przedziale 3-5%, podczas gdy stężenie tlenu w spalinach wynosi 3.4%.

Jak wykazały obliczenia kocioł pracujący w technologii HTAC łączy w sobie dwie zalety: wyrównane strumienie ciepła wzdłuż wysokości komory spalania (jak w przypadku kotłów fluidalnych) oraz wysokie wartości przekazywanych strumieni ciepła (jak w przypadku standardowych kotłów pyłowych z palnikami umieszczonymi na bocznej ścianie). Wymiana ciepła na drodze promieniowania odgrywa dominującą rolę i stanowi 83% całkowitej wymiany ciepła) w komorze spalania.

Trzeci cel pracy dotyczył analizy aspektów ekologicznych związanych z realizacją technologii HTAC w kotłach energetycznych. Szczególną uwagę skupiono na emisji tlenków azotu, tlenku węgla oraz niewypalonych części lotnych i koksiku. Większość tlenków azotu formowana jest w obszarze pomiędzy palnikami, a maksymalna koncentracja wynosi 1195 ppm. Poza tym regionem stężenie tlenków azotu jest niskie i wyrównane; zawiera się w przedziale pomiędzy 300 a 400 ppm. W kotle pracującym w technologii HTAC, 98% całkowitej ilości tlenków azotu jest tworzonych poprzez mechanizm paliwowy. Ważną rolę odgrywa także redukcja powstałych już tlenków azotu. W efekcie, stężenie NO w spalinach jest niskie i wynosi 298 ppm. Długi czas przebywania cząsteczek węgla w kotle i silne recyrkulacje produktów spalania polepszają wypalenie lotnych produktów odgazowania oraz koksiku. Stabilny proces spalania obserwowany w technologii HTAC i bardzo prosta konstrukcja palników stwarza możliwość użycia jako paliwa w tym kotle gorszej jakości węgli.

Czwartym celem pracy było przetestowanie pracy kotła HTAC przy zmiennych parametrach operacyjnych takich jak: podgrzanie powietrza do spalania, moment pędu strugi doprowadzonego powietrza oraz stosunek nadmiaru powietrza. Do wszystkich serii symulacji numerycznych została zaimplementowana ostateczna konfiguracja kotła pracującego w technologii HTAC i stanowiła ona przypadek referencyjny dla obliczeń numerycznych w tej części pracy. Stwierdzono, że poziom podgrzania powietrza nie ma wpływu na poprawną pracę kotła pyłowego w technologii HTAC. Ponadto, zostało potwierdzone, że wysoka prędkość strugi powietrza na dolocie jest jednym z podstawowych warunków koniecznych do realizacji technologii HTAC. Dodatkowo, zauważono potencjał eksploatacji kotła węglowego pyłowego pracującego w technologii HTAC z wartościami stosunku nadmiaru powietrza bliskimi wartości stechiometrycznej.

Piąty cel związany był ze sprawdzeniem pracy kotła HTAC skojarzonego z obiegiem parowym i w efekcie określenie sprawności produkcji energii elektrycznej. Proces projektowania kotła dotyczy zarówno procesu spalania w kotle jak i pracy całego obiegu parowego. Oba te zagadnienie są silnie od siebie zależne ze względu na proces wymiany ciepła zachodzący pomiędzy produktami spalania w komorze spalania kotła, przekazującymi ciepło a mieszanką parowo-wodną w rurach kotła, odbierającą ciepło. Ostateczna konfiguracja kotła HTAC, wraz z warunkami brzegowymi i operacyjnymi, stanowi punkt wyjściowy dla tej serii obliczeń. W celu zamodelowania wymiany ciepła przez ściany kotła napisano program komputerowy, włączony następnie do kodu FLUENT. Rezultatem tej serii obliczeniowej jest otrzymanie rozkładu temperatury na ścianach kotła, zarówno od strony komory spalania jak i od strony czynnika chłodzącego. Kocioł pracujący w technologii HTAC został zaprojektowany jako kocioł przepływowy na parametry ultra-superkrytyczne. Przebadano trzy popularne konfiguracje rur: rury pionowe zasilane od góry, rury pionowe zasilane od dołu oraz rury spiralne. Najbardziej wyrównany profil temperatury wzdłuż rur kotła otrzymano dla orurowania spiralnego.

Przedstawiona praca doktorska potwierdziła, że zastosowanie technologii HTAC w kotłach energetycznych może być praktyczną, wysokoefektywną i czystą metodą spalania pyłu węglowego w celu produkcji energii elektrycznej. Najważniejszą zaletą zastosowania technologii HTAC w kotłach energetycznych są wyrównane i wysokie wartości strumieni ciepła, a tym samym duża gęstość energii w komorze kotła. Skutkuje to mniejszymi rozmiarami komory spalania takiego kotła. Kolejną zaletą jest niska emisja substancji szkodliwych, głównie tlenków azotu, w porównaniu ze standardowymi pyłowymi kotłami energetycznymi. Dodatkowo, zastosowane palniki mają niezwykle prostą konstrukcję: bez stopniowania powietrza, stabilizacji płomienia czy zawirowania, które są powszechnie stosowane w palnikach pyłowych. Mimo stwierdzenia szeregu korzyści z zastosowania technologii HTAC w kotłach energetycznych, istnieje wciąż kilka nierozwiązanych kwestii. Po pierwsze, stężenie cząsteczek w spalinach po spaleniu pyłu węglowego jest prawdopodobnie zbyt wysokie do zastosowania regeneracyjnych wymienników ciepła. W przyszłości zaistnieje potrzeba znalezienia sposobu wykorzystania energii zawartej w spalinach z kotła do podgrzania powietrza do żądanej temperatury. Jednakże, sprawdzono możliwość poprawnej eksploatacji kotła także bez konieczności podgrzewu powietrza. Należy podkreślić, że wykonana praca doktorska jest pierwszą próbą podejścia do tematu wykorzystania technologii HTAC w kotłach energetycznych opalanych pyłem węglowym i koniecznym jest przeprowadzenie wielu dalszych badań zarówno numerycznach jak i eksperymentalnych zanim technologia ta będzie mogła zostać wykorzystana na skalę przemysłową.

Zusammenfassung

Die FLammenlose OXidation (FLOX), ist im englischen Sprachraum entweder als High Temperature Air Combustion (HTAC) oder als MILD (Moderate and Intensive Low-oxygen Dilution) Combustion bekannt. Die wichtigste Eigenschaft der HTAC-Technologie ist die Rückführung/Rezirkulation der Verbrennungsprodukte in die Brennkammer. Der Grund für die Rückführung ist, dass der für die Verbrennung benötigte Luft- und Brennstoffstrom mit dem Abgas verdünnt werden muss, bevor eine Zündung eintritt. Dadurch werden die Temperaturspitzen niedrig gehalten. Ein weiteres Resultat dieser speziellen Mischung ist die homogene Verteilung der Temperatur und des verdünnten Brennstoff-Luftgemisches. Die Besonderheiten der HTAC-Technologie sind folglich niedrige NO_x- und CO-Emissionen, sowie ein gleichmäßig hoher Wärmefluss.

Bisher wurde die HTAC-Technologie hauptsächlich in Industrieöfen eingesetzt, welche mit Brenngasen oder leichten Ölen befeuert werden. In den meisten Industrieanwendungen ist diese Technologie mit Wärmerückgewinnungsanlagen kombiniert, was zu einer beträchtlichen Kraftstoffeinsparung führt.

In dieser Arbeit wurde die Anwendung der HTAC-Technologie in kohlestaubbefeuerten Kraftwerkskesseln untersucht. Folgende Vorteile sind erwartet:

- Gegenüber üblichen Industrieöfen ist der Wärmestrahlung in HTAC-Öfen bedeutend höher. Wenn das Gleiche in Kesseln erreicht werden könnte, würden die Kosten eines Kessels durch eine geringere Wärmeübertragungsfläche reduziert. Durch die Verwendung von Stahlen, welche hohe Temperaturen ermöglichen, könnte der Kessel eine Steigerung den Heißdampfparametern auf ein ultra-überkritisches Niveau erlauben, was insgesamt eine bessere Wärmeausnutzung des Gesamtprozesses bedeutet.

- Ein weiterer Vorteil ist die Verminderung von Schadstoff-Emissionen (hauptsächlich Stickstoffoxide), was teure Abgasreinigungsanlagen überflüssig macht.

Die Anwendbarkeit des HTAC-Technologien in Kraftwerkskesseln könnte in Zukunft die Kohleverbrennung zur saubereren Energieerzeugung werden lassen. Technische und ökologische Aspekte solcher Verfahren sind in dieser Doktorarbeit analysiert und diskutiert.

Das Ziel dieser Arbeit ist es, die Verwendbarkeit der HTAC-Technologie in Kohlekraftwerken für eine umweltfreundlichere Stromerzeugung zu untersuchen. Um das zu erreichen, wurden verschiedene technische Teilziele formuliert. Mithilfe numerischer Modellierungsmethoden, trifft das erste Teilziel Aussagen über den genauen Ablauf der HTAC-Kohleverbrennung. Zu diesem Zweck wurden Messergebnisse einem Experiment durchgeführt bei IFRF anhand mathematischer Modelle beschrieben. Die auf CFD basierten Simulationen sind mit FLUENT Code durchgeführt. Das überprüfte und validierte mathematische Model wird in allen nachfolgenden Untersuchungen verwendet. Das zweite Teilziel beschreibt ein Konzept eines mit Staubkohle befeuerten Kessels unter Verwendung der HTAC-Technologie. Das beinhaltet die Auslegung der Brennkammer, also die Abmessungen, die Abstände zwischen den einzelnen Brennern und die Positionen der Brennerdüsen. Das dritte Teilziel wertet die ökologischen Aspekte der Anwendung der HTAC-Technologie aus. Hauptsächlich werden NO_x, CO, unverbrannte Kohlenwasserstoffe und Kohleausbrand betrachtet. Desweiteren soll die Arbeitsweise eines HTAC-Kessels unter verschiedenen Konditionen überprüft werden. Dazu gehört niedrige Luftverbrennungstemperaturen, niedrige Luftverbrennungsimpuls und eine etwas niedriger Luftzahl. Im weiten Verlauf, das gesamten Dampfkreislaufes wird untersucht, um die Effektivität der elektrischen Energieerzeugung unter Verwendung eines HTAC-Kessels abzuschätzen.

Die gesamte Arbeit wurde mit einem Beschreibung der Technologien, die im Kraftwerkskessel benutzen sind, angefangen. Ferner werden die Grundlagen von Kraftwerkskesselanlagen bereitgestellt. Desweiteren werden in Kürze die Entwicklung, die Stand der Technik und die Problematik der HTAC-Technologie untersucht. Besondere Aufmerksamkeit verdient die Entwicklung des Verbrennungsvorgangs unter HTAC-Bedingungen, speziell mit festen Brennstoffen. Im einen weiten Abschnitt der Arbeit werden die benutzten mathematischen Modelle beschrieben. Im Wesentlichen die Kohleverbrennung, die Stickstoffzusammensetzung zusammen mit Stickstoffreduzierung.

Im Rahmen dieser Arbeit wird zuerst das mathematische Modell, das die Verbrennung von Kohle unter HTAC-Bedingungen beschreibt, mit Hilfe von Messergebnissen validiert, die aus einem IFRF-Experiment stammen, das als HTAC-99 bekannt ist. Verschiedene Untermodelle werden während dieser Validierung und Nachweisprozedur getestet. Je nach Ergebnis wurden folgende Untermodelle ausgewählt:

- $k - \varepsilon$ Modell für Turbulenzen;

- Eddy Dissipation Model für den Zusammenhang zwischen der Chemie und den Turbulenzen;

- diskretes Phasenmodell für die Beschreibung des Partikelverhaltens;

- CPD-Modell des Entgasungsprozess;

- Intrinsic Modell für Kohleausbrandprozess;

- Diskrete Ordinates Model für Strahlungsgleichungslösung;

- Stickstoffsbildung durch Brennstof-, thermischen-, prompt, und N_2O-prozess, sowie die NO-Nachverbrennung in der Gasphase und auf der verkohlten Oberfläche.

Die berechneten Werte gut stimmen mit denen der gemessenen überein. Daher wird ein solches überprüftes Model für die weitere Kesselaufbau-Untersuchungen verwendet.

Der HTAC-Verbrennungsprozess unterscheidet sich sehr von der konventionellen Verbrennung. Deshalb ist ein innovatives Design von Kesseln, die diese Technologie nutzen sollen, notwendig. Es werden verschiedene besondere Konzepte von Kesseln im Zusammenhang mit den folgenden drei Punkten analysiert: Vorhandensein einer intensiven, im Brennkammer vorkommenden Rezirkulation, Gleichverteilung von Temperaturbereichen und chemischen Zusammensetzungen, sowie konstante Wärmeflüsse. Es wurden verschiedene Simulationen durchgeführt, um eine Kesselform zu finden und zu dimensionieren, die optimale Abstände zwischen Brennern und der Platzierung der Brenner selber zu finden.

Basierend auf den vorangegangenen Untersuchungen wurde eine endgültige Konfiguration des HTAC-Kessels ausgewählt. Es muss bedacht werden, dass die Anwendung der HTAC Technologie in Staubkohle befeuerten Kesseln für die Stromerzeugung, hauptsächlich nach technischen und ökologischen Belangen diskutiert wird. Der HTAC-Kessel ist 13 m hoch und hat einen Querschnitt von 7 m mal 6 m. Er ist mit einem Brennerblock ausgestattet, welcher aus 5 identischen Brennern besteht und an der Decke angebracht ist, wodurch der Kessel nach unten feuert. Die Abgassenken sind ebenfalls an der Kesseldecke zu finden und sie sind symmetrisch an den Brennerblockseiten positioniert. Die Senken haben eine quadratische Form mit einer Seitenlänge von 1 m. Jeder der fünf Brenner ist mit einer mittig platzierten Einspritzdüse, welche heiße Luft einbläst, und mit zwei Kohleneindüsen, welche auf beiden Seiten der Düse positioniert sind, ausgestattet. Der Staubkohle wird in den Ofen über Düsen mit einem Durchmesser von 15 mm eingeführt und die Verbrennungsluft mit 48-mm-Düsen. Der Kessel ist mit zwei Aschentrichtern ausgelegt. Die Verbrennungsluft wird bis zu 1200 K vorgewärmt und die Kohle wird mithilfe von Transportluft bei Raumtemperatur (300 K) gefördert. Die Zuführung der Kohle beträgt 3.2 $\frac{kg}{s}$ und die dazu benötigte Transportluft ist etwa zweimal höher. Der Massenstrom der Verbrennungsluft

entspricht einem Wert von 33.1 $\frac{kg}{s}$. Die Strömungsgeschwindigkeit der Luft beträgt 120 $\frac{m}{s}$ und die der Kohle 30 $\frac{m}{s}$. Der Kessel arbeitet insgesamt mit einer Wärmeleistung von 130 MW. Die durch Brennstoff zugeführte Leistung enspricht einem Wert von 100 MW, also arbeitet jeder Brenner mit 20 MW Brennstoffleistung. Die Verbrennungsluft- und die Transportluftmassenströme enthalten beide 23% Sauerstoff und 77% Stickstoff. Die Wandtemperatur in den Berechnungen des Kesselaufbaus liegt bei konstanten 800 K.

In der endgültige Kesselaufbau die interne Gasenrezirkulation ist intensive und die unzureichende Mischung Zone sind kleine. Das ganze Volumen der Brennkammer wird im Verbrennungsprozess ausgenutzt. Die interne Rezirkulation der Verbrennungsprodukte erzeugt eine homogene Temperaturverteilung und eine gleichmäßige Verteilung der chemischen Komponenten. Dank der Verdünnung der Verbrennungsluft und der Brennstoffdüsen findet die Entzündung der Kohle in einem Bereich niedriger Sauerstoffkonzentration statt, und dadurch wird die Temperatur niedrig gehalten. Eine starke Rückführung des heißen Verbrennungsgases beseitigt die Probleme mit Kohlezündung. Der gesamte Kessel ist gefüllt mit Verbrennungsprodukten, die im Temperaturbereich von 1600 bis 2000 K liegen. Die Temperaturspitzen (etwa 2100 K) sind im Wesentlichen geringer als im Vergleich zu konventionellen Verbrennungen mit vorgewärmter Luft. Die Ausgangstemperatur an der Brennkammer beträgt etwa 1400 K und die Enthalpie des Abgases ist sehr hoch. Diese Enthalpie wird in einem Wärmetauscher zurückgewonnen, um damit die Verbrennungsluft vorzuwärmen. Die Sauerstoffkonzentration im Kessel liegt annährend in einem Bereich von 3-5%, die im Abgas liegt bei 3.4%. Die gleichmäßigen und niedrigen Sauerstoffkonzentrationen begründen die niedrige Temperaturspitze. Der HTAC-Kessel hat zwei Vorteile: Gleichmäßige Wärmeflüsse entlang der Kesselhöhe (wie in Wirbelschichtkesseln) und hohe Wärmeflusswerte (wie im Staubkohlegefeuerte Kesseln). Die Wärmeübertragung durch Strahlung hat den größten Einfluss. Es macht etwa 83% der gesamten Wärmeübertragung aus, die restlichen Prozent ergeben sich aus der Wärmekonvektion. Zumeist die NO entsteht in einer Region zwischen den Brennern. Die NO-Konzentrationspitze beträgt 1195 ppm. Unterhalb der höheren NO-Region sind die Stickstoffoxid-Konzentrationen niedrig in einem Bereich von 300 bis 400 ppm. 98% der Stickstoffoxide im HTAC-Boiler resultiert aus dem Brennstoff-NO Weg. Der NO Nachverbrennungsmechanismus spielt eine wichtige Rolle. Demzufolge sind die Stickstoffoxid-Konzentrationen am Kesselausgang gering und betragen 298 ppm. Die lange Aufenthaltszeit der Partikel und die rekursive Rückführung der Verbrennungsprodukte verbessern die Verbrennung von CO so wohl wie Flüchtigenbestandteile und Koks. Gleichmäßige Verbrennungsprozesse

und einfache Brennerkonstruktionen eröffnen die Möglichkeit einer Verwendung von qualitativ schlechter Kohle.

Im weiteren Verlauf die Auswirkungen von drei wichtigen Parametern in HTAC-Kesseln werden getestet: Die Vorwärmung der Verbrennungsluft, die Strömungsgeschwindigkeit der Verbrennungsluft und eine erniedrigte Luftzahl. Für alle Berechnungen werden die Kesselgeometrie und die gleichen Betriebsgrenzen beibehalten. Allerdings sind die Arbeitsbedingungen für jeden Berechnungsdurchlauf verschieden. Der endgültige Kesselaufbau ist immer die Referenz.

Prozeduren für das Design eines Kessels beinhalten die Auswertung des Verbrennungsprozesses, sowie den Dampfkreislauf. Beide sind aufgrund der fortschreitenden Wärmeübertragung von den Verbrennungsprodukten in der Brennkammer zum Wasser/Dampf-Gemisch in den Kesselrohren stark aneinander gekoppelt. In dem letzten Teil der Arbeit findet die Abhängigkeit zwischen HTAC-Kessel und dem kompletten Dampfkreislauf Betrachtung. Die endgültige Kesselgeometrie, sowie die Arbeitsbedingungen und die Betriebsgrenzen sind die Grundlagen für die Berechnungen. Eine benutzerdefinierte Subroutine ist zur Berechnungsdurchführung geschrieben worden. Das Modell berechnet das Temperaturverlauf auf jede Wende im den Kessel. In dieser Doktorarbeit wird der HTAC-Kessel als ein ultra-überkritischer Kessel vorgeschlagen. Drei üblicherweise verwendete Konfigurationen der Durchlaufkesselröhren wurden in einer Serie von Berechnungen getestet. Vertikal abwärts-aufwärts, aufwärts-abwärts und gewunden, bzw. spiralartig. Die meisten gleichmäßigen Temperaturprofile treten im Kessel mit dem spiralförmigen Röhren auf; aufgrund dessen ist die Spiralrohrkonfiguration der brauchbarste HTAC-Kesselaufbau. Allerdings ist diese Konfiguration die technisch aufwendigste Lösung. Der Rankine-Prozesswirkungsgrad des Dampfkreisprozesses mit dem HTAC-Kessel beträgt mehr als 50%.

Insgesamt ergeben die Rechnungen, dass die HTAC-Technologie eine machbare, effiziente und saubere Technologie für Staubkohle befeuerte Kessel ist. Zusammenfassend folgen die wichtigsten Vorteile der mit Staubkohle befeuerten Kessel, die mit HTAC Technologie funktionieren. Da wären zuerst die hohen und gleichmäßigen Wärmeströme, die während des Verbrennungsprozesses abgestrahlt werden, welche ein Resultat der hohen Befeuerungsdichte und der konsequent kleinen Bauart des Kessels sind. Als nächstes seien die, im Vergleich zu Standard-PC-Kesseln, geringen NO_x-Emissionen genannt. Desweiteren sind die Brenner simpel aufgebaut: ohne Luft Stufung, Flammenstabilisator oder Drall Erzeuge, was üblicherweise in kommerziellen Staubkohlebrennern verwendet wird.

Obwohl die HTAC-Technologie eine attraktive Möglichkeit für kohlestaubbefeuerten Kessel ist, so gibt es dennoch viele offene Fragen. Vor allem ist die Partikelkonzentration im Abgas problematisch hoch, um das Verfahren in Verbindung mit Wärmetauschern zu verwenden. In der Zukunft ist es wichtig einen Weg zu finden, die Enthalpie im Abgas zu nutzen. Dennoch wurde untersucht, dass der Kessel ohne eine Luftvorwärmung arbeiten kann, und dass ohne den Zündvorgang in seinen Einzelheiten zu betrachten. Aufgrund der starken Rezirkulation und der hohen Geschwindigkeiten der Kohlepartikel könnte die Erosion ebenfalls ein Problem werden.